

CHARACTERISATION OF THE  
LYSOSOMAL INTEGRAL MEMBRANE PROTEIN TYPE-2  
(LIMP-2) AND ITS INTERACTION WITH  
 $\beta$ -GLUCOCEREBROSIDASE:

IMPLICATIONS FOR  
PARKINSON AND GAUCHER DISEASE

Dissertation

in fulfilment of the requirement for the degree “Dr. rer. nat”  
of the Faculty of Mathematics and Natural Sciences  
at Kiel University

submitted by

**FRIEDERIKE ZUNKE**

Institute of Biochemistry

Kiel, July 2015

**Referee:** Prof. Dr. Paul Saftig

**Co-referee:** Prof. Dr. Axel J. Scheidig

**Date of oral examination:** 13.10.2015

**Approved for publication:**

Prof. Dr. Wolfgang J. Duschl  
(The Dean)



# Table of contents

<b>ABSTRACT</b>	<b>8</b>
<b>ZUSAMMENFASSUNG</b>	<b>9</b>
<b>1 INTRODUCTION</b>	<b>11</b>
<b>1.1 The lysosome</b>	<b>11</b>
1.1.1 Composition of lysosomes	11
1.1.1.1 Soluble lysosomal proteins	11
1.1.1.2 Lysosomal membrane proteins	11
1.1.2 Trafficking of soluble lysosomal enzymes	12
1.1.2.1 Mannose-6-phosphate receptor dependent transport	13
1.1.2.2 Mannose-6-phosphate receptor independent transport	14
1.1.3 Lysosomal storage diseases	15
1.1.3.1 Lipid storage diseases: Sphingolipidoses and cholesterol transport deficiencies	16
1.1.3.1.1 Sphingolipids and sphingolipidoses	16
1.1.3.1.2 Lysosomal accumulation of cholesterol: Niemann-Pick Type C (NPC-1)	17
1.1.3.1.3 Membrane transport of fatty acids and cholesterol	19
<b>1.2 The lysosomal integral membrane protein Type-2 (LIMP-2)</b>	<b>20</b>
1.2.1 Protein structure of LIMP-2	20
1.2.2 LIMP-2 associated diseases	22
1.2.3 LIMP-2-deficient mice	23
<b>1.3 The lysosomal hydrolase <math>\beta</math>-Glucocerebrosidase (GC)</b>	<b>23</b>
1.3.1 Protein structure of GC	24
1.3.2 GC-associated diseases	25
1.3.2.1 Treatment of GC-associated diseases	26
<b>1.4 Lysosomal dysfunction and neurodegenerative diseases</b>	<b>27</b>
1.4.1 Parkinson Disease	27
1.4.2 $\alpha$ -Synuclein: structure and metabolism within the cell	28
1.4.2.1 Lysosomal degradation of $\alpha$ -synuclein	29
1.4.2.2 Proteasomal degradation of $\alpha$ -synuclein	29
1.4.3 Relationship between GC and $\alpha$ -synuclein accumulation	30
<b>2 OBJECTIVES</b>	<b>32</b>
<b>3 MATERIAL AND METHODS</b>	<b>33</b>
<b>3.1 Materials</b>	<b>33</b>
3.1.1 Cell lines	33
3.1.2 Mouse strains	34
3.1.3 Antibodies	35
3.1.3.1 Primary antibodies	35
3.1.3.2 Secondary antibodies	36
3.1.4 Oligonucleotides	37

---

3.1.5	Expression vectors and constructs	37
3.1.5.1	pcDNA3.1 and pfrog vector	37
<b>3.2</b>	<b>Methods</b>	<b>40</b>
3.2.1	Molecular biology	40
3.2.1.1	Polymerase-Chain-Reaction (PCR)	40
3.2.1.1.1	Fusion-PCR	40
3.2.1.2	Agarose electrophoresis	41
3.2.1.3	Cloning experiments: Restriction enzyme digestion and DNA ligation	42
3.2.1.4	Amplification and purification of expression vectors in Escherichia Coli	42
3.2.1.5	Measurement of DNA-concentration	43
3.2.1.6	Mouse perfusion	43
3.2.1.7	Isolation and dissection of murine brain	43
3.2.1.8	Tissue and section preparation	44
3.2.1.8.1	Paraffin embedding, sectioning and removal of paraffin	44
3.2.1.8.2	Succrose embedding	44
3.2.1.9	Histology	45
3.2.1.9.1	Immunohistology	45
3.2.1.9.2	TUNEL staining	46
3.2.1.9.3	Periodic acid-Schiff staining	46
3.2.2	Molecular structural analyses	47
3.2.2.1	LIMP-2-derived peptides	47
3.2.2.2	Recombinant enzymes	48
3.2.2.3	Nanodrop: Proteinconcentration measurement	49
3.2.2.4	Peptide-pulldowns	49
3.2.2.5	Protein modelling	51
3.2.2.6	Circulardichroismus (CD-Spectroscopy)	51
3.2.2.7	Dynamic light scattering (DLS)	52
3.2.2.8	Crystallisation	53
3.2.3	Protein biochemistry	54
3.2.3.1	Lysis of cells and tissue	54
3.2.3.2	Proteinquantification	55
3.2.3.3	Deglycosylation of proteins	55
3.2.3.4	Co-immunoprecipitation (Co-IP) studies	56
3.2.3.5	SDS-PAGE	57
3.2.3.6	Western Blotting	57
3.2.3.7	Incubation with antibodies and stripping of immunoblots	58
3.2.3.8	Coomassie stainings	59
3.2.3.9	Densitometric analysis of immunoblots/coomassie-stained SDS-gels	59
3.2.3.10	Enzyme activity assasy	59
3.2.3.11	In vivo lysosomal activity assay	60
3.2.4	Cell biological methods	61
3.2.4.1	Cultivation of adherent cells	61
3.2.4.2	Transfection of cells	62
3.2.4.3	Transduction of neurons	62
3.2.4.4	Cryopreservation and thawing of cells	63
3.2.4.5	Harvesting of cells	63
3.2.4.6	Uptake assays with recombinant enzymes/LIMP-2-derived peptides	63
3.2.5	Microscopical methods	64
3.2.5.1	Fixing and staining of cells for immunofluorescence	64
3.2.5.2	Filipin stainings	64
3.2.5.3	Microscopical recording	65

3.2.6	Computer software	65
3.2.7	Statistical analysis	66

## **4 RESULTS** **67**

### **4.1 LIMP-2: What does the crystal structure of its luminal domain tell us?** **67**

4.1.1	Lysosomal trafficking of LIMP-2: does it need an M6P-tag?	67
4.1.2	An exciting finding in the three-dimensional structure of LIMP-2: does LIMP-2 exhibit additional functions?	69
4.1.2.1	Is LIMP-2 a transporter of cholesterol?	69
4.1.3	A closer look: where exactly is the GC-binding site on LIMP-2?	75
4.1.3.1	Characterisation of the LIMP-2-GC binding mutants	75
4.1.3.2	GC-binding properties of LIMP-2 mutants	77

### **4.2 Is the helical bundle of LIMP-2 sufficient to mediate interaction with GC?** **79**

4.2.1	Do LIMP-2-derived peptides also modify the function of GC?	82
4.2.1.1	Can the LIMP-2-derived helix 5 peptide be exploited to therapeutically increase GC activity?	86
4.2.2	What causes the positive effect of LIMP-2 peptides on GC function?	87
4.2.2.1	CD-spectroscopy: changes in secondary structure of GC after helix 5 binding?	87
4.2.2.	Dynamic light scattering: changes in quaternary structure of GC after helix 5 binding?	88

### **4.3 Structural analyses of GC: Where does LIMP-2 bind?** **89**

4.3.1	Binding properties of GC mutants towards LIMP-2	94
4.3.2	Subcellular localisation of GC mutants	95
4.3.3	Does LIMP-2 overexpression modulate GC trafficking and function?	101
4.3.4	Validation of the LIMP-2 interaction site of GC protein using LIMP-2-derived peptides	105

### **4.4 LIMP-2 knockout mice – what impact does LIMP-2/GC have on $\alpha$ -synuclein homeostasis in murine brain?** **106**

4.4.1	Storage of GC substrate and undefined material	106
4.4.2	Accumulation of $\alpha$ -synuclein	108
4.4.3	Increased $\alpha$ -synuclein levels lead to neurotoxicity and behavioural abnormalities	110

### **4.5 How does $\alpha$ -synuclein affect human CNS?** **113**

4.5.1	Does $\alpha$ -synuclein interfere with GC function?	113
4.5.2	Does $\alpha$ -synuclein modulate the expression of LIMP-2?	114

### **4.6 What are the effects of LIMP-2-deficiency in humans?** **115**

### **4.7 LIMP-2: A novel therapeutic target for the treatment of synucleinopathies?** **116**

4.7.1	The LIMP-2-derived helix 5 peptide: a novel therapeutic target for PD?	120
-------	--	-----

## **5 DISCUSSION** **122**

### **5.1 New insights on LIMP-2 trafficking and function** **122**

5.1.1	Speculations about the function of the tunnel structure in the LIMP-2 protein	125
-------	---	-----

---

<b>5.2</b>	<b>The interaction of LIMP-2 and GC</b>	<b>128</b>
5.2.1	Analysing the GC binding site on the LIMP-2 protein	128
5.2.2	Analysis of the LIMP-2 binding site on the GC protein	130
5.2.3	The overall picture: combining all data about the LIMP-2 and GC interaction	136
<b>5.3</b>	<b>The LIMP-2-derived helix 5 peptide: a therapeutic target?</b>	<b>138</b>
<b>5.4</b>	<b>The role of LIMP-2 in <math>\alpha</math>-synuclein homeostasis</b>	<b>141</b>
5.4.1	Consequences of LIMP-2 deficiency on lysosomal function in murine brain	142
5.4.2	Reasons for $\alpha$ -synuclein accumulation mediated by the LIMP-2 deficiency	143
5.4.3	Consequences of $\alpha$ -synuclein accumulation in mouse and human CNS	144
5.4.4	The role of LIMP-2 in the development and correction of synucleinopathies: identification of novel therapeutic targets	146
<b>5.5</b>	<b>Conclusion and outlook</b>	<b>150</b>
<b>6</b>	<b>REFERENCES</b>	<b>151</b>
<b>7</b>	<b>APPENDIX</b>	<b>167</b>
<b>7.1</b>	<b>Abbreviations</b>	<b>167</b>
<b>7.2</b>	<b>Equipment, chemicals, enzymes, kits and buffers</b>	<b>168</b>
7.2.1	Machines	168
7.2.2	Consumables	169
7.2.3	Chemicals/Enzymes	170
7.2.4	Kits	172
7.2.5	Buffer and solutions	172
<b>7.3</b>	<b>List of figures and tables</b>	<b>177</b>
7.3.1	Figures	177
7.3.2	Tables	178
<b>7.4</b>	<b>Curriculum Vitae</b>	<b>180</b>
<b>7.5</b>	<b>Publications and scientific participations</b>	<b>181</b>
<b>7.6</b>	<b>Acknowledgments/Danksagung</b>	<b>183</b>
<b>7.7</b>	<b>Declaration</b>	<b>184</b>

## Abstract

The acid  $\beta$ -glucocerebrosidase (GC) is a lysosomal hydrolase for  $\beta$ -glucose-terminated sphingolipids and reaches the lysosome through binding to its transport receptor the Lysosomal Integral Membrane Protein Type-2 (LIMP-2) in a mannose-6-phosphate independent manner. Mutations in GC cause the most common lysosomal storage disorder, Gaucher disease and represent the highest genetic risk factor for the development of Parkinson disease caused by accumulation of  $\alpha$ -synuclein.

In this work properties of LIMP-2 and GC protein structure as well as their binding characteristics were analysed. By mutation and interaction studies, the GC-binding site on the LIMP-2 protein could be narrowed down to an exposed helical bundle comprised of two prominent helices. Surprisingly, a short peptide consisting of the proposed binding region of LIMP-2 was sufficient to mediate interaction with GC. Furthermore the LIMP-2-derived peptide had an activating effect on enzyme activity *in vitro* as well as in cell-based studies.

The respective interaction site of LIMP-2 on the GC protein could also be narrowed down to a hydrophobic patch, verified by mutagenesis, interaction studies as well as peptide pulldown assays.

Furthermore, effects of LIMP-2 deficiency in mouse brain were described exhibiting reduced levels of GC protein and activity, leading to aggregation of its substrates. Dysfunction of GC has been shown to interfere with  $\alpha$ -synuclein homeostasis and its lysosomal degradation. In brain of LIMP-2-deficient mice  $\alpha$ -synuclein accumulation could be observed, which led to severe neurological defects. Additionally, in cell-based experiments a distinct relationship between LIMP-2 expression, GC-activity and lysosomal degradation of  $\alpha$ -synuclein was described. Heterologous expression of LIMP-2 in human and murine cell systems resulted in an increased lysosomal trafficking and activity of GC leading to a reduction of  $\alpha$ -synuclein levels. This underscored the importance of the common function of LIMP-2 and GC in the intracellular regulation of  $\alpha$ -synuclein.

In summary, this study describes the structural characteristics of the interaction of LIMP-2 with GC and the impact of LIMP-2 on GC activity. The experiments performed suggest that an augmented GC activity represents a promising target for the treatment of GC-associated diseases including Gaucher disease and Parkinson disease. This work reveals that this increase in GC activity can either be achieved by enhancing the LIMP-2 expression or by small chaperone-like molecules, as accomplished utilising the LIMP-2-derived peptide.

## Zusammenfassung

Die  $\beta$ -Glukozerebrosidase (GC) ist eine lysosomale Hydrolase, die  $\beta$ -Glukose-ständige Sphingolipide umsetzt. Durch die Bindung an den Transportrezeptor, dem lysosomalen integralen Membranprotein Typ-2 (LIMP-2) gelangt das Enzym vom Endoplasmatischen Retikulum Mannose-6 Phosphat unabhängig an seinen Wirkort –den Lysosomen. Mutationen in der GC führen zu der häufigsten lysosomalen Speichererkrankung, der Gaucher Erkrankung. Außerdem wurde beschrieben, dass Mutationen im Gen der  $\beta$ -Glukozerebrosidase zu den häufigsten genetischen Risikofaktoren der Parkinson Krankheit zählen. Diese neurodegenerative Erkrankung ist durch die Akkumulation des neuronalen Proteins  $\alpha$ -Synuklein charakterisiert.

In dieser Arbeit wurden die strukturellen Eigenschaften des LIMP-2 Proteins sowie der GC untersucht. Dabei war der Fokus auf die strukturelle Untersuchung ihrer Interaktion gerichtet. Durch Mutations- und Interaktionsstudien konnte die GC-Interaktionsstelle im LIMP-2 Protein auf eine exponierte helikale Region eingeschränkt werden. Außerdem konnte gezeigt werden, dass ein Peptid, bestehend aus der potentiellen Binderegion von LIMP-2, ausreichend ist um mit GC zu interagieren und sogar einen positiven Effekt auf die enzymatische Funktion aufweist. Eine erhöhte Enzymaktivität nach Peptid-Zugabe konnte sowohl *in vitro*, als auch in zellkulturbasierten Experimenten bestätigt werden. Zusätzlich konnte die entsprechende LIMP-2 Bindedomäne auf dem GC Protein identifiziert und ebenfalls auf einen hydrophoben helikalen Bereich im Enzym eingeschränkt werden.

Des Weiteren wurden die Auswirkungen einer LIMP-2 Defizienz in Mausgehirnen untersucht. Es konnte gezeigt werden, dass sich einhergehend mit dem Verlust von LIMP-2 auch die Proteinmenge sowie die Aktivität von GC drastisch verringern. Dieses hat einen negativen Effekt auf den lysosomalen Abbau von  $\alpha$ -Synuklein. So konnte in den Gehirnen von LIMP-2-defizienten Mäusen erhöhtes und aggregiertes  $\alpha$ -Synuklein gefunden werden, welches zu weitreichenden neurologischen Defekten in den Tieren führte. Zusätzlich konnte in zellbasierten Experimenten der Einfluss von LIMP-2 Expression und GC Aktivität auf die lysosomale Degradierung von  $\alpha$ -Synuklein gezeigt werden. Eine heterologe Expression von LIMP-2 führte in murinen, sowie humanen Zellsystemen zu einem erhöhten lysosomalen Transport sowie einer gesteigerten Aktivität der Hydrolase und somit zu einer Verringerung der  $\alpha$ -Synuklein Proteinmenge.

Zusammenfassend zeigen die Ergebnisse dieser Arbeit strukturelle Charakteristiken der Interaktion von LIMP-2 und GC, sowie den Effekt von LIMP-2 auf die GC Aktivität. Des Weiteren lassen die Ergebnisse dieser Arbeit darauf schließen, dass die Steigerung der

katalytischen Funktion von GC eine vielversprechende therapeutische Maßnahme für GC-assoziierte Krankheiten wie die Gaucher und die Parkinson Erkrankung darstellt. Eine Erhöhung der Enzymaktivität kann dabei durch eine gesteigerte Expression von LIMP-2 oder durch eine gezielte Aktivierung des Enzyms, wie hier für das LIMP-2 Peptid gezeigt, induziert werden.

# 1 Introduction

## 1.1 The lysosome

The lysosome is a membrane-bound cell organelle ubiquitously found in mammalian cells, except in red blood cells and was discovered in the 1950s by Christian DeDuve (De Duve, Pressman et al. 1955). Lysosomes contain acid hydrolases for degradation and subsequent recycling of macromolecules. The impact of lysosomes in health and disease is further highlighted by a number of diseases resulting from defects in soluble lysosomal proteins and proteins of the lysosomal membrane (Eskelinen, Tanaka et al. 2003). In the last decade it has been realised that lysosomes are not only a recycling organelle but also play a pivotal role in cell metabolism, like repair of the plasma membrane, cell signalling, defence against pathogens, cholesterol metabolism and cell death (Saftig and Klumperman 2009, Yamayoshi, Yamashita et al. 2009, Schulze and Sandhoff 2011, Settembre, Fraldi et al. 2013). Lysosomes emerge from maturation or fusion of early endosomes and are characterised by a pH of 4.6 - 5. Lysosomal proteins are synthesised as soluble or membrane-integrated glycoproteins in the Endoplasmic Reticulum (ER). Mannose-6-phosphate receptors (MPRs) mediate the transport of the majority of lysosomal enzymes. Thereby proteins tagged with mannose-6-phosphate (M6P) terminal residues are recognized in the Trans-Golgi Network (TGN) by MPRs and are delivered to lysosomes (Kornfeld and Mellman 1989, Kornfeld 1992, Ludwig, Le et al. 1995).

### 1.1.1 Composition of lysosomes

#### 1.1.1.1 Soluble lysosomal proteins

To date up to 60 different lysosomal hydrolases responsible for the degradation of different substrates have been described (Settembre, Fraldi et al. 2013). Depending on their degradation products lysosomal enzymes can be classified as proteases, lipases, phosphatases, nucleases, glucosidases, peptidases and sulphatases (Bainton 1981). They require an acidic environment for optimal enzymatic function (De Duve and Beaufay 1959).

#### 1.1.1.2 Lysosomal membrane proteins

The lysosomal hydrolases are enclosed by a lysosomal membrane containing highly glycosylated membrane proteins, which contribute to the lysosomal glycocalyx (Wilke, Krausze et al. 2012, Schwake, Schroder et al. 2013). Most abundant and important for the lysosomal biogenesis and integrity are the Lysosomal Associated Membrane Proteins type 1 and 2 (LAMP-1, -2), the Lysosomal Integral Membrane Protein Type-1 (LIMP-1/CD36) and

the Lysosomal Integral Membrane Protein Type-2 (LIMP-2/SCARB2). A more detailed description of the function and structure of LIMP-2 will be provided in chapter 1.2. Amongst other lysosomal membrane proteins the vacuolar-type  $H^+$ -ATPase is responsible for lysosomal acidification (Ohkuma, Moriyama et al. 1982). The lysosomal cholesterol transporter Nieman-Pick Type C1 (NPC1) plays an important role in cellular cholesterol homeostasis (Infante, Radhakrishnan et al. 2008). Further major integral components of the lysosomal membrane include small molecule transporters like cystinosin and sialin (Eskelinen, Tanaka et al. 2003) (Figure 1.1).

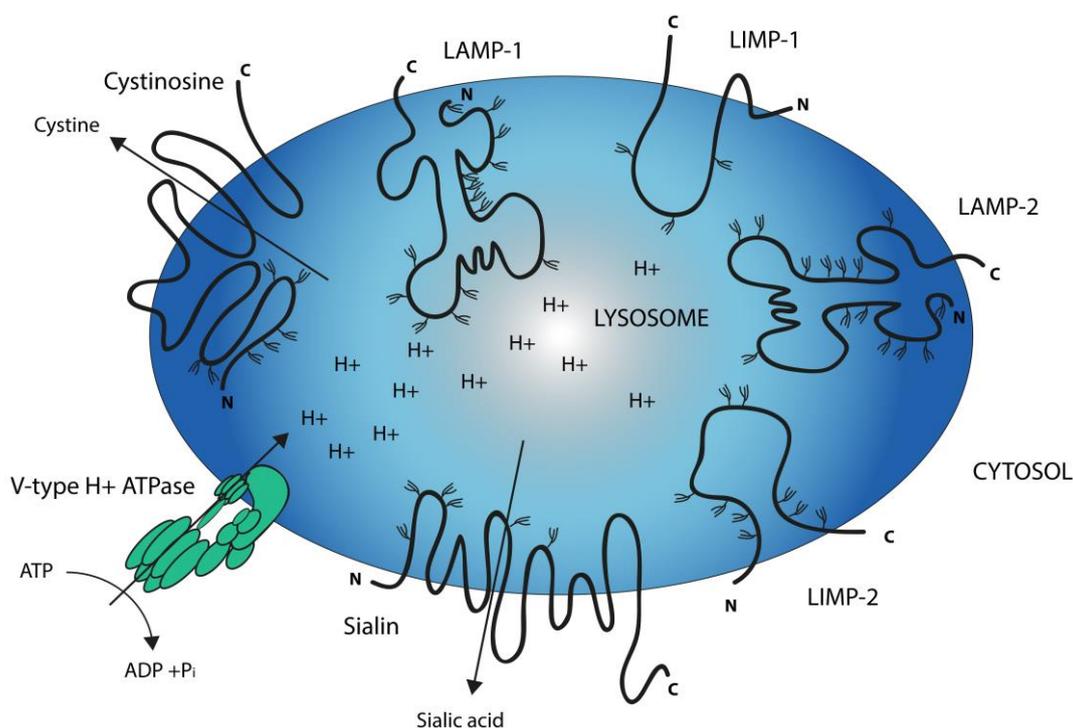


**Figure 1.1: Overview of major lysosomal membrane proteins.**

The lysosomal membrane consists of numerous proteins fulfilling multiple functions like transport across the membrane (sialin and cystinosin), acidification (v-type  $H^+$ -ATPase) and lysosomal transport (LIMP-2) as well as membrane stability (LIMP-1/2, LAMP-1/2). Putative N-glycosylation sites are indicated by black branch-like structures. The illustration was adapted from Eskelinen, Tanaka *et al.* 2003.

### 1.1.2 Trafficking of soluble lysosomal enzymes

Lysosomal enzymes reach the lysosome via the secretory pathway. They are synthesised with an N-terminal signal peptide translocating the proteins into the ER, where the signal sequence is cleaved off. In the ER the proteins get N-glycosylated, which typically involves the binding of an oligosaccharide composed of N-acetylglucosamine, mannose and glucose to an asparagine residue (Kornfeld and Kornfeld 1985). The oligosaccharides undergo further modifications before entering the Golgi apparatus, where the mannose-6-phosphate

recognition marker is added to target most enzymes to the lysosome (see below 1.1.2.1). Additionally M6P-independent lysosomal transport mechanisms have been described (see 1.1.2.2).

In comparison lysosomal membrane proteins are transported to their target organelle by cytoplasmic signal domains (tyrosin or di-leucin). After synthesis in the ER and transport via the Trans-Golgi-Network (TGN), small adaptor proteins binding to the signal domains and accessorise the packaging of the membrane proteins into clathrin-coated vesicles. By vesicular transport, the lysosomal membrane proteins reach the endosomal compartment (Bonifacino and Traub 2003, Braulke and Bonifacino 2009). It has been shown that some lysosomal membrane proteins can escape the lysosomal targeting pathway and get transported to the plasma membrane, where they reach the lysosome by endocytosis (Janvier and Bonifacino 2005).

#### **1.1.2.1 Mannose-6-phosphate receptor dependent transport**

Most enzymes destined for the lysosome are marked with mannose-6-phosphate residues in the Golgi apparatus. Two enzymes are involved in this process and act sequentially (Lazzarino and Gabel 1988): In the first step a GlcNac-1-phosphate is added by N-acetylglucosamine-1-phosphotransferase (GlcNac-1PT) (Ketcham and Kornfeld 1992). The phosphotransferase is composed of three subunits ( $\alpha_2\beta_2\gamma_2$ ) and is encoded by two genes: *GNPTAB* and *GNPTG* (Tiede, Storch et al. 2005). In the second step, N-acetylglucosamine residues are removed by the N-actelyglucosamine-1-phosphodiester  $\alpha$ -N-acetyl glucosamininidase, also known as uncovering enzyme (USE) exposing the M6P recognition marker (Kornfeld, Bao et al. 1999). Subsequent binding of the M6P residue to the M6P-receptors takes place in the TGN and leads to an exit of the receptor-ligand complex in clathrin-coated vesicles, fusing with early endosomes, which further mature to late endosomes. Due to the continuously decreasing pH, receptor and ligand dissociate and MPRs get recycled back to the TGN, with MPRs not found in mature lysosomes (Braulke and Bonifacino 2009) (Figure 1.3).

In mammalian cells two different MPRs have been described; the 46 kDa cation-dependent MPR (CD-MPR, MPR46) and the 300 kDa cation-independent MPR (CI-MPR, MPR300) (Ghosh, Dahms et al. 2003). Both receptors are type-1 glycoproteins but differ in their expression patterns, subcellular localisation and ligand binding properties (Figure 1.2) (Braulke and Bonifacino 2009). For instance only MPR300 is involved in endocytosis of M6P-marked proteins and is also able to bind other ligands lacking glycosylation, like the insulin-like growth factor II (IGF-II) (Braulke 1999).

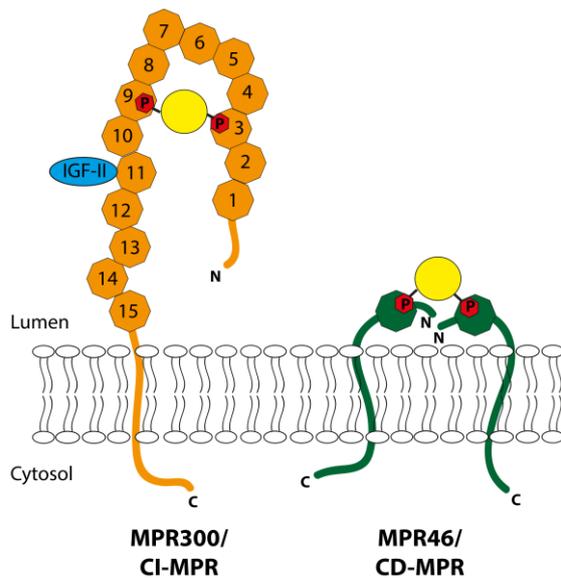


**Figure 1.2: Structure of the two mannose-6-phosphate-receptors (MPR300 and MPR46).**

The cation-independent (CI)-mannose-6-phosphate receptor (MPR300/CI-MPR) is a type I transmembrane glycoprotein with two M6P-binding sites in segment 3 and 9 and a binding domain for IGF-II in segment 11. The cation-dependent (CD)-mannose-6-phosphate receptor (MPR46/CD-MPR) forms a dimer before binding phosphorylated proteins (yellow circle). The picture was adapted from Braulke and Bonifacio 2009.

### 1.1.2.2 Mannose-6-phosphate receptor independent transport

Some lysosomal proteins can be targeted to the lysosome in an M6P receptor independent manner. Such observations could be made in tissues of Inclusion-cell (I-cell) disease patients, who suffer from a complete absence of M6P residues added to lysosomal hydrolases due to a defective phosphotransferase (GlcNac-1PT) (Tsuji, Omura et al. 1988, Rijnboutt, Aerts et al. 1991, Rijnboutt, Kal et al. 1991). Also in an MPR-deficient mouse model it could be shown that some soluble enzymes are able to reach the lysosome via other transport receptors than MPRs in a cell and tissue-specific manner (Dittmer, Ulbrich et al. 1999). An example for such a transporter is the type 1 transmembrane protein sortilin, which has been shown to facilitate lysosomal trafficking of different ligands including, prosaposin, acid sphingomyelinase and potentially cathepsin H (Petersen, Nielsen et al. 1997, Mazella, Zsuzger et al. 1998, Nielsen, Jacobsen et al. 1999, Lefrancois, Zeng et al. 2003, Canuel, Korkidakis et al. 2008, Markmann, Thelen et al. 2015).

Furthermore the soluble hydrolase  $\beta$ -glucocerebrosidase (GC) has been described to be trafficked to the lysosomes in an M6PR-independent manner. In 2007 the lysosomal membrane protein LIMP-2 was revealed as the specific trafficking receptor of GC (Griffiths 2007, Reczek, Schwake et al. 2007). LIMP-2 associates with GC in the ER and travels to the endosomal/lysosomal compartment by traversing the Golgi apparatus. Finally, GC dissociates from LIMP-2 in lysosomes due to a reduction in the pH (Zachos, Blanz et al. 2012).

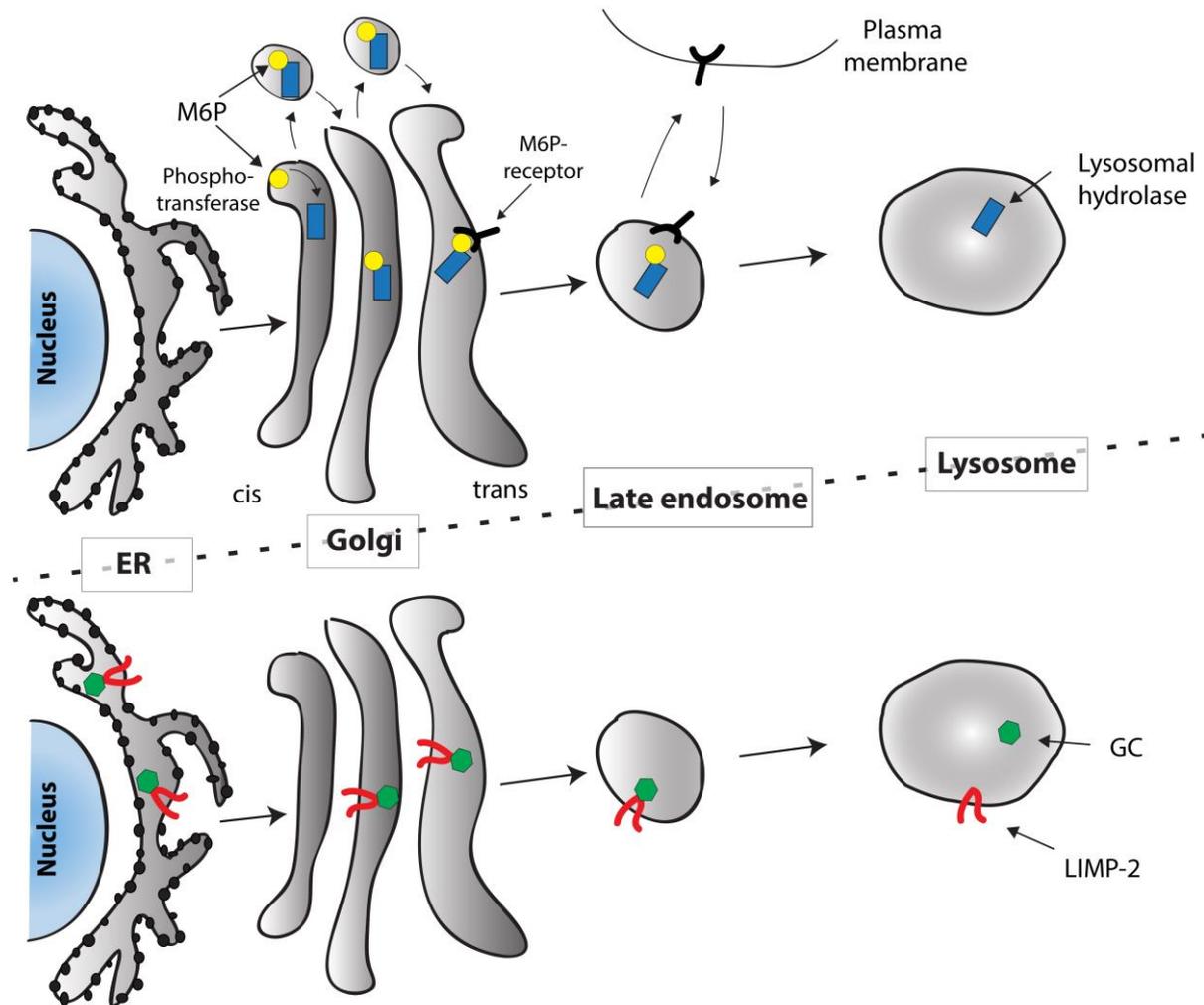


**Figure 1.3: Transport routes to the lysosome: Mannose-6-phosphate dependent and independent.**

On the top panel the mannose-6-phosphate (M6P)-dependent trafficking is shown. In the cis-Golgi the lysosomal hydrolase obtains a M6P-tag transferred by a phosphotransferase. In the trans-Golgi the M6P-receptor binds to the M6P-tag mediating further transport. The receptor and ligand dissociate in late endosomes due to a low pH. In comparison the bottom panel shows the cellular transport of lysosomal hydrolase  $\beta$ -glucocerebrosidase (GC). The hydrolase is transported to the lysosomes in a M6P-independent manner by binding to its transport receptor LIMP-2 early in the ER. After reaching the lysosome, the hydrolase dissociates from the receptor due to the acidic pH.

### 1.1.3 Lysosomal storage diseases

Lysosomal enzymes as well as the lysosomal membrane proteins are important for proper lysosomal function including degradation of various molecules in the cell. In lysosomal storage diseases (LSD) mislocalisation or dysfunction of lysosomal enzymes or other proteins involved in lysosomal integrity or biogenesis result in lysosomal accumulation of the respective substrates (Platt, Boland et al. 2012). The incidence of LSDs has been estimated to 1:5,000 live births (Fuller, Meikle et al. 2006). LSDs comprise a group of around 50 genetic diseases that are primarily classified by their accumulating substrate:

- Lipid storage disorders: including sphingolipidoses (e.g. Gaucher disease) and gangliosidoses (e.g. Tay-Sach's disease)
- Mucopolysaccharidoses
- Glycoproteinoses
- Mucolipidoses

The symptoms of the LSDs vary depending on the accumulating substrate and other factors like age of onset. The clinical presentation of the disease ranges from mild to severe and can include movement disorders, bone abnormalities, organomegaly (spleen and liver), seizures, dementia and deafness (Gieselmann 1995, Fuller, Meikle et al. 2006).

### **1.1.3.1 Lipid storage diseases: Sphingolipidoses and cholesterol transport deficiencies**

#### ***1.1.3.1.1 Sphingolipids and sphingolipidoses***

Sphingolipids are essential components of the plasma membrane and play important roles in signalling processes (Hla and Dannenberg 2012). They can be distinguished in three main groups: ceramides, sphingomyeline and glycosphingolipids. The latter category can be further divided in to cerebroside and gangliosides. Gangliosides differ from cerebroside in containing a sialic acid. Sphingolipids are synthesised in the ER and Golgi apparatus and reach the plasma membrane by vesicular transport. For degradation in the lysosome they are endocytosed in a caveolin- or clathrin-dependent manner (Sillence and Platt 2004). Thereby, any deficiency in the degradation pathway (e.g. in the responsible hydrolase) leads to a buildup of the substrate and subsequently to a pathological manifestation referred to as glycosphingolipidosis (Figure 1.4). Since glycosphingolipids are found in high concentrations in neurons, glycosphingolipidoses often present with neurological symptoms (Yu, Nakatani et al. 2009). Moreover a number of auxiliary proteins are important for proper enzyme function. For example a dysfunction in any of the described sphingolipid activator proteins (saposin A-D) leads to impairments in the lysosomal sphingolipid degradation pathway (Vielhaber, Hurwitz et al. 1996).

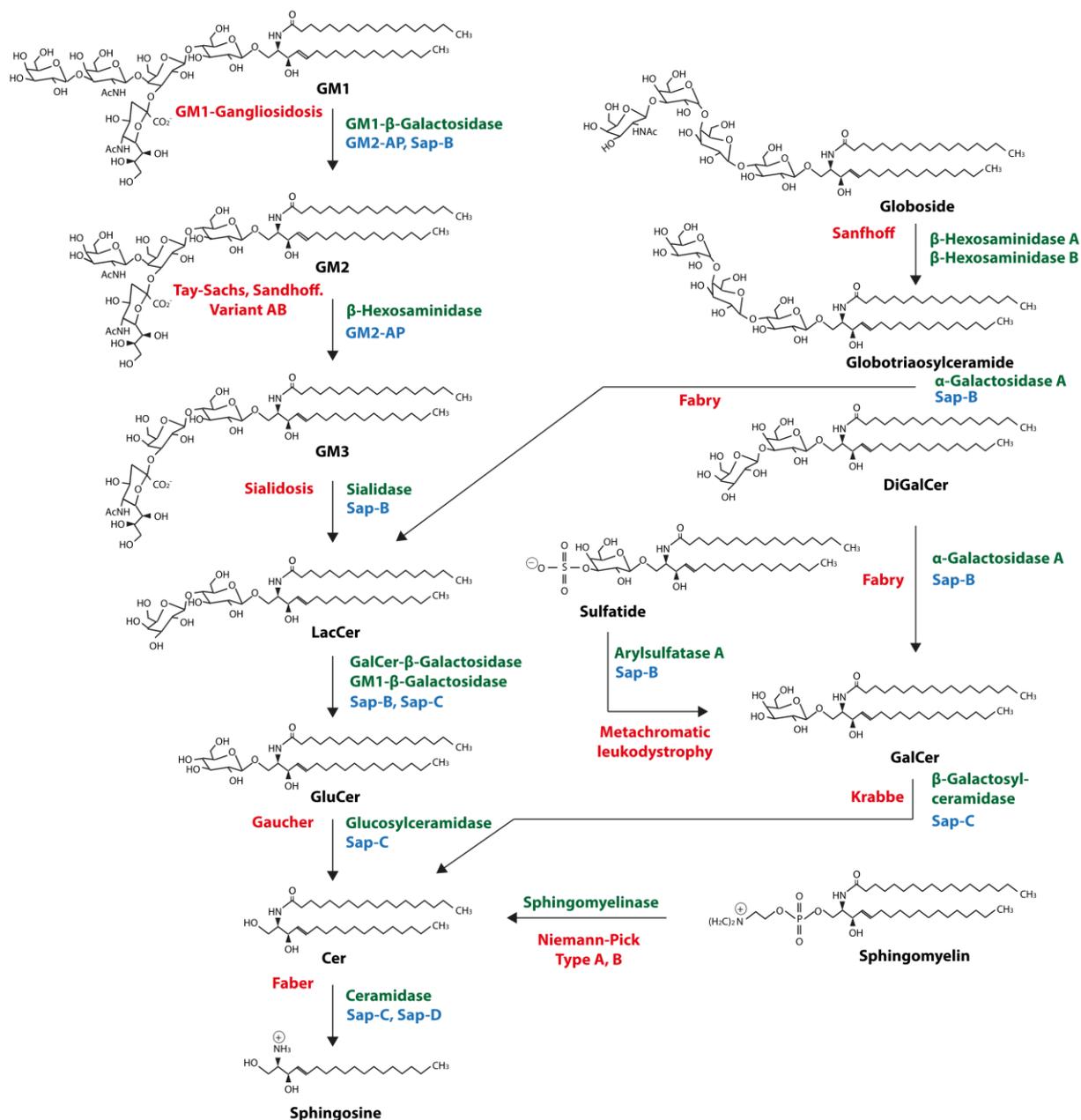


**Figure 1.4: Overview of sphingolipid degradation and sphingolipidoses.**

Single steps of sphingolipid degradation with respective molecular structures (LacCer: lactosylceramide; Cer: ceramide; DiGalCer: digalactosylceramide; GalCer: galactosylceramide). Responsible converting lysosomal enzymes are indicated in green and activator proteins/cofactors required for degradation are shown in blue (GM2-AP: GM2 activator protein; Sap-B/C: saposin B/C). Disease names associated with the accumulation of the respective sphingolipid are indicated in red. The graphic was adapted from Schulze and Sandhoff 2014.

### 1.1.3.1.2 Lysosomal accumulation of cholesterol: Niemann-Pick Type C (NPC-1)

Cholesterol is an essential component of the plasma membrane. Approximately 95% of the total cholesterol is bound to membranes (Spohn and Davison 1972, Chakravarthy, Spence et al. 1985). Cholesterol is also an important precursor for steroid hormones, vitamin D and bile acid. For transport purposes through the blood the highly lipophilic molecule is bound to low

density or high density lipoproteins (LDL and HDL). In humans most of the existing cholesterol is when required synthesised in the body and only small amounts are taken up by intestinal absorption (Ikonen 2006). Cholesterol levels in the body are tightly regulated by diverse control and negative feedback mechanisms in the cells. Here the endocytotic pathway plays a central role: After cellular uptake of the lipoprotein cholesterol via receptor-mediated endocytosis (e.g. by LDL-receptors), it reaches the endocytotic circuits where it gets processed and redistributed to the plasma membrane, Golgi compartments and ER (Brown and Goldstein 1986). Furthermore the recycled cholesterol functions as a regulator for cellular cholesterol uptake, cholesterol synthesis and *de novo* synthesis of the LDL receptor (Ikonen 2008). In endosomes the esterified cholesterol gets hydrolysed by the acid lipase (cholesterol esterase) to fatty acid and free (unesterified) cholesterol (Brown and Goldstein 1986). The export of the cholesterol out of the late endosomes/lysosomes has been suggested to be mediated by a direct interaction of the endosomal membrane with the membranes of the ER or peroxisomes (Chang, Chang et al. 2006, Chu, Liao et al. 2015). However, the molecular mechanisms of endosomal cholesterol export are not well understood.

Lipids reach the endosomal/lysosomal compartments either as part of the limiting membrane or incorporated in the intraendosomal membrane. By inward budding of the endosomal membrane multivesicular bodies (intraendosomal vesicles) are formed (Figure 1.5). Further metabolising of the lysosomal cholesterol is mediated by two indispensable proteins: Niemann-Pick C1 and C2 (NPC1 and NPC2). NPC2 is a soluble protein and removes cholesterol from the intraendosomal/-lysosomal vesicles and delivers it to the membrane-resident NPC1 protein. NPC1, which spans the membrane 13 times, is suspected to facilitate the transport of free cholesterol across the endosomal membrane (Figure 1.5). Mutations in each of the cholesterol-binding proteins causes Niemann-Pick disease type C (NPC), which is characterised by an accumulation of unesterified cholesterol in late endosomes (Patterson, Vanier et al. 2001). Other lipids like sphingosines (Rodriguez-Lafrasse, Rousson et al. 1994), sphingomyeline and gangliosides GM3 and GM2 (Zervas, Dobrenis et al. 2001) accumulate secondary to the storage of cholesterol.

In addition to NPC1 other lysosomal membrane proteins like LAMP-2 have been reported to be involved in the endosomal cholesterol export (Eskelinen, Schmidt et al. 2004, Schneede, Schmidt et al. 2011).

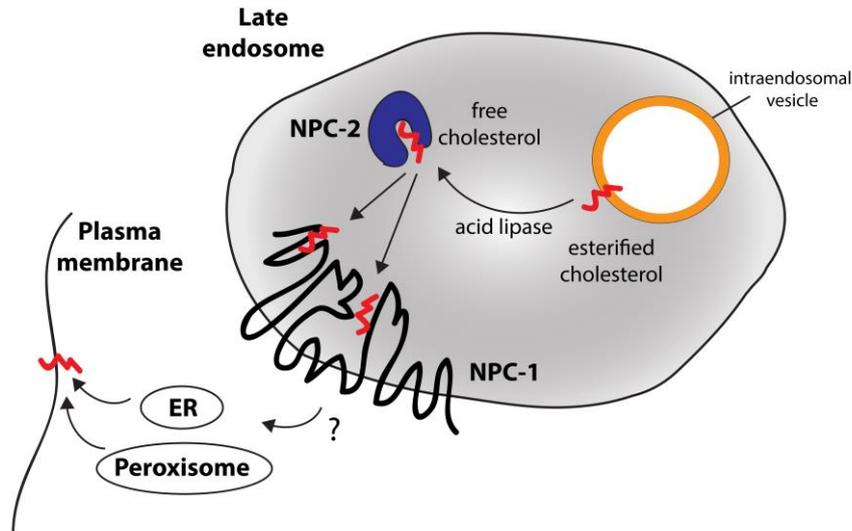


**Figure 1.5: Cholesterol transport in late endosomes: the role of NPC1 and 2.**

Cholesterol can reach the endosomal lumen by inward budding of the endosomal membrane forming intraendosomal vesicles. Within late endosomes/lysosomes the esterified cholesterol gets hydrolysed by acid lipases to free cholesterol. The soluble NPC2 protein transports free cholesterol within the late endosome to the transmembrane protein NPC1. NPC1 transports cholesterol across the endosomal membrane. The mechanisms of cholesterol export out of late endosomes are still poorly understood. Cholesterol also gets delivered back to the plasma membrane most likely by a transport via the ER or peroxisome. The graphic was adapted from Schulze und Sandhoff 2011.

#### ***1.1.3.1.3 Membrane transport of fatty acids and cholesterol***

In general, lipids can passively diffuse through cell membranes due to their hydrophobic nature. However, specific protein-facilitated transport systems of lipids across the membrane exist as well. For example for fatty acids a passive diffusion through the membrane as well as an active transport by membrane-bound proteins has been described (Abumrad, Harmon et al. 1998, McArthur, Atshaves et al. 1999). A transporter of fatty acids is CD36. It belongs to the class B scavenger receptor family, which also includes the scavenger receptor B1 (SR-B1) and lysosomal integral membrane protein type-2 (LIMP-2) (Calvo, Dopazo et al. 1995). CD36 was first identified on platelets, where it was initially described to function as a collagen and thrombospondin receptor (Greenwalt, Lipsky et al. 1992). To date there is strong evidence that CD36 additionally supports the uptake of oxidised lipoproteins (oxLDLs) and fatty acid (Abumrad, Harmon et al. 1998). Furthermore, patients suffering from deficiency of CD36 are associated with an increased risk of suffering from atherosclerotic cardiovascular diseases (Yuasa-Kawase, Masuda et al. 2012). Affected individuals reveal a defective uptake of fatty acids emphasising the important role of CD36 in fatty acid uptake (Nakata, Nakahara et al. 1999, Nozaki, Tanaka et al. 1999).

Recently, the scavenger receptor class B, type I (SR-BI) was identified as cell-surface high-density lipoprotein (HDL) receptor. Thereby, SR-BI selectively mediates the uptake of cholesteryl esters into the cell (Rigotti, Miettinen et al. 2003). Additionally, SR-BI has been shown to facilitate the bidirectional flux of unesterified (free) cholesterol between cells (de la Llera-Moya, Rothblat et al. 1999).

## 1.2 The lysosomal integral membrane protein Type-2 (LIMP-2)

The lysosomal integral membrane protein (LIMP-2/SCARB-2/LGP85) is one of the most abundant proteins of the lysosomal membrane. It is proposed to be required for lysosomal maintenance and biogenesis (Kuronita, Eskelinen et al. 2002, Kuronita, Hatano et al. 2005). LIMP-2 is the receptor for the mannose-6-phosphate (M6P) independent transport of  $\beta$ -glucocerebrosidase (GC), a lysosomal sphingolipidase, from the ER to the lysosome (Reczek, Schwake et al. 2007). LIMP-2 has been described as a receptor for enterovirus 71, the causative pathogen of hand, food and mouth disease (Yamayoshi, Yamashita et al. 2009). Lysosomal transport of LIMP-2 is facilitated by a c-terminal dileucine motif ([DE]XXXL[LI]). It is thought that LIMP-2 is transported by clathrin coated vesicles mediated by an interaction with the adaptor protein complexes AP-1 and AP-3 (Janvier, Kato et al. 2003). By binding of the dileucine motif to AP-1, clathrin-mediated endosomal transport from the trans-Golgi network is associated. By interacting with another adaptor protein complex (AP-3) trafficking of proteins from endosomes to lysosomes is initiated (Honing, Sandoval et al. 1998, Braulke and Bonifacino 2009).

Despite the knowledge of the dependence of GC on LIMP-2, only very little is known about the molecular details of their interaction. Moreover the precise role of LIMP-2 in disease development and additional functions of this abundant lysosomal membrane protein is still poorly understood.

### 1.2.1 Protein structure of LIMP-2

LIMP-2 consists of 478 amino acids representing a total protein size of 85 kDa (glycosylated form). It spans the membrane twice with the large luminal domain exhibiting eleven potential glycosylation sites (Fujita, Ezaki et al. 1991, Neculai, Schwake et al. 2013). Recently, the crystal structure of the ectodomain of LIMP-2 was determined (Neculai, Schwake et al. 2013) (PDB: 4F7B). A helix ( $\alpha 5$ ), which has been predicted to be involved in interaction with GC (Blanz, Groth et al. 2010), could be identified as being exposed at the apical side of the protein, supporting its potential role in GC binding (Figure 1.6).

Surprisingly, the crystal structure revealed a cavity reaching through the entire luminal domain of the LIMP-2 protein (Figure 1.6). The potential function or substrates of this putative channel have not been described yet. As described above, two other family members of the scavenger receptor family (CD36 and SR-BI) are known for binding and transporting lipid proteins, playing an essential role in the lipid metabolism and cholesterol transport (Gu, Trigatti et al. 1998, Rodriguez, Thuahnai et al. 1999, Liu and Krieger 2002, Rigotti, Miettinen et al. 2003, Neculai, Schwake et al. 2013).

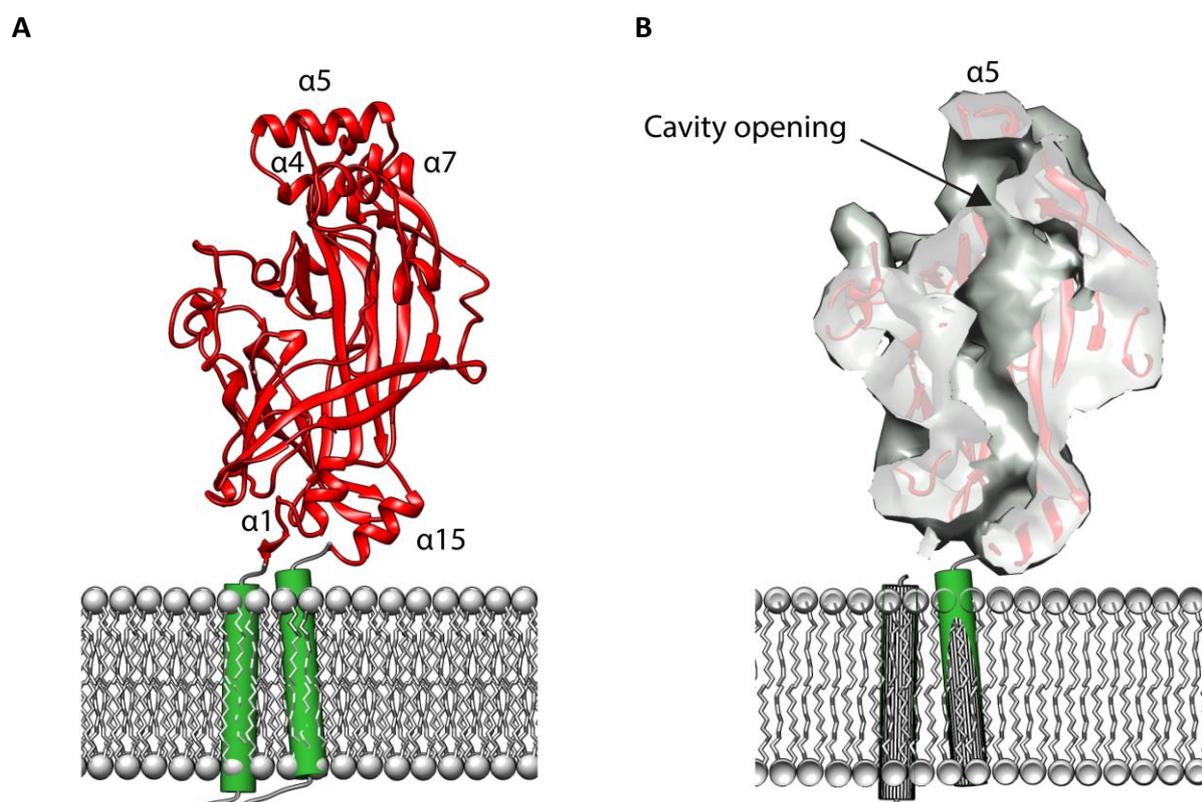


**Figure 1.6: Protein model of the human LIMP-2 with the protein cavity indicated.**

**A)** Structural illustration of the luminal domain of LIMP-2 protein solved by x-ray crystallography. The transmembrane domains (green) as well as the membrane do not belong to the initial crystal complex and were added subsequently to the model. The exposed helix 5 ( $\alpha$  5) has been proposed to be important for ligand binding. **B)** A cross section of LIMP-2 indicates the opening of a cavity, which traverses the whole protein. The structural illustration was performed with UCSF Chimera (PDB: 4F7B) (Neculai, Schwake et al. 2013).

The crystal structure of LIMP-2 was also solved in an independent study revealing a mannose-6-phosphate residue at the N325 glycosylation site (Zhao, Ren et al. 2014). This led the authors to speculate about an M6P-dependent transport of the lysosomal membrane protein and thus GC to the lysosome. The similarities and discrepancies between the two different solved crystal structures of LIMP-2 (Neculai, Schwake et al. 2013, Zhao, Ren et al. 2014) are depicted in an overlay of both protein structures (Figure 1.7). Obvious and of

functional importance are the differences in the carbohydrate chain at position N325, which exhibits the mentioned M6P residue (P-Man9GlcNac2).

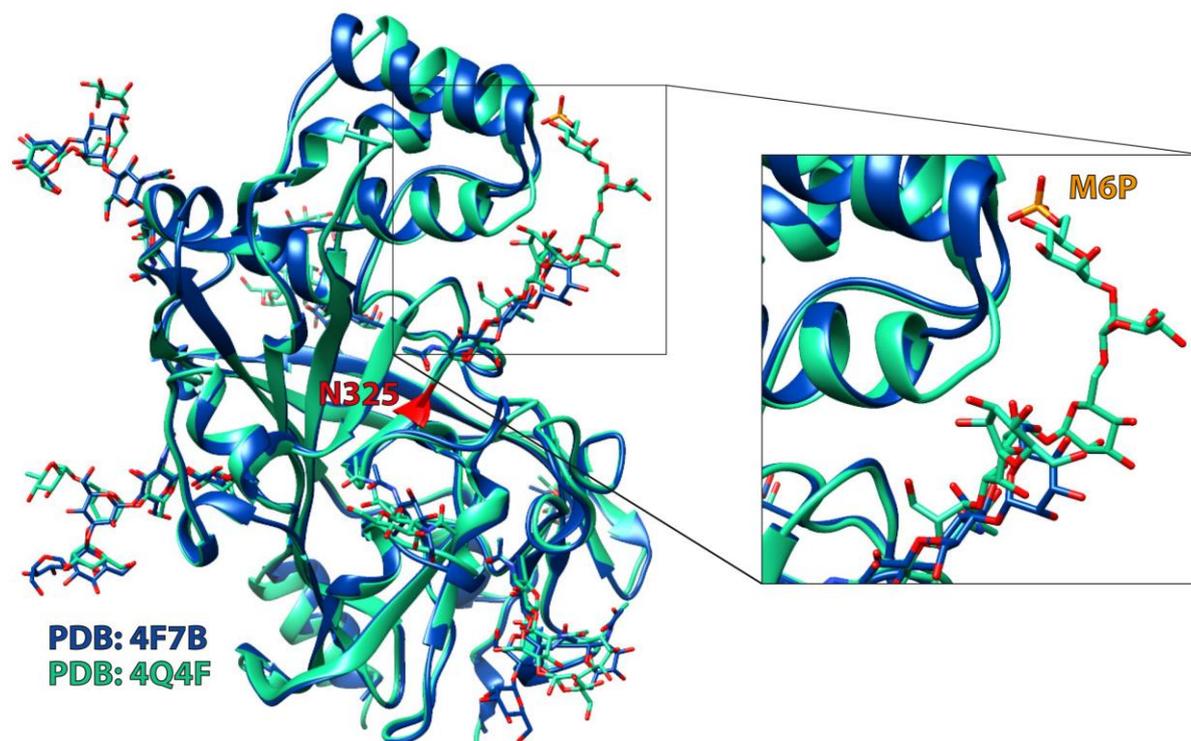


**Figure 1.7: Comparison of two different LIMP-2 crystal structures.**

Blue protein model: Crystal structure of LIMP-2 with a resolution of 3.0 Å in space group  $P2_1$  (PDB: 4F7B; (Neculai, Schwake et al. 2013)). Green model: LIMP-2 crystal structure solved by Zhao, Ren et al. 2014 (PDB: 4Q4F) shows a slightly better resolution of 2.8 Å. Mannose-6-phosphate (M6P) residue at the end of sugar chain emerging from N325 is marked in orange. An overlay of both crystal structures exhibits the similarities of both models, but also the differences, which are predominately in the orientation and length of the glycosylation chains. The structural illustration was performed with UCSF Chimera.

### 1.2.2 LIMP-2 associated diseases

Mutations in the *SCARB2* gene encoding for the LIMP-2 protein have been described to cause a severe autosomal-recessive disorder known as Action-Myoclonus Renal Failure Syndrome (AMRF; OMIM#254900) (Balreira, Gaspar et al. 2008, Berkovic, Dibbens et al. 2008). Patients present a rare form of progressive myoclonic epilepsy (PME) associated with storage material in the brain, renal failure, deafness, a demyelinating peripheral neuropathy and premature death (Berkovic, Dibbens et al. 2008, Hopfner, Schormair et al. 2011). To date, ten disease causing LIMP-2 mutations have been described. Nine of the ten *SCARB2* mutations have been shown to lead to a truncation of the protein, potentially resulting in an impaired ER-exit and incapability of transporting GC to lysosomes (Blanz, Groth et al. 2010, Zachos, Blanz et al. 2012). So far only one missense mutation has been described (H363N)

(Berkovic, Dibbens et al. 2008, Dardis, Filocamo et al. 2009, Dibbens, Michelucci et al. 2009, Dibbens, Karakis et al. 2011).

### 1.2.3 LIMP-2-deficient mice

The LIMP-2 knockout mouse was first established and described in the year 2003 by Gamp and co-workers. The initial phenotypical observations included deafness, peripheral demyelination and hydronephrosis caused by pelvic junction obstruction (Gamp, Tanaka et al. 2003). These mice further revealed ataxia and slight hyperactivity accompanied by an unidentified storage material in the brain (Berkovic, Dibbens et al. 2008). A recent study focused on the consequences of LIMP-2 deficiency on the central nervous system (CNS) and discovered additional neurological deficits accompanied by a premature death in mice lacking LIMP-2 (Rothaug, Zunke et al. 2014). The phenotype of the animal included progressive hind-limb claspings starting from three to five months, which is a general indicator of a dysfunction of the CNS (Rothaug, Zunke et al. 2014). Moreover, LIMP-2 knockout animals presented progressive kyphosis and ataxia, which has been previously reported by Gamp *et al.*

## 1.3 The lysosomal hydrolase $\beta$ -Glucocerebrosidase (GC)

The lysosomal enzyme  $\beta$ -glucocerebrosidase (GC) is the responsible hydrolase for the degradation of the sphingolipid glucosylceramide (GluCer) to ceramide and glucose and is encoded by the Glucosidase Beta 1 (*GBA1*) gene. The *GBA2* gene decodes for the non-lysosomal form of the  $\beta$ -glucocerebrosidase (Matern, Boermans et al. 2001). It has been described to be membrane-associated in the ER and Golgi compartment (Korschen, Yildiz et al. 2013).

The mature human GC protein is composed of 497 amino acids, derived from a precursor protein of 517-536 amino acids (Erickson, Ginns et al. 1985). For maximal enzyme activity the enzyme needs saposin C (SapC) and negatively charged lipids (Grabowski, Gatt et al. 1990). In particular the prosaposin-derived SapC is believed to assist GC to access the short glucosyl-headgroup of its substrate glucosylceramide by remodeling the lipid membrane (Alattia, Shaw et al. 2006, Alattia, Shaw et al. 2007).

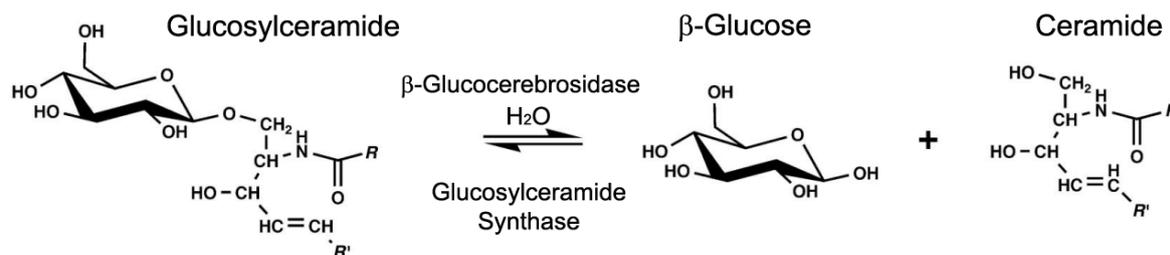


**Figure 1.8: Enzymatic reaction catalysed by  $\beta$ -glucocerebrosidase.**

Glucosylceramide is hydrolysed by the enzymatic activity of the lysosomal  $\beta$ -glucocerebrosidase resulting in  $\beta$ -glucose and ceramide. The reverse reaction is mediated by the glucosylceramide synthase located in the cis-Golgi. A  $\beta$ -glucose is added to a ceramide in a condensation reaction (adapted from Brumshtein *et. al*, 2006).

### 1.3.1 Protein structure of GC

The GC protein is divided into three main domains: domain I (residues 1-27 and 383-414) consists mainly of  $\beta$ -sheets and has been suspected to be important for proper protein folding (Beutler & Grabowski, 2001). The glycosylation on N19 seems essential for enzyme activity *in vivo* (Berg-Fussman, Grace et al. 1993). Domain II (residues 30-75 and 431-497) resembles an immunoglobulin fold with –so far unknown function (Orengo, Michie et al. 1997). The third domain (residue 76-381 and 416-430) is the largest of all three domains and exhibits a  $(\beta/\alpha)_8$  TIM barrel structure containing the catalytic site (Dvir, Harel et al. 2003) (Figure 1.9). The amino acids Glu 235 and Glu 340 are involved in catalysis. Thereby the Glu 340 functions as the nucleophile, whereas Glu 235 acts as the general acid-base residue (Miao, McCarter et al. 1994, Lieberman 2011). The enzyme shows five potential N-glycosylation sites, of which four are believed to be occupied (N19, N59, N146 and N270) (Erickson, Ginns et al. 1985).

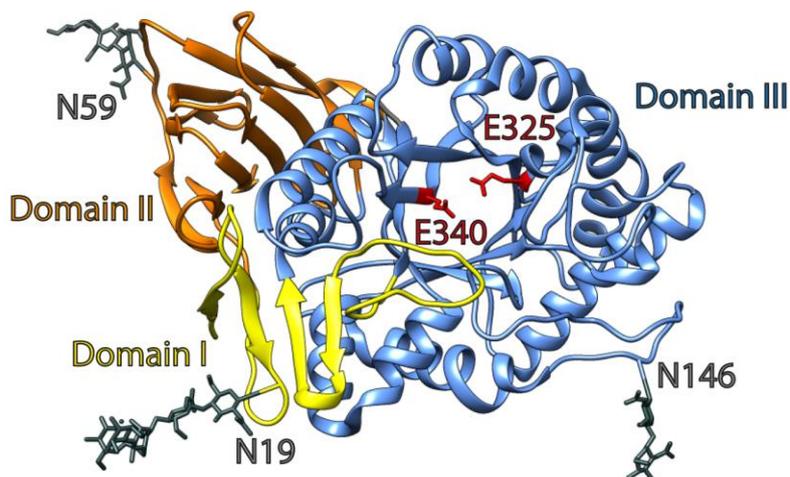


**Figure 1.9: Protein structure of GC subdivided in three domains.**

Structural illustration of glycosylated recombinant GC protein (Cerezyme®) performed utilising UCSF Chimera (PDB: 2J25). The protein can be divided in three domains: domain I (yellow), domain II (orange) and domain III (blue), which includes the active site harbouring the important catalytic amino acids E325 and E340 (shown in red). Furthermore, glycosylation chains linked to N19, N59 and N146 are shown in grey.

The first crystal structure of unglycosylated recombinant GC (Cerezyme®) was published in 2003 (Dvir, Harel et al. 2003). Today 25 different crystal structures of  $\beta$ -glucocerebrosidase exist, varying in the way they were crystallised (incubation and crystallisation conditions). In general differences in the protein structures are minor. In the year 2006 recombinant GC could be crystallised without any deglycosylation treatment (Brumshtein, Wormald et al. 2006). As shown in figure 1.9, the glycosylated form of Cerezyme® exhibits sugar residues on residue N19, N59 and N146. No sugar residues were found on N270 probably due to tight crystal-packing (Brumshtein, Wormald et al. 2006, Lieberman 2011).

### 1.3.2 GC-associated diseases

Almost 300 mutations and polymorphisms have been described in the *GBA1* gene. These mutations are spread over the whole mature GC protein (Dvir, Harel et al. 2003, Hruska, LaMarca et al. 2008) (Figure 1.10). The scattered distribution of mutations underlines the complexity of the enzyme and emphasises the importance of the integrity of the whole protein for proper protein function. A defective function of GC causes the most common lysosomal storage disease ‘Gaucher disease’, which belongs to the class of sphingolipidoses (see chapter 1.1.3.1.1). Gaucher disease is characterized by an accumulation of glucosylceramide (GluCer) (Brady, Kanfer et al. 1966). Most affected by this pathogenic storage are macrophages, forming the so called ‘Gaucher cells’, implicating clinical presentations like organomegaly (e.g. hepato- and splenomegaly) and problems in blood cell as well as bone development. Besides glucosylceramide also the concentration of glucosylsphingosine, another substrate of GluCer, which is known to be neurotoxic (Schueler, Kolter et al. 2003), has been found to be increased in Gaucher patient brain (Nilsson and Svennerholm 1982).

Gaucher disease occurs in a frequency of 1:40,000 – 60,000 in the general population and in a higher frequency in the Ashkenazi Jewish population (1:1000) (Horowitz and Zimran 1994). In general there are three major phenotypes of the disease: type I presents a mild, non-neuronopathic form (OMIM #230800), whereas type II (OMIM #230900) and type III (OMIM #231000) show the involvement of the central nervous system (CNS) including the development of myoclonic epilepsy, seizures and dementia. The clinical presentation of the disease is highly variable between patients –even in twins, sharing the same genotype– indicating that other genetic or environmental factors contribute to the course of disease. Mutations in the LIMP-2 protein have been assumed to act as modifiers in Gaucher disease (Velayati, DePaolo et al. 2011).

Interestingly, mutations in GC represent also the highest genetic risk factor for the development of Parkinson disease (PD) caused by accumulation of  $\alpha$ -synuclein (Westbroek, Gustafson et al. 2011) (see chapter 1.4.3).

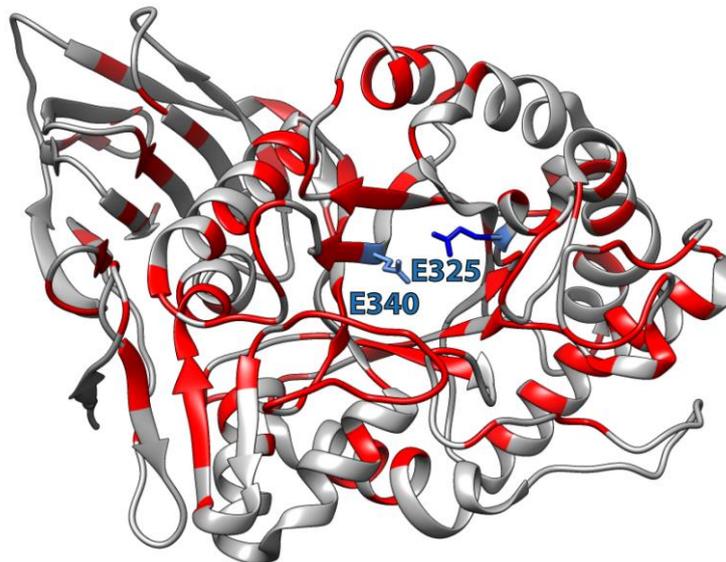


**Figure 1.10: Overview of pathological mutations in the GC protein.**

Protein structure of GC with known missense and nonsense mutations (indicated in red). The disease-causing mutations are spread over the whole protein, with the majority found around the catalytic center with the amino acids E325 and E340. The structural illustration was performed utilising UCSF Chimera (PDB: 2J25).

### 1.3.2.1 Treatment of GC-associated diseases

A number of therapeutic strategies are applied in lysosomal storage diseases -all with the same main goal- to reduce the accumulating substrate. This can be reached by either increasing the activity of the respective enzyme or by the decreasing the level of the substrate of the defective enzyme. The enzyme replacement therapy (ERT) is the first choice for treatment in many lysosomal storage diseases –as described for Gaucher disease (Brady 2006, Rohrbach and Clarke 2007). In Gaucher disease, purified enzyme (GC; Cerezym ®) is administered to the patients by intravenous infusion. Since the exogenous enzyme is not able to cross the blood-brain barrier, ERT is able to improve manifestations of type I Gaucher patients only (Weinreb, Charrow et al. 2002).

The substrate reduction therapy (SRT) represents an alternative way of using small molecules in treating LSD. For this approach a drug is designed to inhibit the biosynthesis of the initial glycosphingolipid (GSL), glucosylceramide. The imino sugar N-butyldeoxynojirimycin (NB-DNJ, miglustat) binds the glucosylceramide synthase (Platt, Neises et al. 1994). Therefore, any residual enzyme activity can better cope with the lower amount of substrate, which needs to be hydrolysed. Miglustat has been shown to be effective in Gaucher disease patients (Cox,

Lachmann et al. 2000, Elstein, Hollak et al. 2004). However SRT is most likely not be the best way to target glucosylceramide storage, since the sphingolipid has been shown to be involved in a range of biological processes like cell differentiation, apoptosis, cell growth as well as neuronal development (Buccoliero, Bodennec et al. 2002).

Next to the ERT and SRT, stabilisation of the affected enzymes is a promising strategy to enhance enzymatic activity either by promoting the protein folding and lysosomal transport or by direct stabilisation of the active site. Several small molecules have been identified to serve as ‘molecular chaperones’. For example isofagomine and miglustat act as competitive inhibitors for the GC protein, augmenting enzyme stability and activity simultaneously (Alfonso, Pampin et al. 2005, Kornhaber, Tropak et al. 2008, Shen, Edwards et al. 2008).

## **1.4 Lysosomal dysfunction and neurodegenerative diseases**

There is increasing evidence for a role of the lysosome as the main digestive and recycling organelle of the cell to contribute to age-related neurodegenerative diseases, such as Alzheimer Disease, Huntington Disease and Parkinson disease.

An efficient degradation of metabolic substrates (e.g. proteins, lipids, carbohydrates, etc.) is essential for neuronal survival, since neurons are particularly sensitive to alterations in the lysosomal degradation pathway. It could be shown that abnormal protein accumulation lead to intraneuronal inclusions and subsequently to neuronal cell death (Hara, Nakamura et al. 2006, Komatsu, Waguri et al. 2006). Also, in postmortem brain from PD patients an impairment of lysosomal activity, including a reduced number of intraneuronal lysosomes, decreased levels of lysosomal-associated proteins and aggregations of autophagosomes have been observed (Chu, Dodiya et al. 2009, Dehay, Bove et al. 2010).

### **1.4.1 Parkinson Disease**

Parkinson disease is a slowly progressive neurodegenerative disorder, that is most common in the elderly population affecting about two percent of adults above the age of 65 and with a prevalence of one in 300 in the general population (Schapira, Bezdard et al. 2006). The early causes of PD are characterized by movement abnormalities including tremor, bradykinesia and rigidity. In later stages also non-motor symptoms may arise including dementia, behavioral problems and depression (Chaudhuri, Healy et al. 2006). Clinical manifestations result from the loss of dopaminergic neurons in the substantia nigra, which is a part of the midbrain (Davie 2008). This loss of neurons observed in PD patient brains may be due to an accumulation of Lewy bodies, which are intraneuronal aggregates of proteins mainly containing accumulated  $\alpha$ -synuclein. Since  $\alpha$ -synuclein is the major component of

intraneuronal Lewy bodies, its aggregation is considered as a hallmark of PD and other synucleinopathies, like demetia with Lewy body and multiple system atrophy (Baba, Nakajo et al. 1998, Xia, Liao et al. 2008).

#### 1.4.2 $\alpha$ -Synuclein: structure and metabolism within the cell

$\alpha$ -Synuclein is a small soluble neuronal protein consisting of 140 amino acids (Figure 1.11) encoded by the *SNCA* gene. The synuclein protein family further consist of  $\beta$ - and  $\gamma$ -synuclein with all three forms being present in the cytosol and predominantly found in the pre-synaptic terminals of neurons (George 2002). It seems that  $\alpha$ - and  $\beta$ -synuclein play an important role in synaptic transmission and stability with their exact function remaining elusive (Chandra, Fornai et al. 2004).  $\alpha$ - and  $\beta$ -synucleins seem to be able to compensate each other's function (Chandra, Gallardo et al. 2005). However to date, only the accumulation of  $\alpha$ -synuclein is associated with PD disease progression (Han, Weinreb et al. 1995, Polymeropoulos, Lavedan et al. 1997).

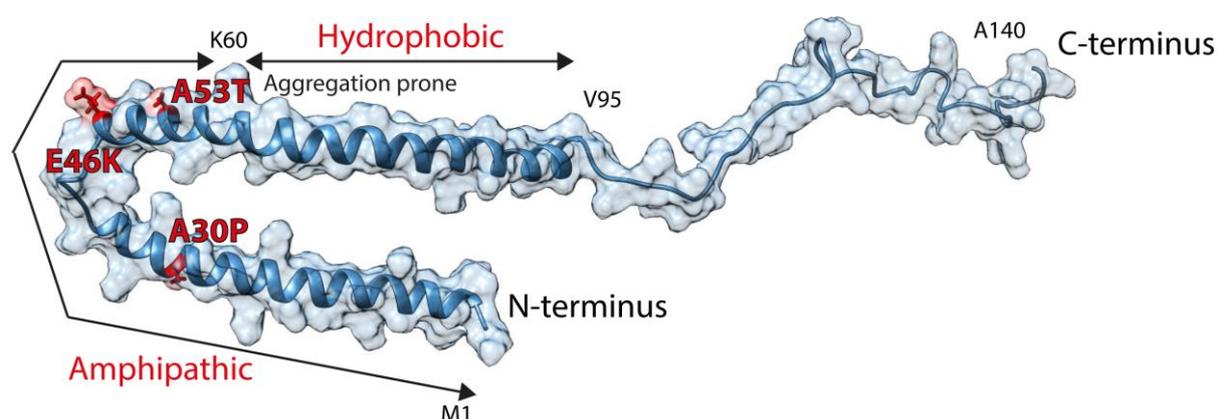


**Figure 1.11: Structure of the  $\alpha$ -synuclein protein.**

Protein model of  $\alpha$ -synuclein crystal structure subdivided in different regions. Met1-Lys60: Amphipathic structure including disease-related mutants (Ala30P, Glu46K and Ala53T). Lys60-Val95: Hydrophobic region with aggregation prone area. Val95-Ala140: proline rich C-terminus. The structural illustration was performed using UCSF Chimera (PDB: 1XQ8).

In aqueous solution  $\alpha$ -synuclein exists as an unfolded protein. It forms  $\alpha$ -helical structures when  $\alpha$ -synuclein binds to negatively charged lipids and  $\beta$ -sheet rich structures indicating its affinity to form aggregates (Davidson, Jonas et al. 1998). Disease-related mutants (A30P, E46K and A53T (Figure 1.11)) but also wild-type  $\alpha$ -synuclein are able to lead to formation of amyloid-like fibrils (Conway, Lee et al. 2000). During the formation of the fibrils various intermediate forms of  $\alpha$ -synuclein appear including soluble as well as insoluble oligomers. The soluble oligomeric form is likely more neurotoxic than the insoluble fibrillary forms (Volles and Lansbury 2002, Karpinar, Balija et al. 2009, Winner, Jappelli et al. 2011). A

possible explanation is the ability of soluble oligomeric  $\alpha$ -synuclein to block the release of proteins from the endoplasmic reticulum (ER) by interaction with respective SNARE protein complexes, important for vesicular fusion (Mazzulli, Xu et al. 2011). Specifically,  $\alpha$ -synuclein was found to interact with the SNARE-protein synaptobrevin-2/VAMP2 (Burre, Sharma et al. 2010, DeWitt and Rhoades 2013). Furthermore, the smaller oligomeric forms of  $\alpha$ -synuclein have been shown to induce mitochondrial fragmentation inducing mitochondrial dysfunction and cell death (Kamp, Exner et al. 2010, Nakamura, Nemani et al. 2011).

In general it is assumed that  $\alpha$ -synuclein leads to pathological manifestations through a toxic *gain-of-function* mechanism when critical levels of the aggregation-prone protein are reached (Lashuel, Petre et al. 2002, Lashuel and Lansbury 2006).

Additionally it has been revealed that aberrant  $\alpha$ -synuclein exerts a negative effect on the protein degradation systems.  $\alpha$ -Synuclein itself is degraded after import in the lysosome by chaperone-mediated autophagy (CMA) and by macroautophagy (Webb, Ravikumar et al. 2003, Cuervo, Stefanis et al. 2004, Vogiatzi, Xilouri et al. 2008, Mak, McCormack et al. 2010, Ebrahimi-Fakhari, Cantuti-Castelvetri et al. 2011) as well as by the proteasome (Tofaris, Layfield et al. 2001, Webb, Ravikumar et al. 2003). Thus, dysfunction in either degradation pathway contributes to  $\alpha$ -synuclein accumulation creating a vicious loop resulting in the different types of synucleinopathies (Xilouri, Vogiatzi et al. 2008).

#### **1.4.2.1 Lysosomal degradation of $\alpha$ -synuclein**

Monomeric  $\alpha$ -synuclein is thought to be degraded mostly through chaperone-mediated autophagy (CMA), oligomeric and aggregated forms of the protein are degraded via macroautophagy (Verhoef, Lindsten et al. 2002, Webb, Ravikumar et al. 2003, Cuervo, Stefanis et al. 2004). Degradation of the monomeric  $\alpha$ -synuclein, involves binding to the CMA transporter LAMP-2 after being recognised by the cytosolic chaperone Hsc70 (Cuervo, Stefanis et al. 2004). In contrast, the aggregated and in most cases mutant  $\alpha$ -synuclein is polyubiquitinated by PARKIN and sequestered into autophagic vacuoles to be directed to lysosomes. For degradation these vesicles fuse with lysosomes (Komatsu, Waguri et al. 2006). This process is called macroautophagy. Inside the lysosome cathepsin D is discussed as an important protease for  $\alpha$ -synuclein degradation (Qiao, Hamamichi et al. 2008, Cullen, Lindfors et al. 2009, Cullen, Sardi et al. 2011).

#### **1.4.2.2 Proteasomal degradation of $\alpha$ -synuclein**

Monomeric wild-type  $\alpha$ -synuclein can also be degraded by the proteasomal system (Tofaris, Layfield et al. 2001, Webb, Ravikumar et al. 2003). The ubiquitin ligases PARKIN/PARK2

(Kitada, Asakawa et al. 1998) and Ubiquitin Carboxy-terminal Hydrolase Like-1 (UCHL-1) (Leroy, Boyer et al. 1998) have been identified to be responsible for tagging  $\alpha$ -synuclein for degradation. Once the protein is aggregated it cannot be degraded by the proteasomal system but can be a substrate for removal by macroautophagy (Verhoef, Lindsten et al. 2002).

#### 1.4.3 Relationship between GC and $\alpha$ -synuclein accumulation

Recently it could be shown by genetic and clinical studies that mutations in *GBA1* are linked to aberrant  $\alpha$ -synuclein degradation. The precise role of GC in the pathogenesis of the accumulation of  $\alpha$ -synuclein and the development of synucleinopathies is still a mystery. It was shown that mutations in the *GBA1* either in homo- or heterozygous form are linked to a about 20-fold increase in the risk to develop PD (Beavan and Schapira 2013). Genetic studies suggest that 5-10 % of PD patients carry mutations in *GBA1* (Sidransky, Nalls et al. 2009, Lesage, Anheim et al. 2011, McNeill, Duran et al. 2012). In these patients neuropathological findings including  $\alpha$ -synuclein positive Lewy bodies were described similar to those found in brains of PD patients without *GBA1* mutations (Goker-Alpan, Lopez et al. 2008). However, increased  $\alpha$ -synuclein levels have been described in brains of sporadic PD cases, exhibiting also reduced GC activity (Murphy, Gysbers et al. 2014).

Gaucher disease patients also show a higher risk to develop PD. In genetic screens it was revealed that especially first-degree relatives of Gaucher disease patients are prone to develop PD (Goker-Alpan, Schiffmann et al. 2004, Lwin, Orvisky et al. 2004). Patients with mutations in *GBA1* seem to develop earlier symptoms of PD with a higher frequency of cognitive changes (Sidransky, Nalls et al. 2009).

There are two major ideas describing how GC impacts  $\alpha$ -synuclein homeostasis. The '*gain-of-function*' theory implies that the mutant enzyme has a direct effect on  $\alpha$ -synuclein aggregation through a biochemical interaction of both proteins. Cullen et al. supported this view showing overexpression of different GC mutants triggering the accumulation of  $\alpha$ -synuclein in cell culture (Cullen, Sardi et al. 2011) and in a transgenic mouse model (Sardi, Clarke et al. 2011). However, there are more data in support of the '*loss-of-function*' theory. It is thought that the consequences of the GC dysfunction of the enzyme cause an imbalance in the metabolism of  $\alpha$ -synuclein. GC mutations lead to a progressive build-up of its substrate glucosylceramide, which possibly stabilises oligomeric  $\alpha$ -synuclein thus promoting  $\alpha$ -synuclein aggregation (Mazzulli, Xu et al. 2011) (Figure 1.12). Furthermore a negative pathogenic loop has been suggested, where soluble oligomers of  $\alpha$ -synuclein may block ER-Golgi trafficking (Cooper, Gitler et al. 2006, Thayanidhi, Helm et al. 2010, Mazzulli, Xu et al. 2011). This block in

intracellular trafficking also leads to an impairment of the transport, maturation and function of lysosomal enzymes including GC creating a negative feedback loop (Figure 1.12).

Another model is linked to the increased cell stress caused by the accumulation of mutant GC in the ER leading to unfolded protein response (UPR) and ER-associated degradation (ERAD) (Ron and Horowitz 2005, Mu, Ong et al. 2008). Increased levels of UPR markers were found in brain of PD patients independently of the presence of *GBA1* mutations, indicating a general role for the ERAD-pathway in the clinical course of PD (Bendikov-Bar and Horowitz 2012, Gegg, Burke et al. 2012).

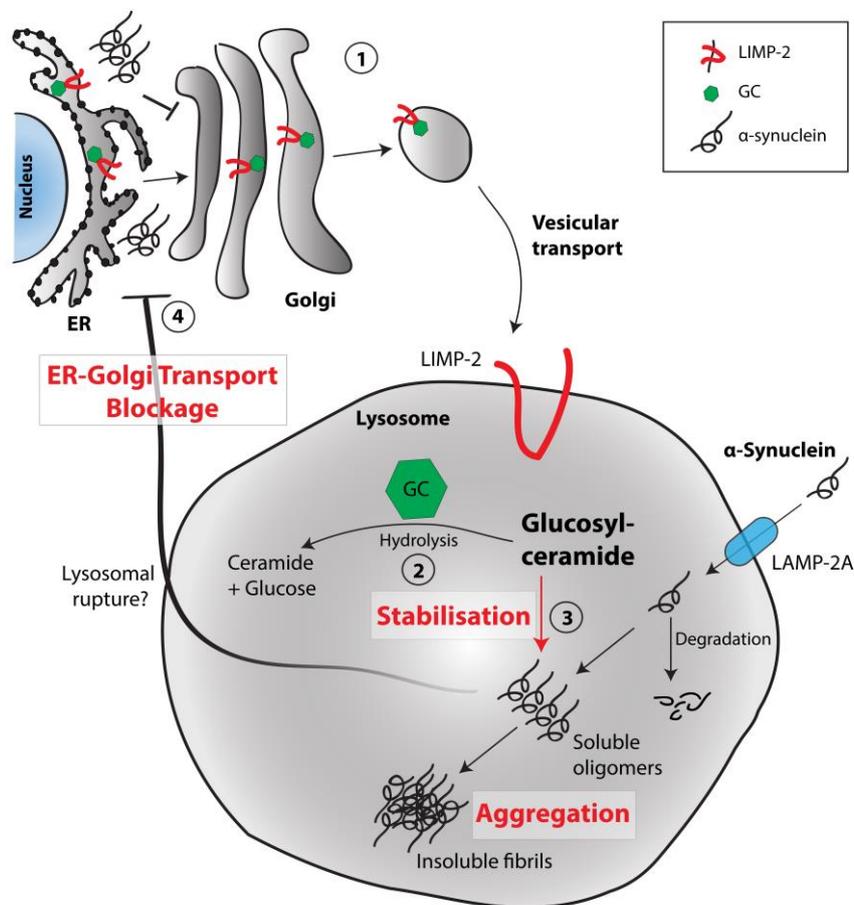


**Figure 1.12: The role of LIMP-2 and GC in lysosomal degradation and aggregation of  $\alpha$ -synuclein.**

(1) GC gets transported to the lysosome by interaction with LIMP-2. Both proteins associate in the ER and dissociate in the lysosome. (2) In the lysosome GC fulfils its enzymatic function by hydrolysing glucosylceramide to ceramide and glucose. (3) Glucosylceramide itself is able to interact and stabilise  $\alpha$ -synuclein oligomers. Initially it has been proposed that  $\alpha$ -synuclein gets transported into the lysosome for degradation by CMA via LAMP-2A. (4) The soluble oligomers of  $\alpha$ -synuclein possibly exhibit a negative effect on ER-Golgi transport. To date it is not known how the  $\alpha$ -synuclein oligomers manage to leave the lysosome. A possible way of lysosomal exit may be the rupture of the lysosomal membrane. Since  $\alpha$ -synuclein is an accumulation-prone protein the soluble oligomers are highly susceptible to form insoluble fibrils. The interference of the intracellular trafficking by  $\alpha$ -synuclein further leads to decreased levels and activity of lysosomal GC accompanied by an increase in glucosylceramide, which is able to further stabilise  $\alpha$ -synuclein creating a negative pathogenic loop.

## 2 Objectives

The central aim of this study is to characterise structural and functional properties of the Lysosomal Integral Membrane Protein Type 2 (LIMP-2) and its ligand the lysosomal hydrolase  $\beta$ -glucocerebrosidase (GC). Biochemical analyses including site-directed mutagenesis of the LIMP-2 and GC proteins followed by molecular interaction studies as well as subcellular localisation should be applied to identify the interaction sites of both proteins.

Additionally, a small peptide comprising the GC-binding region of LIMP-2 and its ability to mediate a specific interaction with GC was analysed. A putative chaperone-like effect of the LIMP-2 protein as well as the LIMP-2-derived peptide on GC should be assessed. To verify the potential positive effect of LIMP-2 on GC function, stabilisation and GC activity assays are performed *in vitro* and in cell-based studies. Further studies to validate a specific interaction of the LIMP-2-derived peptide and GC were designed to support a potential application of the peptide in a therapeutic context.

The identification of a close relationship between GC activity and lysosomal degradation of  $\alpha$ -synuclein, the accumulating protein in Parkinson disease, was a further aim of this project to clarify the role of LIMP-2 -the transport receptor of GC- in  $\alpha$ -synuclein metabolism. In this respect, the consequences of LIMP-2 deficiency in the central nervous system of mice will be analysed in detail.

In addition therapeutic approaches to enhance GC activity in order to decrease neuronal  $\alpha$ -synuclein protein levels should be studied. Under the assumption that an increase in the expression of LIMP-2 is followed by enhanced lysosomal trafficking and activity of GC leading to increased turnover of  $\alpha$ -synuclein, the therapeutic potential of LIMP-2 –as well as the LIMP-2-derived peptide- will be evaluated.

### 3 Material and methods

#### 3.1 Materials

##### 3.1.1 Cell lines

The cells were kept in a sterile incubator at 37°C and 5 % CO<sub>2</sub>. Human fibroblasts (AMRF, patient cells and NPC patient cells) were cultivated in RPMI® media (GE Healthcare) including 10 % FCS and 1 % Penicillin/Streptomycin. Human H4 neuroglioma cells were grown in Opti-MEM® (Thermo Fisher Scientific) with 5 % FCS, 1 % Penicillin/Streptomycin, 200 µg/ml G418 and 200 µg/ml Hygromycin. All other murine embryonic fibroblasts and standard cell lines were cultivated in DMEM® High Glucose media (GE Healthcare) and 10 % FCS and 1 % Penicillin/Streptomycin. Human midbrain dopaminergic neurons were cultivated in SM1-NB media (additive: 10% FCS) without phenol red (Thermo Fisher Scientific). Cultivation of these cells was performed in the laboratory of Dr. Dimitri Krainc (Harvard Medical School/MGH, Boston, USA).

A table of utilised cell culture media can be found in the appendix (Table 7.7).

**Table 3.1: Cell lines utilised in this study.**

Name	Description	Reference
LIMP-2 KO MEFs (E5)	Primary murine embryonic fibroblasts; LIMP-2 deficient	(Reczek, Schwake et al. 2007)
LIMP-2 KO MEFs (583-2)	Primary murine embryonic fibroblasts; LIMP-2 deficient	Dr. J. Schröder, laboratory of Prof. Saftig, University of Kiel; (Blanz, Groth et al. 2010)
WT MEFs (583-3)	Wild-type murine embryonic fibroblasts	Dr. J. Schröder, laboratory of Prof. Saftig CAU Kiel; (Blanz, Groth et al. 2010)
AMRF patient cells (EH, OR)	Human fibroblasts from skin biopsy of two AMRF patients (EH, OR)	(Berkovic, Dibbens et al. 2008)
CD/CI MPR deficient MEFs	Primary murine embryonic fibroblasts; deficient for CD- and CI-MPR	Laboratory of Prof. Thomas Bräulke, UKE Hamburg; (Kollmann, Damme et al. 2012)
Cos7	Kidney cell line from African green monkey; SV40 immortalised	ATCC / DSMZ, established cell line
Gnptab <sup>c.3082insC</sup> MEFs	Primary murine embryonic fibroblasts; GlcNAc-1-Phosphotransferase defective	Laboratory of Prof. Thomas Bräulke, UKE Hamburg; (Kollmann, Damme et al. 2012)
H4	Human neuroglioma cells stably overexpressing wild-type $\alpha$ -synuclein under the control of a tetracycline-inducible promoter ('tet-off')	Provided by Pamela J. McLean, Mayo Clinic, Jacksonville, USA and Dr. Joseph R. Mazzulli, University of Chicago; (Mazzulli, Xu et al. 2011)
HeLa	Cervical carcinoma cells (Henrietta Lacks)	DSMZ, established cell line

Human midbrain dopaminergic neurons (iPSC-derived)	iPSC: cultured and maintained (over 90 days) as described in (Mazzulli, Xu et al. 2011). Differentiation into midbrain dopamine neurons according to (Kriks, Shim et al. 2011)	Cultured, maintained and kindly provided by Dr. Joseph R. Mazzulli, University of Chicago, USA
J774E	Murine macrophages, optimised for endocytosis	Originally from Dr. Philip Stahl, Washington University School of Medicine, St Louis, USA; (Fiani, Beitz et al. 1998)
LAMP 1/2 dKO MEFs	Primary murine embryonic fibroblasts; LAMP-1 and LAMP-2 double deficient	Laboratory of Prof. Saftig, University of Kiel
mGBA KO MEFs	Primary murine embryonic fibroblasts, GC-deficient	Dr. E. Sidransky, NIH Bethesda, MD USA
N2a	Murine neuroblastoma cell line	ATCC / DSMZ, established cell line
Nieman-Pick Type C (NPC) fibroblasts	Human fibroblasts from biopsy of two NPC-1 patients	Laboratory of Prof. Kohlschüttler, UKE Hamburg

### 3.1.2 Mouse strains

LIMP-2 knockout mice were first established and described in the year 2003 by Gamp *et al.*. The LIMP-2-deficient mice contain a neomycin cassette, which disrupts the transcription of LIMP-2 within exon 8. The animals were maintained in a mixed genetic background (SVJ129\_C57BL/6J Harlan) (Gamp, Tanaka et al. 2003, Berkovic, Dibbens et al. 2008). In this mouse model no cognitive decline –like seen in AMRF-patients, lacking functional LIMP-2 protein- was observed. An explanation might be the chromosomal deletion of the  $\alpha$ -synuclein locus in the C57BL/6J strain from Harlan (Specht and Schoepfer 2001). For the studies shown in this work, LIMP-2 knockout mice were backcrossed into C57BL/6N from Charles River exhibiting normal  $\alpha$ -synuclein level (Rothaug, Zunke et al. 2014). An immunoblot of brain lysates of the two different mouse strains indicates a drastic drop of  $\alpha$ -synuclein protein in C57BL/6J compared to C57BL/6N strain (Figure 3.1A). Quantitative real-time PCR shows the decrease of  $\alpha$ -synuclein transcript level. For the LIMP-2 mRNA a constant expression could be identified in all different mouse strains (Figure 3.1 B).

Before mice in the age of 2-10 months were sacrificed for biochemical and histological analyses, they were monitored for behavioural and movement abnormalities including ataxia and hind-limb clasping.

The animals were maintained in a conventional animal facility (University of Kiel) and all experiments were carried out under guidelines of the National Animal Care Committee of Germany.

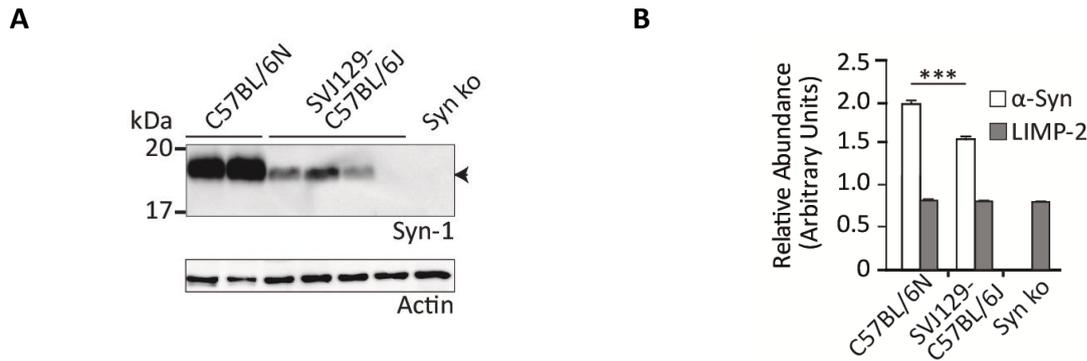


**Figure 3.1: Analysis of  $\alpha$ -synuclein levels in mice of two different genetic backgrounds.**

**A)** Comparison of  $\alpha$ -synuclein protein levels in brain lysates from C57BL/6N and C57BL/6J mouse strain utilising the Syn-1 antibody, showing a drop in the absence in  $\alpha$ -synuclein protein expression in the C57BL/6J background. **B)** Quantitative real-time PCR reveals mRNA levels of  $\alpha$ -synuclein being decreased in C57BL/6J mouse strain, whereas LIMP-2 mRNA levels are unchanged between different strains (Rothaug, Zunke et al. 2014).

### 3.1.3 Antibodies

#### 3.1.3.1 Primary antibodies

**Table 3.2: Overview of primary antibodies.**

Immunofluorescence (IF), Western-Blot (WB), immunohistochemistry (IHC), immunohistology-fluorescence (IH-IF).

Name	Source	Host	Dilutions			
			IF	WB	IHC	IH-IF
$\alpha$ -Actin	Sigma Aldrich, Steinheim, DE	rabbit	-	1:2000	-	-
$\alpha$ -Alpha-synuclein (Syn-1; BD 610787)	Transduction Laboratories, Franklin Lakes, NJ, US	mouse	1:100	1:1000	1:1000	1:200
$\alpha$ -Alpha-synuclein (LB509)	Thermo Fisher Scientific, Rockford, US	mouse	-	1:500	-	-
$\alpha$ -Alpha-synuclein (C-20, sc-7011-R)	Santy Cruz Biotechnology, Santa Cruz, US	rabbit	-	1:500	1:1000	1:200
$\alpha$ -Alpha-synuclein (4D6)	Abcam	mouse	-	1:500	1:1000	1:200
$\alpha$ -Biotin (labelled with Alexa Fluor® 488)	Jackson Immuno Research	mouse	1:200	-	-	-
$\alpha$ -CD68	Serotec, Oxford, UK	rat	-	-	1:3000	-
$\alpha$ -mGC (4171)	Sigma Aldrich, Steinheim, DE	rabbit	1:100	1:1000	-	-
$\alpha$ -hGC (4171)	Prof. Johannes Aerts, NL	mouse	1:250	1:500	-	-
$\alpha$ -GFAP	Sigma Aldrich, Steinheim, DE	mouse/ rabbit	-	-	1:3000	-
$\alpha$ -HA (3F10)	Roche, Penzberg, DE	rat	-	1:500	-	-
$\alpha$ -LAMP-1 (1D4B)	DSHB, Iowa City, US	rat	1:50	1:500	-	-

$\alpha$ -LAMP-2 (ABL93c)	DSHB, Iowa City, US	rat	1:100	1:500	-	-
$\alpha$ -LIMP-2 (Tier 2; L2T2)	Pineda, Berlin, DE	rabbit	1:500	1:2000	1:3000	1:200
$\alpha$ -myc (9B11)	Cell Signalling, Boston, US	mouse	1:250	1:1000	-	-
$\alpha$ -myc (GTX)	Santa Cruz, Biotechnology, Santa Cruz, US	goat	1:250	1:1000	-	-
$\alpha$ -NeuN (MAB 377)	Chemicon, Billerica, US	mouse	-	-	1:2000	-
$\alpha$ -NSE (neuronal specific enolase)	Polyscience, Warrington, US	rabbit	-	1:2000	-	-
$\alpha$ -PDIA6 (protein disulphide-isomerase; ab11432)	Abcam, Cambridge, UK	rabbit	1:750	-	-	-
$\alpha$ -Tubulin	Sigma Aldrich, Steinheim, DE	mouse	-	1:5000	-	-
$\alpha$ -Tyrosine hydroxylase (ab112)	Abcam, Cambridge, UK	rabbit	-	-	1:3000	-

### 3.1.3.2 Secondary antibodies

**Table 3.3: Overview of secondary antibodies.**

Immunofluorescence (IF), Western-Blot (WB), immunohistochemistry (IHC), immunohistology-fluorescence (IH-IF).

Name	Source	Host	Dilutions			
			IF	WB	IHC	IH -IF
$\alpha$ -Mouse Biotinylated	Abcam, Cambridge, UK	goat	-	-	1:500	-
$\alpha$ -Rabbit Biotinylated	Abcam, Cambridge, UK	goat	-	-	1:500	-
$\alpha$ -Rat Biotinylated	Abcam, Cambridge, UK	goat	-	-	1:500	-
$\alpha$ -Mouse-HRP	Dianova GmbH, Hamburg, DE	sheep	-	1:10,000	-	-
$\alpha$ -Rabbit-HRP	Dianova GmbH, Hamburg, DE	sheep	-	1:10,000	-	-
$\alpha$ -Rat-HRP	Dianova GmbH, Hamburg, DE	rabbit	-	1:10,000	-	-
$\alpha$ -Mouse-Alexa Fluor 488/594/647	Invitrogen, Darmstadt, DE	goat or donkey	1:500	-	-	1:2000
$\alpha$ -Rabbit-Alexa Fluor 488/594/647	Invitrogen, Darmstadt, DE	goat or donkey	1:500	-	-	1:2000
$\alpha$ -Rat-Alexa Fluor 488/594/647	Invitrogen, Darmstadt, DE	goat or donkey	1:500	-	-	1:2000

### 3.1.4 Oligonucleotides

All primers used for site-directed mutagenesis, cloning and sequencing were obtained from Sigma Aldrich (Steinheim, DE) in a concentration of 100  $\mu$ M, diluted in ddH<sub>2</sub>O and stored at 4°C or -20°C.

**Table 3.4: Overview of primer for cloning and site-directed mutagenesis.**

Name	Sequence (5'-3')
pfrog forward	gagaaccactgcttactgg
pfrog reverse	gagactccattcgggtgttct
hGC_L91E forward	gacagatgctgctgctGAGaacatccttgcctg
hGC_L91E reverse	cagggcaaggatggtCTCagcagcagcatctgtc
hGC_L94E forward	gctgctctcaacatcGAGgccctgtcacccct
hGC_L94E reverse	agggggtgacagggcCTCgatgttgagagcagc
hGC_L156E forward	gaggaagataccaagGAGaagatacccctgattc
hGC_L156E reverse	gaatcaggggtatcttCTCcttggtatcttctc
hGC_R211E forward	accagacctgggccGAAtactttgtgaagttcctg
hGC_R211E reverse	caggaactcacaagtaTTCggcccaggtctggt
hGC_P159L forward	ataccaagctcaagataCTTctgattcaccgagc
hGC_P159L reverse	gctcggatgaatcagAAGtatcttgagcttggtat
hGC_I161S forward	agctcaagatacccctgTCGcaccgagccctgcag
hGC_I161S reverse	ctgcagggctcgggtCGAcaggggtatcttgagct
hGC_R213E forward	gacctgggccagataGAAgtgaagttcctgga
hGC_R213E reverse	tccaggaactcacTTCgtatctggcccaggtc

### 3.1.5 Expression vectors and constructs

#### 3.1.5.1 pcDNA3.1 and pfrog vector

Two expression vectors were utilized in this study: pFrog3 (Gunther et al., 1998) and pcDNA3.1 Hygro<sup>+</sup> (Invitrogen, Darmstadt, DE) (Table 3.5). The pFrog vector (Figure 3.2) was derived from the pcDNA3 vector (Invitrogen, Darmstadt, DE) and was cloned by Dr. Michael Schwake (Faculty for Chemistry/Biochemistry III, University of Bielefeld, DE). A T7-promoter and cytomegalovirus (CMV) promoter control transcription and a poly-adenylation signal from bovine growth hormone (BGH) stabilising the RNA after transcription. The Simian Virus 40 (SV40) promoter controls transcription of a neomycin resistance gene for selection in eukaryotic cells. A CoIEI gene allows replication in bacteria and an ampicillin resistance gene growth and selection of the vector in E.coli. All LIMP-2 and human GC mutants were expressed in the pFrog-vector and tagged on the N-terminus with a myc-sequence (EQKLISEEDL). The LIMP-2 constructs as well as the human GC-wild-type-construct were previously generated by Dr. Michael Schwake (Faculty for Chemistry/Biochemistry III, University of Bielefeld).

The vector pcDNA3.1 Hygro<sup>+</sup> has 3 promoters that allow a high expression of the transcript including the CMV-promoter a T7-promoter and an SV40 promoter, which allows transcription of hygromycin and thus selection of transfected cells. It also exhibits an ampicillin resistance gene and pUC origin for growth and selection in *E. coli*.

The human  $\alpha$ -synuclein (SNCA) construct was cloned in the pcDNA3.1 Hygro<sup>+</sup> vector by Dr. Michelle Rothaug (Institute of Biochemistry, University of Kiel, DE) containing an HA-tag (YPYDVPDYA) at the C-terminus.

Additionally, an  $\alpha$ -synuclein construct was used for lentiviral transduction and generated by Dr. Joseph Mazzulli (Northwestern University of Chicago, US) using a gateway cloning system (Invitrogen, LR recombination reaction). The  $\alpha$ -synuclein cloning sequence was transferred from the pENTRA1A-vector (Invitrogen) to the SIN-W-PGK lentiviral vector containing the mouse phosphoglycerate kinase promoter (Mazzulli, Xu et al. 2011).

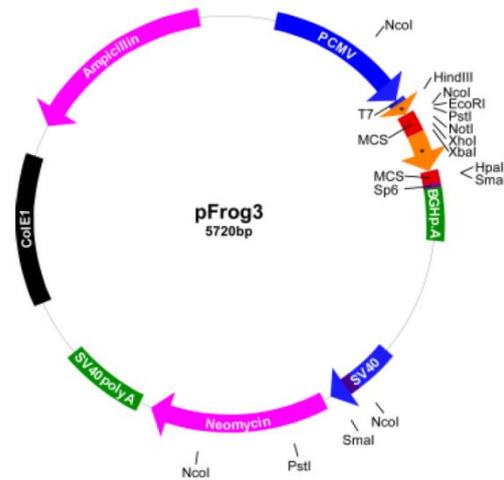


**Figure 3.2: Map of pFrog3 vector.**

Vectormap indicating genes for resistance, promoter regions and splice sites for inserting expression constructs.

**Table 3.5: Overview of utilised expression constructs.**

$\alpha$ -Synuclein (SNCA), wild-type (WT), ER-retention mutant (ERret), murine LIMP-2 (mLIMP-2), human GC (hGC).

<b>Name and description:</b> <i>Vector name—construct- tag</i>	<b>Resistance in e.coli</b>	<b>Source</b>
<i>SIN-W-PGK- SNCA</i>	Kanamycin	generated by Dr. Joseph R. Mazzulli
<i>pcDNA3.1-Hygro<sup>+</sup> - SNCA- HA</i>	Ampicillin	generated by Dr. Michelle Rothaug
<i>pFrog-mLIMP2-WT- myc</i>	Ampicillin	generated by Dr. Michael Schwake
<i>pFrog-mLIMP2-ERret- myc</i>	Ampicillin	generated by Dr. Michael Schwake
<i>pFrog-mLIMP2-L155D- myc</i>	Ampicillin	generated by Dr. Michael Schwake
<i>pFrog-mLIMP2-I156D- myc</i>	Ampicillin	generated by Dr. Michael Schwake

<i>pFrog</i> -mLIMP2-M159D- <b>myc</b>	Ampicillin	generated by Dr. Michael Schwake
<i>pFrog</i> -mLIMP2-L160D- <b>myc</b>	Ampicillin	generated by Dr. Michael Schwake
<i>pFrog</i> -mLIMP2-A162D- <b>myc</b>	Ampicillin	generated by Dr. Michael Schwake
<i>pFrog</i> -mLIMP2-Y163D- <b>myc</b>	Ampicillin	generated by Dr. Michael Schwake
<i>pFrog</i> -mLIMP2-K166D- <b>myc</b>	Ampicillin	generated by Dr. Michael Schwake
<i>pFrog</i> -mLIMP2-I184D- <b>myc</b>	Ampicillin	generated by Dr. Michael Schwake
<i>pFrog</i> -mLIMP2-L187D- <b>myc</b>	Ampicillin	generated by Dr. Michael Schwake
<i>pFrog</i> -mLIMP2-F191D- <b>myc</b>	Ampicillin	generated by Dr. Michael Schwake
<i>pFrog</i> -mLIMP2-D400K- <b>myc</b>	Ampicillin	generated by Dr. Michael Schwake
<i>pFrog</i> -hGC-WT- <b>myc</b>	Ampicillin	generated by Dr. Michael Schwake
<i>pFrog</i> -hGC-L91E- <b>myc</b>	Ampicillin	self-produced
<i>pFrog</i> - hGC-L94E- <b>myc</b>	Ampicillin	self-produced
<i>pFrog</i> - hGC-L156E- <b>myc</b>	Ampicillin	self-produced
<i>pFrog</i> - hGC-L211E- <b>myc</b>	Ampicillin	self-produced
<i>pFrog</i> - hGC-P159L- <b>myc</b>	Ampicillin	self-produced
<i>pFrog</i> - hGC-I161S- <b>myc</b>	Ampicillin	self-produced
<i>pFrog</i> - hGC-N188S- <b>myc</b>	Ampicillin	generated by Dr. Christina Zachos
<i>pFrog</i> - hGC-F213E- <b>myc</b>	Ampicillin	self-produced

A detailed list of the utilised chemicals, machines, kits and buffers can be found in the appendix.

## 3.2 Methods

### 3.2.1 Molecular biology

#### 3.2.1.1 Polymerase-Chain-Reaction (PCR)

In general, the polymerase-chain-reaction (PCR) is utilized to amplify specific DNA regions. Specific oligonucleotides (primers) bind to single-stranded template DNA and determine the starting point for the DNA-polymerases (see Table 3.6: Annealing temperature usually 3-5°C below melting point of primers). These enzymes synthesise the complementary DNA strand in 5' → 3' direction and work most efficiently at a temperature optimum at 72°C (see Table 3.6: Elongation step). The forward and reverse primers span the sequence to be amplified. PCRs consist of three cyclically repeating annealing steps (usually 30-45 times).

**Table 3.6: Standard-PCR procedure: Ingredients and protocol**

5 µl	10x PCR-buffer			
0.5 µl	dNTPs (2 µM)			
2.5 µl	DMSO			
1 µl	forward-Primer (20 µM)			
1 µl	reverse-Primer (20 µM)			
xx µl	Template (20 ng - 1 µg)			
0.1 µl	Taq DNA Polymerase			
<b>total 50 µl</b>		H <sub>2</sub> O		
Temp.	Time (mins)	Cycles	Function	
95 °C	2:00		Denaturation	
95 °C	0:30		35 - 40	
52-58 °C	0:30			
72 °C	1:00			
72 °C	X (2min/1000bp DNA)		Elongation	
4 °C	∞		End	

##### 3.2.1.1.1 Fusion-PCR

The fusion-PCR is a special method used to insert a point mutation within a DNA sequence. The PCR was performed following the above described PCR-protocol. Primers with the desired point mutation were designed (see Table 3.4). The primers are usually around 30 base-pairs long and exhibit the mutation (three base-pairs encoding for one amino acid) in the middle of the oligonucleotide sequence. In two single PCR reactions the forward primer including the mutation (FM) is incubated with the external reverse primer (R) and vice versa the mutated reverse primer (RM) is incubated with the external forward (F) primer. As annealing temperature a standard temperature of 62°C was applied. In the end of the first two reactions there are two overlapping PCR-reaction products, which are incubated in the same PCR-reaction together with the external forward and reverse primers (fusion-PCR). The PCR-

result is a DNA-fragment including the desired point-mutation (Figure 3.3). Subsequently this fragment was cloned into the respective vector in the presence or absence of a myc- or HA-tag by digestion with restriction enzymes (for more details see 3.2.1.3). All here described point-mutants (LIMP-2 and GC) were designed following this protocol.

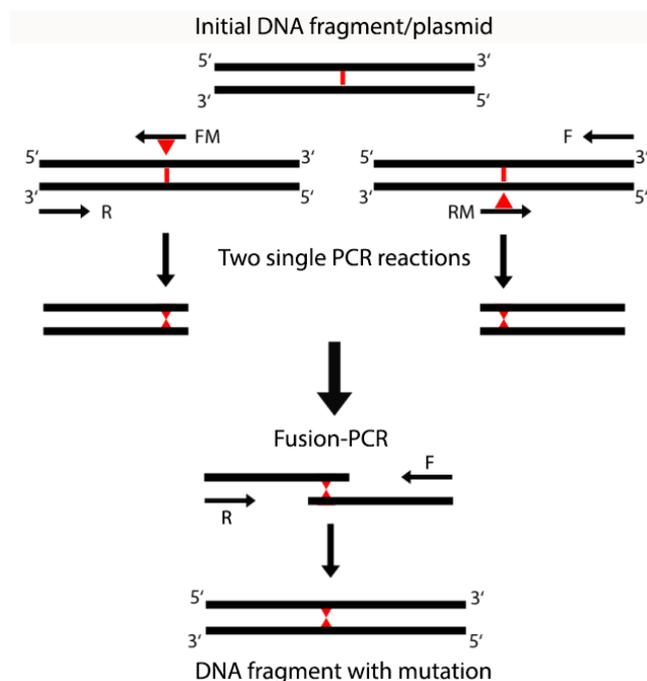


**Figure 3.3: Principle of fusion-PCR.**

The red bar indicates the desired point mutation. Primers including the mutated sequence (red triangle; FM and RM) are utilised in two separate PCR-reaction steps. The two single PCR-products exhibiting the desired mutation (red triangle) and are mixed in the subsequent fusion-PCR. Together with the framing forward (F) and reverse (R) primer this PCR-approach results in a DNA-fragment with desired point-mutation (red triangle).

### 3.2.1.2 Agarose electrophoresis

Agarose-gel electrophoresis is used for separation of DNA molecules according to their molecular weight. DNA/PCR products were detected and analysed using 1-2% agarose gels in 1x TAE buffer (see Table 7.6) and including ethidium bromide (endconcentration of 1%), which visualises DNA by its intercalation with the oligonucleotide strengths. The DNA/PCR products were mixed with loading buffer (Thermo Fisher Scientific, Waltham, US) in a ratio of 6:1 and loaded onto the gel. A size-reference of 100 bp or 1 kb ladders (Thermo Fisher Scientific, Life Technologies) was additionally applied on the agarose-gel. DNA fragments were separated at 90-120 mV for 30-45 minutes and visualised under UV light (Gel Jet Imager;  $\lambda=312$  nm). For cloning DNA-fragments were cut out of the gel and purified according to instructions of the kit manual (High Pure PCR-Purification Kit, Roche).

### 3.2.1.3 Cloning experiments: Restriction enzyme digestion and DNA ligation

In this work several cDNA constructs were utilised for overexpression studies. Changes on the cDNA level were made by PCR and point-mutations were introduced by fusion-PCR (see 3.2.1.1.1). For cloning of a specific PCR-fragment/cDNA sequence (insert) into an expression vector, the insert (50 µl PCR-product) as well as the vector (~2 µg) were digested with the respective restriction enzymes (Thermo Fisher Scientific). Restriction enzymes are able to cut specific palindromic DNA-sequences resulting in so called 'sticky ends'. The amount and relation of enzymes and buffer were applied as recommended in the manufacturer's manual (Thermo Scientific) or suggested by the 'DoubleDigest Calculator' on the Thermo Fisher Scientific webpage ([www.lifetechnologies.com](http://www.lifetechnologies.com)). To prevent re-ligation, the vector was dephosphorylated by adding 1 µl FastAP (Thermo Fisher Scientific) to approximately 20 ng of a cDNA plasmid. For ligation of the insert and the cDNA vector, 1 µl plasmid-DNA and 7 µl of the insert were mixed with 1 µl T4-ligase and 1 µl 10x ligation buffer and incubated at 37°C overnight. As a negative control ddH<sub>2</sub>O was added instead of the insert. The ligase has to be deactivated by incubating the sample at 62°C for 15 minutes according to the manufacturer's manual (Thermo Scientific).

### 3.2.1.4 Amplification and purification of expression vectors in *Escherichia Coli*

For amplification of ligated expression plasmids (see above) or for retransformation of established expression vectors, electro competent XL1-Blue *Escherichia Coli* (*E. coli*) were transformed with the DNA plasmids by electroporation (2.5 kV, 400 Ω and 25 µF; Biorad, Hercules, US). After thawing the cells on ice, 1 µl of plasmid cDNA were added to 50 µl cells, no cDNA was added to negative controls. The cells were then resuspended in 1 ml LB media and incubated at 37°C for 30 mins. Following, electroporated cells were squirted onto the centre of a LB agar plate with antibiotics (100 µg/ml ampicillin). Plates were inverted and incubated at 37°C overnight. The following day single colonies were picked and grown overnight either in 3 ml or in 100 ml LB-medium (see appendix Table 7.6) in a 37°C shaking incubator.

After growing single colonies overnight in 3 ml or 100 ml LB medium, the DNA was isolated and purified using the 'plasmid miniprep kit' (Thermo Fisher Scientific) for small volumes and the 'plasmid midiprep kit' (Promega) for larger volumes. The plasmid isolation was performed as suggested in the manufacturers' protocols.

### **3.2.1.5 Measurement of DNA-concentration**

The DNA concentration was measured with the help of a Synergy HT microplate reader (BioTec). Nucleic acids exhibit a specific absorption spectrum between 250 and 280 nm (maximum at 260 nm). An optical density (OD) of 1 at 260 nm reveals a concentration of 50 µg/ml. Furthermore a quotient of the absorption at 260 nm and 280 nm (A<sub>260</sub>/A<sub>280</sub>) was determined to control for contaminations with proteins or solvents. A value between 1.8 and 2.0 is a generally expected value for pure DNA.

### **3.2.1.6 Mouse perfusion**

For histochemical analyses of brain samples, LIMP-2-deficient as well as wild-type animals were perfused before harvesting of the tissue. Animals were anaesthetised with 10 µg/mg weight of a mixture of 1.2 % xylazine/0.16 % ketamine in phosphate buffered saline (PBS). By checking for the pinch-withdrawal reflexes of the animals, the depth of the narcosis was monitored. The mouse was fixed on a clean platform and opened by a lateral incision from the neck to the torso. To get access to the heart the diaphragm and the rib-cage were cut. Next a butterfly needle was inserted to the left ventricle and the right atrium was cut. The animal was perfused with 0.1 M PBS until the inner organs turned pale. Subsequently mice were perfused with 4 % paraformaldehyde (PFA) in PBS.

### **3.2.1.7 Isolation and dissection of murine brain**

Mice were perfused or subjected to CO<sub>2</sub> and sacrificed by cervical dislocation. The head was detached and the brain was isolated by removing skin and skull caudal to rostral utilising a bone-scissor and forceps. If brains were used for histological analysis, they were post-fixed at room temperature for 4 hours in 4 % PFA in PBS. For separation of specific brain areas the whole brain was cut sagittally. Under the microscope the different regions (Figure 3.4) were separated, frozen in liquid nitrogen and stored at -80°C. This study mainly focuses on the pons and the midbrain including the substantia nigra (Figure 3.4).

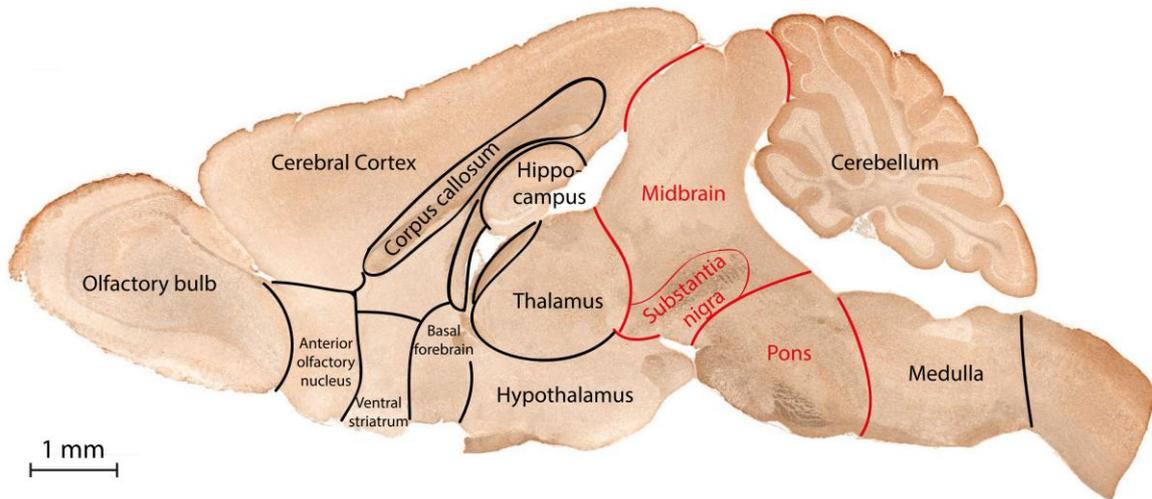


**Figure 3.4: Different brain regions in a sagittal murine brain section.**

A mouse brain roughly subdivided in the different main brain regions indicated in a brain section in brightfield modus. The brain sections focused on in this work (pons and midbrain including the substantia nigra) are highlighted in red. The illustration was modified from the ‘gensat brain atlas’ ([www.gensat.org](http://www.gensat.org)).

### 3.2.1.8 Tissue and section preparation

For further histological analysis the brain sections were either embedded in paraffin or sucrose.

#### 3.2.1.8.1 Paraffin embedding, sectioning and removal of paraffin

The fixed brains were dehydrated in an ascending alcohol series (30 min. in 50 %, 60 %, 70 % ethanol, 15-30 mins in 96 % and finally 45-60 mins in 100 % ethanol). Subsequently they were cleared with xylol (2 x 1 hour), incubated with RotiPlast® paraffin (Roth) and heated to ~60°C. The sections were cut sagittally in 5 µm thick slices using a Leica SM 2000R microtome (Leica).

For all performed histological stainings the paraffin embedded sections were deparaffinised in Rotihistol® (Roth) two times for 10 minutes. Subsequently the sections were rehydrated in a descending alcohol series (5 minutes each in 100 %, 96 %, 70 % and 50 % ethanol) and rinsed in ddH<sub>2</sub>O.

#### 3.2.1.8.2 Succrose embedding

For immunohistology stainings (see section 3.2.1.9.1) the tissue was incubated in 30 % sucrose in 0.1M PB for at least 24 hours at 4°C. To generate free-floating sections, the brain samples were cut sagittally utilising the Leica SM 2000R microtome (Leica).

### **3.2.1.9 Histology**

To visualise morphological changes in the brains of LIMP-2-deficient and wild-type animals, histochemical stainings were performed.

#### ***3.2.1.9.1 Immunohistology***

For immunohistological analysis antibodies are applied for visualisation. It can be distinguished between a direct and indirect staining. A direct staining deciphers the application of a fluorophore-coupled secondary antibody, which is targeted against the constant region (Fc) of a primary antibody. If an amplification of the signal is needed, a streptavidin/biotin system may be used (ABC-system; Vector Laboratories, Enzo Life Sciences). Hereby, a biotinylated primary antibody is applied. To each biotin-labelled antibody multiple streptavidin molecules coupled to horse-radish peroxidases (HRP) are able to amplify the signal.

An indirect staining utilises a chromogenic substrate as for example the chemical reagent 3,3'-diaminobenzidine (DAB). The DAB staining was followed after using the ABC kit. The HRP, which is coupled to streptavidin molecules, is able to cause a reduction of the DAB leading to an insoluble brown precipitate. This precisely indicates where a primary antibody has bound. ABC as well as DAB stainings were performed as suggested in the manufacturer's handbooks (Vector Laboratories, Enzo Life Sciences).

Free floating and human paraffin sections were subjected to immunohistological stainings either utilising DAB or fluorophore-labelled secondary antibodies. To retrieve the epitopes in paraffin sections, the samples were boiled in citrate buffer (pH6) for 10 minutes. Before immunohistochemistry stainings were performed, endogenous peroxidase activity was stopped by incubation in 0.3 % H<sub>2</sub>O<sub>2</sub> in 0.1M PB for 30 minutes. The sections were rinsed in 0.1 M PB and blocked in 0.1 M PB with 4 % normal goat serum, and 0.25 % triton x-100 for 30 minutes at room temperature. The first antibody was incubated overnight, and the secondary biotinylated antibody was incubated for one hour at room temperature. After washing the sections with 0.1 M PB/0.25 % triton x-100, 0.1M PB followed by 0.01 M PB and finally ddH<sub>2</sub>O the ABC kit was applied. Subsequently the DAB staining kit was utilized. DAB sections were dehydrated and prepared for mounting before microscopical analysis using a BX50 microscope (Olympus). Hereby the sections were dehydrated by incubation in ascending ethanol concentrations (5 minutes each in 50 %, 70 %, 96 % and 100 ethanol). The

alcohol was removed by incubating two times 10 minutes in RotiHistol® (Roth) before mounting of the sections with Eukitt® (Sigma).

Sections for immunofluorescence were mounted in a mixture of 1, 4-diazabicyclo [2, 2, 2] octane (DABCO)/Mowiol (17 % Mowiol, 33 % Glycerol), 50 mg/ml DABCO, 1 µg/ml 4',6-diamidino-2-phenylindole (DAPI) and hardened in the dark at room temperature. The immunohistologically stained sections were visualised using a confocal laser scanning microscope (CLSM) FV1000 (Olympus).

### ***3.2.1.9.2 TUNEL staining***

By Terminal deoxynucleotidyl Transferase (TdT) deoxyuridine triphosphate (dUTP) Nick End Labeling (TUNEL) apoptotic cells were stained within brain tissue. This is a method, which detects DNA fragments resulting from apoptotic cell death by labelling the terminal end of fragmented DNA. The enzyme TdT catalyses the transfer of dUTPs, that are secondarily labelled by a marker onto the 3' end of a DNA strand.

Paraffin sections (section 3.2.1.8.1) were stained using the ApopTag® Peroxidase In situ Apoptosis Detection Kit (Millipore) according to the manufacturer's instructions. After deparaffinising and rehydrating of the paraffin sections they were incubated in 20 µg/ml proteinase K diluted in PBS for 15 minutes. Subsequently, endogenous peroxidase was quenched by incubating the sections in 3 % H<sub>2</sub>O<sub>2</sub> in PBS for 5 minutes. Following the samples were incubated with equilibration buffer before adding the TdT enzyme for an hour at 37 °C. In this step the labelled dUTP (digoxigenin) was conjugated to the ends of nicked DNA strands and the reaction was terminated by adding the "stop buffer". The sections were washed with PBS before incubation with an anti-digoxigenin antibody attached to a peroxidase for 30 minutes. Following the sections were washed again in PBS for (4 x 2 minutes). The 3,3'-diaminobenzidine (DAB) staining was utilised according to the manufacturer's instructions (Vector Laboratories, Enzo Life Sciences) to visualise the antibody signals. Finally, the sections were dehydrated and prepared for mounting before analyzing the samples microscopically by using a BX50 microscope (Olympus).

### ***3.2.1.9.3 Periodic acid-Schiff staining***

To detect glycogen or carbohydrate conjugates (also attached to lipids or proteins) in tissue the Periodic acid-Schiff (PAS) was utilised. This reaction selectively oxidises glucose/galactose residues creating aldehydes, which react with the Schiff's reagent resulting

in a magenta positive signal. Thus, an increased staining may indicate a metabolic disorders leading to storage e.g. glycolipids or glycoprotein. The staining was in deparaffinised sections from murine brain tissue following the protocol outlined in table 3.7. The stainings were analysed microscopically by using a BX50 microscope (Olympus).

**Table 3.7: Protocol for PAS-staining of brain sections.**

Reagents	0.05 % periodic acid Schiff's reagent Haematoxylin Basic water (NaOH pH 7.8) Acid Alcohol (1 % HCl in 70 % ethanol) Alcohol dilution series (50 % - 100 %) Rotihistol®
Protocol	- 5 minutes periodic acid - Rinse in ddH <sub>2</sub> O - Schiff's reagent 30 minutes - Wash in running water 5 minutes - Haematoxylin 5 minutes - Wash in running water 5 minutes - Acid alcohol: dunk 2-3 times until the sections turn pink. - Tap water: rinse 3-5 minutes - Basic water 5-6 slow dunks; until sections darken - Dehydrate in alcohol: 2 minutes each - 50 %, 70 %, 96 %, 100 % - Clear in Rotihistol® and mount in Eukritt®

### 3.2.2 Molecular structural analyses

#### 3.2.2.1 LIMP-2-derived peptides

All peptides were purchased from jpt Peptide Technologies (Berlin) in a purity of >95%. A biotin-tag was N-terminally coupled to the peptides via a Ttds linker (TTDS = 1,13-diamino-4,7,10-trioxatridecan-succinic acid) (Figure 3.5). The peptide sequences were derived from the LIMP-2 interaction site. The 3xD helix 5 peptide was utilised as a negative binding control. The helix 5, 3xD helix 5 as well as helix 7 peptide end with an acid COOH-group at the C-terminus. In addition uptake-optimised 'TAT-peptides' of helix 5 and 3xD helix 5 were designed. Auxiliary they exhibit a CMA-sequence (KFERQ) linked to the N-terminus and TAT-sequence (YGRKKRRQRRR) on the C-terminus. Both of the peptides were designed to have an amide-group at the end of the C-terminus to make the peptides more stable for cell culture experiments. All peptides and the recombinant GC (Cerezyme ®, Genzyme Therapeutics, Boston, US) were dissolved in NaPhosphate buffer (50mM, 150mM NaCl, pH7). The peptides were solved in 0.1% HCl before dilution in 10% volume of the total amount of NaPhosphate buffer (e.g. the peptide was solved in 30 µl 0.1% HCl and

subsequently 270  $\mu$ l buffer was added). For peptide studies including pulldown, activity and uptake assays, recombinant GC was incubated with 10 times higher concentrated peptides (in molarities). The concentration of the peptides as well as recombinant proteins was assessed spectroscopically by using a nanodrop (see paragraph 3.2.2.3).

**Table 3.8: Overview and properties of utilised peptides**

Peptide name	Sequence (N-terminus-----C-terminus)
Helix 5	Biotin-Ttds-LREIIEAMLKAYQQKLFVTHTVDE (acid) M=3404 g/mol; $\epsilon$ =0.45
3xD Helix 5	Biotin-Ttds-LREDDEAMDKAYQQKLFVTHTVDE (acid) M=3409 g/mol; $\epsilon$ =0.45
Helix 7	Biotin-Ttds- TVDELLWGYKDEILSLIHVFRPD (acid) M=3287 g/mol; $\epsilon$ =2.53
Helix 5 TAT	Biotin-Ttds- <i>KFERQLREIIEAMLKAYQQKLFVTHTVDEYGRKKRRQRRR</i> (amide) M=5107 g/mol; $\epsilon$ =0.50
3xD Helix 5 TAT	Biotin-Ttds- <i>KFERQLREDDEAMDKAYQQKLFVTHTVDEYGRKKRRQRRR</i> (amide) M=5113 g/mol; $\epsilon$ =0.50

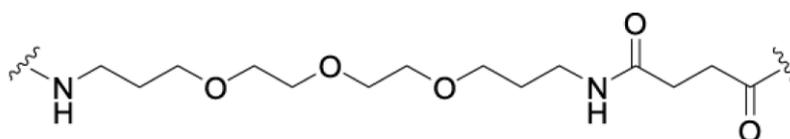


**Figure 3.5: Structure of the Ttds-linker.**

The Ttds-linker was incorporated N-terminally between the biotin-tag and the sequence of the helices through an amide linkage.

### 3.2.2.2 Recombinant enzymes

In this study recombinant enzymes were utilised in a number of different experimental approaches including peptide-pulldown, enzyme-activity and cell-based uptake assays. For example the recombinant GC (Cerezyme ®) was used to validate the ability the LIMP-2-derived peptides to specifically interact with this enzyme *in vitro*. To validate the binding specificity of the LIMP-2-derived peptides, the recombinant lysosomal acid  $\alpha$ -mannosidase (LAMAN; Zymenex) was applied as negative control. In addition the effect of the whole luminal domain of LIMP-2 on GC function was assessed.

Information about the individual recombinant enzymes can be found in table 3.9.

**Table 3.9: Overview and description of utilised recombinant enzymes.**

Name	Description
hLIMP-2 LD	Luminal domain of LIMP-2 with c-terminal human IgG-tag; R&D Systems (Minneapolis, US) diluted in 100 µg/ml in PBS
GC (Cerezyme®)	Imiglucerase for injection (enzyme replacement therapy), produced in CHO cells; Genzyme (Sanofi Company, Boston, US). Diluted in 50 mM NaPhosphate buffer, 150 mM NaCl, pH7; Gift of Dr. med. Eugen Mengel (University paediatric clinic of Mainz) M = 60,430 g/mol; $\epsilon$ = 1.67
rhLAMAN	Recombinant human $\alpha$ -mannosidase for injection (enzyme replacement therapy) diluted in PBS; Zymenex (Hillerod, DK) (Roces, Lullmann-Rauch et al. 2004, Blanz, Stroobants et al. 2008) M = 113,744 g/mol; $\epsilon$ = 1.71

### 3.2.2.3 Nanodrop: Proteinconcentration measurement

After getting recombinant protein and peptides into solution, they were quantified by utilising a NanoDrop® spectrophotometer (ND-100, Thermo Fisher Scientific, US). After calibrating and blanking with 1 µl nuclease-free water, 2 µl protein/peptide solution was applied and a spectrum from 220 - 350 nm measured. Aromatic amino acids in protein/peptides absorb light at 280nm. The more light is absorbed, the higher is the protein concentration in the sample. Using the Beer-Lambert law it is possible to relate the amount of absorbed light to the concentration of sample:

$$c = \frac{E}{\epsilon} \quad (E = \text{Extinction and } \epsilon = \text{specific extinction coefficient})$$

The extinction coefficient of each peptide/recombinant protein was identified by using the protein calculator (online version 3.3 on the server of the Scripps Research Institute, La Jolla, US).

### 3.2.2.4 Peptide-pulldowns

*In vitro* pulldown: for the pulldown of recombinant protein utilising LIMP-2-derived peptides, 2 nmol of protein (GC, LAMAN and BSA) were incubated overnight at 4°C or 1-2 hours at room temperature with the tenfold molecular amount (20 nmol) of biotinylated LIMP-2-derived peptides (helix 5, 3xD and helix 7 as well as TAT-peptides (see Table 3.8)). The total incubation volume was filled up to 250 µl with NaPhosphate buffer (50 mM, 150 mM NaCl, pH7). Simultaneously ‘High Capacity Streptavidin Beads’ (Thermo Fisher Scientific, Life Technologies) were blocked with 1 % BSA solution. The next day the beads were equilibrated

with the respective buffer (50 mM NaPhosphate, 150 mM NaCl, pH7) by washing them four times (centrifugation step at 4000 rpm, 4°C). For each pulldown 50 µl of beads were utilised and incubated with 200 µl enzyme/peptide mixture for 30 minutes at room temperature. The remaining 50 µl of the enzyme/peptide samples were prepared for SDS-PAGE (25 µl + 5 µl 5x Laemmli → 'LOADED fraction') and kept in the fridge for further analysis (e.g. GC activity assay or nanodrop analysis). After incubation of the beads with the enzyme/peptide mixture the samples were centrifuged for 1 min. at 1,500 x g at 4°C.

The supernatant was removed from the beads and stored at 4°C as 'UNBOUND fraction'. Following, the beads were washed three times for 10 minutes with 250 µl of NaPhosphate buffer and centrifugation at 4000 rpm at room temperature. Finally, the washing buffer was removed from the beads and incubated with 30 µl 1x laemmli buffer at 60°C for 20 minutes. In this step the precipitated enzyme and peptide were released from the streptavidin agarose beads ('BOUND fraction'). The LOADED and BOUND fractions of the pulldown-down experiments were loaded on a NuPAGE® Novex® 4-12 % Bis-Tris gel with NuPAGE® MES buffer (NuPAGE system: Thermo Fisher Scientific, Life Technologies), subjected to electrophoresis (paragraph 3.2.3.5) and stained with coomassie (Brilliant Blue, R-250; BioRad; for protocol see 3.2.3.7). The gels were destained (for buffer ingredients see appendix Table 7.9) until the background staining was minimised. Gels were kept air-locked in a humid plastic bag at 4°C and digitalised by scanning.

Pull down from cell lysates: for pulldown of endogenous and overexpressed GC from N2a cell lysates 20 nmol of LIMP-2-derived peptide (Helix 5 and 3xD) were incubated with 50 µl cell lysate at 4°C overnight. The cells were harvested in EBC-buffer. As described above the 'High Capacity Streptavidin Beads' (Thermo Fisher Scientific, Life Technologies) were blocked with BSA and equilibrated in NaPhosphate buffer as described above. The cell lysate/peptide mixture was incubated with the streptavidin beads for 30 minutes at room temperature. The supernatant was removed and the beads were washed three times in NaPhosphate buffer. The bound enzyme was released from the streptavidin agarose beads by incubation with 40 µl 1x Laemmli and incubation at 60°C for 20 minutes. After centrifugation for 2 minutes at 17,000 x g the supernatant was removed ('BOUND fraction') and subjected to SDS-Page (section 3.2.3.5) and western-blotting (chapter 3.2.3.6). An antibody against the human variant of GC (anti-hGC, for details see Table 3.2) was used to detect the pulldown of the overexpressed GC mutants, whereas an antibody against the murine form of GC (anti-mGC, for details refer to Table 3.2) was applied to detect the endogenous GC enzyme.

### 3.2.2.5 Protein modelling

Molecular analyses, graphics and animations were performed with the UCSF Chimera package (<http://www.cgl.ucsf.edu/chimera>) (supported by NIGMS P41-GM103311).

### 3.2.2.6 Circular dichroism (CD-Spectroscopy)

In this study the CD-spectroscopy was applied to characterise the secondary structure of recombinant proteins and LIMP-2-derived peptides. The principle of this technique is based on the difference in the absorption of left- and right-handed circularly polarised light and occurs when a molecule contains one or more chiral chromophores.

Every single protein secondary structure including  $\alpha$ -helices,  $\beta$ -sheets and random coils reveals a specific CD-spectrum (Figure 3.6). Thus every protein exhibits a characteristic CD-spectrum, which is a mixture of the spectra of the individual secondary structures.

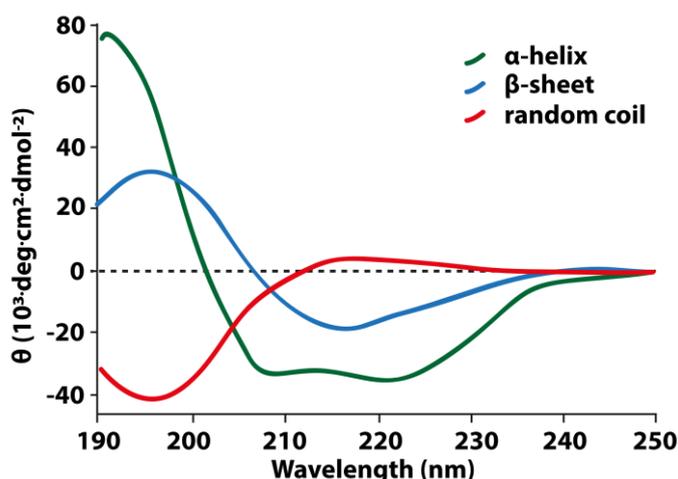


**Figure 3.6: Characteristic CD-spectra of individual secondary structures.**

Every protein secondary structure exhibits a characteristic UV CD-spectrum (250 nm-190 nm). A spectrum of a random coil (lack of structure) is shown in red, a typical  $\beta$ -sheet curve progression is exposed in blue and a typical 'W'-shaped  $\alpha$ -helical spectrum is revealed in green. The ellipticity ( $\theta$ ) is stated as  $10^3 \cdot \text{deg} \cdot \text{cm}^2 \cdot \text{dmol}^{-2}$ .

The CD-measurements were carried out with a Jasco-J-720-CD spectropolarimeter (Japan Spectroscopic Company) at 20°C. The LIMP-2-derived peptides (helix 5, 3xD helix 5 and helix 7) were dissolved in 50 mM NaPhosphate buffer (+ 10 mM NaCl, pH7) in a concentration of 0.2  $\mu\text{g}/\mu\text{l}$  in a total volume of 300  $\mu\text{l}$  and measured from 250 nm – 200 nm with settings as depicted in table 3.10.

Furthermore the CD-spectrum of GC and its changes in the presence and absence of the helix 5 peptide was assessed. Initially 2 nmol GC (Cerezyme®) were incubated with 20 nmol of helix 5 and 3xD peptide overnight at 4°C. For CD-analysis the samples were diluted 1:15 resulting in a concentration of 0.05 – 0.07  $\mu\text{g}/\mu\text{l}$  in a total volume of 300  $\mu\text{l}$ . For stabilisation/

melting curve analysis the temperature was increased from 20°C to 90°C (1°C/min) and spectral changes were recorded every degree at a wavelength of 220 nm (for further settings of measurements see table 3.10).

**Table 3.10: Settings of CD-spectrum measurements.**

<b>Settings:</b>	
Data pitch	1 nm
Scanning mode	continuous
Speed	5 nm/min
Response	8 sec.
Band width	2.0 nm
Accumulation	3 measurements
Wavelength	250 nm – 200 nm; for melting curve analysis: 220 nm
Width of cuvette	0.05 cm

### 3.2.2.7 Dynamic light scattering (DLS)

This technique is applied to determine the size distribution of small molecules (down to 1 nm diameter) in solution. The principle of this experimental setup relies on the fact, that the moving particles hit the monochromatic light (laser) and diffract it in all directions. Together with the frequency of passing the laser beam it is possible to conclude the size of these particles. The set-up of a DLS-experiment is shown in figure 3.7

In this study it was assessed if the presence of the GC-binding helix 5 peptide is causing changes in the quaternary structure (e.g. multimerisation or aggregation) of the GC protein. Protein and peptide were pre-incubated overnight in a molar ratio of 1:10 in 50 mM NaPhosphate buffer (+ 10 mM NaCl, pH7). The measurements were carried out at room temperature in a laser-spectroscatter 201 (RiNA GmbH). The best signals were obtained when GC was applied in a concentration of 50 µM.

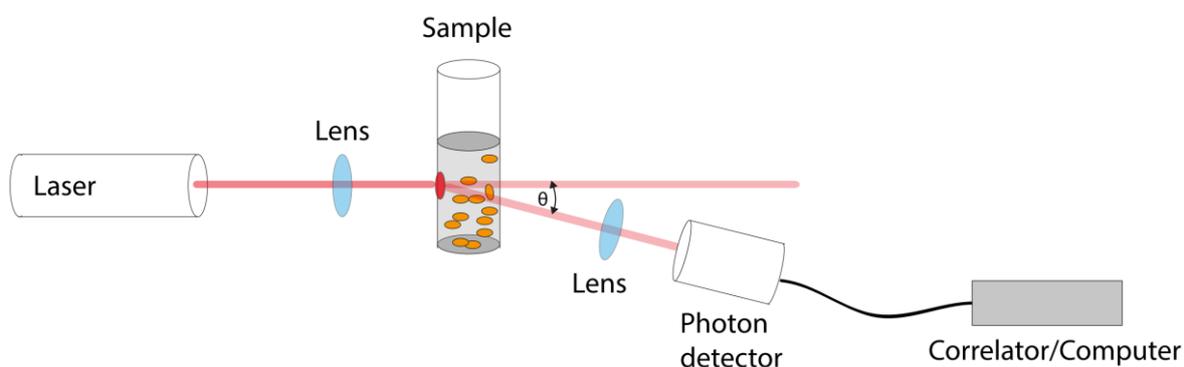


**Figure 3.7: Principle of dynamic light scattering technique.**

A monochromatic light source (laser) is shot through a polariser (lens). The light hits the molecules in the sample (orange circles) and gets diffracted in all directions. At a certain angle ( $\theta$ ) the light is detected by going through another lens and a photon detector. The repetition of events and thus the change in wavelengths can be correlated to a specific size of the particle (calculated by the correlator/computer).

### 3.2.2.8 Crystallisation

For crystallisation experiments recombinant GC (Cerezyme®) and the peptide were solved in MES-buffer (50mM MES, 100 mM NaCl). By using spin columns (Vivaspin 500, Sartorius) GC was concentrated to approximately 4 mg/ml and GC was incubated with the peptide (10 fold higher molarity compared to GC) at 4°C overnight. The crystallisation buffers were modified from a published protocol for crystallisation of glycosylated GC (Brumshtein, Wormald et al. 2006).

On 96 well crystallisation plates the best conditions were screened by variation of the buffer in pH and concentration of the different buffer components. Best results were observed under following crystallisation buffer conditions: 100 mM Bis-Tris buffer, 2.0-2.4 M Ammonium sulphate, pH4.9-5.1. Crystals were grown and kept consistently at 20°C. In addition, growing the crystals under oil (Al's oil; Paraffin and Silicon oil (50:50); Hampton Research) had a positive impact on the number and size of the crystals (experimental set-up see Figure 3.8). After 3-5 days first crystals could be observed, gaining in size over time. An IZIT® (Hampton Research, CA, US) staining was performed to verify the protein content of the cultured crystals. The GC/peptide mixture (in MES buffer) and crystallisation solution (Bis-Tris buffer) were mixed 1:1 (100 nl each) and then covered by 2-3 µl of oil. The neighbouring reservoir was filled with 50 µl crystallisation solution (Bis-Tris) and the batch was sealed with plastic tape (Figure 3.8). The obtained crystals were monitored every second day and harvested at a size around 50 µm. Utilising a mounted cryoloop (MicroMesh 400/50, Jena Bioscience) the crystals were harvested, stored in liquid nitrogen and measured at the BESSY II in Berlin (Helmholtz Zentrum Berlin, DE) using the MX\_beamline\_14.1. The BL14.1 is a tunable energy beamline for macromolecular crystallography. It can perform X-ray diffraction experiments of very small crystals up to 15 µm (for further properties of the beamline see Table 3.11). The crystallisation experiments were performed in the laboratory of Prof. Dr. Axel Scheidig ('Zentrum Molekulare Biowissenschaften', University of Kiel, DE) and supported by Dr. Annette Faust.

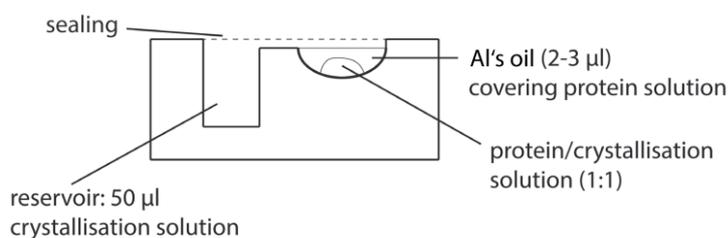


**Figure 3.8: Side view of under oil crystallisation batches.**

The protein (in MES buffer) was mixed with the same amount of crystallisation buffer (Bis-Tris) and covered by oil. A neighbouring reservoir was filled with 50 µl crystallisation buffer and the batch was sealed with plastic tape.

**Table 3.11: Properties of the BL14.1 beamline.**

<b>Beamline data</b>	
Source	7T-WLS-2
Monochromator	KMC-1
Energy range	5- 15.5 keV
Energy resolution	2 eV
Flux	$1.4 \cdot 10^{11}$ (Photons/s/100mA)
Polarisation	Horizontal
Divergence horizontal	0.5 mrad
Divergence vertical	0.5 mrad
Focus size (hor. x vert.)	170x90 $\mu\text{m}$
	110x90 $\mu\text{m}$
	80x70 $\mu\text{m}$
	60x50 $\mu\text{m}$
	40x30 $\mu\text{m}$
Distance Focus/last valve	300 mm
Height Focus/floor level	1400 mm
Free photon beam available	Yes
Fixed end station	Yes

### 3.2.3 Protein biochemistry

#### 3.2.3.1 Lysis of cells and tissue

Cells harvested from cell culture dishes were pelleted (1,500 g, 4°C) and lysed in a lysing buffer, which is specific for each experiment. As a standard lysis buffer PBS (pH7.4) including protease inhibitors (Complete®, Roche) and 1 % of the detergent triton-x-100 was utilised. For Co-IP the cells were lysed in EBC-buffer (Table 7.6). Depending on the size of the cell pellets 20-150  $\mu\text{l}$  lysis buffer was applied and the samples were sonicated 2 x 10 seconds, incubated on ice for 30 minutes and sonicated again 2 x 20 minutes. Lysates were then centrifuged at 17,000 g for 10 minutes at 4°C. The lysed cell sample (supernatant) was transferred to a clean tube and used for protein concentration quantification (see next paragraph).

In addition, a special lysing buffer and a sequential extraction protocol was used for cells and tissue analysed for  $\alpha$ -synuclein (brain samples and H4 cells). For studies of midbrain and pons it was distinguished between soluble and insoluble fractions utilising two different buffer systems (triton-x-100 and Sodium-Dodecyl-Sulfate (SDS)) carried out as described in Mazzulli *et. al*, 2006. Briefly, cells/brains were lysed in triton buffer (10 volumes; 1 % triton x-100, 20 mM HEPES, 10 % glycerol, 150 mM NaCl, 1 mM  $\text{MgCl}_2$ , 50 mM NaF, 2 mM  $\text{NaVO}_3$ , protease inhibitors; pH 7.4). Lysates were subjected to 4 freeze and thaw cycles (on dry ice) and ultracentrifuged (Optima™ TLX ultracentrifuge, Beckman) at 100,000 g for 30

minutes. This step was repeated twice and the two supernatants were pooled as the triton soluble fraction. The remaining pellets were lysed in 5 volumes of SDS-lysis buffer (2 % SDS, 50 mM Tris-HCl-pH7.4), boiled for 10 minutes, sonicated 4 times with 3 seconds pulses, at 50 % power, boiled for 10 minutes and centrifuged at 20,000 g for 30 minutes, resulting in the SDS (insoluble) fraction.

### 3.2.3.2 Protein quantification

Protein quantification was performed by using a BCA-kit (Pierce <sup>TM</sup>, Thermo Fisher Scientific) according to the manufacturer's manual. This method relies on the ability of proteins containing 3 or more amino acids to reduce  $\text{Cu}^{2+}$  to  $\text{Cu}^{+}$  in an alkaline medium. Subsequently the  $\text{Cu}^{+}$  reacts with the bicinchoninic acid (BCA) resulting in a purple-coloured reaction product. The absorbance can be measured in a plate reader (Synergy HAT, BioTek) at a wavelength of 562 nm together with a standardised protein curve.

### 3.2.3.3 Deglycosylation of proteins

Glycoproteins like LIMP-2 and GC can be characterised by two enzymes able to cleave N-linked glycosylations: endoglycosidase H (endo H) and Peptide-N-Glycosidase F (PNGase F). Both enzymes exhibit a unique specificity in the digestion of N-glycosylations, which makes it possible to monitor protein trafficking. The core N-glycosylation occurs in the ER, where the glycoproteins are still sensitive to endoglycosidase H digestion (high mannose and hybrid structures; Figure 3.9). After entering the Golgi-compartment complex modifications are made to the glycans (complex glycan structures; Figure 3.9) and the proteins get resistant to EndoH digestion. In contrast the PNGaseF enzyme is still able to cleave these complex N-linked carbohydrates and thus provides a positive control for digestion assays (Figure 3.9).

To study the subcellular localisation and transport of the various GC mutants (ER, post ER localisation) an endoglycosidase H as well as PNGaseF digestions were performed utilising a glycosidase-kit from New England Biolabs (NEB). For both reactions 20  $\mu\text{g}$  of protein was applied and the experimental procedure was performed according to the manufacturer's handbook (NEB). Briefly, the protein samples were denatured by adding a denaturing buffer and boiling the samples (95°C, 10 minutes). After cooling down 1  $\mu\text{l}$  of the enzyme (EndoH/PNGaseF) was applied together with the respective amount of buffer and incubated at 37°C for 1 hour. Reducing laemmli buffer (appendix Table 7.9) was added to the samples, heated at 60°C for 20 minutes and analysed by SDS-PAGE and immunoblotting. A positive digestion resulted in a molecular size shift of the protein.

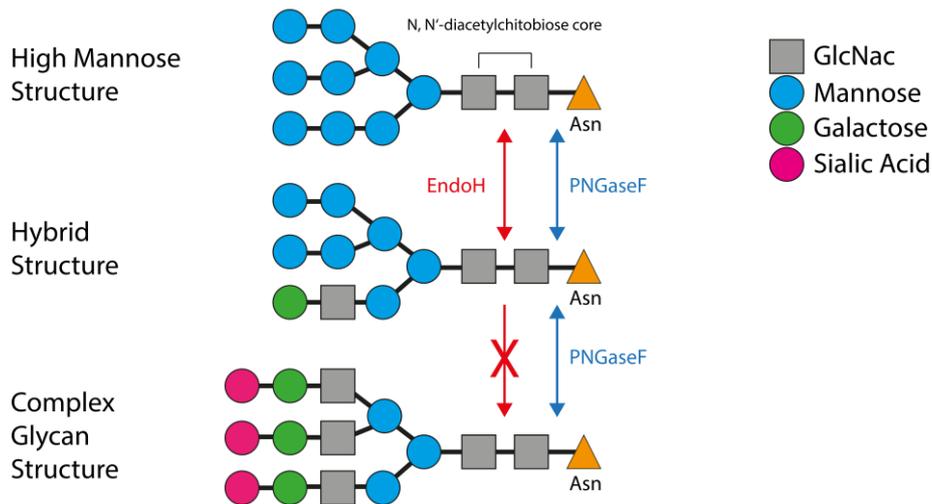


**Figure 3.9: Illustration of endoglycosidase H/PNGaseF cleavage.**

N-Glycosylation is protein modification and occurs in the ER resulting in high mannose carbohydrate chains. Endoglycosidase H (endoH) and PNGaseF are able to cleave the glycosylation chains. During protein trafficking from the ER to the Golgi compartment, modifications on the carbohydrate chains take place. A hybrid glycan structure is still cleaved by both enzymes, whereas the complex glycan residue is only sensitive to the PNGaseF enzyme. Since this form of glycosylation can only be found in the Golgi, it is possible to monitor protein trafficking by performing endoglycosidase H digestion. Illustration was modified from [www.promega.de](http://www.promega.de).

### 3.2.3.4 Co-immunoprecipitation (Co-IP) studies

Co-IP studies are performed to analyse the interaction of one protein with another. Hereby one target protein is precipitated utilising a specific antibody. In this study LIMP-2 was precipitated and the ability of its interaction with GC and numerous GC mutants was assessed. For Co-IP studies cells were lysed in EBC-buffer (Table 7.6) including protease inhibitor (complete®, Roche). Next, 500-1000 µg protein lysate (approximately one 10 cm cell culture dishes needed) was incubated with 1.5 µl of LIMP-2 antibody overnight at 4°C. At the same time the 30 µl/sample magnetic agarose G beads (Thermo Fisher Scientific, Life Technologies) were blocked with 1 % BSA. The next day the beads were incubated with the lysate/antibody mixture for 30 minutes at room temperature. During this step the antibody interacts with the protein G of the beads. Subsequently, the beads were washed 4 times with 200 µl EBC buffer/complete. The supernatant was discarded and the beads were incubated with 60 µl of 1x Laemmli and heated at 60°C for 15 minutes. Finally, the Co-IP samples were analysed by SDS-PAGE and immunoblotting (see following chapters). The co-precipitated GC was visualised using an anti-human GC antibody (Table 3.2).

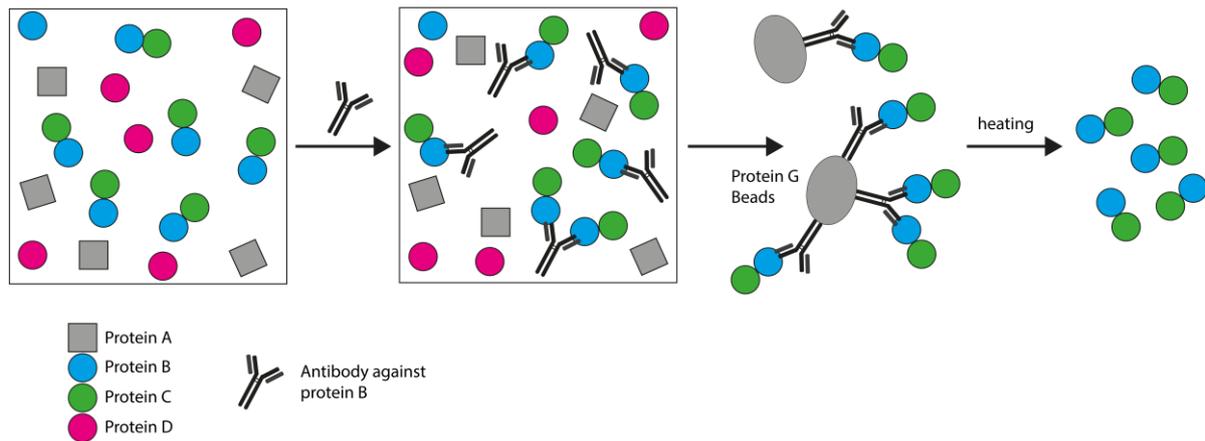


**Figure 3.10: Principle of Co-Immunoprecipitation.**

A sample containing a mixture of proteins (A, B, C and D) is incubated with an antibody against protein B (blue). Since protein B interacts with protein C (green), both proteins get precipitated by the antibody. Protein G agarose beads then interact with the antibody. The agarose beads can be precipitated by centrifugation and the proteins are released from the antibody by heating. In this way a primary and secondary target of the antibody can be precipitated from a protein mixture (e.g. cell lysate).

### 3.2.3.5 SDS-PAGE

Sodium dodecyl sulfate polyacrylamide gel electrophoresis (SDS-PAGE) is a technique to separate proteins according to their molecular weight regardless of their electric charge. Extracted proteins were denatured beforehand in a SDS-containing reducing buffer containing DTT (Laemmli, see appendix Table 7.9). The protein samples were then heated at 60°C for 10 minutes. Samples for  $\alpha$ -synuclein analysis were incubated 10 min. at 95°C. Together with a protein-size standard (Thermo Fisher Scientific) the protein samples were loaded on a polyacrylamid gel (10% selfmade and 4-12% NuPAGE gradient gels; Thermo Fisher Scientific, Life Technologies) and exposed to voltage: 120 V for first 10 minutes followed by 140V.

### 3.2.3.6 Western Blotting

To visualise proteins by antibodies after separation by SDS-PAGE, the proteins were transferred onto membranes (nitrocellulose (GE Healthcare) and PVDF for  $\alpha$ -synuclein) by applying voltage. The PVDF-membranes (Millipore) are equilibrated in methanol before use. In this study the TANK-blot system was performed. The SDS-gels were assembled with the respective membrane together with *whatman*-filter papers between cathode (-) and anode (+) as shown in figure 3.10. The complete ‘sandwich’ of SDS-gel, membrane and filter papers was placed in a TANK-blotting chamber (Bio-Rad), filled with blotting buffer and subjected to voltage as follows:

- 1) Over night (4°C): 20 V constant; next morning: 30 mins 70 V
- 2) 2hrs (4°C): 0.85A constant
- 3) 1 hr (4°C): 100 V constant

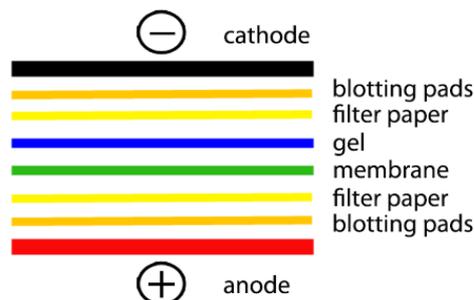


**Figure 3.11: Set-up of TANK-blot system.**

In a tank-blot system proteins are transferred from the SDS-gel to membrane by attaching voltage. This picture illustrates the assembly of the SDS-gel, the respective membranes and filter papers between the cathode and anode.

After transferring the proteins onto membranes they were blocked for 30 minutes at room temperature in 5 % milk in TBS-T. For studying  $\alpha$ -synuclein the membranes were post-fixed 20 minutes in 0.4 % PFA (room temperature) before blocking in milk.

### 3.2.3.7 Incubation with antibodies and stripping of immunoblots

After blocking the membranes with milk, they were subjected to antibody incubation. The antibodies were diluted in the respective concentration (Table 3.2) in 5 % milk in TBS-T (0.1 % tween-20). Primary antibodies were incubated overnight at 4°C. After three washing steps in TBS-T the membranes were incubated for 1 hour with the respective secondary antibody at room temperature. This antibody was diluted 1:10,000 in 5 % milk (TBS-T) and linked to a horseradish peroxidase (HRP). After washing the membrane three times, the signal of the antibody was detected in a chemiluminescence detection system (LAS4000, Fujifilm). Hereby a chemiluminescent substrate (ECLadvanced, Amersham) was applied. The antibody bound peroxidase (HRP) converts hydrogen peroxide to water and reactive oxygen, which oxidises luminol. This oxidation is followed by a release of light, which is detected by the detection system.

For re-probing the membrane with another antibody it is possible to strip off the initially bound antibodies. The membranes were incubated either in stripping buffer containing  $\beta$ -mercaptoethanol ( $\beta$ -ME) or SDS (Table 7.9). For stripping in the  $\beta$ -ME containing buffer, the membranes were heated to 70°C for 20 minutes, and subsequently washed in ddH<sub>2</sub>O and TBS-T until the smell of  $\beta$ -mercaptoethanol was negligible. The membranes were incubated in the SDS-stripping buffer (pH 2.2) for 1 hour at room temperature. After both stripping protocols

the membranes were blocked again in 5 % milk in TBS-T and re-probed with a new round of primary and secondary antibodies as described above.

### **3.2.3.8 Coomassie stainings**

After subjecting proteins samples to SDS-PAGE analyses, it is also possible to visualise proteins in-gel by incubation of the SDS-gels with a coomassie blue staining. This stain is a triphenylmethan dye and binds to all basic side chains of amino acids.

SDS-gels were incubated with coomassie brilliant blue (R-250, Bio-Rad) for 30 minutes at room temperature. Subsequently the gels were destained with a destaining solution containing 10 % methanol and 10 % acetic acid until the background signal was negligible. Gels can be kept in water at 4°C for a few days and scanned for analysis.

### **3.2.3.9 Densitometric analysis of immunoblots/coomassie-stained SDS-gels**

The signal intensities released from individual protein bands either by indirect chemiluminescence reactions or by direct protein stains with coomassie can be determined. Usually for immunoblot-analysis the band intensity was normalised to the respective signal of the loading control. For statistical analysis the intensity of each individual protein band, the Image J software (Table 3.12) was utilised. A rectangle was placed around the signals and the intensity was calculated by integral calculus. In addition the background signal was subtracted from the signal of the protein band.

### **3.2.3.10 Enzyme activity assay**

Using artificial substrates the activity of enzymes (for example hydrolases) can be assessed. In this study 4-nitrophenyl-conjugated carbohydrates were applied. The activity of enzymes leads to the hydrolytic cleavage of both components (sugar and 4-nitrophenyl) under acid pH. When a basic stop solution was added the reaction of the enzymatic reaction was stopped and the p-nitrophenols become fully deprotonated. This leads to a yellow colour shift, which can be detected in a plate reader (Synergy HAT, BioTek) at 405 nm.

In this study activity of GC and  $\alpha$ -mannosidase (LAMMAN) were measured using 10 mM 4-nitrophenyl  $\beta$ -D-glucopyranoside and 10 mM p-nitrophenyl-N-acetyl- $\beta$ -D-glucosaminide, respectively. The artificial substrates were solved in citrate buffer (0.2 M Na-Citrate, 0.4 % BSA, pH 4.6). All activity assays were performed in 1.5 ml Eppendorf tubes and in duplicates.

To assess the enzymatic activity of cell or tissue lysates 20-200  $\mu$ g of protein was applied to and incubated with 100  $\mu$ l of the specific substrate. To determine GC activity the assay was

incubated approximately 2 hours at 37°C and for  $\alpha$ -mannosidase activity the assay was incubated for 5 hours at 37°C. The reaction was stopped applying 500 – 1000  $\mu$ l of the stop solution (0.4 M Glycine, pH10.4). To determine the enzymatic activity of the recombinant enzymes 0.2 nmol of Cerezyme ® and LAMAN (Table 3.9) were applied (in absence or presence of 2 nmol LIMP-2-derived peptides) and incubated for 15-30 minutes at 37°C and the enzymatic reaction was stopped as described above. After centrifugation of the samples at full speed for 10 minutes 161  $\mu$ l of the supernatants were pipetted onto a 96 well plate and measured at 405 nm in a plate reader (Synergy HAT, BioTek). The absolute enzyme activities were calculated by using following formula:

$$Activity \left[ \frac{U}{mg} \right] = \left( \frac{\Delta E \times V_{\text{end}}}{t \times \varepsilon \times d \times V_{\text{lysate}}} \right) \div c_{\text{lysate}}$$

U	enzyme activity ( $\mu$ mol/minute)
$\Delta E$	change in absorbance at 405 nm
$V_{\text{end}}$	final volume in the reaction tube
$V_{\text{lysate}}$	volume of lysate used
d	path-length of 1 cm
T	time in minutes
$\varepsilon$	molar absorption coefficient

### 3.2.3.11 In vivo lysosomal activity assay

Since the above described activity assay only detects GC activity in whole cell lysates, the development of an assay where it could be distinguished between lysosomal and non-lysosomal enzyme activity has advantages. Furthermore this newly developed assay is able to measure enzyme activity in living cells by pulse-chasing a fluorescent substrate.

GC activity was also assessed in living H4-cells as well as in living human midbrain neurons. Cells were plated in 96 well dishes (BD, black well) at  $8 \times 10^4$  cells/well. On the day of the assay, neurons were treated with DMSO or lysosomal inhibitor bafilomycin A1 (Calbiochem, Millipore) at 200 nM for 1 hr. Subsequently, cells were loaded with 100  $\mu$ g/ml of the cell-permeable artificial enzyme substrate 5-(pentafluoro-benzoylamino) fluorescein di- $\beta$ -D-glucopyranoside (PFB-FDGlu) (Thermo Fisher Scientific, Life Technologies) that fluoresce upon cleavage. After 1 hour of incubation of the substrate the cells were washed with warm media 3 times, and replaced with fresh media. The fluorescence intensity was recorded every 30 minutes for 3-4hrs in a spectramax i3 plate reader (Molecular Devices) (PFB-FDGlu: Ex=485nm, Em=530nm). After the final read, cells were fixed in 4% formaldehyde / PBS, stained with draq5 and sapphire 700 as described (Mazzulli, Xu et al. 2011) to ensure for integrity of cells and measure cell volume. The plate was scanned on an odyssey infrared imager (Li-cor). Fluorescence intensities were graphed as fluorescence intensity versus the

time, and analysed by measuring the area under the DMSO and bafilomycin (Baf) curves (AUC). Total cellular activity was obtained by calculating the AUC of the DMSO curve. Non-lysosomal activity was obtained by calculating the AUC of the bafilomycin curve. And lysosomal activity was obtained by subtracting the AUC of the bafilomycin from the DMSO curve (Figure 3.12).

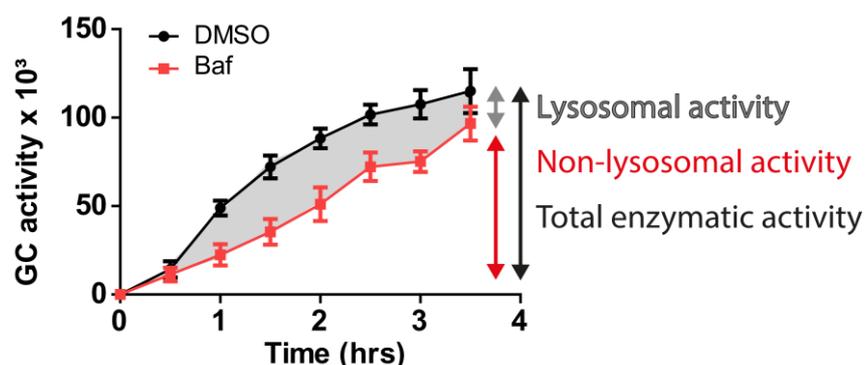


**Figure 3.12: Principle of measuring and calculating lysosomal GC activity.**

Living cells were chased with a fluorescent artificial substrate and GC activity was measured on a plate reader over 3.5 hours. Cells treated DMSO (black) exhibit total cell activity, whereas cell treated with the lysosomal inhibitor bafilomycin (Baf; red) reveal the non-lysosomal activity. For calculation of the lysosomal activity the areas under the curves (AUC) were calculated. By subtracting the non-lysosomal (Baf) AUC from the total (DMSO) AUC, the lysosomal activity could be determined (grey area).

### 3.2.4 Cell biological methods

#### 3.2.4.1 Cultivation of adherent cells

The cells utilised in this work are listed in table 3.1 and were kept consistently in an incubator at 37°C and 5 % CO<sub>2</sub>. The cells were maintained in the respective media additionally containing 1 % Penicillin/streptomycin and 10 % FCS (see 3.1.1 and appendix Table 7.7) and grown on 6 to 10 cm cultivation dishes. For immunofluorescence studies cells were grown on glass coverslips in 6 well dishes. To maintain the cells in cell culture over a longer time period they were passaged (usually 1:10) by adding 0.5 – 1 ml trypsin (0.5 mg/ml)/EDTA to the cells. After incubation of 10-30 min at 37°C the cells detached from the cell culture dish and could be cultivated in a new dish with fresh media. To prevent contamination, all cell culture work was performed under a sterile hood utilising only sterile utensils.

*H4 cells:* The H4 cell line (human neuroglioma) stably overexpresses wild-type  $\alpha$ -synuclein under the control of a tetracycline-inducible promoter (“tet-off”). Cells were cultured in OptiMEM® media (Thermo Fisher Scientific, Life Technologies). To suppress *de novo*  $\alpha$ -synuclein transcription the H4 cells were treated with 2  $\mu$ g/ml of doxycycline (Invitrogen).

For the  $\alpha$ -synuclein turnover assay cells were harvested after 0, 8, 24, 48 and 72 or 74 hours of doxycycline treatment (ice cold PBS with protease inhibitors) and lysed in a triton-x-100 lysis buffer (Mazzulli, Xu et al. 2011) (refer also to 3.2.3.1) and prepared for western-blot analysis as well as GC activity assays.

### **3.2.4.2 Transfection of cells**

Transfection is the process of introducing nucleic acids into eukaryotic cells. Transfection of animal cells typically involves opening transient pores in the cell membrane to allow the uptake of material. This can be achieved by mixing a cationic lipid with the material to produce liposomes. These then fuse with the cell membrane and deposit their cargo (e.g. DNA plasmids) inside the cell. Cells given in 3.1.1 were transfected with plasmids utilising Turbofect® (Thermo Fisher Scientific), FuGene® HD (Promega) or Polyethylenimin (PEI; Sigma). Standard cell lines as Cos7, HeLa and N2a cells were transfected using PEI or Turbofect®. For murine and human fibroblasts like GC-deficient and LIMP-2-deficient MEF cells and fibroblasts from patients, FuGene was utilised for transfection. The respective amount of plasmid DNA (3  $\mu$ g for a 10 cm dish and 1  $\mu$ g for a 6 cm dish) was incubated with twice (Turbofect and PEI) and three times (FuGene) the amount of transfection reagent and incubated for 20 minutes in 100 – 500  $\mu$ l DMEM only (without any addition of FCS or antibiotics) before pipetting the transfection sample on the cells. When Turbofect or PEI was applied for transfection the cell culture media was changed after ~6 hours. The constructs were expressed 24 – 72 hours (depending on the expression constructs).

### **3.2.4.3 Transduction of neurons**

Since neurons do not undergo any cell division, they were transduced utilising a lentiviral strategy. This experiment was carried out in the laboratory of Dr. Dimitri Krainc (to that time: Medical School Harvard/MGH, Boston, USA). The cloning and establishing of the lentivirus was done by Dr. Joseph R. Mazzulli (to that time: Medical School Harvard/MGH, Boston, USA) and the procedures have been described in detail in Mazzulli, Mishizen et al., 2006. Briefly, the supernatant from transfected HEK-FT cells was concentrated 500 times in neurobasal medium containing 10% fetal bovine serum. Viral titers were determined using a p24 ELISA kit (Zeptomatrix). Aged human midbrain dopaminergic neurons (> 90 days old) were grown in 96-well plates and infected with lentiviral constructs. Analysis of lentiviral experiments were done at 14 days post infection at a multiplicity of infection (MOI) of 5 for wild-type- $\alpha$ -synuclein. Expression of the construct was verified by western blot analysis (data

not shown here). Furthermore cells were subjected to live cell lysosomal GC activity assays (as described in section 0).

#### **3.2.4.4 Cryopreservation and thawing of cells**

Cells can be cryopreserved in liquid nitrogen. Adherent cells were trypsinised as described above and resuspended in freezing media (see appendix Table 7.7). The cells were centrifuged at 200 g for 10 minutes in a tabletop centrifuge (Universal 32, Typ 1605, Hettich) and the pellet was resuspended in 1 ml freezing media per 10 cm dish (each ~80 % confluency) and transferred into cryotubes. The cells were gently frozen by cooling them down on ice, dry ice and for 24 hours at -80°C. The next day the cells were frozen and stored in liquid nitrogen.

For thawing the samples, cryotubes were removed from the liquid nitrogen tank and slightly opened. Cells were incubated shortly in a 37°C water bath and subsequently suspended in 5 ml fresh media. The samples were then centrifuged at 200 g for 10 minutes and the pellet was dissolved in fresh media and plated on 10 cm dish. The next day the cells were briefly washed with PBS and the media was changed again.

#### **3.2.4.5 Harvesting of cells**

Before harvesting the cells were washed two times in PBS in order to remove residual media. Then 1 ml of ice cold PBS including a cocktail of protease inhibitors (Complete®: 1 tablet in 50 ml PBS; Roche) was applied and cells were scraped on ice using a cell scraper. Subsequently cells were pelleted at 1,500 g for 10 minutes (4°C). The pellets were either stored at -20°C or directly processed by lysing in the respective lysing buffer (see section 3.2.3.1).

#### **3.2.4.6 Uptake assays with recombinant enzymes/LIMP-2-derived peptides**

For the uptake of recombinant GC and LIMP-2-derived peptides three different cell lines were utilised: The murine macrophage cell line J774E, GC-deficient MEF cells and the human brain neuroglioma cell line H4. In initial experiments J774E cells were incubated with 50 µM peptides applied to 2 ml media in a 6 cm dish and incubated for ~12 hours. To control for the uptake of the peptide, cells were prepared for immunofluorescence studies using a fluorophore-labelled (Alexa Fluor, 488 nm) antibody targeted against biotin (1:200; Jackson Immuno Research). In a second approach GC-deficient murine fibroblasts were incubated with 0.2 nmol of recombinant GC (Genzyme) pre-incubated with 10x molar amount of peptides (2 nmol). The mixture was incubated in a total amount of 40 µl 50 mM NaPhosphate buffer including 100 mM NaCl (pH7) and incubated at least 2 hours at room temperature or

overnight at 4°C. Subsequently the protein/peptide mixture was added to 2 ml cell medium in a 6 cm dish. Success of uptake was confirmed by SDS-PAGE and immunoblotting (see chapter 3.2.3.6) utilising an anti-mGC antibody (Sigma, 4171, Table 3.2).

H4 cells constantly overexpressing  $\alpha$ -synuclein were incubated with 2 nmol of uptake-optimised TAT-peptides (helix 5 and 3xD helix 5; see 3.2.2.1) in 2 ml cell medium of a 6 cm dish. New TAT-peptides were applied to the cell media every 24 hours if a longer incubation time was needed.

### 3.2.5 Microscopical methods

#### 3.2.5.1 Fixing and staining of cells for immunofluorescence

Applying an immunofluorescence (IF) staining protocol proteins can be specifically labelled and visualised by microscopy. For IF stainings of cells, they were grown in 6-well dishes on glass cover-slips. If necessary the cells were treated or transfected according to the established protocols. When reaching a confluency of ~80 % the cells were fixed with 4 % PFA/PBS for 20 minutes at room temperature. Following they were washed three times with PBS. To permeabilise the cells they were incubated 5 minutes in 0.2 % saponin/PBS and subsequently 10 minutes in 0.2 % saponin/0.12 % glycine/PBS at room temperature. To reduce unspecific binding of the antibodies the cells were incubated for 20 minutes in 0.2 % saponin/10 % FCS/PBS. The primary as well as the secondary antibody was diluted in this blocking solution. A dark, wet chamber was prepared, where the primary as well as secondary antibody was pipetted onto parafilm and the coverslip was put on top (the side with the cells facing the antibody drop). The primary antibody was either incubated one hour at room temperature or overnight at 4°C. Before incubating in secondary antibody the coverslips were washed four times in 0.2 % Saponin/PBS. The secondary antibody exhibits a fluorophore-labelling (Alexa Fluor 488 nm, 594 nm or 647 nm) and was applied in a concentration of 1:500 (see Table 3.3) for 1 hour at room temperature. After washing the cover slips three times in 0.2 % saponin/PBS and one time in ddH<sub>2</sub>O they were embedded on microscope slides with a mixture of Dapi/Dabco/Mowiol (see appendix Table 7.10). The next day the samples could be analysed by laser scanning microscopy.

#### 3.2.5.2 Filipin stainings

To stain for free (unesterified) cholesterol in cells a filipin staining was performed. Filipin (Sigma) is a fluorescing antibiotic (extremely sensitive to light), which specifically stains free cholesterol and therefore can be used for molecular studies analysing the cholesterol

metabolism. In this study filipin stainings were performed in cells exhibiting increased cholesterol storage in lysosomes: Niemann-Pick Type C (NPC) patient fibroblasts, LIMP-1/2 double deficient MEF cells and HeLa cells treated with 0.3 – 3.0  $\mu\text{M}$  U18666A for 24 hours according to manufacturer's manual (Cayman Chemicals). This chemical blocks the exit of free cholesterol from lysosomal compartments resulting in cholesterol accumulation (Liscum and Faust 1989). According to each individual protocol the cells were transfected and prepared for immunofluorescence stainings as described above. A 100 x stock of filipin (= 50 mg/ml) was prepared in DMSO and stored in the dark in liquid nitrogen. After fixing the cells in 0.4 % PFA, they were incubated in the dark with 750  $\mu\text{l}$  of filipin solution (1:100 dilution of the filipin stock). The cells were washed with PBS and if needed antibody-stained (following the protocol as described above). Before embedding the coverslips in Mowiol/Dapco (no Dapi, since filipin likewise exhibits blue fluorescence), they were washed three times in ddH<sub>2</sub>O. For visualising filipin the blue Dapi channel was applied at the Axiovert 200 M (Carl Zeiss Jena GmbH). Filipin exhibits an extinction of 240 nm – 380 nm and an emission between 385 nm – 470 nm.

### 3.2.5.3 Microscopical recording

After embedding and hardening of the cover slips, they could be analysed by using confocal laser microscopy (Fluoview 1000; Olympus) or -in the case of filipin stainings- an inverted epifluorescence microscope (Axiovert 200 M; Zeiss). Depending on the utilised secondary antibody and staining of cell the respective laser was utilised. The pictures were taken in the 'sequential mode' to prevent an overlay of the different colour channels. Cells were visualised 60 – 100 times enlarged utilising oil objectives. The pictures were compiled by the FV1000-ASW 3.0 Viewer-Software and exported to Photoshop (Adobe) for further changes e.g. in the contrast.

### 3.2.6 Computer software

**Table 3.12: List of utilised software for data handling and analysis.**

Programme	Supplier
Adobe Illustrator	Adobe Systems Inc., San Jose, US
Adobe Photoshop	Adobe Systems Inc., San Jose, US
Chimera USCF	<a href="http://www.cgl.ucsf.edu/chimera">www.cgl.ucsf.edu/chimera</a>
DNASTAR Lasergene 8	Lasergene, Madison, US
EndNoteX6	Thomson Reuters, Carlsbad, CA, US
Fluo View 1000 ASW 3.0	Olympus, Hamburg, DE
Image J	<a href="http://rsbweb.nih.gov/ij/">http://rsbweb.nih.gov/ij/</a>

---

MS-Office 2010

Microsoft Corporation, Redmond, US

GraphPad Prism 5

Graphpad Incorporated, LaJolla CA, US

---

### 3.2.7 Statistical analysis

All data is expressed as mean  $\pm$  standard error of the mean (s.e.m.), where  $n$  equals the number of independent repetitions of experiment. To determine significance between two groups a two-tailed independent Student's t-test was utilised, if data was parametric. For comparing more than two groups a one-way analysis of variances (ANOVA) was applied. A value of  $p < 0.05$  was considered to indicate statistical significance. \*, \*\* and \*\*\* denote  $p < 0.05$ ,  $p < 0.01$  and  $p < 0.001$ . All statistical calculations were performed in GraphPad Prism 5.01 software (Graphpad Software Inc).

## 4 Results

### 4.1 LIMP-2: What does the crystal structure of its luminal domain tell us?

Since the crystal structure of the extracellular domain of LIMP-2 (amino acids 252-255) was solved in 2013 (Neculai, Schwake et al. 2013), the three dimensional information was applied to analyse the structural and functional characteristics of the protein. For instance it was used to verify the interaction site to its ligand, the lysosomal enzyme GC (see chapter 4.1.3). Furthermore, the LIMP-2 protein exhibits properties pointing to additional function(s) of this lysosomal membrane protein (section 4.1.2). To date only its function as a GC transport receptor has been studied in detail.

Recently an independent crystal structure of LIMP-2 was published, differing mainly by a mannose-6-phosphate (M6P) residue at the end of the N325 carbohydrate chain (Zhao, Ren et al. 2014). This led the authors to the assumption that LIMP-2 is transported in an M6P-dependent pathway to lysosomes (section 4.1.1).

#### 4.1.1 Lysosomal trafficking of LIMP-2: does it need an M6P-tag?

Data on LIMP-2 trafficking consistently showed an M6P-independent transport of LIMP-2 and its ligand GC to the lysosome (Reczek, Schwake et al. 2007, Braulke and Bonifacino 2009). However, a recently solved crystal structure of LIMP-2 is questioning this understanding: in the three-dimensional structure of Zhao *et al.* an M6P-residue is found attached to the carbohydrate chain linked to N325. Experiments using plasmon resonance and fluorescence lifetime imaging led the authors to claim that an M6P-dependent transport of LIMP-2 and GC exists by forming a trimeric complex with the M6P-receptor (MPR) (Zhao, Ren et al. 2014). To resolve the paradox between the previous data and the study by Zhao *et al.*, LIMP-2 trafficking was reanalysed in cell-based experimental set-ups utilising immunofluorescence stainings and immunoblotting. To study the impact of the putative M6P-modification on the lysosomal localisation of LIMP-2, MPR-double-deficient cells (CD-MPR<sup>-/-</sup> / CI-MPR<sup>-/-</sup>) as well as mouse embryonic fibroblasts (MEFs) lacking activity of the phosphotransferase GlcNAc-1PT (Gnptab<sup>c.3082insC</sup>) (Kollmann, Damme et al. 2012) were analysed. The presence of MPRs as well as the GlcNAc-1PT, which catalyses the formation of the M6P-residues, is crucial for proteins, which are trafficked to the lysosomes in an M6P-dependent manner. Immunofluorescence stainings of LIMP-2 together with a lysosomal marker (LAMP-1) were performed, revealing endogenous LIMP-2 in LAMP-1 positive vesicles in all cell types regardless of the presence of MPRs or M6P residues (Figure 4.1).

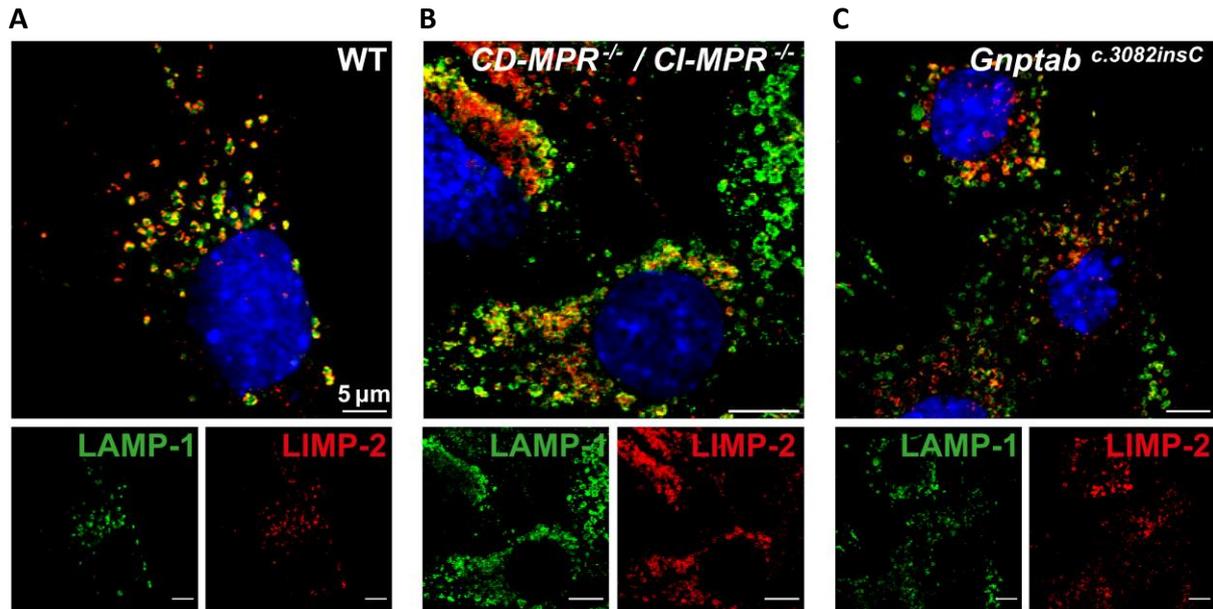


**Figure 4.1: Subcellular localisation of endogenous LIMP-2 in dependence of MPR and M6P.**

Immunofluorescence stainings for LIMP-2 (red) in wild-type MEF cells (A), MPR double deficient cells (CD-MPR<sup>-/-</sup> / CI-MPR<sup>-/-</sup> (B)), and fibroblasts lacking GlcNAc-1PT-activity (Gnptab<sup>c.3082insC</sup>; (C)). A costaining with the lysosomal marker LAMP-1 (green) indicates colocalisation of both proteins (yellow) implying unimpaired cellular transport and lysosomal localisation of LIMP-2 in all three cell types. Scale bars indicate 5 μm.

In another approach, immunoblots of purified liver lysosomes from wild-type, LIMP-2- and GlcNAc-1PT-deficient mice were stained for LIMP-2, its ligand GC as well as NPC2 and LAMP-1 to control for an additional lysosomal membrane protein. The expression level of LIMP-2 and GC were unchanged in GlcNAc-1PT-deficient (Gnptab<sup>c.3082insC</sup>) samples in comparison to wild-type lysosomes. As expected the signal for LIMP-2 as well as the GC protein was strongly reduced in LIMP-2 KO samples (Figure 4.2). This result indicates that lysosomal GC transport is facilitated by LIMP-2, in an M6P-independent manner. Confirming this conclusion, the transport of NPC2 was found to be MPR-mediated, displaying reduced protein levels in the absence of M6P residues (Gnptab<sup>c.3082incC</sup>; Figure 4.2)

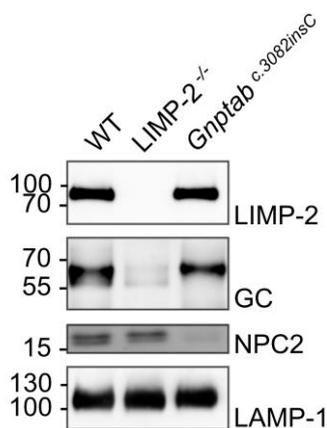


**Figure 4.2: Immunoblot analysis indicating MPR-independent transport of LIMP-2 to the lysosome.**

Western blot staining of lysates from enriched liver lysosomes derived from wild-type (WT), LIMP-2 and GlcNAc-1PT-deficient (Gnptab<sup>c.3082insC</sup>) mice. The GC protein level is unchanged when M6P residues are absent (Gnptab<sup>c.3082insC</sup>). On the other hand no signal for NPC2 could be observed, indicating MPR dependence. No change was seen for the expression level of LAMP-1 in either sample.

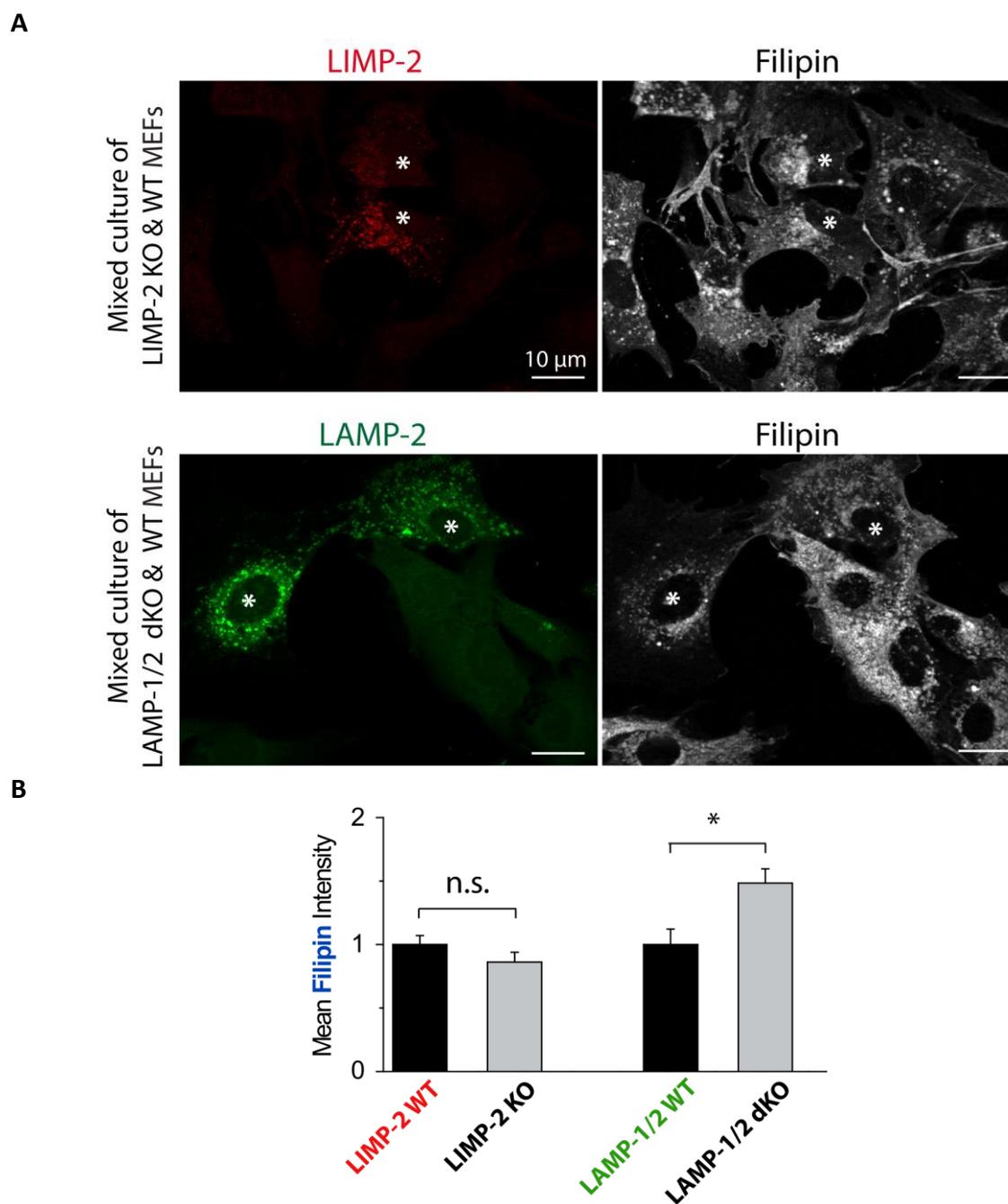
In conclusion, the results clearly reveal a lysosomal localisation of LIMP-2 together with GC independent of the existence of MPRs (CD and CI) or M6P residues. This supports the idea of an M6P-independent trafficking of LIMP-2 and its ligand GC to lysosomes (Reczek, Schwake et al. 2007, Braulke and Bonifacino 2009).

#### 4.1.2 An exciting finding in the three-dimensional structure of LIMP-2: does LIMP-2 exhibit additional functions?

Having solved the crystal structure of the luminal domain of LIMP-2, new structure-function assumptions could be drawn from the three-dimensional protein model. An outstanding finding was the presence of a cavity traversing the entire protein (Figure 1.6), indicating a putative role of LIMP-2 in transport processes.

##### 4.1.2.1 Is LIMP-2 a transporter of cholesterol?

Since members of the CD36 superfamily have been shown to play an important role in lipid transfer, a potential function of LIMP-2 in cholesterol transport was investigated (Rodrigueza, Thuahnai et al. 1999, Liu and Krieger 2002, Rigotti, Miettinen et al. 2003, Neculai, Schwake et al. 2013). To study the impact of LIMP-2 in lysosomal cholesterol transport, filipin stainings were performed on fixed cells. Filipin is an antibiotic able to bind to free (unesterified) cholesterol (Katzenstein, Spielvogel et al. 1974). A mixture of LIMP-2-deficient and wild-type cells was incubated with filipin showing no differences in staining intensities (Figure 4.3). As a positive control LAMP-1/LAMP-2 double-deficient MEFs, known to accumulate free cholesterol in lysosomes were used (Schneede, Schmidt et al. 2011), exhibiting stronger filipin signals when compared to wild-type cells (Figure 4.3). Wild-type cells could be distinguished from knock-out cells using antibodies against the respective endogenous proteins (LIMP-2 or LAMP-2) (Figure 4.3 A). Absence of LIMP-2 did not affect endogenous cholesterol levels.

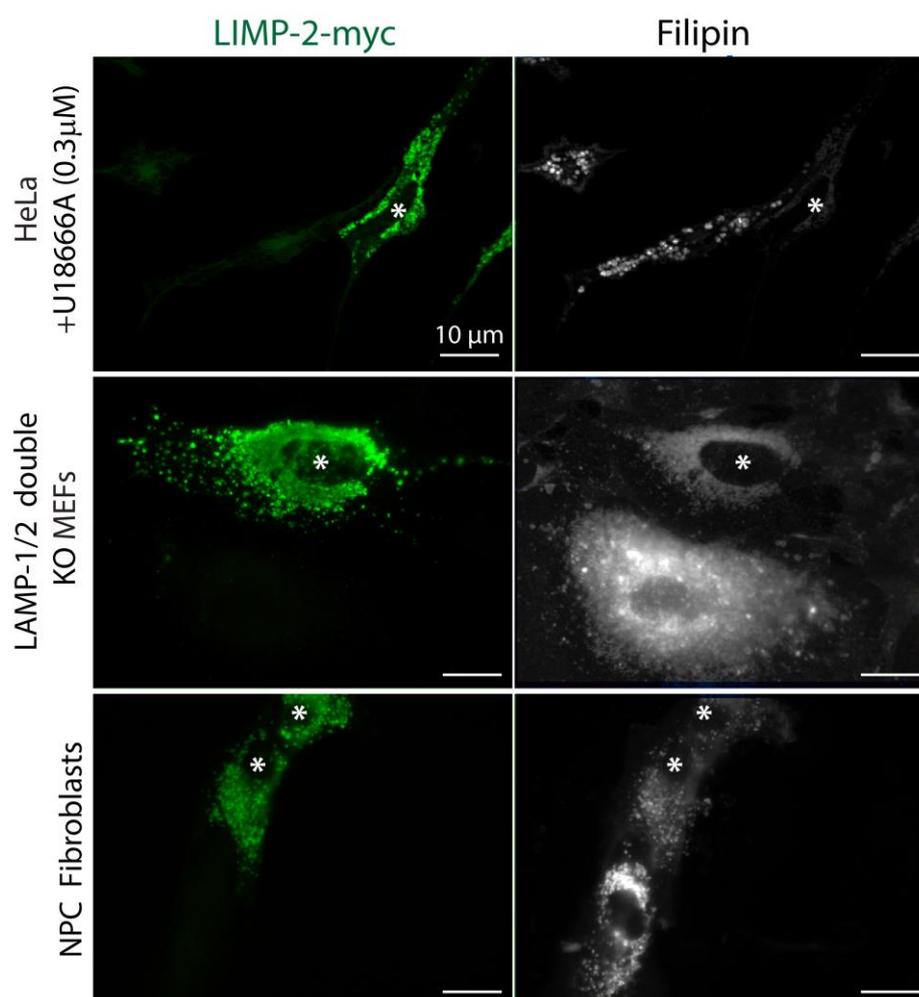


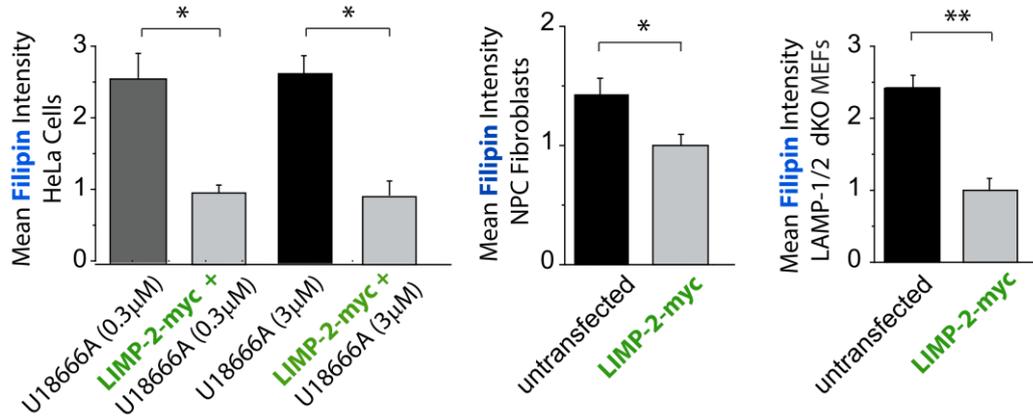
**Figure 4.3: Filipin stainings in LIMP-2 KO and LAMP-1/2 double KO MEFs.**

**A)** Wild-type (WT) and knockout cells were mixed, cultured on coverslips and stained against the respective endogenous proteins (LIMP-2 (red) or LAMP-2 (green)) to identify wild-type cells (indicated by asterisks). Subsequently filipin stainings were performed. **B)** The quantification of the fluorescence intensity of each single cell was performed using ImageJ. Scale bars indicate 10  $\mu$ m. No difference in staining of free cholesterol could be observed between LIMP-2 WT and LIMP-2-deficient cells but a more intense signal could be detected for LAMP-1/2 double knockout (dKO) cells validating the assay. The mean filipin intensity of single cells was normalised to the respective WT cell line. Statistical analysis was performed using an independent two-sided Student's t-test with \* denoting  $p < 0.05$  (LIMP-2 KO:  $n=6-10$  and LAMP-1/2 dKO:  $n=4-7$ ).

Having observed no effect of the LIMP-2 deficiency on endogenous cholesterol, the ability of LIMP-2 to reverse already existing lipid accumulation was assessed in cell systems exhibiting

enhanced lysosomal cholesterol levels. The elevated lipid storage in these cells was induced by treatment with a chemical or by a genetically modified background. In the first experimental setup HeLa cells were incubated with 0.3-3.0  $\mu$ M U18666A for 24 hours, which blocks the exit of free cholesterol from lysosomal compartments resulting in cholesterol accumulation (Liscum and Faust 1989). In this case overexpression of LIMP-2 could reduce the lysosomal cholesterol levels, as revealed by a reduced intensity of filipin staining (Figure 4.4). Secondly, LAMP-1/LAMP-2 deficient cells, which accumulate free cholesterol in lysosomes (Schneede, Schmidt et al. 2011), were transfected with LIMP-2. Cells positive for LIMP-2 exhibited a significant decrease in filipin signal (Figure 4.4). Finally, lysosomal cholesterol accumulation could also be decreased in Niemann-Pick disease type C patient (NPC) fibroblasts positive after overexpression of LIMP-2 (Figure 4.4). For densitometric analysis of the filipin signal intensities see figure 4.4 B on the next page.

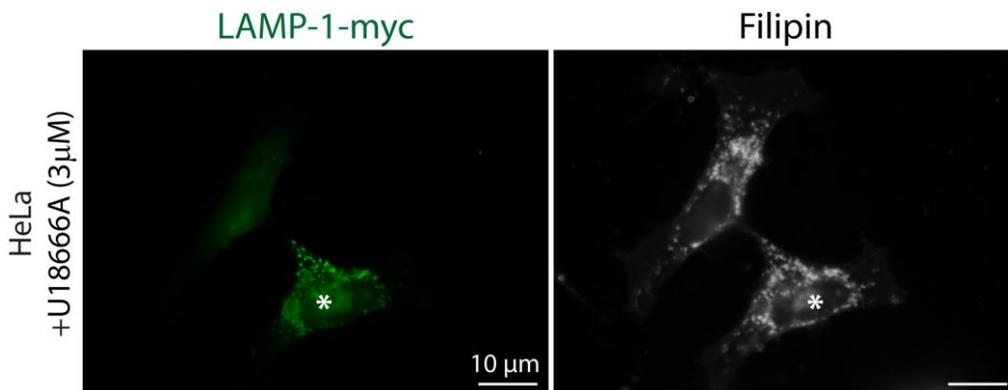
**A**

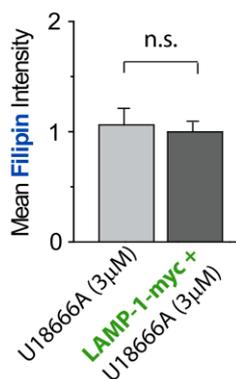
**B**

**Figure 4.4: Filipin staining in HeLa, LAMP-1/2 dKO cells and NPC fibroblasts after overexpression of LIMP-2.**

**A)** Three different cell models with lysosomal cholesterol accumulation were transfected with LIMP-2-myc. Upper panel: HeLa cells were treated with 0.3 mM U18666A for 24 hours, leading to impaired lysosomal cholesterol export and cholesterol accumulation. Cells positive for LIMP-2 (myc; green) were able to overcome this effect and show a significant reduction in the filipin signal. Middle panel: LAMP-1/2 dKO cells, which are characterised by accumulation of cholesterol, show a reduction in filipin signal after transfection of LIMP-2-myc (green). Lower panel: NPC patient cells transfected with LIMP-2-myc (green), show significant reduction in cellular cholesterol, when transfected with LIMP-2. White asterisks indicate cells positive for LIMP-2-myc. Scale bars indicate 10 μm. **B)** Densitometric analysis of mean filipin intensities of single cells was performed in ImageJ. For statistical analysis an independent two-sided Student's t-test was applied. \*, \*\* denote  $p < 0.05$ ; 0.01 (HeLa:  $n = 14-37$ ; LAMP-1/2 dKO:  $n = 6$ ; NPC-fibroblasts:  $n = 6-19$ ).

To control for unspecific effects, for example induced by transfection, HeLa cells were transfected with LAMP-1 and treated with 3.0 μM U18666A for 24 hours. Subsequent filipin stainings revealed no decrease in cholesterol levels in LAMP-1 positive cells in contrast to those after transfection of LIMP-2 (Figure 4.5). The densitometric analysis of the filipin staining can be found on the next page (Figure 4.5 B).

**A**

**B**

**Figure 4.5: Filipin stainings in HeLa cells treated with U18666A after overexpression of LAMP-1.**

**A)** HeLa cells induced with 3µM U18666A for 24 hours were transfected with LAMP-1-myc and stained for the overexpressed protein (anti-myc; green). No effect of LAMP-1 on intracellular cholesterol levels was observed. The white asterisk indicates a LAMP-1 positive cell. Scale bars indicate 10 µm. **B)** Statistical analysis of filipin signals in single cells. A two-sided Student's t-test was applied. n.s.: not significant; n=3.

In the structure of LIMP-2 (Figure 4.6 A) a continuous cavity inside the protein is found, which is known to be large enough to accommodate free or esterified cholesterol (Neculai, Schwake et al. 2013). To further analyse the role of LIMP-2 being involved in direct cholesterol transport, a 'tunnel mutant' was designed. The rationale of this approach was to block the tunnel and perform a rescue experiment as outlined before. The two amino acids V415 and A379 are located within the tunnel pointing towards the inside of the cavity (see magnification in Figure 4.6 A). Both amino acids were substituted with a bulky tryptophan (V415W, A379W) aiming to block the putative channel. An endoglycosidase H digestion reveals post ER localisation of the mutant similar to the LIMP-2 wild-type situation, indicating structural integrity of the mutant protein (Figure 4.6 B). The ability of this mutant to transport cholesterol was verified in a similar set-up as shown above. HeLa cells were transfected with the LIMP-2 tunnel mutant (anti-myc; green) and treated with 3.0 µM U18666A for 24 hours. The subsequent filipin staining revealed no differences between untransfected cells and cells positive for the 'tunnel mutant' (Figure 4.6 C). This indicates that the mutant is not able to rescue the lysosomal cholesterol accumulation as observed for the LIMP-2 wild-type. Additionally, these results point to a direct transport of the lipid through the hydrophobic cavity of the LIMP-2 protein.

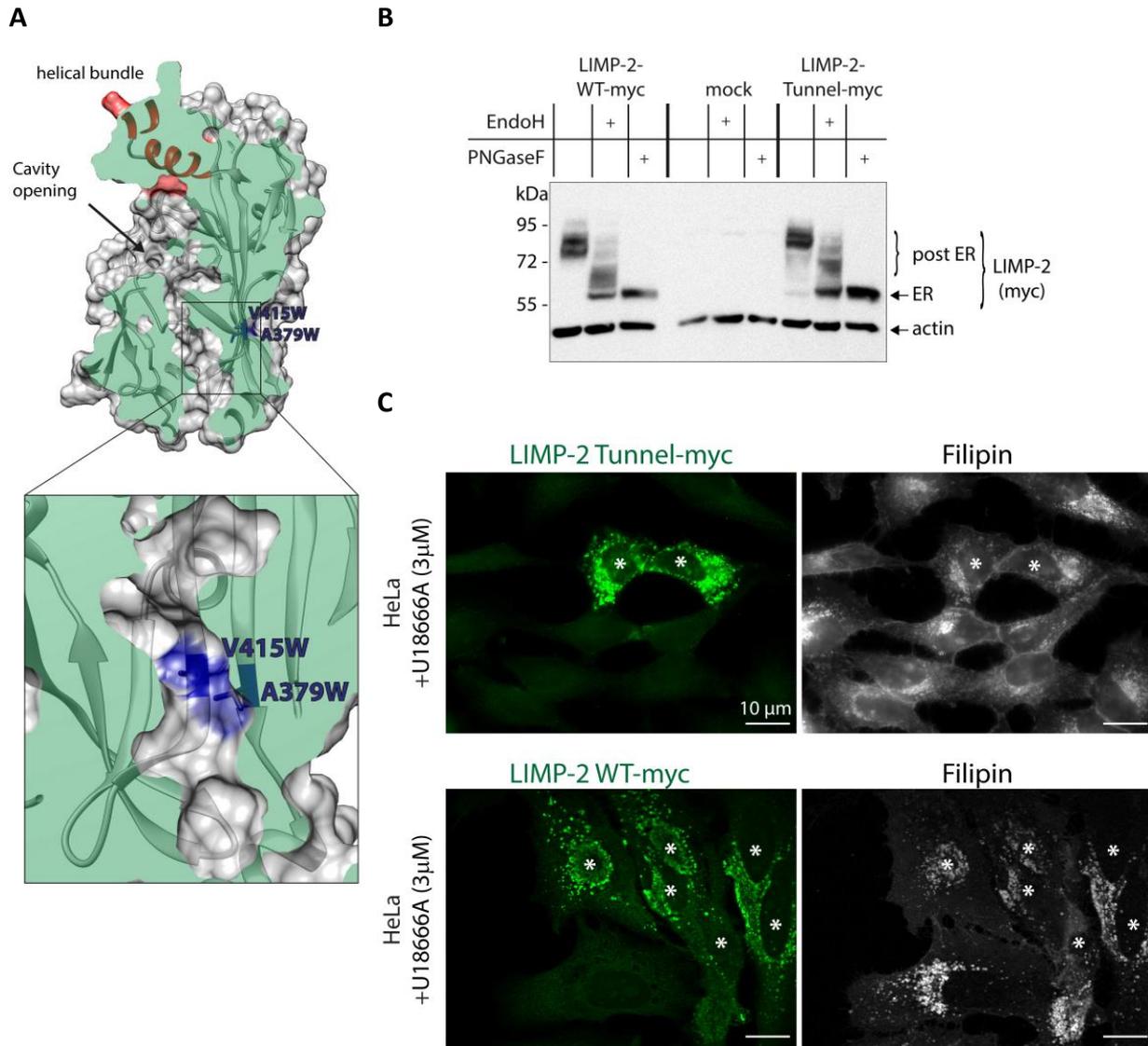


**Figure 4.6: Mutational analysis of the LIMP-2 tunnel mutant (V415W, A379W).**

**A)** The protein model reveals a cross section of the ectodomain of LIMP-2 visualising a tunnel traversing the whole protein. The opening to the cavity is indicated by an arrow and the helical bundle is depicted in red. Amino acids V415 and A379 (blue) are located at a narrow part of the cavity. Both amino acids were substituted to a tryptophan. A box indicates the area of magnification. Molecular illustrations were performed using UCSF Chimera; (PDB: 4F7B). **B)** Immunoblot analysis of endoglycosidase H and peptide-N-Glycosidase F (PNGaseF) digestions of LIMP-2 WT (myc) and LIMP-2 tunnel (myc) mutant lysates (V415W, A379W) revealing comparable post ER and ER-protein levels. The PNGaseF digestion was applied to control for a complete digestion. **C)** HeLa cells were transfected with the LIMP-2 wild-type and tunnel mutant (anti-myc; green) and treated with 3  $\mu$ M U18666A for 24 hours. Cells were stained for free cholesterol with filipin showing no differences in staining intensities. Transfected cells are marked with white asterisks. Scale bars indicate 10  $\mu$ m.

This result part can be summarised as follows: firstly, no endogenous free cholesterol accumulation could be observed in LIMP-2-deficient MEFs. Secondly, overexpression of the LIMP-2 wild-type protein was able to rescue lipid storage when lysosomes were loaded with cholesterol. Thirdly, there are indications that the tunnel traversing the entire LIMP-2 protein is directly involved in cholesterol transport.

#### 4.1.3 A closer look: where exactly is the GC-binding site on LIMP-2?

An outstanding finding in the crystal structure of LIMP-2 (PDB: 4F7B) was the identification of a distinct and apical ‘helical bundle’ consisting of helix 4, 5 and 7. This triple-helical fold is found opposite of the transmembrane domains. Finally, especially helix 5 and 7 seem to be predestined for protein interaction due to their highly exposed position (Figure 4.7).

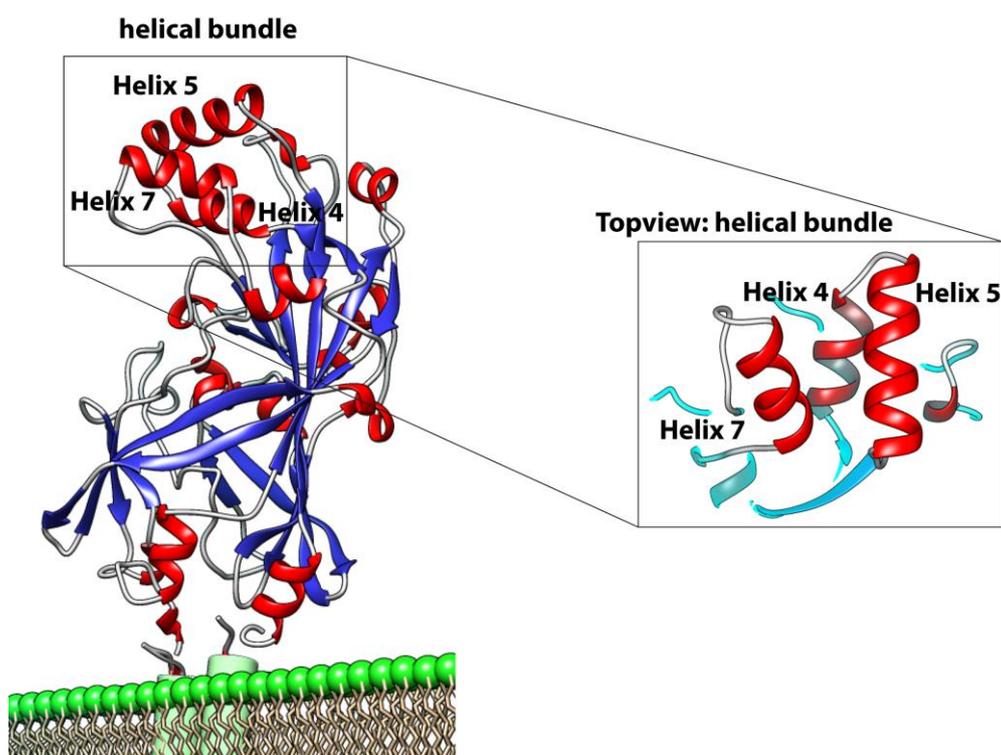


**Figure 4.7: Crystal structure of LIMP-2 with an exposed helical bundle.**

The crystal structure of LIMP-2 (PDB: 4F7B) (Neculai, Schwake et al. 2013) presented in a ribbon view with  $\alpha$ -helical structures shown in red,  $\beta$ -sheets highlighted in blue. An enlargement of the helical bundle shows the orientation of helix 4, 5 and 7 indicating helix 5 and 7 being most surface exposed. The transmembrane domains of LIMP-2 (green) and the lysosomal membrane were modelled into the crystal structure by using UCSF Chimera.

##### 4.1.3.1 Characterisation of the LIMP-2-GC binding mutants

Since helix 5 and 7 of the helical bundle in LIMP-2 were suspected to be important for the interaction with GC, site-directed mutagenesis was applied. Subsequently the mutants were characterised regarding their subcellular localisation and GC-binding properties. Single point mutations were introduced into helix 5 and 7 of the helical bundle of LIMP-2. To disturb the hydrophobic character of the proposed GC-binding site, hydrophobic amino acids were substituted by negatively charged aspartates (D) (Helix 5: L155D, I156D, M159D, L160D, A162D, Y163D and helix 7: L184D, L187D, F191D, see also Figure 4.10 A, B). The protein integrity of the resulting mutants was verified by analysing their cellular localisation utilising

immunofluorescence microscopy (Figure 4.8) and endoglycosidase H digestion (Figure 4.9, see also 3.2.3.3). For immunofluorescence stainings Cos7 cells were transfected with myc-tagged LIMP-2 mutants. The cells were labelled with an antibody against myc (red) and for the lysosomal membrane protein LAMP-2 serving as a lysosomal marker. All analysed LIMP-2 constructs with mutations in helix 5 and helix 7 co-localised with endogenous LAMP, confirming their correct lysosomal localisation (Figure 4.8). In addition, endoglycosidase H and peptide-N-Glycosidase F (PNGaseF) digestions were performed after transfection of the LIMP-2 mutants into Cos7 cells. Comparable to the LIMP-2 wild-type, all helix 5 mutants (L155D, I156D, M159D, L160D, Y163D) showed partial resistance to the endoglycosidase H (Figure 4.9). Sensitivity to endoglycosidase H indicates ER localisation of proteins. Since insensitive to the enzyme suggests a post ER localisation, it can be concluded that the helix 5 LIMP-2 mutants have left the ER comparable to wild-type LIMP-2 (Figure 4.9). The helix 7 mutants (I184D, L187D, F191D) were also found in post ER compartments –although to a lesser extent as compared to the wild-type situation (Figure 4.9). A PNGaseF digestion was included to control for a complete removal of carbohydrates, resulting in migration of the backbone of the protein at ~58 kDa in electrophoresis.

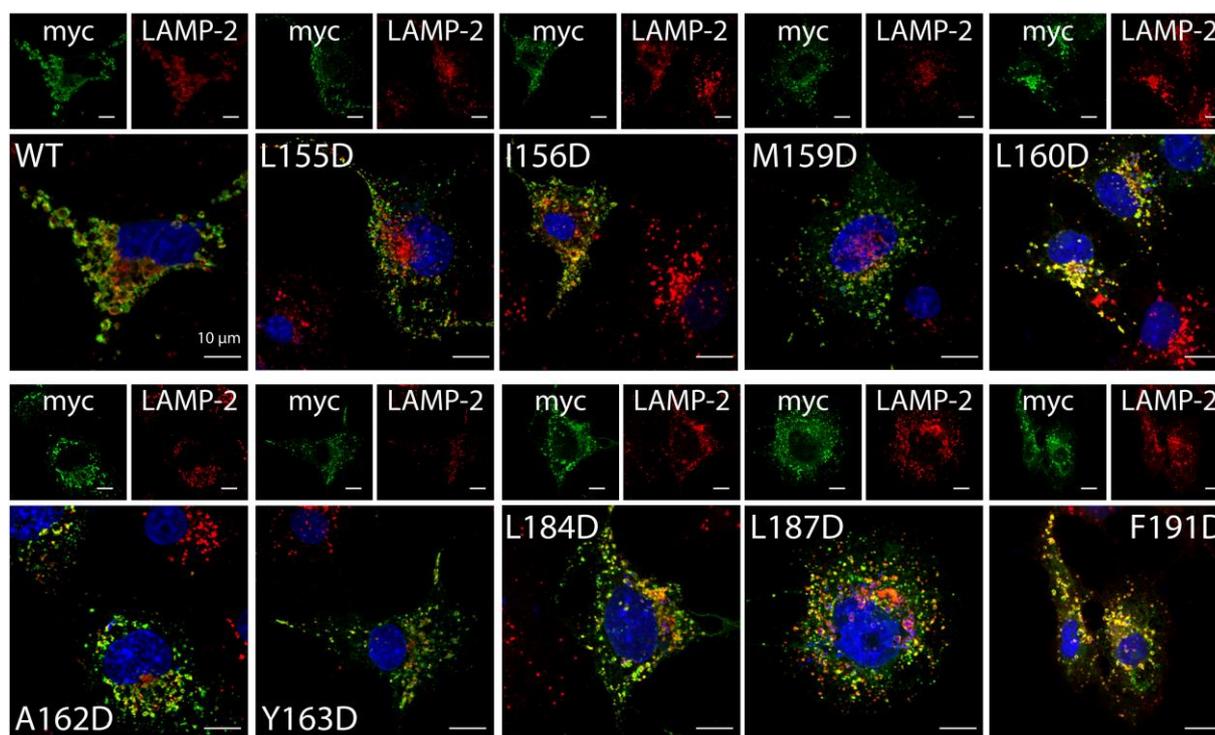


**Figure 4.8: Subcellular localisation study of LIMP-2-GC binding mutants.**

Cos7 cells were transfected with the indicated LIMP-2-myc construct (wild-type (WT) or point mutants in helix 5 and 7) and stained against anti-myc (488 nm; green). To validate cellular localisation of the mutants a co-staining with the lysosomal marker LAMP-2 (495 nm; red) was performed. An overlay of both colour channels revealed co-localisation (yellow) of all mutants similar to the expressed wild-type indicating lysosomal localisation of all LIMP-2 mutant tested. Scale bars indicate 10  $\mu$ m.

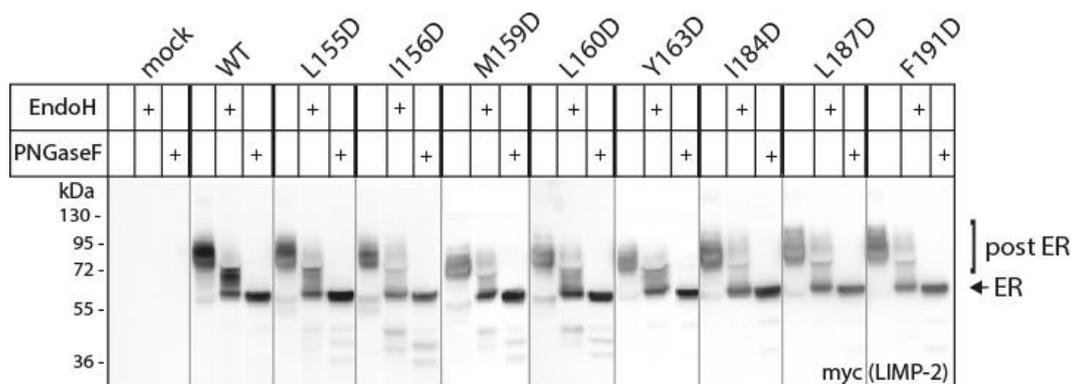


**Figure 4.9: Endoglycosidase H and PNGaseF digestion of LIMP-2 mutants.**

Analysis of LIMP-2 mutants by endoglycosylation H and PNGaseF digestion after overexpression in Cos7 cells verifying their subcellular localisation. For the following immunoblot analysis an anti-myc antibody was utilised. Protein fractions resistant or partly resistant to the endoglycosylation H enzyme indicate post ER localisation (~65-90 kDa), whereas fully deglycosylated proteins suggests localisation in the ER (~58 kDa).

#### 4.1.3.2 GC-binding properties of LIMP-2 mutants

Since LIMP-2 is the described transport receptor of the lysosomal enzyme GC from the ER to the lysosome (Reczek, Schwake et al. 2007), the interaction of the LIMP-2 mutants with the lysosomal enzyme was assessed. Therefore co-immunoprecipitation (co-IP) studies and GC-activity assays in LIMP-2-deficient cells transfected with the indicated LIMP-2 point-mutants were performed (Figure 4.10).

For the direct interaction studies the LIMP-2 constructs were overexpressed in Cos7 cells and precipitated utilising an anti-myc antibody. Expression of each construct was validated by immunoblot before co-IP was performed. Only LIMP-2 wild-type and the control mutant D400K, which is not located in the predicted interaction site of LIMP-2 are able to bind and precipitate GC (Figure 4.10 D). None of the other mutants in helix 5 and 7 could co-precipitate GC. This suggests a complete loss of GC-interaction highlighting the important role for both helices in GC-binding (Figure 4.10).

Taking advantage of LIMP-2 deficient cells, the capability of the artificially engineered LIMP-2 mutants to bind and transport GC was assessed by measuring the enzyme activity.

In the case of the expressed LIMP-2 wild-type a rescue effect could be observed with almost full recovery of GC activity. This is due to proper interaction of both proteins and transport of the enzyme to the lysosome, where optimal enzymatic conditions are present. Consequently, only mutants still able to bind and transport GC to the lysosome will show GC activity above background. A mutant localised outside the suspected interaction site (D400K; Figure 4.10 B) showed GC activity comparable to the wild-type (Figure 4.10 E). GC activities in the low range are detected for the mutants in helix 5 and 7 and most likely due to ER retention of the enzyme.

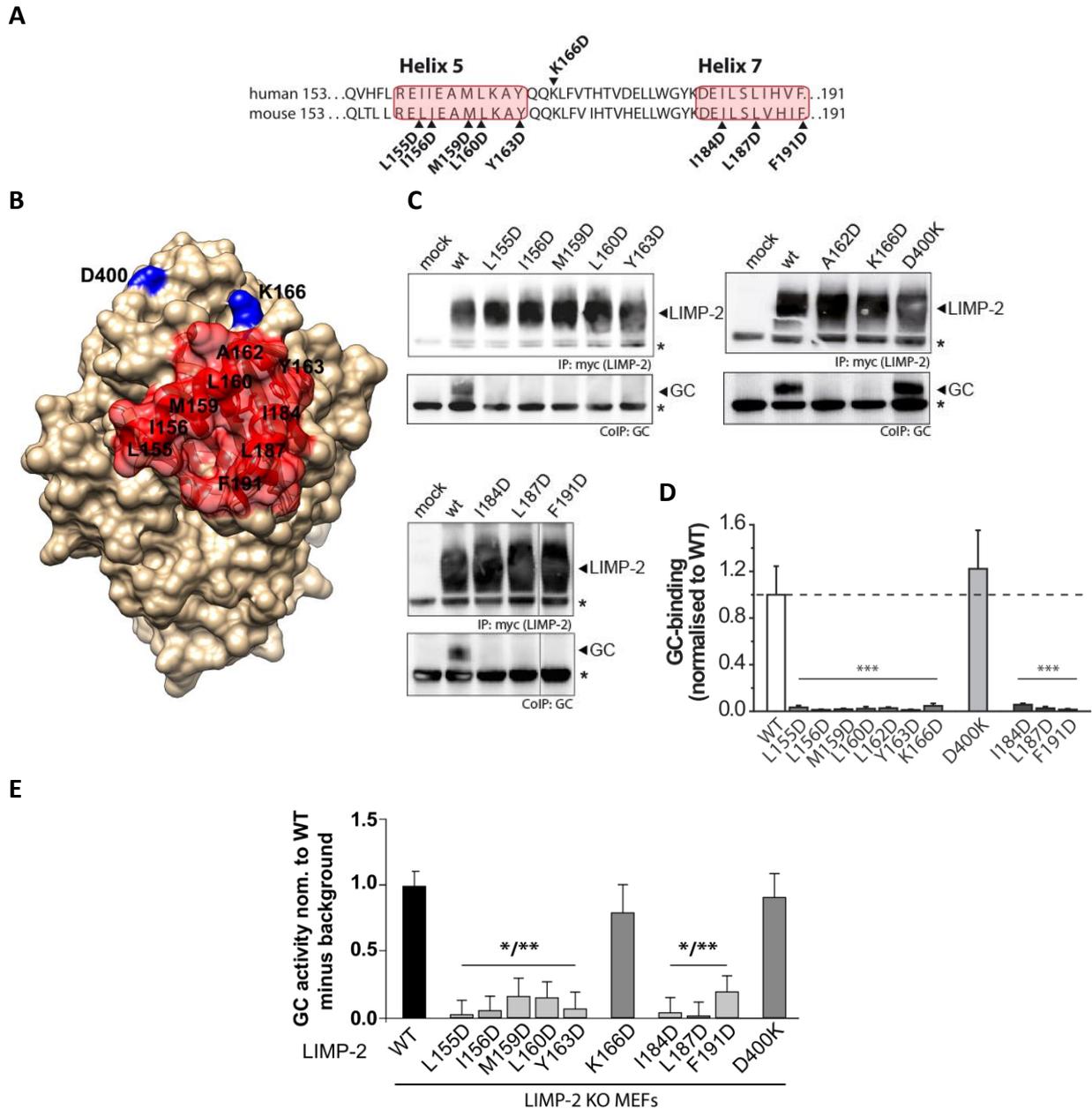


**Figure 4.10: Structural overview of LIMP-2 mutants and interaction studies to determine the binding site of LIMP-2 to GC.**

**A)** The human and murine amino acid sequence of the LIMP-2 binding region with indication of selected point mutations in helix 5 and 7. **B)** The three dimensional protein structure of LIMP-2 shows mutated amino acids and indicates their surface exposure. The helical bundle is shown in red (PDB: 4F7B; designed in UCSF Chimera). **C)** For direct interaction studies of LIMP-2 to GC, murine LIMP-2 constructs were expressed in Cos7 cells and binding abilities of the mutants were assessed by co-immunoprecipitation studies. Immunoblots stained for LIMP-2 (anti-myc) show precipitated LIMP-2. Below each LIMP-2 blot the respective immunoblot of the co-IP (anti-GC) is presented. Interaction of the enzyme could only be observed for wild-type LIMP-2 and the control mutant D400K. Asterisks denote the antibody heavy chains. **D)** Densitometry of the GC co-IP. Data are presented as bound GC in relation to precipitated LIMP-2, normalised to LIMP-2 wild-type (n=3). **E)** GC activity after transfection of individual LIMP-2 point mutants in LIMP-2 deficient MEFs. Only LIMP-2 constructs, which are still able to bind and transport GC to the lysosome, are able to rescue GC activity similar to the LIMP-2 wild-type. The GC background activity was deducted from the determined GC activity and values were normalised to LIMP-2 wild-type (n=4-7). A one-way ANOVA with a subsequent Tukey-Kramer posthoc test was utilised for all statistical tests. \*, \*\*, \*\*\* denote  $p < 0.05$ ; 0.01; 0.001 comparing all mutants to cells transfected with GC wild-type.

In conclusion, the point mutants in helix 5 and 7 of LIMP-2 exhibit a comparable lysosomal localisation as observed for the LIMP-2 wild-type. In direct interaction studies the inability of the mutants to precipitate GC or rescue GC activity in GC-deficient cells emphasises the important role of helix 5 and 7 in GC binding.

## 4.2 Is the helical bundle of LIMP-2 sufficient to mediate interaction with GC?

The GC binding site in the LIMP-2 protein could be narrowed down to the helical bundle especially involving helix 5 and 7. These two helices seem to be most likely involved in the interaction with GC. To test this hypothesis, peptides consisting of each single helix were designed and synthesised by JPT Peptide Technologies GmbH (Berlin, Germany). Each peptide consists of 23-24 amino acids resembling either helix 5 (amino acid 152-175) or helix 7 (amino acid 172-194) of the helical bundle of LIMP-2 (Figure 4.7; Table 4.1). Previously, the substitution of three hydrophobic amino acids within helix 5 (I155, I156 and L160) to highly charged aspartic acid (D) has been shown to disable the interaction of LIMP-2 with GC (Blanz, Groth et al. 2010). Thus, a control peptide was designed in the same way with a triple D motif (3xD) included into the helix 5 amino acid sequence. A biotin-tag was attached n-terminally to all peptides by a linker (TTDS = 1,13-diamino-4,7,10-trioxatridecan-succinic acid; consisting of 19 atom bonds). The c-terminus was left unprotected (negatively charged).

**Table 4.1: Overview of the three peptide sequences.**

Peptide name	Sequence (N-terminus-----C-terminus)
<b>Helix 5</b>	Biotin-Ttds-LREIIEAMLKAYQQKLFVTHTVDE (24 aa)
<b>3xD Helix 5</b>	Biotin-Ttds-LRE <b>DD</b> EAM <b>D</b> KAYQQKLFVTHTVDE (24 aa)
<b>Helix 7</b>	Biotin-Ttds- TVDELLWGYKDEILSLIHVFRPD (23 aa)

The structural properties of the synthetic peptides were analysed by circular dichroism (CD) spectroscopy. For determination of the secondary structure the ‘far-UV’ spectral region ( $\lambda=200-250$  nm) was used. Each secondary structure ( $\alpha$ -helix,  $\beta$ -sheet or random coil) gives rise to a characteristic shape and magnitude of CD spectrum. The helix 5 as well as the helix 7 peptide exhibited a clear  $\alpha$ -helical folding (Figure 4.11). In comparison the CD spectrum of the control peptide (3xD helix 5) did not reveal a helical structure anymore (Figure 4.11 A). This indicates that the residues I155, I156 and L160 are important for helix 5 to form an  $\alpha$ -helical structure. Furthermore, this data confirms that the helical structure of helix 5 and 7 as

found in the crystal structure can be recapitulated in the form of biotin-tagged 23-24 amino acid long peptides.

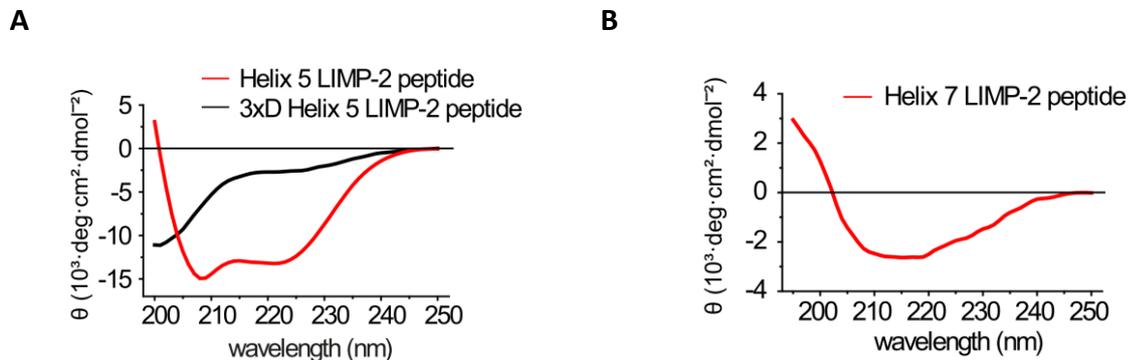


**Figure 4.11: Circular dichroism (CD) spectroscopy of the LIMP-2-derived peptides.**

CD spectroscopy in the "far-UV" spectral region (200-250 nm) was utilised to determine the secondary structure of the LIMP-2-derived peptides (helix 5, 3xD helix 5 and helix 7). The spectra of the helix 5 (A; red spectrum) and helix 7 (B) exhibit a helical folding. In comparison the 3xD helix 5 peptide loses the helical structure and indicates a random coil folding (A; black spectrum). The CD-measurements were performed in 50 mM sodium-phosphate buffer and 150 mM NaCl at pH7 and 20°C and are shown in ellipticity ( $\theta$ ) as the legacy of polarimetry.

To determine if helix 5 and helix 7 directly interact with GC, we used purified GC (Cerezyme®) in an *in vitro* binding assay. GC was co-incubated with biotin-bound LIMP-2 peptides, and precipitated with agarose-bound streptavidin (Figure 4.12 A). This revealed a preferential interaction with helix 5 compared to the 3xD peptide or the helix 7 peptide (Figure 4.12 B, C).

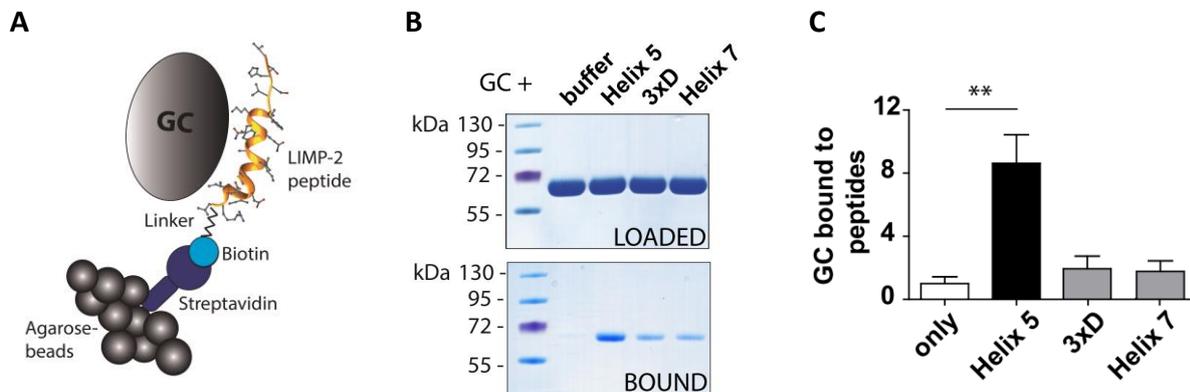


**Figure 4.12: Pulldown experiment using LIMP-2 peptides and recombinant GC.**

A) Principle of the *in vitro* pulldown of recombinant GC: peptides were incubated with enzyme and then subjected to precipitation using streptavidin coupled agarose beads. Binding of GC to peptide was validated by subjecting loaded and bound fraction to SDS-PAGE. Proteins were visualised by coomassie blue staining (recombinant GC: ~65 kDa) (B). Binding efficiencies of each peptide were densitometrically evaluated (ImageJ) and normalised to GC bound to buffer only. Precipitation of GC with the helix 5 peptide is significantly increased compared to the buffer control (C). A One-Way ANOVA with a subsequent Tukey-Kramer posthoc test was utilised for statistical analysis. \*\* denotes  $p < 0.01$ ;  $n = 3-5$ .

To control for the binding specificity of the LIMP-2-derived peptides, interactions to recombinant lysosomal acid  $\alpha$ -mannosidase (LAMAN) and bovine serum albumin (BSA)

were assessed. A precipitation experiment revealed no specific interaction between the LIMP-2 helix 5 peptide and the two control proteins (LAMAN and BSA; Figure 4.13).

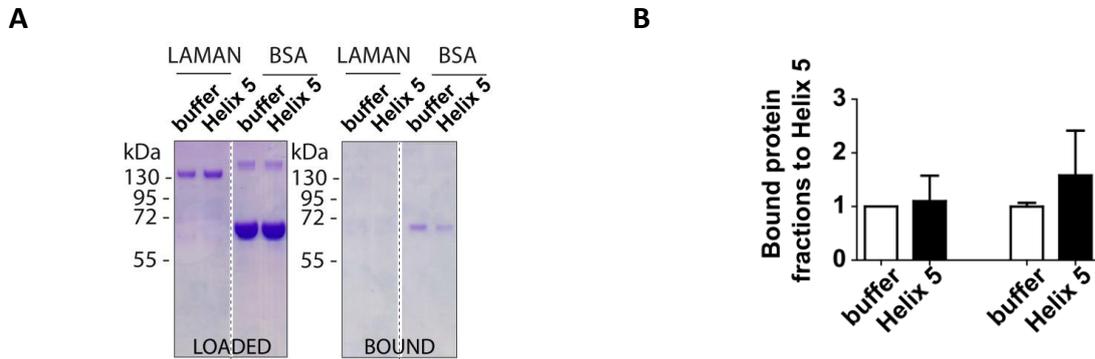


**Figure 4.13: Specificity control: precipitation experiment of recombinant LAMAN and BSA.**

**A)** Loaded and bound fractions of the peptide pulldown from recombinant LAMAN (~ 130 kDa) and bovine serum albumin (BSA) (~ 61 kDa). The samples were subjected to SDS-PAGE and visualised by coomassie blue staining. **B)** Densitometric analysis (ImageJ) of LAMAN and BSA fractions bound to helix 5 were normalised to protein bound to the peptide after incubation with buffer only (n=2).

Peptide pulldown assays were also performed directly from endogenous cellular GC (Cos7 cells). Following the same protocol as for the *in vitro* precipitation (see above), helix 5 peptide and buffer only were incubated with cell lysates and subjected to precipitation with streptavidin linked agarose beads (Figure 4.14 A). The loading after cell lysis and the bound fractions were separated on an SDS-PAGE. The GC protein was visualised after immunoblot analysis, demonstrating successful binding of the endogenous enzyme to the synthetic helix 5 peptide (Figure 4.14 B, C).

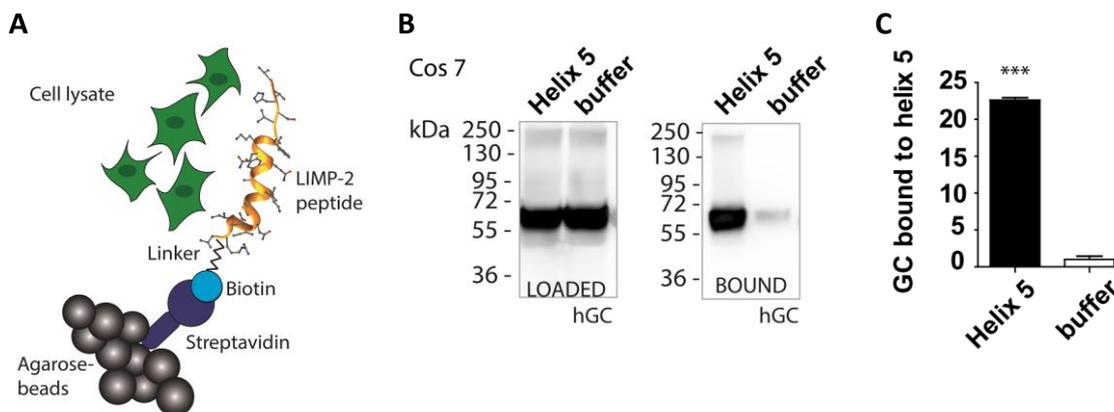


**Figure 4.14: Pulldown experiment revealing endogenous GC-precipitation from Cos7 cellular lysate.**

**A)** Sketch of the used precipitation assay: Pulldown of endogenous GC from cell lysate after incubation with biotin-tagged helix 5 peptide. Binding of enzyme to the peptide was validated by subjecting loaded and bound fractions to SDS-PAGE followed by western-blotting utilising an antibody against human GC (**B**). Binding efficiencies of endogenous GC to helix 5 peptide was analysed by densitometry indicating a significant pulldown of enzyme with the helix 5 peptide (**C**). An independent two-sided t-test was utilized for statistical analysis. \*\*\* denotes  $p < 0.001$ ; n=3-5.

These results indicate that helix 5 alone is sufficient to interact with recombinant GC as well as with endogenous GC derived from cell lysates.

#### 4.2.1 Do LIMP-2-derived peptides also modify the function of GC?

Having shown that the helix 5 peptide can be used to precipitate recombinant and cellular GC it was interesting to analyse if the LIMP-2-derived peptides additionally affecting the function of GC. To determine if these peptides are able to modify enzymatic activity, recombinant GC was incubated with 10 fold excess of peptides. GC activity was assessed using an artificial substrate. After incubation with the helix 5 peptide a fourfold increase in GC activity was found. In comparison the buffer control and the non-binding 3xD control peptide, only a 2-3 fold enhancement of GC activity could be observed when the helix 7 peptide was co-incubated with GC (Figure 4.15 A). In addition a random helical control peptide consisting of 24 amino acids was applied to control for the specificity of this assay. This peptide was not able to increase GC activity like observed for the helix 5 peptide (Figure 4.15 A). As a further negative control recombinant lysosomal acid  $\alpha$ -mannosidase (LAMAN) was subjected to incubation with LIMP-2 peptides. No change in GC activity was detected (Figure 4.15 B). To determine if LIMP-2 peptides also enhance the activity of endogenous GC enzyme, the effect of the peptides on N2a lysate was assessed through an activity assay. For this experiment the N2a cell lysate was incubated with 20 nmol of helix 5 and 3xD control peptide and subsequently subjected to a GC activity assay. As shown in Figure 4.15 C the helix 5 peptide was able to increase endogenous GC activity  $\sim$ 1.6 fold compared to the buffer and the non-interacting 3xD peptide control.

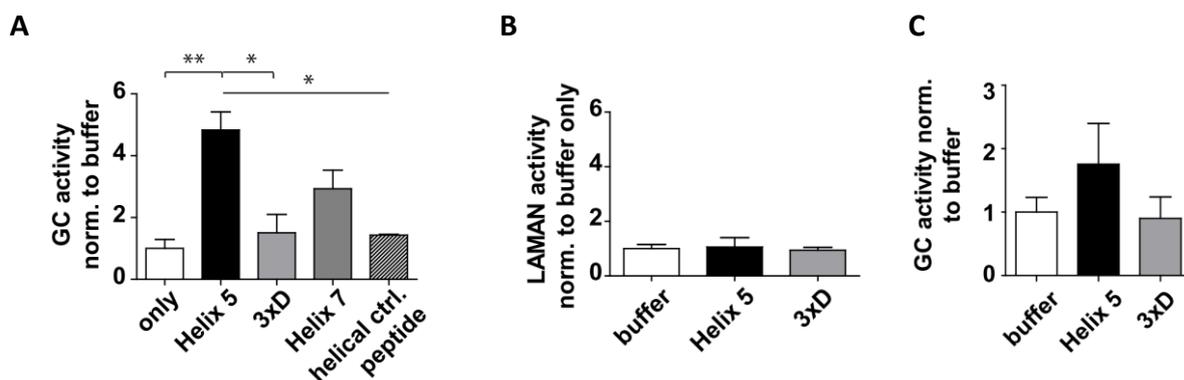


**Figure 4.15: Activity assays of recombinant and endogenous enzymes after incubation with LIMP-2-derived peptides.**

Activity assay of recombinant GC (A) and LAMAN (B). Both enzymes were incubated with 10 fold molar excess of the indicated peptide. Whereas the helix 5 peptide was able to increase GC activity  $> 4$  fold, no change in LAMAN activity could be observed after incubation with the peptides (GC:  $n=2-4$ ; LAMAN:  $n=2$ ). C) Activity assay of endogenous GC. N2a cell lysate was incubated with helix 5 and 3xD control peptides. The helix 5 peptide was able to increase GC activity of the enzyme derived from the N2a cell lysate  $\sim$ 1.6 fold ( $n=2-9$ ). All enzyme activities were normalised (norm.) and compared to buffer only. A one-way ANOVA with a subsequent Tukey-Kramer posthoc test was utilised for statistical analysis. \*, \*\* denote  $p < 0.05$ ,  $0.01$ .

In an additional experiment the effect of the complete LIMP-2 ectodomain -which includes the GC interaction site containing helix 5 and helix 7- on GC activity, was evaluated.

Recombinant GC was incubated with increasing molarities of the LIMP-2 ectodomain as well as the helix 5 peptide and as a negative control bovine serum albumin. The incubation with the recombinant LIMP-2 led to an increased GC activity immediately after mixing both recombinant proteins (same molarities; 1x mol; Figure 4.16 A). The helix 5 peptide starts to enhance enzyme activity from a 5 fold molar excess of the peptide compared to GC (5x mol, Figure 4.16 A). After adding a 10 molar excess of the peptide or the LIMP-2 ectodomain (10x mol) the augmentation of GC activity was most efficient (Figure 4.16 A). In contrast, no activation of LAMAN was detected after incubation with the LIMP-2 ectodomain or the helix 5 peptide (Figure 4.16 B).

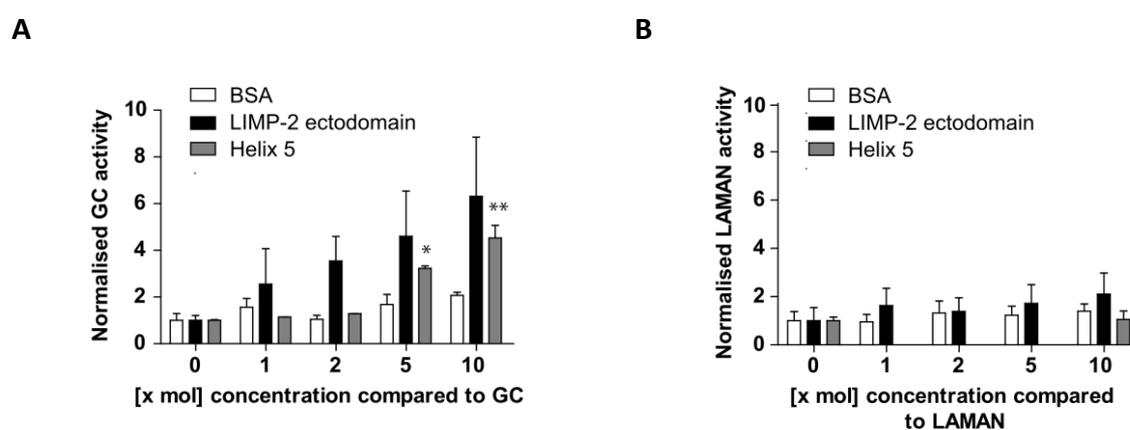


**Figure 4.16: Effect of the recombinant LIMP-2 ectodomain and the helix 5 peptide on GC activity.**

Activity assays of recombinant GC (A) and LAMAN (B). Recombinant GC was incubated with different molarities (1x -10x) of helix 5 peptide or the recombinant luminal domain of LIMP-2 (n=2-5). GC activities were normalised and statistical analyses \* and \*\* denote  $p < 0.05$  and  $0.01$  referring to a comparison to the 0 value [0 x mol] of the respective sample. For statistical analysis a one-way ANOVA with a subsequent Tukey-Kramer posthoc test was performed.

The effect of peptide binding on GC protein stability was also assessed by measuring GC activity at increasing temperatures (20-60°C) at pH7. Therefore a 10 fold molar excess of the peptides was applied and GC activity was measured every 10°C. As shown above (Figure 4.15) the helix 5 peptide is able to increase GC activity ~4 fold after incubation at room temperature. When the temperature was increased up to 40°C, the enhancement of GC activity remained stable compared to buffer and 3xD control. Helix 7 peptide alone was able to increase GC activity slightly (Figure 4.17). When reaching > 40°C the enzyme was denatured, resulting in a loss of activity. Sigmoidal dose-response curves were fitted to the graphs (see small inlay, Figure 4.17) and inflexion points of curves are presented as LogEC50 underneath the diagram. LogEC50 deciphers the temperature of half maximal GC activity and describes the protein stability. Incubation of recombinant GC with helix 5 peptide increased this value

slightly (46°C) in comparison to the buffer control (42°C), indicating a stabilising effect of the peptide.

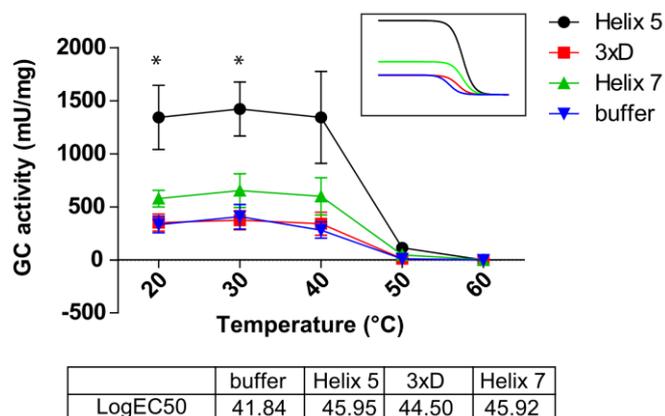


**Figure 4.17: Impact of LIMP-2 peptides on protein stability and function.**

Protein stability assay: GC was incubated with buffer only, helix 5, 3xD helix 5 and helix 7 peptide and the temperature was increased in 10°C steps from 20-60°C. Samples were subjected to GC activity assays. Sigmoidal response curves were fitted (see inset at top right corner) and LogEC50 values are shown in the table underneath. A one-way ANOVA with a subsequent Tukey-Kramer posthoc test was used to describe increase in GC activity after incubation with helix 5 peptide compared to buffer. \* denotes  $p < 0.05$ ;  $n = 3$ .

Since the detectable effect of the helix 5 peptide on GC stability was minor in the assay above, another approach was used to assess the consequences of peptide binding to GC. A mixture of enzyme and peptide was incubated at 37°C and pH7. The activity of the enzyme was measured over a time period of 270 hours (Figure 4.18). The GC activity indicates that the helix 5 peptide is able to increase the activity of the enzyme at early time points (0-40 hours). After ~40 hours of incubation at 37°C a drop in GC activity was detected for all samples. However, when compared to the buffer and non-binding 3xD helix 5 peptide the decrease in enzyme activity was not as strong in the sample incubated with helix 5. Furthermore, the GC activity stays constant from ~80 hours on; whereas the control samples (buffer and 3xD helix 5 peptide) showed complete loss of activity after 60 hours of incubation at 37°C. The half maximal enzyme activity (LogEC50) for GC incubated with buffer only and 3xD control peptide were reached for both samples after 24 hours, whereas the time point for the helix 5 incubated sample was twice as high (~48 hours). This indicates the ability of the interacting LIMP-2-derived peptide (helix 5) to stabilise GC. The helix 5 peptide can increase the GC activity at a physiological temperature and at a neutral pH.

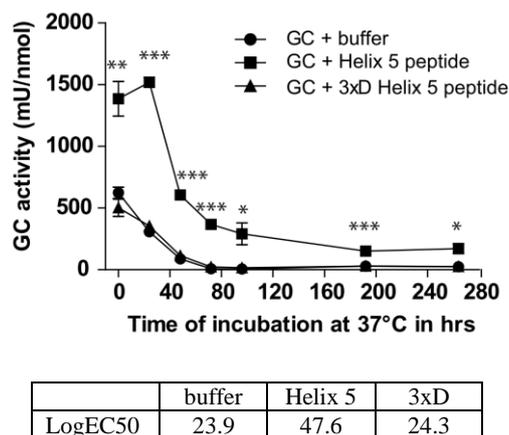


**Figure 4.18: Stabilisation assay of GC after incubation at 37°C.**

GC activity was measured after incubation of the enzyme with buffer, helix 5 and the 3xD helix 5 control peptide at 37°C for 270 hours. Incubation with helix 5 peptide led to stabilisation of the enzyme indicated by a constantly higher activity of the enzyme compared to buffer and 3xD control peptide. Response curves were fitted with LogEC50 values indicating half maximal enzyme activity (values are depicted in the table underneath the graph). A one-way ANOVA with a subsequent Tukey-Kramer posthoc test was used to describe increase in GC activity after incubation with the helix 5 peptide compared to buffer and the 3xD peptide. \*, \*\*, \*\*\* denote  $p < 0.05$ , 0.01, 0.001;  $n=2-3$ .

Having observed that the helix 5 peptide specifically interacts with GC, it was of interest to analyse if the complete  $\alpha$ -helix is required for this interaction or if a small fragment of the helix 5 is sufficient to mediate binding to GC. The 24 amino acid long helix 5 peptide was fragmented into four small peptides consisting of 5-7 amino acids. Each small peptide contains at least two hydrophobic amino acids (Table 4.2).

**Table 4.2: Overview of small peptide sequences.**

Peptide name	Sequence (N-terminus-----C-terminus)
<b>Helix 5 full sequence</b>	152-LREIIEA-MLKAYQ-QKLFV-THTVDE-175
<b>Helix 5, Peptide 1</b>	- LREIIEA - (7 aa)
<b>Helix 5, Peptide 2</b>	- MLKAYQ - (6 aa)
<b>Helix 5, Peptide 3</b>	- QKLF - (5 aa)
<b>Helix 5, Peptide 4</b>	- THTVDE - (6 aa)

To evaluate the interaction of the small unlabeled peptides 1-4 with GC, a GC activity assay was applied. None of the fragmented peptides could affect the activity of GC after co-incubation with recombinant GC. It is likely, that the whole helical structure of helix 5 is required to exert a positive function on GC activity (Figure 4.19).

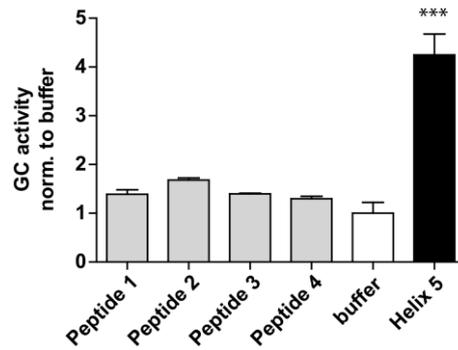


**Figure 4.19: GC activity assay after incubation with fragmented peptides derived from the helix 5 sequence.**

Activity assay of recombinant GC incubated with a 10 fold molar excess of the indicated helices. Whereas helix 5 is able to increase GC activity > 4 fold, no statistically significant effects could be observed for the smaller peptides 1-4. Enzyme activity was normalised (norm.) to the buffer-incubated sample. A One-Way ANOVA with a subsequent Tukey-Kramer posthoc test was utilised for statistical analysis. \*\*\* denotes  $p < 0.001$  comparing the helix 5-incubated sample with the buffer the buffer control;  $n=4-5$ .

#### 4.2.1.1 Can the LIMP-2-derived helix 5 peptide be exploited to therapeutically increase GC activity?

As shown above especially helix 5 is able to efficiently enhance the enzymatic function of GC. Thus, the peptide might be considered as a therapeutic tool to increase GC activity in cells exhibiting impaired enzyme function. To test the therapeutic potential of helix 5, it was determined if this peptide could be internalised by cells and subsequently reach the lysosomal compartment. This was tested by incubating murine macrophages (J774E) with 50  $\mu\text{M}$  of the helix 5 peptide. Endocytic uptake of the peptide was visualised by staining cells with a fluorescently labelled biotin antibody (488 nm; green) and co-staining for endogenous GC (anti-murine GC; red) revealing co-localisation (Figure 4.20 A). Furthermore, the effect of the internalised peptide could be shown by a ~1.3 fold increase in cellular GC activity (Figure 4.20 B).

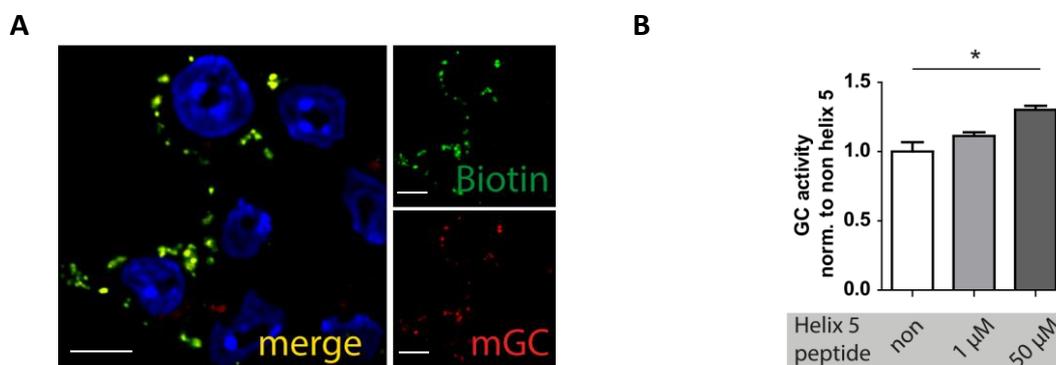


**Figure 4.20: Uptake and effect of helix 5 peptide in J774E mouse macrophages.**

**A)** Immunofluorescence stainings of J774E macrophages incubated with 50  $\mu\text{M}$  helix 5 peptide. Biotin-labelled helix 5 peptide (anti-biotin; 488 nm, green), which was taken up by the cells show co-localisation with endogenous GC (anti-murine GC; red) confirming lysosomal localisation of the peptide in cells. Scale bars indicate 10  $\mu\text{m}$ . **B)** GC activity assay showing a ~1.3 fold increase in enzyme activity after uptake of 50  $\mu\text{M}$  helix 5 peptide. A one-way ANOVA with a subsequent Tukey-Kramer posthoc test was used for statistical analysis. \* denotes for  $p < 0.05$ ;  $n=2$ .

To further enhance the cellular uptake of the helix 5 peptide, recombinant GC (0.2 nM) was pre-incubated with the peptide (2 nM) and then added to the media of GC-deficient MEFs cells. Uptake of the enzyme pre-incubated with the respective peptides was visualised by immunoblotting (Figure 4.21 A). The uptake rate of the enzyme/peptide mixtures was similar for the different peptides tested (helix 5, 3xD helix 5 and helix 7) (Figure 4.21). However, the cellular GC activity was significantly increased when the helix 5 peptide was applied (Figure 4.21 B). The advantage of the pre-incubation of recombinant enzyme is that a much smaller concentration (1  $\mu$ M) of peptide is necessary to improve enzyme activity (compare with Figure 4.20).

In summary, these results indicate that a positive effect of the helix 5 peptide on GC function can be found in *in vitro* assays but also in cell-based experiments.

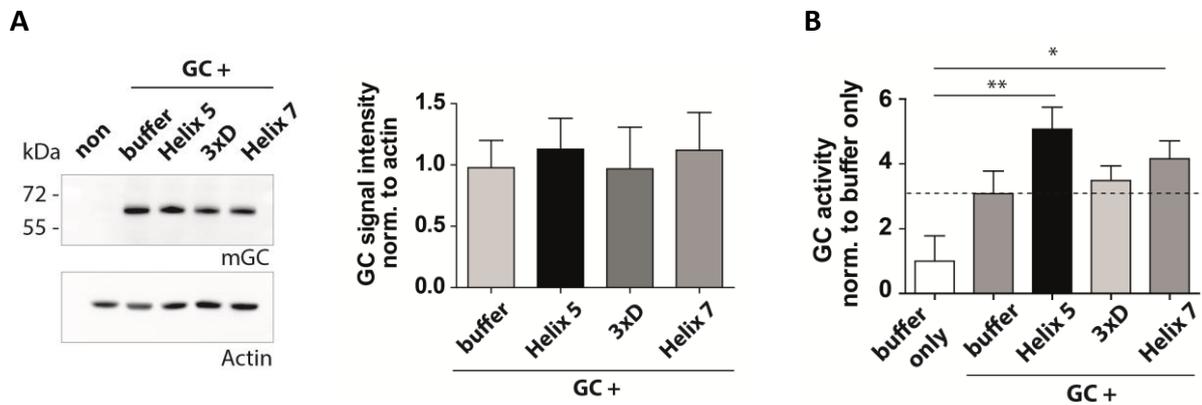


**Figure 4.21: Uptake and effect of GC pre-incubated with LIMP-2 peptides into GC KO MEFs.**

**A)** Immunoblot analysis of uptake of recombinant enzyme pre-incubated with the indicated peptide visualised by an anti-mGC antibody. A densitometric analysis reveals an equal uptake of GC independent of the peptide. Subsequently GC activity of cell lysate was measured showing a significant increase after uptake of the GC-helix 5 peptide mixture compared to buffer only (**B**). A one-way ANOVA with a subsequent Tukey-Kramer posthoc test was used for statistical analysis. \*, \*\* denotes  $p < 0.05, 0.01$ ;  $n=4$ .

#### 4.2.2 What causes the positive effect of LIMP-2 peptides on GC function?

To explain the positive effect of the LIMP-2 peptide helix 5 on GC function, analyses to understand potential structural changes of GC protein after peptide binding were performed. This included studies evaluating the secondary as well as quaternary structure of the protein after incubation with the LIMP-2-derived peptides by CD-spectroscopy and dynamic light scattering (DLS).

##### 4.2.2.1 CD-spectroscopy: changes in secondary structure of GC after helix 5 binding?

To analyse conformational changes in the secondary structure of GC in order to control for a stabilising and chaperone-like effect of the helix 5 peptide on the GC protein a thermal

stability assay was performed. In this assay, recombinant GC was incubated with buffer, with helix 5 or with 3xD helix 5 peptides, subjected to ascending temperatures (20-90°C). Starting from ~40°C the protein began to denature (Figure 4.22 B). The CD-spectrum ( $\lambda=250-200$  nm) of GC after heating to 90°C revealed a loss of the secondary structure of the protein (Figure 4.22 A). To follow the melting/denaturing of the GC protein when it is subjected to increasing temperatures, CD-spectra at 220 nm were recorded. The values measured at 220 nm were plotted against the temperature resulting in a melting curve of the GC protein. These graphs were fitted to a sigmoidal dose-response curve (Figure 4.22 B; red graphs). The inflexion points in the curves are shown as LogEC50 in the table underneath the graph. These values decipher the temperature where half of the GC protein was still properly folded. For the different GC samples similar LogEC50 values could be observed (Figure 4.22 A). This indicates that the binding of the helix 5 peptide to GC does not lead to a permanent change in the secondary structure of the protein, which would possibly make GC more susceptible to heat.

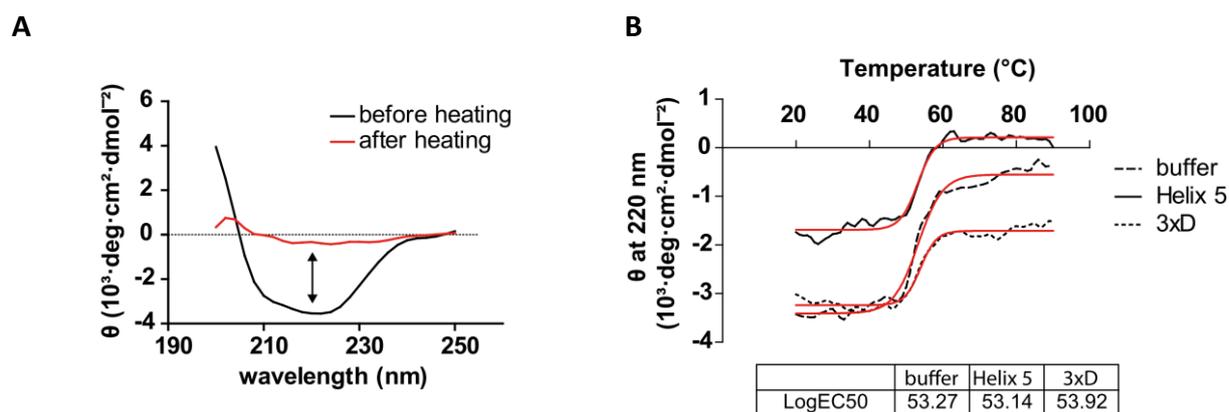


**Figure 4.22: Thermal protein stability: CD-analysis of GC after incubation with helix 5 peptide.**

**A)** CD-spectrum of GC protein before and after heating, indicating the denaturation of the protein after exposing the protein to heat (90°C; red graph). The arrow indicates a wavelength of 220 nm, at which the following measurements were performed to track the denaturation of the protein. **B)** GC incubated with buffer, helix 5 and 3xD peptide subjected to temperatures from 20-90°C. CD-spectroscopic analyses were performed at 220 nm. Sigmoidal curves (red) were fitted to the graphs and the LogEC50 values could be determined and used as a measurement of the stability of secondary protein structure. The CD-measurements were performed in 50 mM sodium-phosphate buffer and 150 mM NaCl at pH7 and are shown in ellipticity ( $\theta$ ) as the legacy of polarimetry.

#### 4.2.2.2 Dynamic light scattering: changes in quaternary structure of GC after helix 5 binding?

To investigate potential changes in the quaternary structure of GC after incubation with the helix 5 peptide (e.g. on the level of multimerisation of the protein), dynamic light scattering (DLS) experiments were performed. As shown in Figure 4.23 no difference in the molecule radius of GC plus buffer and GC incubated with helix 5 peptide could be observed. In both

conditions the mean effective diameter of GC molecules remained in the same range (~8 nm). It can be concluded, that the incubation of the enzyme with the interacting helix 5 peptide did not lead to multimerisation or aggregation of GC.

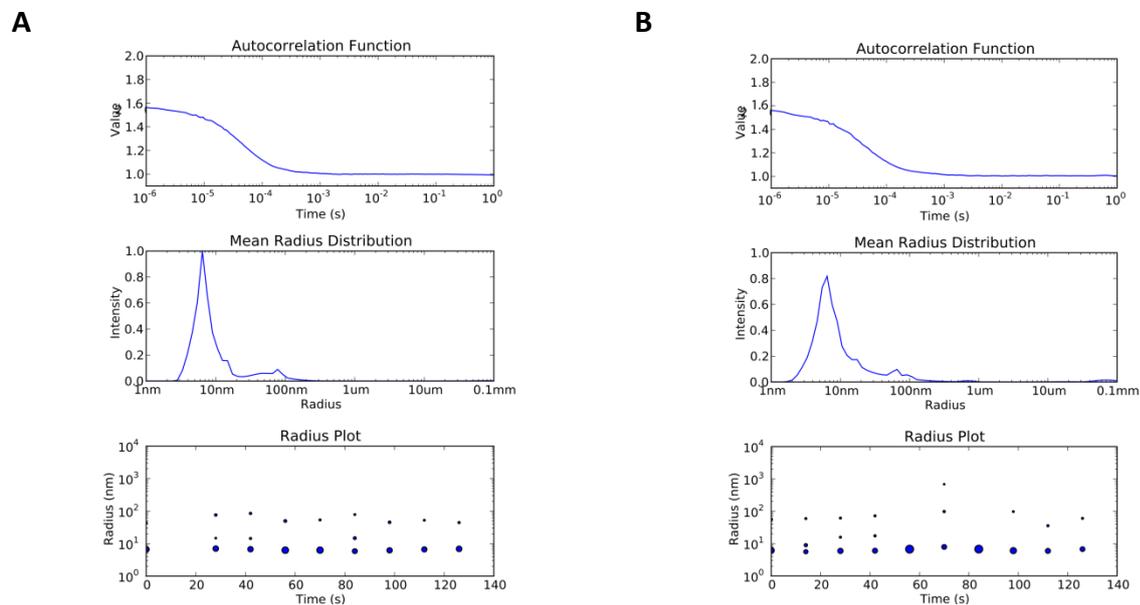


**Figure 4.23: Dynamic light scattering (DLS) of GC in the presence or absence of the helix 5 peptide.**

DLS analysis of the quaternary structure of GC after adding buffer (A) and helix 5 peptide (B), respectively. The upper graph presents the incidence (time in seconds) of GC molecules passing and staying in the laser beam. Analysis of this data, radius of particles (GC) can be plotted (lower graph) and mean radius distribution was calculated (middle graph), revealing a size of ~8 nm per particle. No obvious difference in the size of GC molecules could be observed after incubation with the helix 5 peptide. The DLS-measurements were performed in 50 mM sodium-phosphate buffer and 150 mM NaCl at pH7.

In summary, the molecular mechanism of the positive effect of the LIMP-2 peptide (helix 5) on GC function still remains elusive. With the applied assays no changes in the secondary structure of GC protein or multimerisation could be observed.

### 4.3 Structural analyses of GC: Where does LIMP-2 bind?

Since the LIMP-2 interaction site on the GC enzyme is not known, co-crystallisation experiments with recombinant GC and the LIMP-2 helix 5 peptide were performed. Protein and peptide were mixed (10 fold molar excess of the peptide) and incubated on crystallisation plates. The protein solutions were covered with oil (details of crystallisation procedure see material and methods paragraph 3.2.2.8). First crystals with a diameter of around 20  $\mu\text{m}$  could be observed after a few days. Further incubation resulted in a size of up to 50  $\mu\text{m}$  in the following days. Blue IZIT<sup>®</sup> staining (Hampton research, CA, USA) confirmed that grown crystals were proteins (Figure 4.24 B). Single crystals were then frozen in liquid nitrogen and measured at an x-ray beam line in Berlin (BESSYII, Helmholtz Centrum; for more details of

the beam line please see material and methods Table 3.11) with a beneficial diffraction and a resolution of  $\sim 2$  Å. Further parameters including the length (sides: a, b, c) and the angles ( $\alpha$ ,  $\beta$ ,  $\mu$ ) of the unit cell of the crystal are depicted in table 4.3. Overlays of electron densities of GC only and GC incubated with helix 5 peptide revealed exact conformity, indicating that helix 5 peptide was not present in the analysed crystals.

**Table 4.3: X-ray parameters of the protein crystals.**

Space group:	C222 <sub>1</sub>
Unit cell:	
Length [Å]	Angles [°]
a: 111.26	alpha: 90
b: 286.03	beta: 90
c: 92.03	gamma: 90

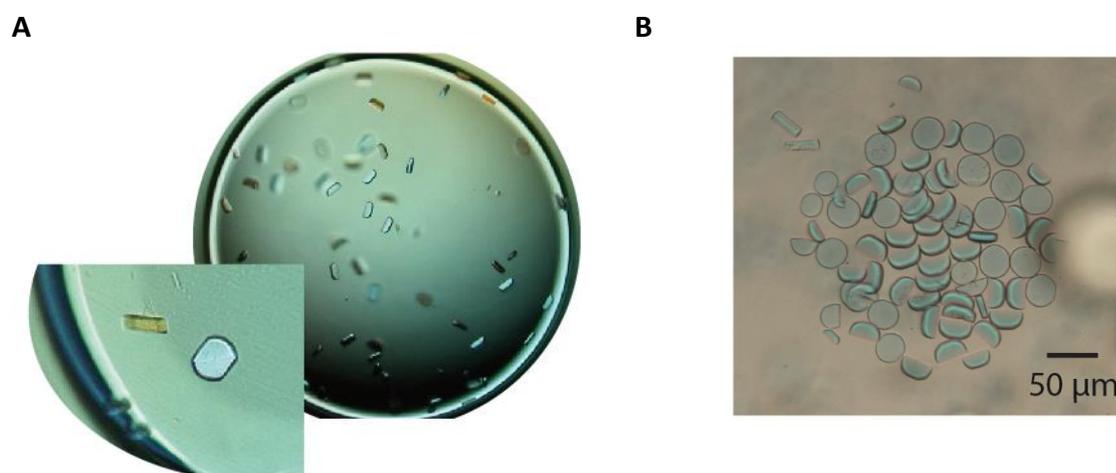


**Figure 4.24: Crystallisation approach showing shape and properties of GC crystals.**

**A)** The shape of crystals raised under oil at pH 5 displaying a size of  $\sim 50$   $\mu\text{m}$ . The space group of crystals was C222<sub>1</sub>. For further parameters of the crystals see table 4.3. **B)** A blue IZIT<sup>®</sup> staining of ‘young’ crystals confirms protein content of the crystals.

Since a co-crystallisation approach was not successful to determine the LIMP-2 binding site on GC, further structural and molecular studies were applied to narrow down the interaction site on GC.

For the design of the following experiments the crystal structures of the glycosylated GC protein (Cerezyme<sup>®</sup>; PDB: 2J25) and the luminal domain of LIMP-2 (PDB: 4F7B) were studied. On the basis of this structural information, experimental approaches as well as site-directed mutagenesis experiments were designed.

By surface charge analyses hydrophobic interfaces, indicated by little to no surface charge (white colour; Figure 4.25), could be found on LIMP-2 and GC. In the LIMP-2 protein this hydrophobic patch is exactly localised to the exposed helical bundle - the GC interaction site, which has been described before (see results 4.1.3). The hydrophobic surface area of the GC

protein could be located in a helical bundle as well (helix 1: T86-S110; helix 2: P150-A168). This helical motif is found on the opposite side of the catalytic pocket. The crystal structure of GC (Cerezyme ®; PDB: 2J25) exhibits three sugar residues bound to asparagines via N-glycosylation, showing no interference with the potential hydrophobic interaction site (Figure 4.25).

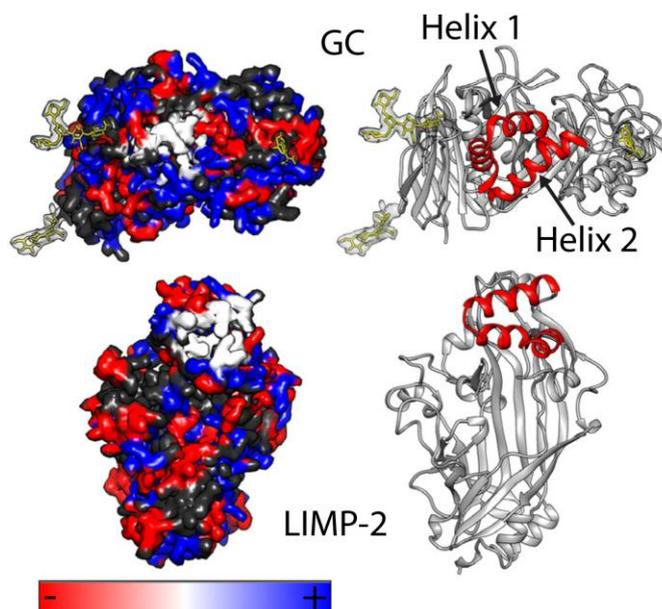


**Figure 4.25: Surface charge analysis of LIMP-2 and GC protein.**

Surface charge of the LIMP-2 structure (PDB: 4F7B) and the GC protein (PDB: 2J25) with hydrophobic patches (Leu, Ala, Val, Ile, Met and Phe) indicated in white. Negatively charged amino acids are shown in red, whereas positively charged amino acids are shown in blue. Additionally the GC structure contains three sugar residues indicated in yellow. On the right hand side the clusters of hydrophobic amino acid are indicated in red suspecting a possible interaction of both proteins via two helical bundles.

Considering the structural surface analysis, GC point mutants in the helical bundle, likely involved in protein-protein interaction, were designed (Figure 4.26, Table 4.4). Surface resident hydrophobic amino acids (leucines) were substituted by highly charged amino acids (glutamic acid; L91E, L94E, L156E). A mutant on the other side of protein (R211E) was used as a negative control. The chosen R211E mutation is in close proximity to the patient mutant F213I (Kawame and Eto 1991, He, Grace et al. 1992) but is exposed to the surface of the protein and thus could have a direct impact in protein-protein interaction (Figure 4.26 A, C). Furthermore, Gaucher disease clinical mutants were designed and analysed as well (I161S, P159L, F213E and N188S) (Eyal, Firon et al. 1991, Cormand, Harboe et al. 1998, Demina and Beutler 1998, Hodanova, Hrebicek et al. 1999, Filocamo, Mazzotti et al. 2004). From the two patient mutations located in the predicted binding region of GC (I161S, P159L) only one amino acid was found to be exposed to the outside of the protein (P159L) and thus might be

directly involved in LIMP-2 binding (Figure 4.26 D, E). Two clinical mutants located on the opposite side of the predicted binding area were established as well (N188S and F213I). Only the N188 mutant exhibits protein surface exposure (Figure 4.26 D, E) (Kawame and Eto 1991, He, Grace et al. 1992, Kim, Liou et al. 1996, Park, Orvisky et al. 2003, Montfort, Chabas et al. 2004). An overview of all inserted GC point mutations can be found in table 4.4.

To validate the integrity of the mutant proteins and to exclude indirect changes of the protein structure on binding properties by the inserted point mutations, each mutant was analysed for its enzymatic activity (Figure 4.26 F, G). N2a cells were transfected with the individual GC mutants. Since N2a cells express endogenous GC, the activity of mock transfected cells indicates the background/endogenous GC activity of the cell lysates.

All analysed mutants reveal activity above background suggesting their structural integrity. They were further subjected to direct LIMP-2 interaction studies and cellular localisation analyses.

**Table 4.4: Overview of the introduced GC point mutations.**

Name of GC mutant	Description	
<b>L91E</b>	in helical bundle/proposed interaction site	'Glutamic acid mutants'
<b>L95E</b>		
<b>L156E</b>		
<b>R211E</b>	opposite of the proposed interaction site	
<b>P159L</b>	in helical bundle/proposed interaction site	Clinical Gaucher disease mutants
<b>I161S</b>		
<b>N188S</b>		
<b>F213I</b>		

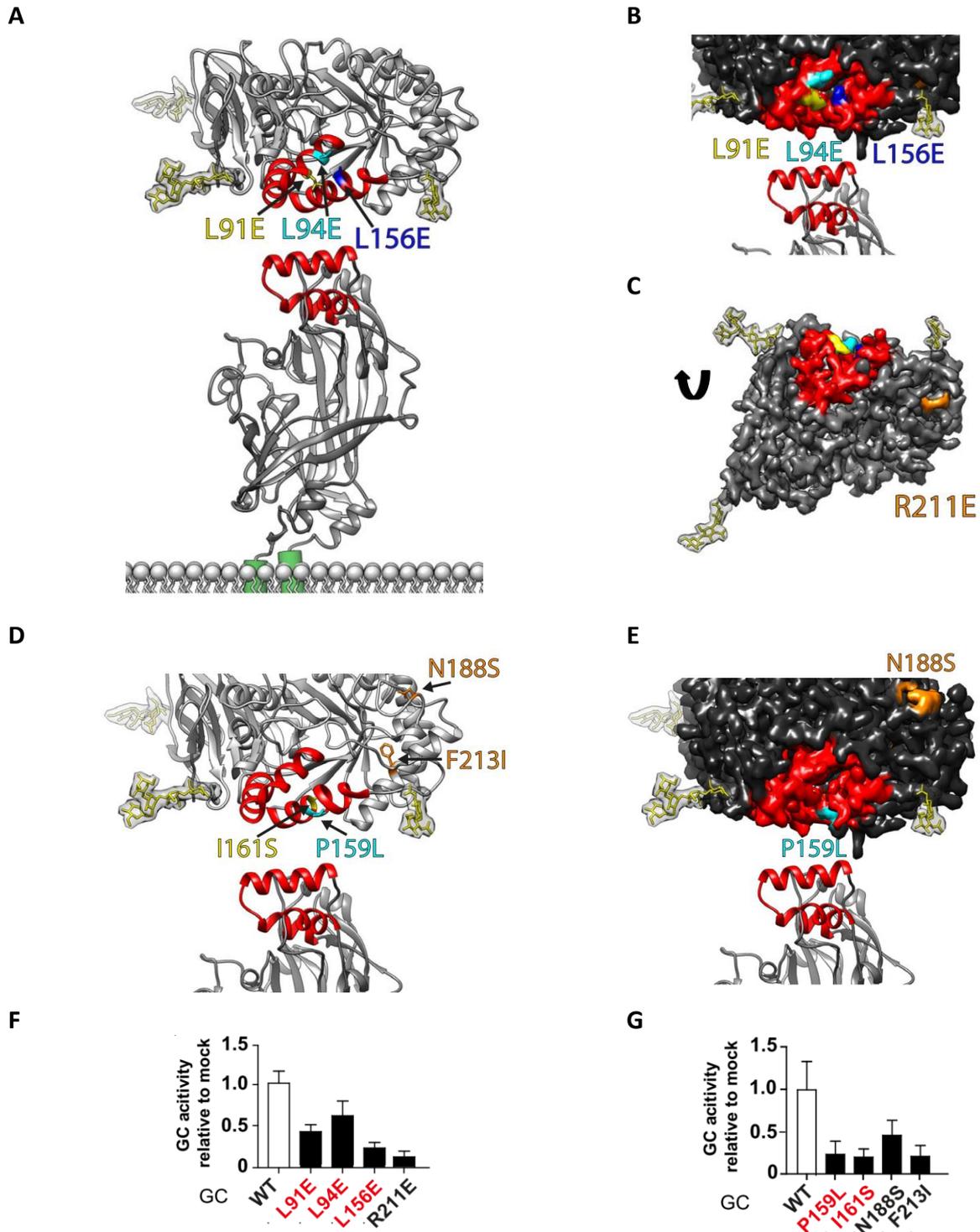


**Figure 4.26: Structural and functional characterisation of GC mutants analysed in this study.**

A) A model of the interaction of LIMP-2 and GC. Helical bundles in both proteins as potential interaction sites are shown in red and the introduced point mutants of GC to demonstrate the GC-LIMP-2-interaction are indicated. Hydrophobic amino acids (leucins) were substituted to highly charged glutamic acids. **B**) Magnification and surface view of the GC protein reveals exposed localisation of the analysed amino acids (cyan: L91E, yellow: L94E, blue: L156E). **C**) A control mutant R211E (orange) was introduced on the other side of the protein. **D**) Human Gaucher disease mutants located in the potential helical interaction site: P159L (turquoise) and I161S (yellow). Also control patient mutants outside of the predicted interaction site were designed: N188S (surface exposed; orange) and F213E (no surface exposure; orange). **E**) Surface view exhibits exposed localisation of the mutated amino acids P159 and N188S. **F**) 'Glutamic acid' mutants shown in A and **G**) Gaucher patient mutants shown in D were subjected to enzyme activity assays after overexpression in N2a cells. The background/endogenous GC activity was subtracted before the enzyme activity was normalised to GC wild-type (WT) (n=3-10). Amino acids located in the predicted interaction site are presented in red.

### 4.3.1 Binding properties of GC mutants towards LIMP-2

The ‘Glutamic acid mutants’ (in the potential binding site: L91E, L94E, L156E and control mutant on the opposite protein side: R211E) were analysed to determine their binding affinity towards LIMP-2. A co-immunoprecipitation study followed by subsequent immunoblot analysis was performed. The GC mutants were overexpressed in N2a cells. Endogenous LIMP-2 was precipitated using a monoclonal antibody against LIMP-2. The amount of GC protein bound to LIMP-2 indicates the ability of each GC mutant to interact with LIMP-2. When compared to GC wild-type and the control mutant R211E, GC point mutants within the helical bundle (L91E, L94E and L156E) were unable to interact with LIMP-2 (Figure 4.27 A, B).

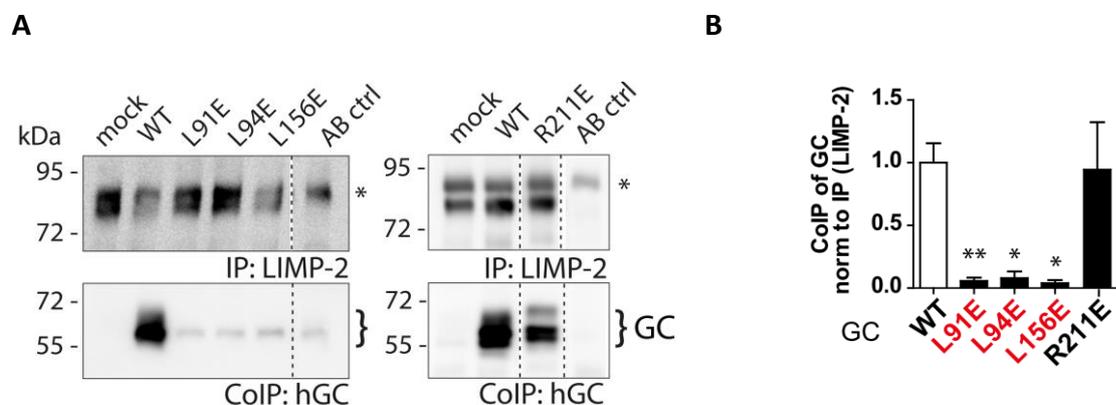


**Figure 4.27: Co-Immunoprecipitation studies of GC ‘glutamic acid mutants’.**

**A)** Co-immunoprecipitation studies in N2a cells after transfection of the indicated GC. For IP an anti-LIMP-2 antibody was used and interaction to GC could be determined using an antibody specific for the human (transfected) variant of GC (anti-hGC). \* indicates a signal of the antibody used for IP (AB ctrl: antibody control). The dotted lines indicate splicing within the same blot. **B)** Quantification of the co-IP study (n=2-10). GC mutants located in the predicted interaction site are shown in red. Bound GC was normalised to precipitated LIMP-2 (IP). GC mutants within the predicted interaction site (L91E, L94E, L156E) show impaired binding to LIMP-2. Control mutant R211E has a similar interaction towards LIMP-2 as compared to wild-type (WT) GC. A one-way ANOVA with a subsequent Tukey-Kramer posthoc test was utilised for statistical analyses. \*, \*\* denote  $p < 0.05$ ;  $0.01$  with comparison of the mutants to cells transfected with GC wild-type.

A similar type of experiment was performed for the Gaucher patient mutants (P159L and I161S) including the clinical control mutants, which are located on the opposite protein side (N188S, F213I). In this set-up, all analysed mutants showed a reduced binding towards LIMP-2. The two GC mutants located within the predicted interaction site (P159L and I161S) were the most affected revealing a binding capacity of less than 10 % compared to the wild-type GC (Figure 4.28).

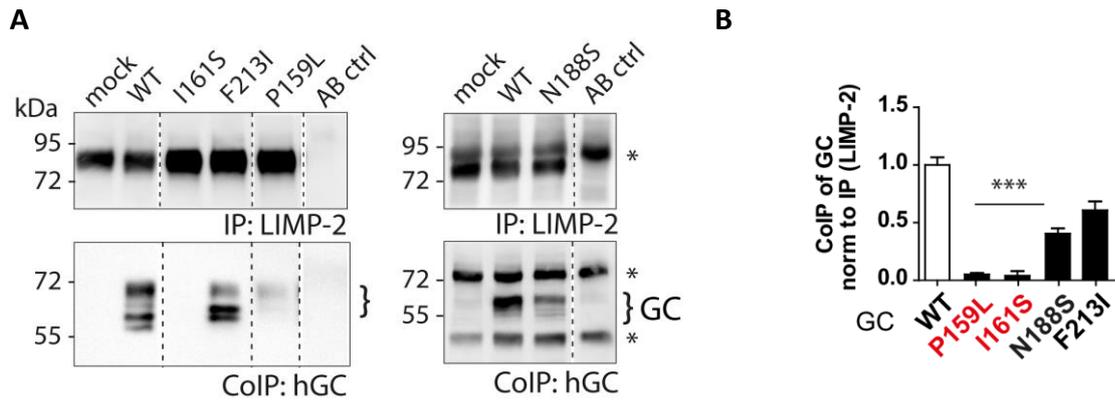


**Figure 4.28: Co-Immunoprecipitation study of Gaucher patient mutants.**

A) Co-immunoprecipitation study of GC patient mutants transfected into N2a cells. For IP an anti-LIMP-2 antibody was used and interaction to GC was determined using an antibody specific for the human (overexpressed) variant of GC (anti-hGC). \* indicating a band of the antibody used for IP (AB ctrl: antibody control). The dotted lines indicate splicing within the same blot. B) Densitometry of the co-IP studies. The signal of co-precipitated GC was normalised to the IP of LIMP-2 (n=2-9). Amino acids located within the predicted binding site are presented in red and show impaired binding to LIMP-2. A one-way ANOVA with a subsequent Tukey-Kramer posthoc test was utilised for statistical analyses. \*\*\* denote  $p < 0.001$  with comparison of the mutants to cells transfected with GC wild-type.

#### 4.3.2 Subcellular localisation of GC mutants

The interaction of the described GC mutants to LIMP-2 was further validated by cellular localisation studies utilising immunofluorescence microscopy (Figure 4.29 and Figure 4.32) and an endoglycosidase H digestion (Figure 4.31 and Figure 4.34). Both experimental approaches investigate the impact of the helical binding domain in GC and the cellular localisation of the enzyme.

The ‘glutamic acid mutants’ were overexpressed in GC-deficient mouse embryonic fibroblasts and visualised by an anti-human GC antibody (Figure 4.29). A co-staining against endogenous LIMP-2 was performed, indicating a co-localisation of LIMP-2 with GC wild-type and R211E mutant (Figure 4.29 A). For the mutants localised in the potential binding site of GC (L91E, L94E and L156E) almost no lysosomal localisation could be observed (Figure 4.29 A). To further validate the cellular localisation of the expressed GC a triple staining including LAMP-2 as an independent lysosomal marker was included (Figure 4.30). Co-localisation of endogenous LIMP-2 and LAMP-2 is indicated by purple colour. ER-retention of the LIMP-2 binding-deficient mutants was visualised by co-staining with the ER marker PDI (protein disulfid isomerase). Mutants showing no interaction towards LIMP-2 (L91E, L94E and L156E) did co-localise with PDI. In contrast, GC wild-type and the control mutant (R211E) showed considerably less overlay with the PDI staining (Figure 4.29 B). The level of co-localisation either to LIMP-2 or PDI was expressed as Pearson’s index. A value of one

defines the highest value for co-localisation (Figure 4.29 C, D). An interaction of GC (green) with both lysosomal markers LIMP-2 (blue) and LAMP-2 (red) led to a white signal, as seen for GC wild-type and the control mutant R211E but not for the L91E mutant (Figure 4.30)..

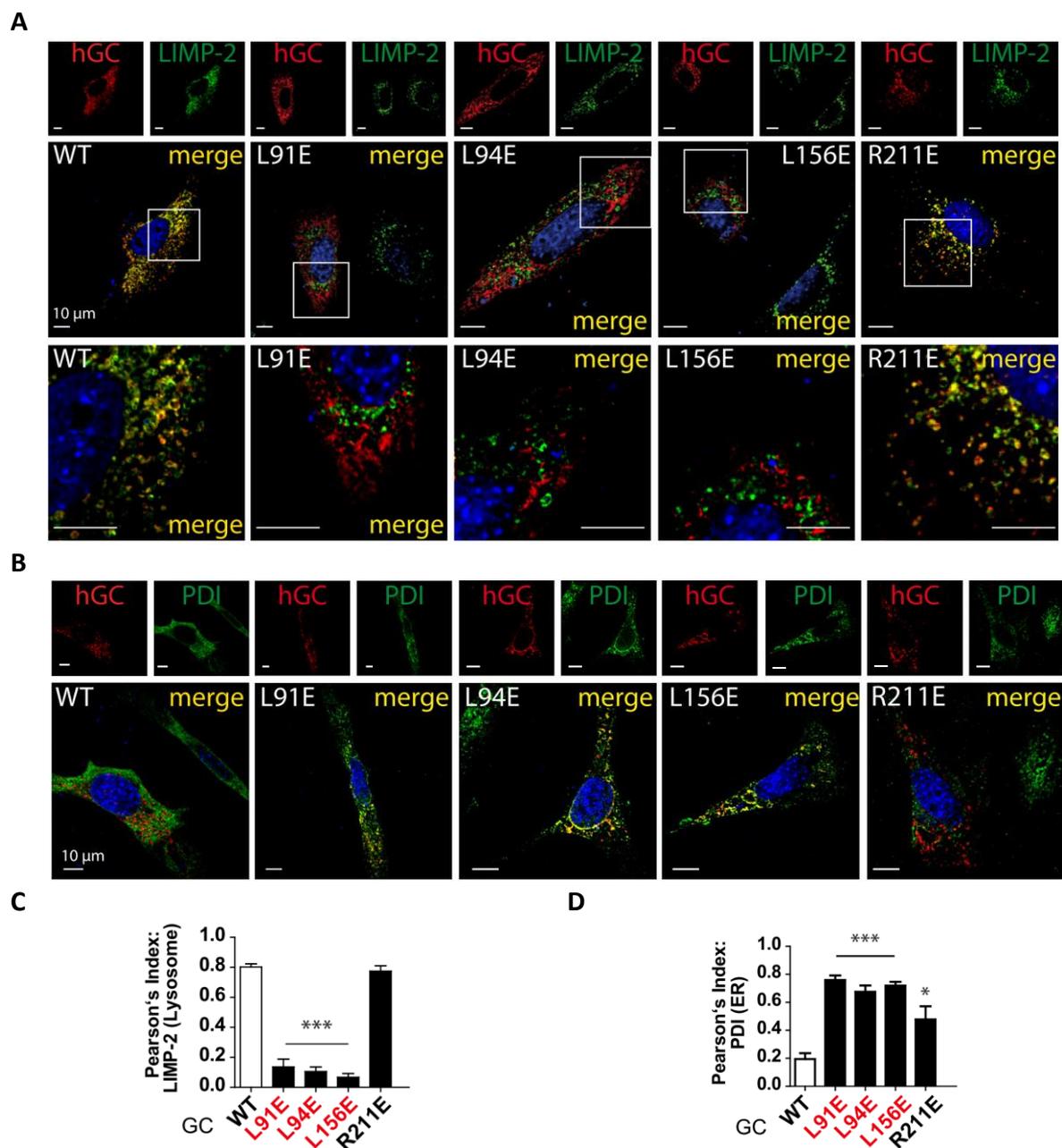


**Figure 4.29: Analysis of cellular localisation of GC ‘glutamic acid mutants’ by immunofluorescence.**

Immunofluorescence stainings of GC mutants transfected into GC-deficient cells. **A**) An anti-human GC antibody (594nm, red) was used together with an antibody against endogenous LIMP-2 (488nm, green). Interaction of both proteins indicates lysosomal localization of GC and is visualized by a yellow colour. The area of magnification is indicated by a white box. **B**) To validate ER localisation of the GC constructs co-staining with the ER-marker PDI (488nm, green) was performed. The intensity of co-localisation of GC with either LIMP-2 (**C**) or PDI (**D**) was presented as a Pearson’s index. A value of one defines the highest value for co-localisation (n=2-10). Point-mutants within the predicted interaction site are indicated in red. A one-way ANOVA with a subsequent Tukey-Kramer posthoc test was utilised for statistical analyses. \*, \*\*, \*\*\* denote p<0.05; 0.01; 0.001 with comparison of all GC mutants to cells transfected with GC wild-type. The scale bars indicate 10 μm in all panels.

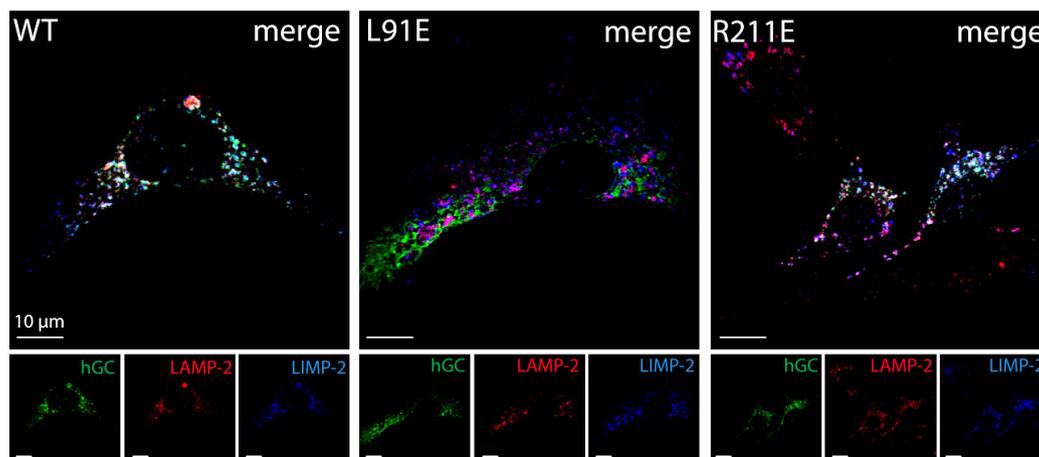


**Figure 4.30: Triple stainings of GC constructs with LIMP-2 and an additional lysosomal marker LAMP-2.** For further validation of lysosomal localisation of GC mutants a triple staining including LAMP-2 was performed, indicating GC in green, LAMP-2 in red and LIMP-2 in blue. The interaction LAMP-2 and LIMP-2 is shown in purple. Additionally, the interaction of GC (green) with the two lysosomal markers is indicated in white as seen for GC wild-type and R211E, but not for the LIMP-2 binding deficient L91E mutant. The scale bars indicate 10  $\mu$ m.

To further biochemically analyse the cellular localisation of the LIMP2-binding-deficient GC mutants L91E, L94E and L156E endoglycosidase H (EndoH) and PNGaseF digestions were performed (Figure 4.31). The proteins were overexpressed in N2a cells and subjected to enzymatic digestions and subsequent immunoblotting using an anti-human GC antibody. Protein fractions resistant to endoglycosidase H digestion (~70 kDa) indicate post ER localisation, whereas a completely deglycosylated protein indicates localisation of the protein within the ER (~56 kDa). The PNGaseF enzyme was utilised as a control to show the fully deglycosylated protein.

The LIMP-2-binding-deficient GC mutants L91E, L94E and L156E show impaired trafficking out of the ER compared to wild-type GC indicated by a sensitivity to endoglycosidase H cleavage. The mutants L91E and L94E seem to be most affected revealing a ~75% decrease of post ER localisation in comparison to the wild-type (Figure 4.31 B). The results of this study support the data obtained from the interaction studies (see results 4.3.1). In conclusion, when interaction of GC with LIMP-2 is impaired as revealed by the co-IP studies, also the transport of these proteins out of the ER appeared to be decreased.

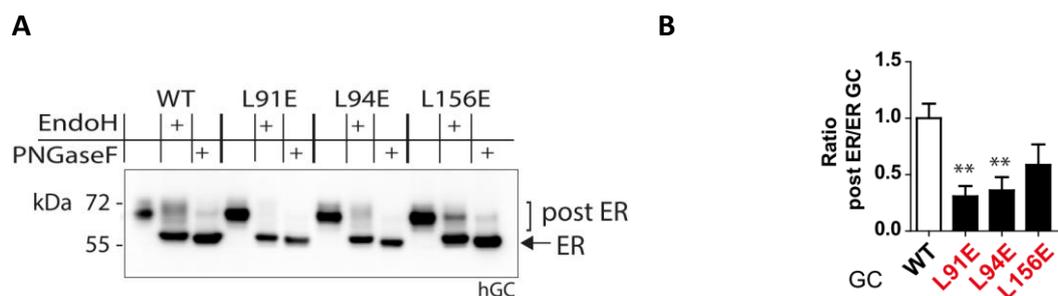


**Figure 4.31: Analysis of cellular localisation of GC mutants by endoglycosidase H digestion.**

**A)** Endoglycosidase H and PNGaseF digestion of ‘glutamic acid GC mutants’ (L91E, L94E, L156E) after overexpression in N2a cells. The subsequent immunoblot was stained for anti-human GC. Protein fractions resistant to EndoH digestion decipher post ER localisation, whereas fully deglycosylated protein indicates localisation in ER. **B)** Densitometry of endoglycosidase H sensitive (ER) and insensitive (post ER) band, calculating the post ER/ER ratio. Values are normalised to the wild-type (WT) GC. A one-way ANOVA with a subsequent Tukey-Kramer posthoc test was utilised for statistical analysis. \*\* denotes  $p < 0.01$  with comparison of each mutant to GC wild-type ( $n=3-8$ ).

The potential LIMP-2 interaction site in the GC protein was further characterised by analysing the Gaucher disease mutants. Thus, the same methods including immunofluorescence microscopy and an endoglycosidase H digestion -as described above- were utilised.

The GC constructs (P159L, I161S, N188S, F213I) were overexpressed in GC-deficient cells and co-stained for endogenous LIMP-2 (Figure 4.32 A). A co-localisation of both proteins is indicated by a yellow colour in the IF pictures and expressed as a Pearson’s index (Figure 4.32 C). Clear co-localisation with LIMP-2 could be seen for GC wild-type, N188S and F213I and no co-localisation was observed for the P159L and the I161S mutants (Figure 4.32 A, C). Triple immunofluorescence staining using an independent lysosomal marker (LAMP-2) confirmed lysosomal localisation of N188S but not I161S (Figure 4.33). PDI-stainings revealed clear co-localisation with the LIMP-2-binding-deficient mutants P159L and I161S indicating their ER residence (Figure 4.32 B, D).

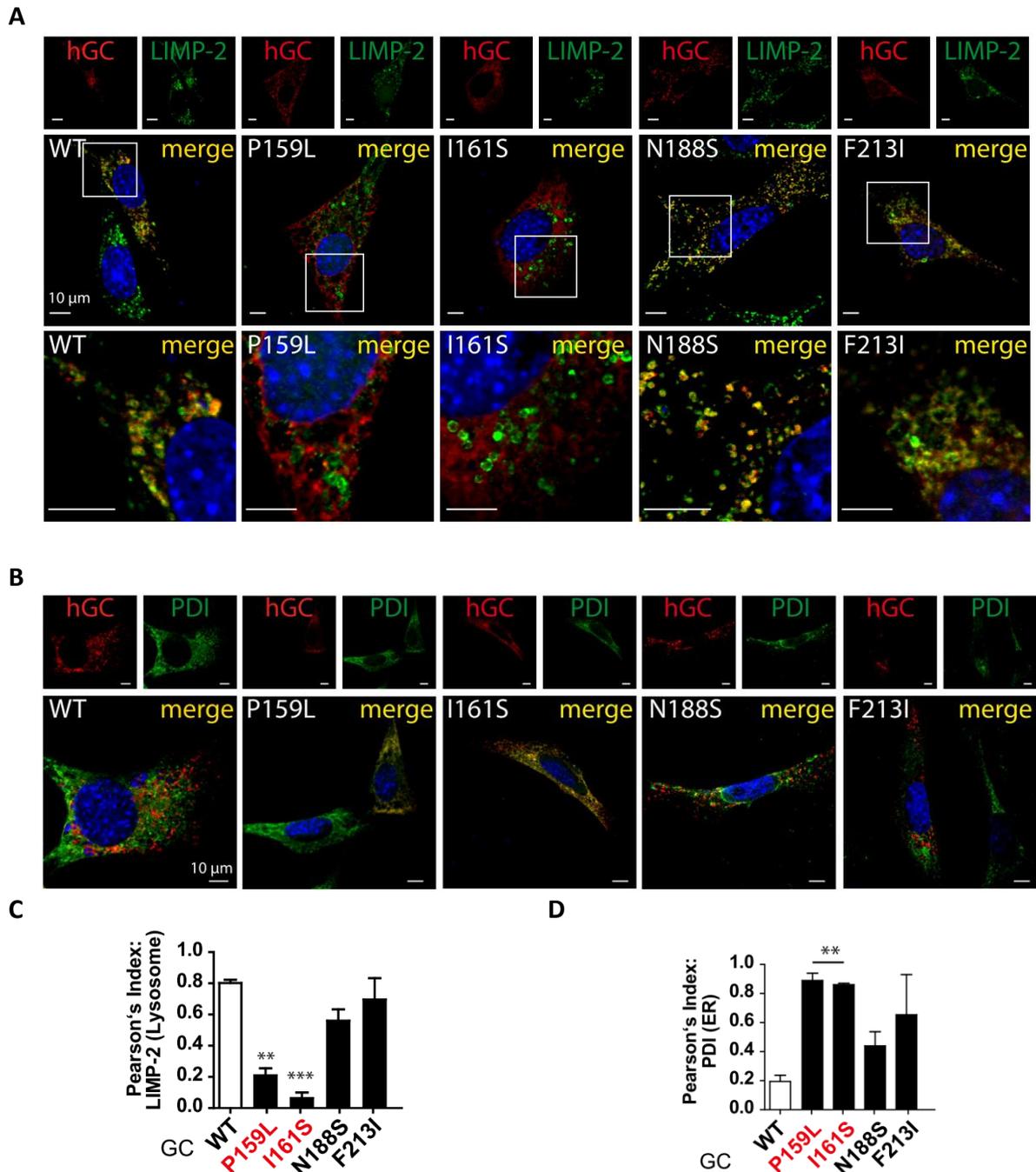


**Figure 4.32: Analysis of cellular localisation of GC patient mutants by immunofluorescence microscopy.**

Visualisation of Gaucher patient mutants transfected into GC deficient MEFs by immunofluorescence. An anti-human GC antibody was used to detect the transfected GC constructs (red) together with an antibody against endogenous LIMP-2 (**A**; green) and ER-marker protein disulfid isomerase (PDI) (**B**; green). Interaction of GC with LIMP-2 indicates lysosomal localisation whereas interaction with PDI suggests ER-retention. The degree of co-localisation of GC with LIMP-2 (**C**) and PDI (**D**) was expressed as a Pearson's index, with one being the highest value for interaction ( $n=2-6$ ). A one-way ANOVA with a subsequent Tukey-Kramer posthoc test was utilized for statistical analyses. \*\*, \*\*\* denote  $p < 0.01$ ;  $0.001$  with comparing all mutants to cells transfected with GC wild-type. The scale bars indicate  $10 \mu\text{m}$  in all panels.

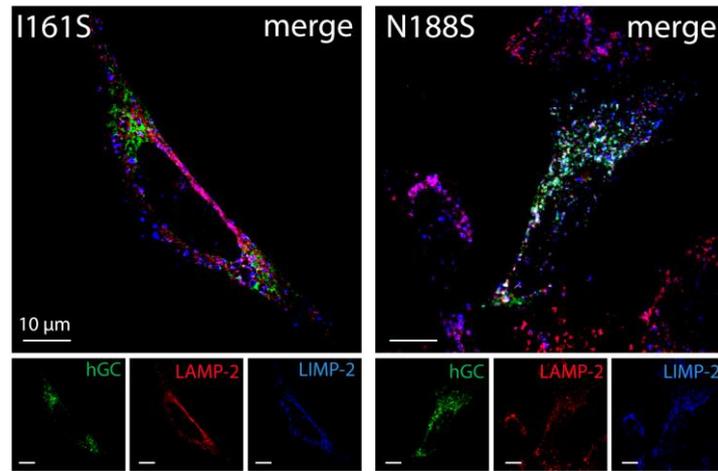


**Figure 4.33: Triple stainings of GC patient mutants with LIMP-2 and LAMP-2.**

For further validation of lysosomal localisation of GC a triple staining including LIMP-2 and LAMP-2 was performed in GC-deficient MEF cells (GC: green; LAMP-2: red and LIMP-2: blue). Co-localisation of both lysosomal markers LIMP-2 and LAMP-2 is indicated by a purple colour and an additional overlay with GC is shown in white colour and can be observed for the GC control mutant N188S, but not for the GC mutant I161S. The corresponding wild-type GC control is presented in figure 4.30. The scale bars indicate 10 µm.

The inability of the GD mutants (P159L and I161S) to transport GC to lysosomes was also analysed biochemically using endoglycosidase H digestions (Figure 4.34). As shown in figure 4.35 A, hardly any endoglycosidase H-resistant protein (~70 kDa), which deciphers post ER localisation, was observed for the P159L and I161S mutants, respectively. In comparison the control mutant N188S shows a similar pattern of protein bands and thus transport out of the ER as observed for the GC wild-type protein. (Figure 4.34 A, B).

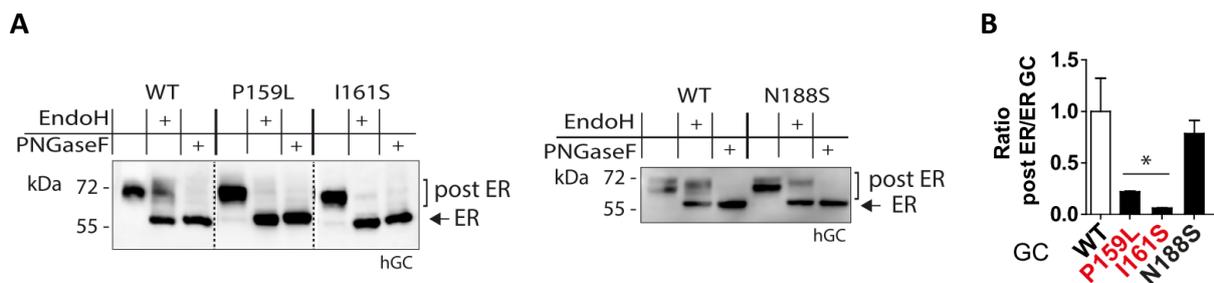


**Figure 4.34: Analysis of cellular localisation of GC mutants by endoglycosidase H digestions.**

**A)** The GC mutants P159L, I161S and N188S were overexpressed in N2a cells and subjected to endoglycosidase H and PNGaseF digestion and analysed by immunoblot using anti-human GC antibody. Protein fractions resistant to the endoglycosidase H enzyme, indicate post ER localisation (~70 kDa), whereas a fully deglycosylated protein deciphers ER-localisation (~56 kDa). **B)** Densitometrical analysis with calculation of the post ER/ER ratio normalised to the GC wild-type situation. A one-way ANOVA with a subsequent Tukey-Kramer posthoc test was utilized for statistical analysis. \* denotes  $p < 0.05$  with comparing mutants to GC wild-type ( $n=2-3$ ).

Taking the findings together, two independent experiments (immunofluorescence stainings and endoglycosidase H digestions) in combination with the two different ER sets of GC mutants – including clinical Gaucher patient mutants – clearly underline the importance of the helical

binding domain in GC, revealing less LIMP-2 interaction with GC and decreased lysosomal/post ER localisation of the enzyme.

#### 4.3.3 Does LIMP-2 overexpression modulate GC trafficking and function?

Having determined the binding site between LIMP-2 and GC on both proteins, it was evaluated if an increased LIMP-2 expression may be of potential therapeutic benefit to facilitate transport of GC wild-type and GC mutants to the lysosome. Studies were performed in two different cell systems (N2a and GC-deficient MEFs). In addition co-expression of LIMP-2 together with GC mutants (LIMP-2-binding-deficient as well as control mutants localised outside the predicted interaction motif) followed by an analysis of the subcellular localisation of the GC protein was used to further validate the identified LIMP-2 interaction site of the GC protein.

Co-expression of LIMP-2 together with GC in GC-deficient as well as N2a cells led to a slight decrease in migration of the GC protein in SDS-PAGE. This is due to the interaction of the ligand GC with its specific transport receptor LIMP-2, resulting in an increased transport out of the ER and an increased glycosylation due to enzyme maturation in the secretory pathway (Figure 4.35 A, C).

As expected for the wild-type GC as well as the control Gaucher mutant N188S showed an increase in the molecular weight of GC (Figure 4.35 A). In contrast, GC mutants suspected to be limited in LIMP-2 binding (L91E, L94E, L156E) did not exhibit a significant increase in molecular weight and thus post ER localisation (GC KO: Figure 4.35 A, B and N2a cells: Figure 4.35 C, D). Since even LIMP-2 overexpression did not result in more post ER localisation of the GC mutants, it can be concluded that this failure is due to a lack of protein-protein interaction.

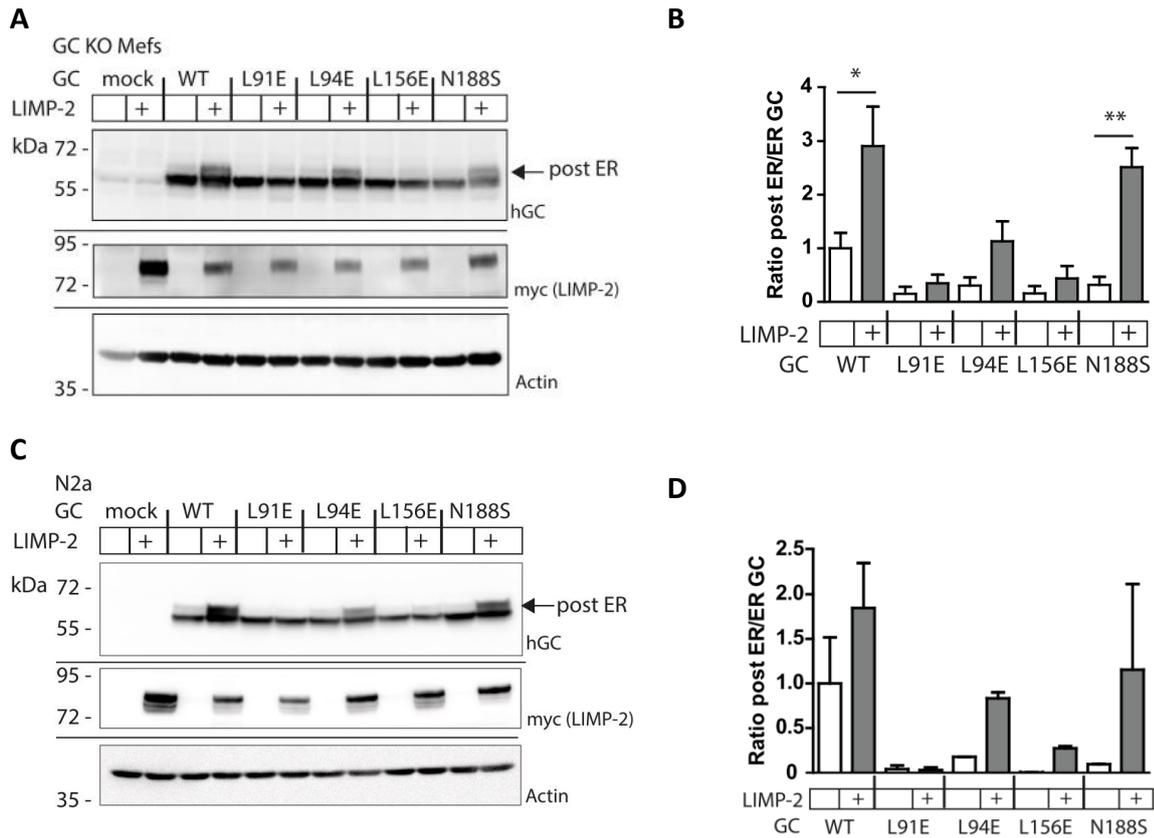


**Figure 4.35: LIMP-2 co-expressed with GC leads to a molecular weight shift due to transport to lysosomes.**

Immunoblots of GC using an anti-human GC antibody. GC mutants were co-expressed with LIMP-2 (anti-myc) in GC KO cells (A) and N2a cells (C) with actin was used as a loading control. The upper band of GC represents a higher glycosylated GC form due to ER exit. The lower protein band indicates GC retained in the ER. **B, D**) Quantification of post ER and ER forms of GC of respective western-blot. Post ER/ER ratio normalised to GC wild-type are indicated (n=2-3). A two-sided independent Student's t-test was utilised to compare the effect of LIMP-2 co-expression within each construct. \*, \*\* denote  $p < 0.05$ ;  $0.01$ .

For a better discrimination between post ER- and ER-forms of GC, endoglycosidase H digestions were performed in the presence or absence of a LIMP-2 co-expression. The results were again obtained in two different cell systems (GC-deficient MEF and N2a cells). Protein fractions resistant to endoglycosidase H digestion (~70 kDa) decipher post ER localisation and a complete deglycosylation of the protein indicates its ER-residence (~56 kDa). An enhanced transport of GC to post ER compartments indicated by an increase in the molecular weight of the GC protein (~70 kDa) was observed for wild-type GC and the patient mutant N188S in the presence of LIMP-2 expression (Figure 4.36). The LIMP-2-binding-deficient GC mutants L91E, L94E and L156E did not show a significant increase in post-ER GC after LIMP-2 co-expression, indicating their retention in ER-compartments (Figure 4.36). Interestingly, a small fraction of the L94E mutant seems to be able to overcome this ER-retention after LIMP-2 co-expression (Figure 4.36). This indicates that this point-mutation still allows transport and thus interaction with LIMP-2 to a certain degree.

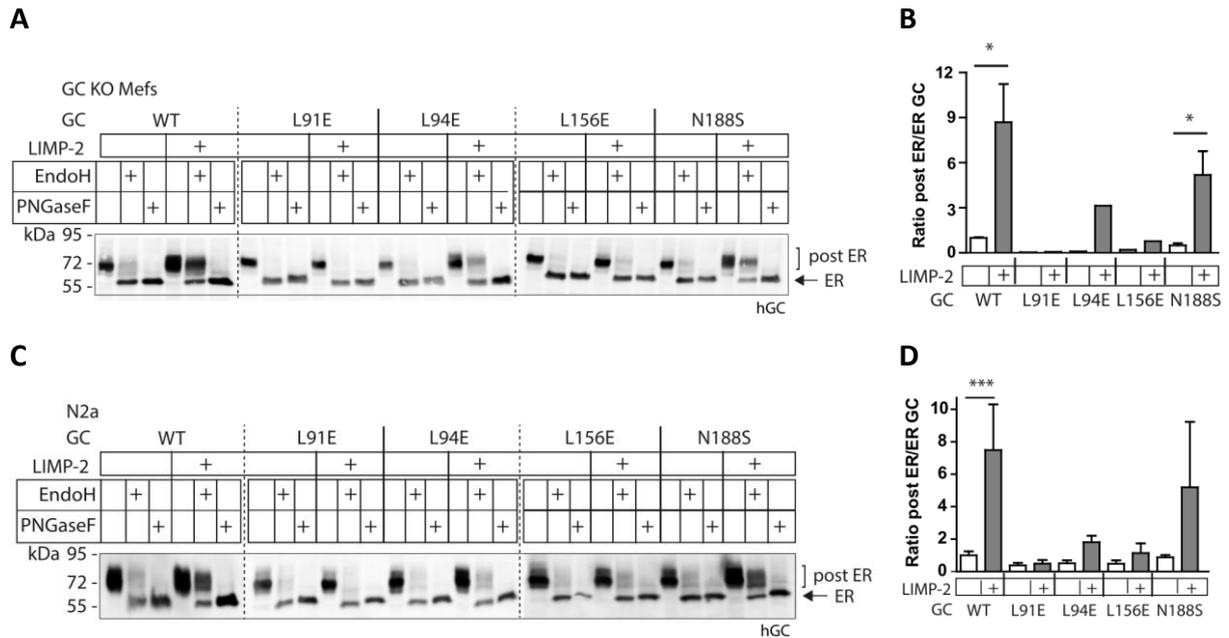


**Figure 4.36: Biochemical analysis of the cellular localisation of the GC mutants by endoglycosidase H digestion.**

Immunoblot of EndoH and PNGaseF digestions of GC mutants detected using an anti-human GC antibody. The GC mutants were expressed in the absence and presence of LIMP-2 in GC-deficient MEF (A) and N2a cells (C). Protein fractions resistant to endoglycosidase H digestion indicate a post ER localisation (~70 kDa), whereas a complete digestion of the enzyme (~56 kDa) indicates the protein to be retained in the ER. A PNGaseF digestion was performed to control for the completeness of the carbohydrate digestion. Quantification of endoglycosidase H digestions, showing GC post ER/ER ratio in GC KO MEFs (B; n=1-3) and N2a cells (D; n=2-6). A two-sided independent Student's t-test was utilised to compare the effect of LIMP-2 co-expression within each GC construct. \*, \*\*\* denote  $p < 0.05$ , 0.001.

In addition, immunofluorescence stainings of the expressed GC mutants in presence with co-expressed LIMP-2 as detected using an anti-myc antibody were performed (Figure 4.37 A). The co-localisation of each GC protein with co-overexpressed LIMP-2 was expressed as a Pearson's index (Figure 4.37 B). The GC wild-type and Gaucher mutant N188S show the same level of co-localisation with LIMP-2 (Pearson's value ~0.85). The potential LIMP-2 binding-deficient GC mutants L91E, L94E and L156E show less co-localisation with lowest co-localisation observed when the L91E mutant was expressed (Pearson's value ~0.3) (Figure 4.37 B).

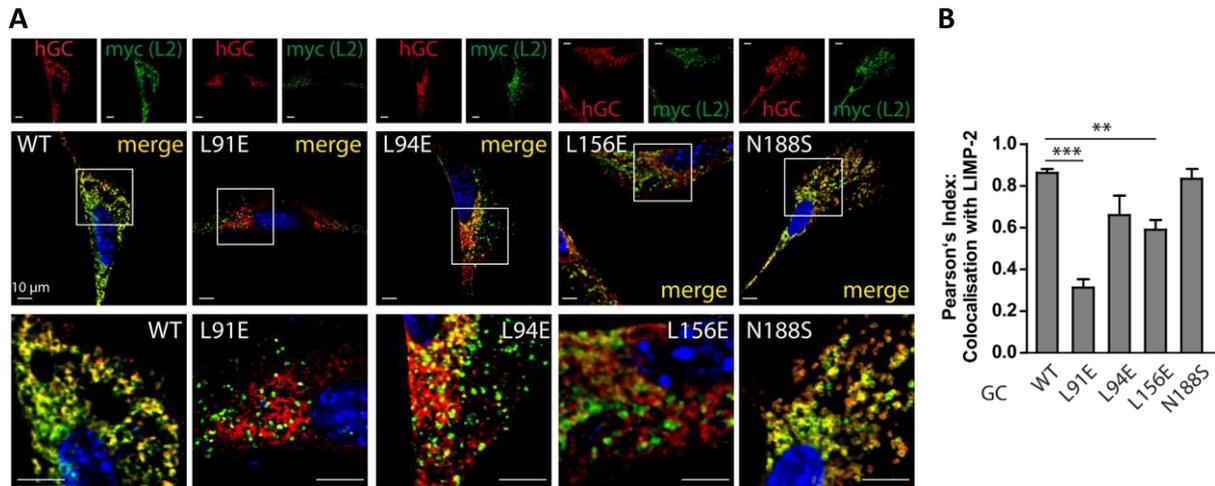


**Figure 4.37: Immunofluorescence microscopy to evaluate co-localisation of GC mutants and LIMP-2.**

**A)** Immunofluorescence stainings showing GC-deficient cells transfected with the indicated GC mutants (anti-hGC (red)) and LIMP-2 (anti-myc (green)). The degree of co-localisation of GC with overexpressed LIMP-2 is indicated by a yellow colour. Areas of magnification are marked by white boxes. Scale bars indicate 10  $\mu$ m. **B)** Quantification of the IF stainings using the Pearson's index to analyse the co-localisation of transfected GC and co-expressed LIMP-2 (n=2-7). A one-way ANOVA with a subsequent Tukey-Kramer posthoc test was applied for all statistical analyses. \*\*, \*\*\* denote  $p < 0.01$ ;  $0.001$ .

Moreover, a putative effect of enhanced LIMP-2 expression on GC function was assessed. Enzyme activity assays utilising an artificial substrate were performed in N2a cell lysates after overexpression of the individual GC constructs in presence and absence of overexpressed LIMP-2. Only the wild-type GC revealed a significant increase of GC activity after co-expression of LIMP-2. To a much lesser extent the Gaucher mutant N188S as well as the L94E mutant could be activated after LIMP-2 overexpression (Figure 4.38).

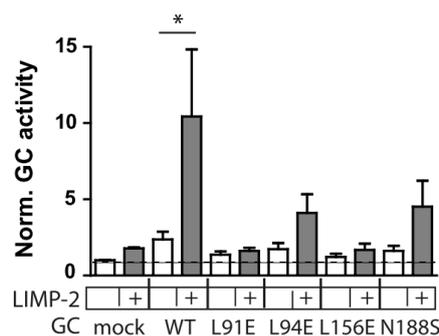


**Figure 4.38: Effect of LIMP-2 co-expression on GC activity.**

GC activity measurement of GC mutants (L91E, L94E, L156E and N188S) overexpressed in N2a cells with and without co-expression of LIMP-2. The GC activity was normalized (norm.) to the mock transfected control, indicating background/endogenous GC activity of this assay (dotted line). A One-Way ANOVA with a subsequent Tukey-Kramer posthoc test was applied for statistical analysis. \* denotes  $p < 0.05$  with  $n=4$ .

In summary, LIMP-2 overexpression exhibits a positive effect on GC trafficking and activity. However, these effects could only be observed if the GC protein was able to interact with its lysosomal transport receptor.

#### 4.3.4 Validation of the LIMP-2 interaction site of GC protein using LIMP-2-derived peptides

As shown above, endogenous GC was successfully precipitated from cell lysates by a peptide derived from the binding site (helix 5) of LIMP-2 (Figure 4.14). This specific interaction was further exploited to study the binding abilities of the different GC mutants to this helix 5 peptide. A pull-down assay to precipitate the overexpressed GC mutants from N2a cells using the helix 5 peptide was designed (Figure 4.39 A). The pull-down was visualised by immunoblotting. Staining for GC revealing a strong interaction of the GC wild-type as well as the N188S mutant to the helix 5 peptide. The interactions of the LIMP-2-derived peptide to the GC mutants (L91E, L94E, L156E) was reduced to one third compared to the GC wild-type (Figure 4.39 B, C). The same mutants already exhibited impaired interaction with LIMP-2 in co-immunoprecipitation studies (Figure 4.27).

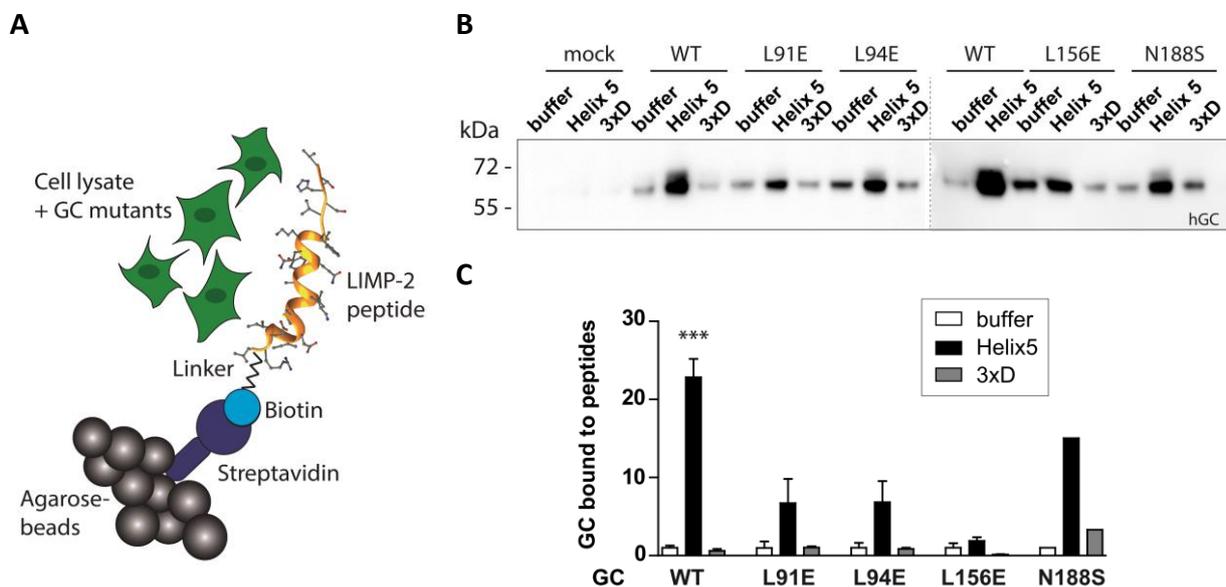


**Figure 4.39: Pull-down of overexpressed GC mutants with LIMP-2-derived peptides from cell lysates.**

**A)** Principle of peptide-pulldown of overexpressed GC (Wildtype (WT), L91E, L94E, L156E and N188S) from N2a cell lysates. **B)** Immunoblot of pulldown using an anti-human GC (hGC) antibody. Buffer only and 3xD helix 5 were used as negative binding control. **C)** Quantification of the signal intensity of the precipitated GC proteins, indicating binding of the GC wild-type as well as N188S mutant to the helix 5 peptide. The L91E, L94E and L156E GC mutants only exhibit weak interaction with the helix 5 peptide. Each construct was normalised to buffer only. A one-way ANOVA with a subsequent Tukey-Kramer posthoc test was applied for statistical analysis. \*\*\* denotes  $p < 0.001$  ( $n = 2-4$ ).

In summary, these data reveal another strategy to analyse the LIMP-2 interaction site of the GC protein by utilising LIMP-2-derived peptides.

#### 4.4 LIMP-2 knockout mice – what impact does LIMP-2/GC have on $\alpha$ -synuclein homeostasis in murine brain?

The enzymatic activity of GC has been directly linked to the intracellular  $\alpha$ -synuclein homeostasis (Mazzulli, Xu et al. 2011, Westbroek, Gustafson et al. 2011). However, the role of LIMP-2, as the specific lysosomal transporter of GC, has not been assessed. In this study LIMP-2-deficient mice were analysed for neuronal  $\alpha$ -synuclein accumulation and impairment of the central nervous system (CNS). LIMP-2 knockout mice were backcrossed into the C57BL/6N background exhibiting normal  $\alpha$ -synuclein level (see introduction section 1.2.3 and Figure 3.1). The following studies mainly focus on the midbrain and pons as these regions are most affected in synucleinopathies like Parkinson disease (Davie 2008).

Immunoblot analysis of LIMP-2 deficient pons and midbrain lysates showed no expression of LIMP-2 and strong reduction in GC protein levels (Figure 4.40 A). A GC activity assay revealed a significant decline in GC-activity (less than 50 % when compared to the wild-type samples) in lysates from both brain regions (Figure 4.40 B).

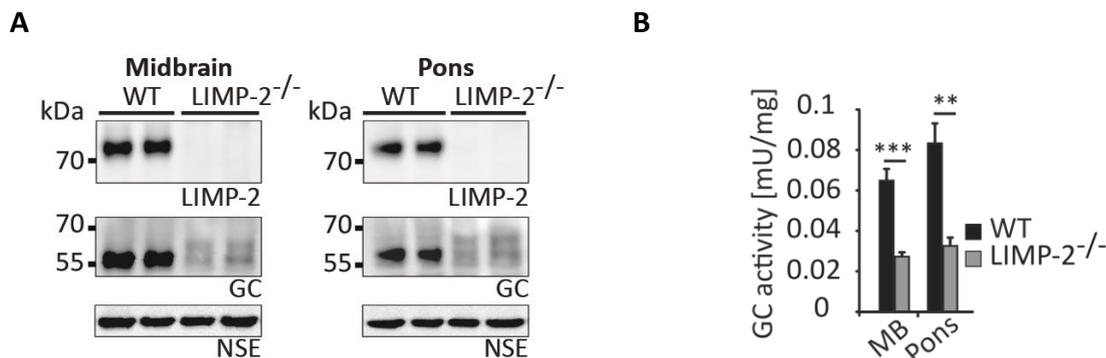


**Figure 4.40: LIMP-2 deficiency causes decreased GC expression and activity in murine pons and midbrain.**

**A)** Immunoblot of pons and midbrain lysates of wild-type (WT) and LIMP-2-deficient mice showing complete absence of LIMP-2 protein in the knockout and only residual GC protein levels. Neuronspecific enolase (NSE) was used as a loading control. **B)** Pons and midbrain lysates were subjected to GC activity assays indicating a significant decrease in GC activity in both tissues of LIMP-deficient mice. An independent two-sided Student's t-test was used for statistical analysis. \*\*, \* \*\* denote  $p < 0.01$ ,  $0.001$ ;  $n = 4$ .

##### 4.4.1 Storage of GC substrate and undefined material

In the following studies it was assessed to what extent the observed reduction in GC activity affects intracellular levels of the GC substrate glucosylceramide. Since no reliable antibodies are available to stain for the lipid, brain sections (pons and midbrain) of wild-type and LIMP-2-deficient mice were subjected to a periodic-acid-Schiff staining (PAS), detecting carbohydrates including the glycosyl-residues of the GC substrate. PAS positive accumulation was

found in the midbrain and pons of LIMP-2-deficient mice (Figure 4.41 A). Analyses in 2, 4, 6 and 10 months old animals further revealed a progressive accumulation of the carbohydrate conjugates especially in the pons of LIMP-2-deficient mice (Figure 4.41 B). Additionally electron micrographs of the pons revealed unidentified storage material (arrows; Figure 4.42) and lipid droplets (red asterisks; Figure 4.42) in LIMP-2 knockout but not in wild-type neurons.

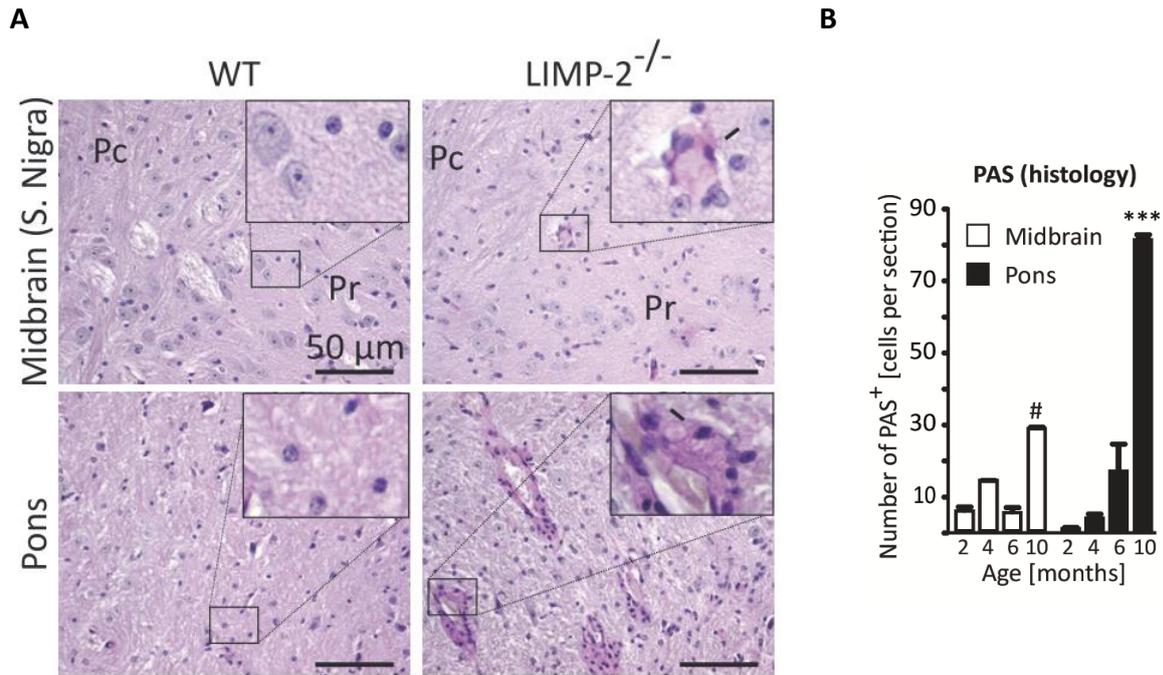


**Figure 4.41: Periodic-acid-Schiff staining (PAS) of brain sections at different ages.**

**A)** Pons and midbrain sections of wild-type (WT) and LIMP-2 KO (-/-) mice at different ages (2, 4, 6 and 10 months) were subjected to PAS staining. Depicted images are from 10 months old mice with inserts showing magnified area of image. Pc = pars compacta; Pr = pars reticulata. Scale bars indicate 50  $\mu$ m. **B)** Respective quantification of PAS positive cells highlighting progressive accumulation of the carbohydrate-conjugates in LIMP-2-deficient compared to wild-type brain. A one-way ANOVA with a subsequent Tukey-Kramer posthoc test was applied for statistical analysis. # and \*\*\* denote  $p > 0.05$  and  $p < 0.001$ . The stainings and densitometric analysis were performed in collaboration with Dr. Michelle Rothaug (Biochemical Institute, University of Kiel).

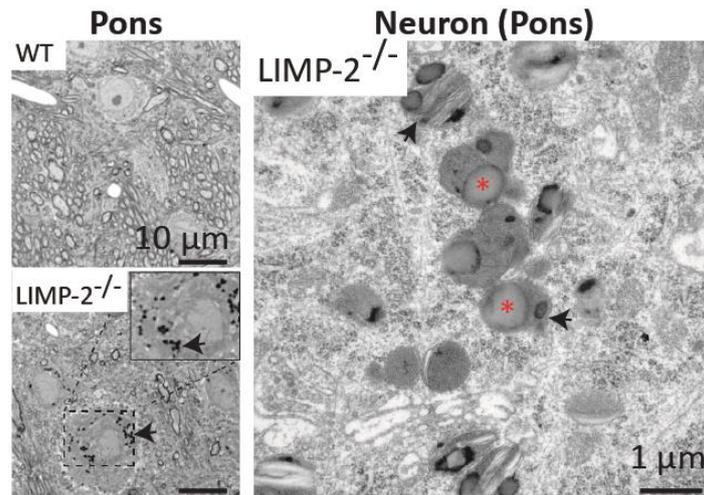


**Figure 4.42: Electron micrographs indicating storage material in the pons of LIMP-2 KO mice.**

Sections of the pons of 10 months old LIMP-2 deficient and wild-type animals were subjected to toluidine blue staining for ultrastructural analysis. Accumulation of storage material (highlighted by arrows) and lipid droplets (indicated by red asterisks) were evident in sections of LIMP-2 KO compared to wild-type. Scale bars indicate 10 and 1  $\mu\text{m}$ . EM stainings were performed by Dr. Michaela Schweizer (ZMNH, UKE Hamburg).

In summary, LIMP-2-deficient mice revealed a reduction in GC protein and enzymatic activity in pons and midbrain. The decline in functional GC ultimately led to accumulation of PAS-positive deposits.

#### 4.4.2 Accumulation of $\alpha$ -synuclein

Dysfunction of GC and accumulation of its substrate (glucosylceramide) have been shown to negatively influence neuronal  $\alpha$ -synuclein levels and its degradation (see introduction 1.4.3) (Mazzulli, Xu et al. 2011, Westbroek, Gustafson et al. 2011). Hence, LIMP-2-deficient brain was analysed for  $\alpha$ -synuclein accumulation via immunoblotting and immunohistochemistry. Before performing SDS-PAGE, brain lysates were separated into Triton soluble (T-Sol) and insoluble (SDS) fractions. Three different  $\alpha$ -synuclein antibodies (Syn-1, C-20 and 4D6; for more information see material and methods chapter 3.1.3) were utilised depicting three forms of  $\alpha$ -synuclein (~17 kDa, ~23 kDa and ~58 kDa), that were not present in lysates from mice deficient for  $\alpha$ -synuclein (Figure 4.43). It should be considered that each antibody detects the various  $\alpha$ -synuclein forms with different preferences. For the monomeric form (~17 kDa) no significant changes could be observed in the absence of LIMP-2 (Figure 4.43). This is in contrast to the 23 kDa and 58 kDa forms of  $\alpha$ -synuclein, which showed to be elevated at least twice as much in the midbrain of LIMP-2-deficient mice in comparison to wild-type samples (Figure 4.43).

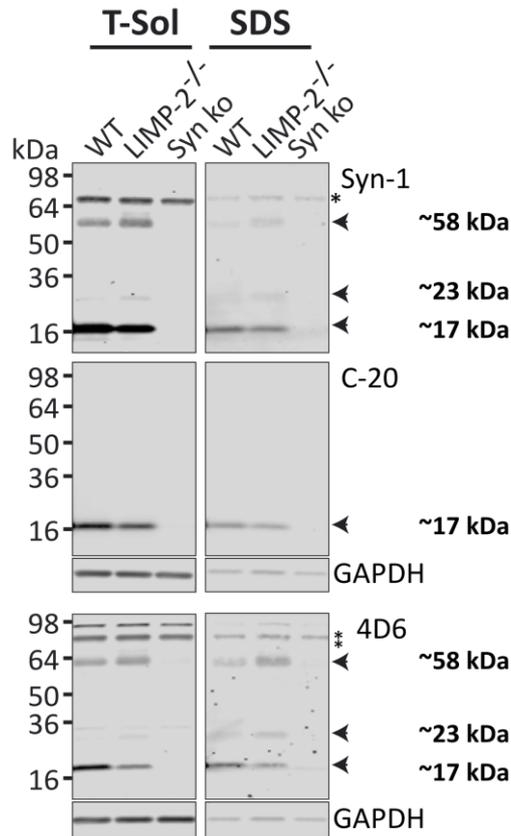
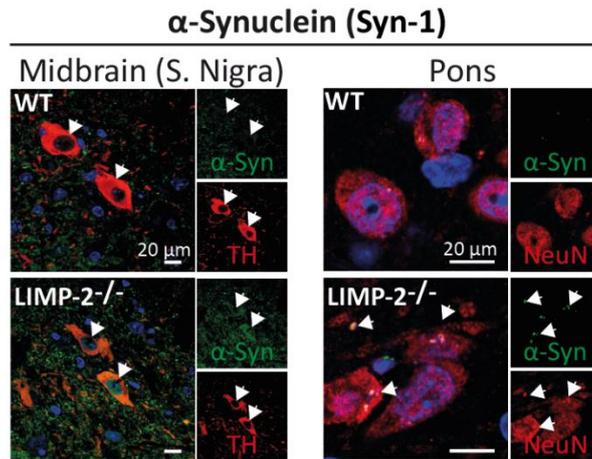


**Figure 4.43: Immunoblot analysis revealing  $\alpha$ -synuclein accumulation in the midbrain of LIMP-2-deficient animals.**

Immunoblots of soluble (T-Sol) and insoluble (SDS) fractions of wild-type (WT) and LIMP-2 knockout (-/-) as well as  $\alpha$ -synuclein deficient (Syn ko) midbrain samples. Three different antibodies (Syn-1, C-20 and 4D6) were used to detect three species of  $\alpha$ -synuclein (17 kDa, 23 kDa and 58 kDa). Arrowheads indicate  $\alpha$ -synuclein forms and the asterisks indicate non-specific bands. **B**) Quantification of immunoblots utilising the syn-1 and 4D6 antibody. Unchanged levels of the 17 kDa form, but a statistical increase in the 23 kDa and 58 kDa forms of  $\alpha$ -synuclein in LIMP-2 deficient samples of both fractions was observed (T-Sol and SDS). An independent two-sided Student's t-test was performed for statistical analysis with \* and \*\* denoting  $p < 0.05$  and  $0.01$ ;  $n = 3-7$ . The  $\alpha$ -synuclein immunoblots were performed in collaboration with Dr. Joseph Mazzulli (Northwestern University of Chicago, US).

Neuronal accumulation of  $\alpha$ -synuclein in pons and midbrain, including the substantia nigra was confirmed by immunohistochemistry, using the three  $\alpha$ -synuclein specific antibodies (Syn-1, 4D6 and C-20). Immunofluorescence stainings of  $\alpha$ -synuclein were performed in pons and midbrain revealing neuronal  $\alpha$ -synuclein accumulation (Syn-1 antibody: Figure 4.44 A; 4D6 and C-20: Figure 4.44 B). The pons and midbrain samples were co-stained for a neuronal marker (NeuN) and tyrosine-hydroxylase (TH) to identify dopaminergic neurons. Additionally, DAB-immunohistochemical and immunofluorescence stainings confirmed accumulation of  $\alpha$ -synuclein in the pons using the 4D6 and C-20 antibody (left panels; Figure 4.44 B).

A



B

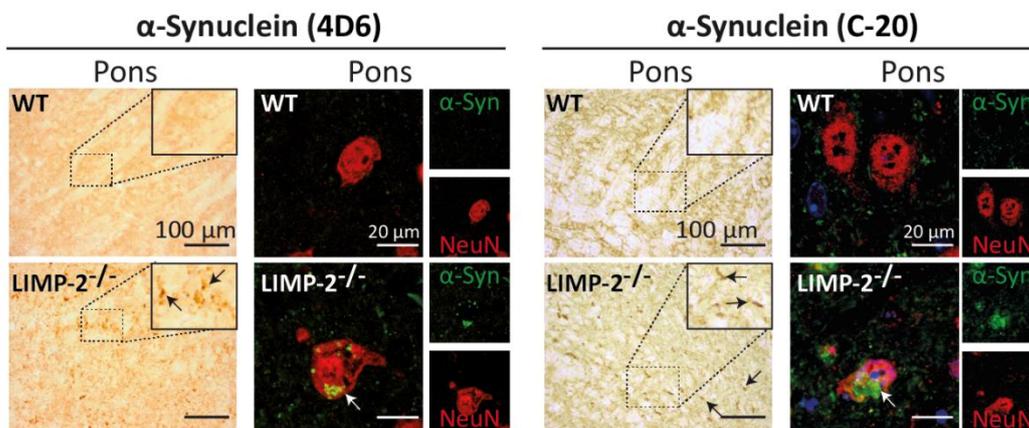


**Figure 4.44: Immunohistochemical stainings of  $\alpha$ -synuclein in midbrain and pons.**

**A)** Immunofluorescence stainings of  $\alpha$ -synuclein (green, 488 nm) in the pons and midbrain co-stained with a neuronal marker (NeuN; red, 594 nm) and tyrosine-hydroxylase (TH; red, 594 nm) comparing 10 month old littermates. White arrows point towards accumulated  $\alpha$ -synuclein (S. Nigra: substantia nigra). **B)** DAB (left panels) and immunofluorescence (right panels) stainings of  $\alpha$ -synuclein (green; 488 nm) using the 4D6 and C-20 antibody (NeuN; red; 694 nm). Arrows highlight accumulated  $\alpha$ -synuclein with inlays showing magnified sections of the DAB stainings. Scale bars indicate 20  $\mu$ m for immunofluorescence stainings and 100  $\mu$ m for DAB-stained sections. All stainings shown here were performed in collaboration with Dr. Michelle Rothaug (Biochemical Institute, University of Kiel).

These results confirm an accumulation of  $\alpha$ -synuclein in the pons and midbrain of LIMP-2-deficient mice. This suggests a possible contribution of  $\alpha$ -synuclein in the pathological processes observed in LIMP-2-deficient mice.

#### 4.4.3 Increased $\alpha$ -synuclein levels lead to neurotoxicity and behavioural abnormalities

It has been shown that  $\alpha$ -synuclein accumulation can cause neurotoxicity in cells and animal models (Xu, Kao et al. 2002). Especially dopaminergic neurons in the substantia nigra of the

midbrain are affected by aggregation of the cytosolic protein, thus undergoing neurodegeneration in Parkinson disease (Xu, Kao et al. 2002, Periquet, Fulga et al. 2007).

To study the effect of the described  $\alpha$ -synuclein accumulation, histochemical assays were established to verify the viability and characteristics of neurons in brain sections of midbrain and pons. Apoptotic cell stainings were performed by terminal deoxynucleotidyl transferase dUTP nick end labeling (TUNEL) on brain sections from mice of different ages (2-10 months). In the pons an abrupt increase of apoptotic cells (TUNEL positive) could be observed starting from the age of 6 months. TUNEL-staining in the midbrain of LIMP-2-deficient mice revealed an increase in apoptotic cell death at the age of 10 months (Figure 4.45 A).

In PD mouse models and patients astrogliosis as well as microgliosis have been observed (Hirsch, Hunot et al. 2005, Zhang, Wang et al. 2005). Hence, DAB-immunohistochemistry was utilised to check for both neuropathological changes in brain sections of LIMP-2-deficient mice with markers for astrocytes (glial fibrillary acidic protein, GFAP) (Figure 4.45 B) and microglia (macrosialin/CD68) (Figure 4.45 C). Sections of pons and midbrain from mice at the age of 2, 4, 6 and 10 month were subjected to GFAP and CD68 stainings. An increased number of GFAP- as well as CD68-positive cells could be found in both tissues of LIMP-2-deficient mice when comparison to wild-type mice. Furthermore, an age-dependent progression of astro- as well as microgliosis in the brain of LIMP-2-deficient mice could be observed (Figure 4.45 B, C).

Consequently, the above described pathological changes in the brain of LIMP-2-deficient mice are accompanied by behavioural abnormalities. LIMP-2 knockout mice exhibited severe neurological impairments starting in the age of 4 months including tremor and hind-limb claspings, which finally resulted in partial paralysis. Finally, LIMP-2-deficient mice did not survive beyond 10 months and showed reduced weight (wild-type:  $34,2 \pm 5.4$  g; LIMP-2 knockout:  $22.2 \pm 2.8$  g).

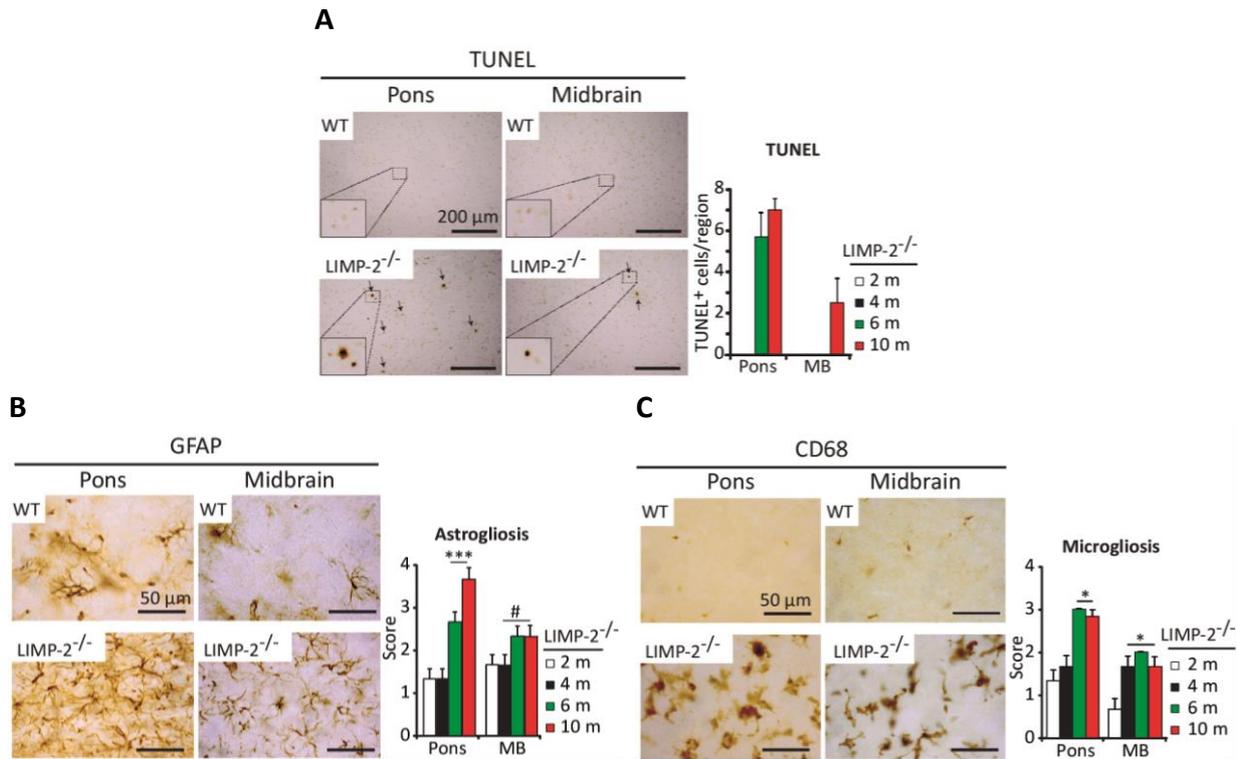


**Figure 4.45: DAB-immunohistochemistry showing highly progressive neurotoxic effects of  $\alpha$ -synuclein.**

**A)** TUNEL-staining of positive apoptotic cells (highlighted by arrows) showing a progressive increase in apoptotic cells in the pons and midbrain of LIMP-2-deficient (-/-) compared to wild-type (WT) mice (2, 4, 6 and 10 months). DAB-stainings to check for astroglia (GFAP; **B**) and microglia (CD68; **C**) in pons and midbrain of wild-type (WT) and LIMP-2 KO mice (2, 4, 6 and 10 months of age) show progressively increasing number of positive cells. A one-way ANOVA with a subsequent Tukey-Kramer posthoc test was used for statistical analysis. #, \* and \*\*\* denote  $p > 0.05$  and  $p < 0.05$  and  $0.001$ ;  $n = 3-4$  mice per age. All stainings show representative results and were taken from wild-type and LIMP-2 knockout littermates at the age of 10 months. Scale bars indicate  $200 \mu\text{m}$  in TUNEL-stainings and  $50 \mu\text{m}$  in GFAP/CD68 stainings. The stainings as well as the densitometric analyses were performed in collaboration with Dr. Michelle Rothaug (Biochemical Institute, University of Kiel).

In summary, the results indicate that accumulation of  $\alpha$ -synuclein, triggered by LIMP-2-deficiency, is accompanied by significant apoptotic cell death and gliosis in the pons and midbrain. Due to these profound impairments of the CNS the LIMP-2-deficient mouse also showed strong behavioural abnormalities (data not shown).

## 4.5 How does $\alpha$ -synuclein affect human CNS?

### 4.5.1 Does $\alpha$ -synuclein interfere with GC function?

The results shown above describe an accumulation of  $\alpha$ -synuclein in murine brain induced by a deficiency of LIMP-2 with a simultaneous loss of GC activity. The impaired GC function is thought to be the initial cause of the observed pathogenic increase in  $\alpha$ -synuclein. Neuronal accumulation of  $\alpha$ -synuclein in murine brain resulted in a cascade of events: neurotoxicity, inflammation (astro- and microgliosis) and neuronal death.

To study a possible interference of the accumulated  $\alpha$ -synuclein with GC, human dopaminergic neurons from midbrain derived from induced pluripotent stem cells (iPSC) were utilised and transduced with  $\alpha$ -synuclein by lentiviral delivery. After 48 hours expression time, the effect on GC activity was measured using a newly developed method to measure lysosomal GC activity in living cells. These experiments were performed in the laboratory of *Dr. Dimitri Krainc* (Harvard Medical School/Massachusetts General Hospital, Boston, USA). To measure the lysosomal GC activity the transduced cells were treated with DMSO or bafilomycin, which largely prevents lysosomal hydrolase activity. A pulse chase experiment with a fluorescent GC substrate was performed and GC activity was measured every 30 minutes over a time period of three hours. The GC activity was assessed in the presence of DMSO and bafilomycin A1. Since bafilomycin is a specific inhibitor of the vacuolar type H<sup>+</sup> ATPase, lysosomal function including GC activity is diminished in these cells. In order to calculate the lysosomal GC activity the total cellular GC activity (DMSO treated cells) was subtracted from the activity measured in the presence of bafilomycin. Since GC activity was expressed as the area under the curve (AUC), the area between DMSO and bafilomycin treated cells indicates the lysosomal activity only (for more details see material and methods 3.2.3.11). A significant reduction in lysosomal GC activity could be observed in human midbrain dopaminergic neurons after  $\alpha$ -synuclein overexpression when compared to the vector control (Figure 4.46). This indicates a negative effect of  $\alpha$ -synuclein on lysosomal GC activity.

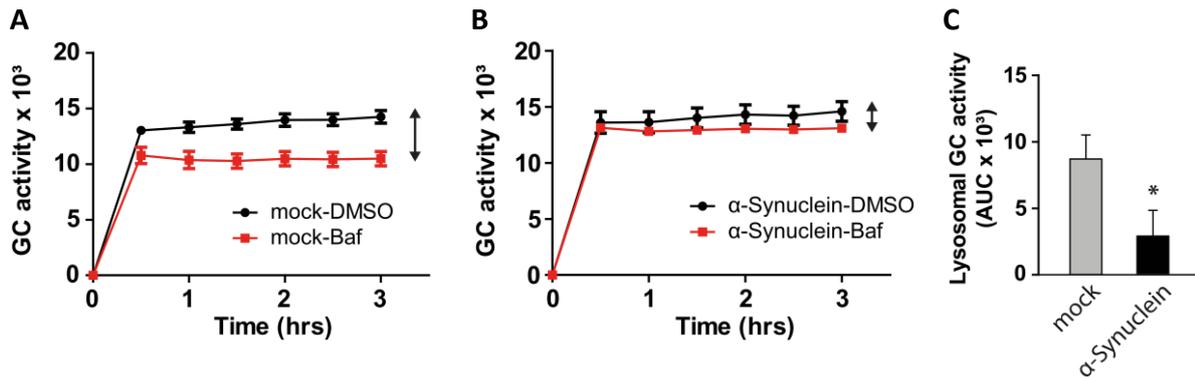


**Figure 4.46: Effect of  $\alpha$ -synuclein on lysosomal GC activity in human midbrain dopaminergic neurons.**

Human dopaminergic neurons were transduced with a mock vector (A) and  $\alpha$ -synuclein (B). In a pulse chase experiment with a fluorescent GC substrate GC activity was measured in living cells over a time period of three hours. The areas between the DMSO (black) and bafilomycin (Baf; red) treated samples indicate the lysosomal GC activity in the living cells (indicated by an arrow). The activity is depicted in arbitrary units as the intensity of the fluorescent substrate. C) The area between the DMSO and bafilomycin curve (AUC) was quantified revealing a decrease in lysosomal GC activity after  $\alpha$ -synuclein overexpression. A two sided independent Student's t-test was utilised for statistical analysis. \* denotes  $p < 0.05$ ;  $n = 4$ .

#### 4.5.2 Does $\alpha$ -synuclein modulate the expression of LIMP-2?

The role of LIMP-2 on cellular GC function and  $\alpha$ -synuclein metabolism could be demonstrated in brain of LIMP-2-deficient mice. This leads to the question if LIMP-2 protein expression is also altered when abnormal  $\alpha$ -synuclein levels are present in the cells. To address this question, Parkinson disease post-mortem midbrain samples were analysed for LIMP-2 protein expression by immunofluorescence. In the case of a synucleinopathy increased levels of neuronal LIMP-2 could be observed (Figure 4.47). Consequently, this resulted in enlarged vesicles (referred to as circumference in figure 4.47). Dopaminergic (DA) neurons within the midbrain were identified by their high neuromelanin content (Figure 4.47).

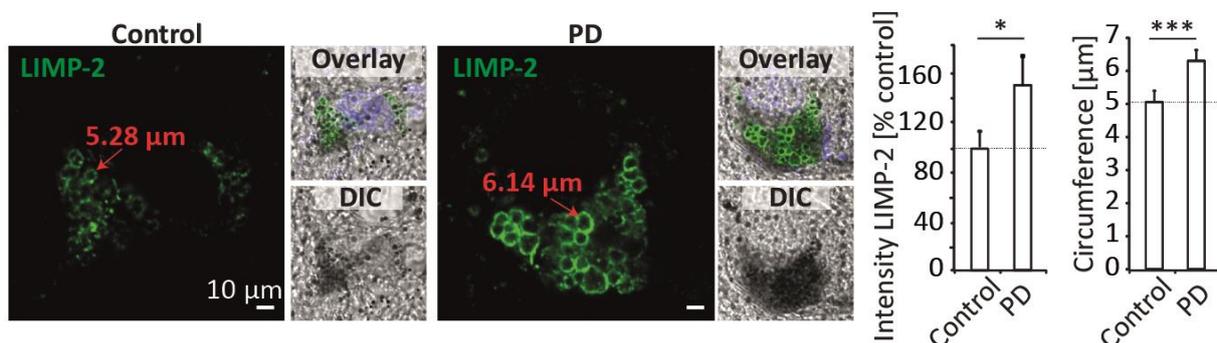


**Figure 4.47: Immunohistological stainings of LIMP-2 in control and PD midbrain sections.**

Control and Parkinson disease midbrain sections were stained for LIMP-2. Dopaminergic (DA) neurons were identified by their high neuromelanin content (black structures in differential interference contrast (DIC) image). As indicated in the stainings, circumferences of LIMP-2 positive vesicles are increased in size in PD samples (6.14  $\mu\text{m}$  compared to 5.28  $\mu\text{m}$ ). The total LIMP-2 signal was divided by the circumference of vesicles compensating for variations in vesicle size revealing a significant increase in LIMP-2 signal in PD DA neurons when compared to healthy control. For statistical analysis an independent two-sided Student's t-test was performed with \* and \*\*\* denoting  $p < 0.05$  and 0.001; Control patients:  $n = 5$ ; PD patients:  $n = 7$ . Scale bars decipher 10  $\mu\text{m}$ . The samples were stained by Dr. Hermann Altmeppen (University Hospital Hamburg, UKE, DE). The pictures were taken in collaboration with Dr. Michelle Rothaug (University of Kiel, DE).

In summary, these results not only show that dysfunction of GC negatively effects  $\alpha$ -synuclein homeostasis, but also that  $\alpha$ -synuclein interferes with GC activity and influences neuronal LIMP-2 expression. The augmented expression of LIMP-2 and increased vesicle size in human PD midbrain sections further indicates an important role of the lysosomal protein in the pathological cascade in PD.

#### **4.6 What are the effects of LIMP-2-deficiency in humans?**

In patients a deficiency in LIMP-2 leads to the Action Myoclonus Renal Failure syndrome (AMRF), which is characterised by progressive myoclonic epilepsy (PME) associated with ataxia, undefined storage material in the brain and in most cases causing renal failure (see introduction 1.2.2). Although the LIMP-2-deficient mouse seems to be a valid disease model (Gamp, Tanaka et al. 2003, Berkovic, Dibbens et al. 2008, Rothaug, Zunke et al. 2014), differences between the murine and human situation exist. For example the consequences of LIMP-2 deficiency in AMRF patients appear to be even more severe than in mice, resulting in premature death between 20-35 years (Badhwar, Berkovic et al. 2004, Rubboli, Franceschetti et al. 2011).

Unfortunately, the current experimental approaches are restricted to fibroblasts, making it difficult to evaluate  $\alpha$ -synuclein homeostasis. The fibroblasts used here were derived from AMRF patient 1 (Case A) and patient 2 (Case B) (Berkovic, Dibbens et al. 2008). Like the majority of AMRF causing mutations, both cases result in a truncated LIMP-2 protein, which cannot be detected by the utilised antibody, which is designed against the c-terminus of the protein. Hence, immunoblots of AMRF patient fibroblasts show a complete loss of the LIMP-2 signal (Figure 4.48 A). Furthermore, GC was dramatically reduced in AMRF patients cells with residual amounts of the enzyme located in the ER (endoglycosidase H positive signal; Figure 4.48 A). Consequently, GC activities were diminished in AMRF patient cells compared to control. The GC inhibitor Condurotol-B-epoxide (CBE) was used to control for specificity of GC activity assay (Figure 4.48 B). Also in immunofluorescence stainings with a LIMP-2 antibody no signal could be detected in AMRF patient cells, whereas control cells exhibit positive LIMP-2 signals co-localising with the lysosomal marker LAMP-2 (Figure 4.48 C).

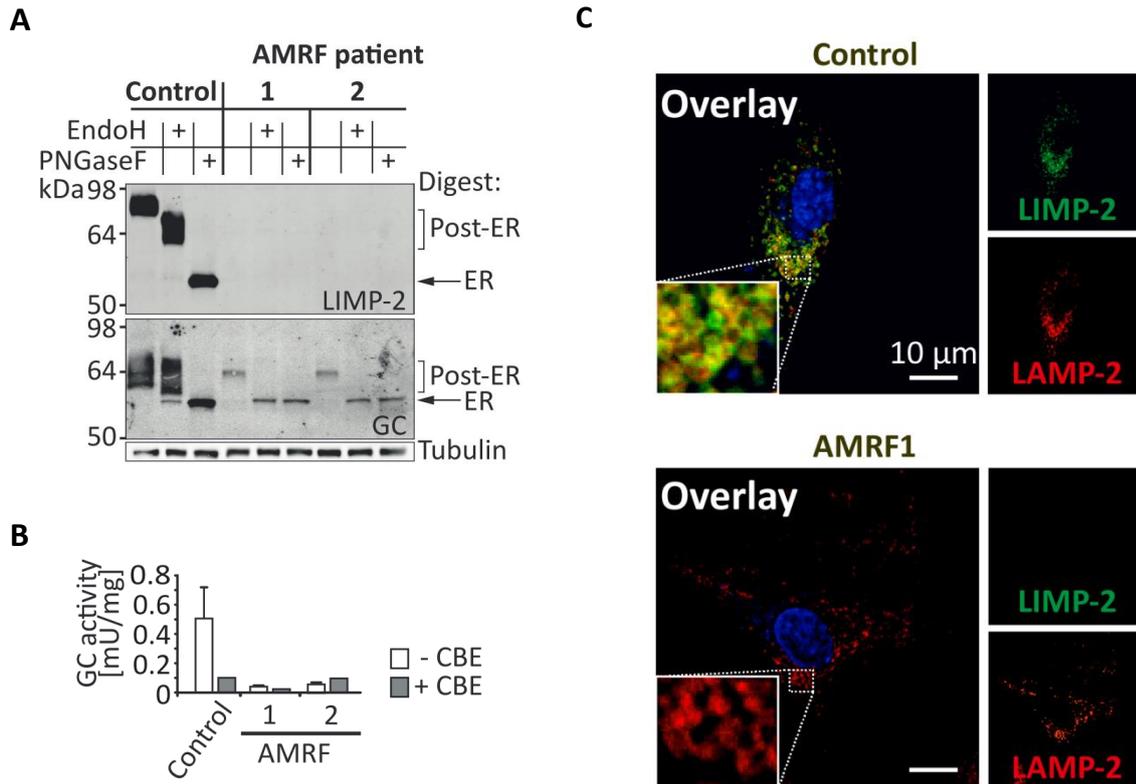


**Figure 4.48: Biochemical analyses of fibroblasts derived from AMRF patients.**

**A)** Immunoblot analysis of endoglycosidase H and PNGaseF digested lysates of human control and LIMP-2-deficient fibroblasts (AMRF patient 1 and 2). In AMRF cell lysates no LIMP-2 signal was detectable and residual GC protein was completely sensitive to endoglycosidase H digestion, indicating ER retention. Tubulin was used as loading control. **B)** GC activity assays indicate very little enzyme activity of human LIMP-2-deficient fibroblast compared to control. A GC inhibitor (CBE) was used to control for the specificity of the GC-activity measurement. **C)** Immunofluorescence of control and AMRF fibroblasts (AMRF1) staining for LIMP-2 (green; 488 nm) and the lysosomal marker LAMP-2 (red, 594 nm). No LIMP-2 signal could be observed in LIMP-2-deficient fibroblasts (AMRF1: Case A) whereas the LIMP-2 signal in control fibroblasts shows a co-localisation with the lysosomal marker LAMP-2. Scale bars indicate 10  $\mu$ m.

The two analysed AMRF mutations resulting in a truncated form of LIMP-2 protein seem to have the same consequences on GC protein expression and activity as seen in the mouse model with a complete deficiency of LIMP-2.

#### 4.7 LIMP-2: A novel therapeutic target for the treatment of synucleinopathies?

The findings in the murine and human CNS as well as in neuronal cell culture implicate an important role of LIMP-2 in regulating  $\alpha$ -synuclein levels. As shown in paragraph 4.3.3, an increase in LIMP-2 expression leads to a shift of GC to post ER compartments and an enhancement of its enzymatic activity (Figure 4.35, 4.36 and Figure 4.38).

Thus, it was of interest to evaluate if this augmentation in GC activity is sufficient to reverse  $\alpha$ -synuclein accumulation and the resulting pathological events.

In murine neuroblastoma cells (N2a) the cellular cell GC activity was found to be increased twofold after LIMP-2 overexpression ( $p < 0.05$ ). Additionally, the lysosomal GC activity was assessed in a human neuroglioma cell line (H4) constitutively overexpressing  $\alpha$ -synuclein. The cells were transfected with an empty vector control (Figure 4.49 A) and a LIMP-2 expression vector (Figure 4.49 B). The area between the two GC activity curves (DMSO and bafilomycin) indicates the lysosomal GC activity in living cells assessed over 3.5 hours. When compared to the vector control, lysosomal GC activity was increased after LIMP-2 transfection (compare white area and grey area between both curves; Figure 4.49 A and B).

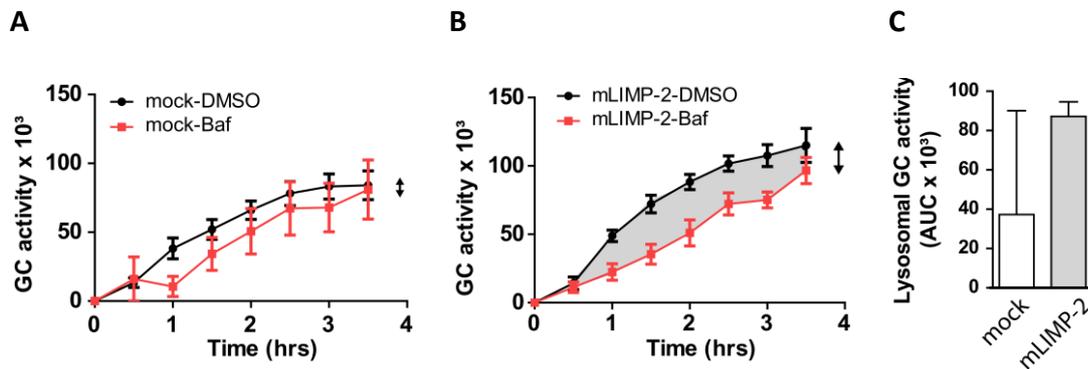


**Figure 4.49: Whole cell and lysosomal GC activity is increased after LIMP-2 overexpression.**

Analysis of lysosomal GC activity in human H4 cells overexpressing empty vector control (A) and LIMP-2 (B). The area between the curves of cells treated with DMSO (black) and bafilomycin (Baf; red) show lysosomal GC activity (indicated by an arrow). The chase of fluorescent GC substrate was performed for 3.5 hours indicating enhanced GC activity in lysosomes after LIMP-2 expression (grey area). The activity is depicted in arbitrary units as intensity of the fluorescent substrate. The area between the two curves (DMSO and Baf) was quantified and graphed (C). Although the variance in the mock transfected sample seems to be large, a tendency of augmented lysosomal GC activity after overexpression of LIMP-2 could be revealed ( $n=4$ ).

After verifying the positive effects of increased LIMP-2 expression on lysosomal GC localisation and activity, the consequences of enhanced LIMP-2 levels on  $\alpha$ -synuclein homeostasis were assessed. Wild-type LIMP-2 and as a control ER-resident LIMP-2 were co-expressed in murine neuroblastoma cells (N2a) with a HA-tagged  $\alpha$ -synuclein construct. As shown in the immunoblot of figure 4.50, overexpression of wild-type LIMP-2 resulted in decreased levels of the  $\alpha$ -synuclein protein when compared to samples co-transfected with the ER-resident LIMP-2 or mock control.

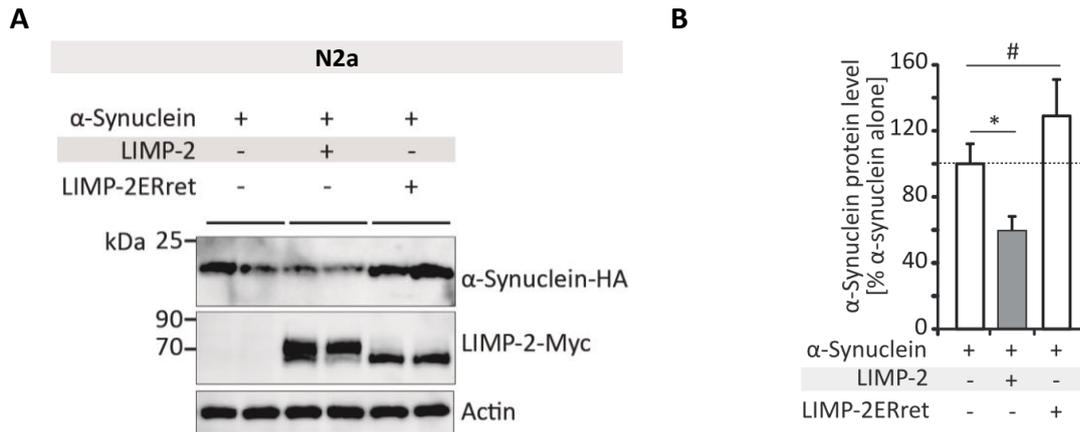


**Figure 4.50: LIMP-2 overexpression leads to a decrease in  $\alpha$ -synuclein protein levels in murine N2a cells.**

**A**) Immunoblot of N2a lysates after overexpression of wild-type and an ER-retention mutant of LIMP-2. An anti-myc antibody (9B11) was used to control for the transfection and an anti-HA antibody (3F10) was used to detect changes in the  $\alpha$ -synuclein protein levels. A drop in  $\alpha$ -synuclein signal was revealed after LIMP-2 overexpression. Actin was used to control for loading. No significant changes in the  $\alpha$ -synuclein level were identified after co-expression of the ER-resident LIMP-2 protein. **B**) Quantification of  $\alpha$ -synuclein protein levels normalised to actin and expressed as percentage of  $\alpha$ -synuclein level alone. For statistical analysis a one-way ANOVA with a subsequent Tukey-Kramer posthoc test was applied. \* denotes  $p < 0.05$  and #  $p > 0.05$ ;  $n = 4$ .

In the following experiment, the observed effects in the murine N2a cells were verified in a human H4 cell system stably overexpressing  $\alpha$ -synuclein (Figure 4.51). Like in the murine cells, immunoblots of H4 cells revealed a decrease in  $\alpha$ -synuclein levels after overexpression of LIMP-2 compared to the GFP control (Figure 4.51 A, B). Furthermore, an intracellular shift of GC towards post ER compartments could be observed after LIMP-2 expression in the human neuroglioma cell line (Figure 4.51 A, C).

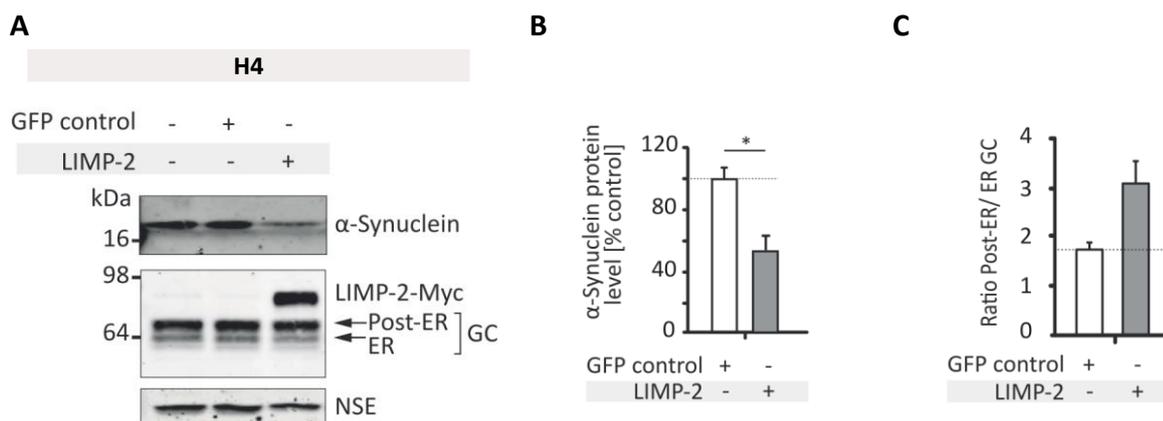


**Figure 4.51: LIMP-2 overexpression leads to a decrease in  $\alpha$ -synuclein protein levels in human H4 cells.**

**A**) Human neuroglioma cells were transfected with LIMP-2 (anti-myc) and a GFP control. Immunoblots were stained for the human variant of  $\alpha$ -synuclein (LB509), GC and the neuronspecific enolase (NSE), which was utilised as a loading control. **B**) Quantification of  $\alpha$ -synuclein protein levels normalised to NSE. **C**) Furthermore the post ER and ER fractions of the GC protein were densitometrically analysed, revealing an increase in the post ER fraction of GC protein after LIMP-2 expression. An independent two-sided Student's t-test was used for statistical analyses with \* indicating  $p < 0.05$ ,  $n = 3$ .

Since  $\alpha$ -synuclein exhibits a high turn-over rate, the effect of enhanced LIMP-2 expression was assessed over time in H4 cells. This human neuroglioma cell line stably overexpresses  $\alpha$ -synuclein under the control of a tetracycline-inducible promoter ('Tet-off'). To study the clearance of  $\alpha$ -synuclein, cells were transfected with a mock control as well as wild-type LIMP-2 and harvested between 0 and 72 hours. In parallel the cells were treated with doxycycline to stop further *de novo* transcription of  $\alpha$ -synuclein. This led to a decrease in  $\alpha$ -synuclein protein levels. However, in the presence of additional LIMP-2 (expression of the protein starts after 24 hours) a faster clearance of  $\alpha$ -synuclein could be observed (Figure 4.52 A, B). In a same type of experiment the steady state expression of  $\alpha$ -synuclein was visualised by immunoblot after 72 hours of LIMP-2 expression indicating a significant decrease of  $\alpha$ -synuclein (Figure 4.52 C, D).

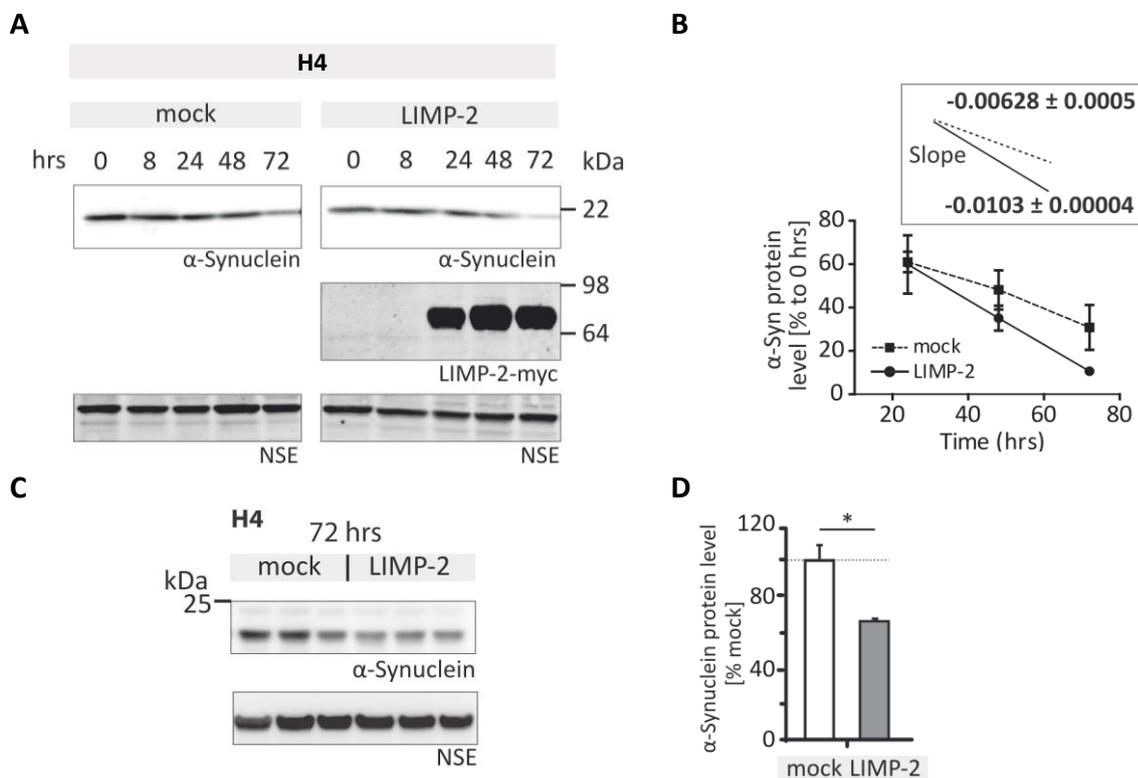


**Figure 4.52: Turn-over rate of  $\alpha$ -synuclein after overexpression of LIMP-2 in human H4 cells.**

**A)** Immunoblot detecting  $\alpha$ -synuclein turnover in human H4 cells after treatment with doxycycline to stop  $\alpha$ -synuclein transcription. For detection of the  $\alpha$ -synuclein protein an antibody specifically targeting the human variant of the protein was utilised (LB509). The expression of the LIMP-2 protein started after 24 hours (anti-myc) and cells were harvested at time point between 8-72 hours. **B)** Intensity of  $\alpha$ -synuclein protein band of immunoblots shown in **A** were normalised to the neuronspecific enolase (NSE). Results are presented as a curve over time highlighting enhanced clearance of  $\alpha$ -synuclein in the presence of LIMP-2. Since the expression of LIMP-2 starts after 24 hours of transfection, also the protein levels of  $\alpha$ -synuclein reveal changes from this time point on. The graph shows the  $\alpha$ -synuclein protein levels from 24-72 hours and indicates a steeper slope for cells transfected with LIMP-2 in comparison to the mock transfected control cells (n=3). The absolute slope values are highlighted in the box above the graph. **C)** Immunoblot of H4 cell samples analysed after 72 hours expression of LIMP-2 stained for  $\alpha$ -synuclein. NSE was utilised as a loading control. **D)** Densitometric analysis of  $\alpha$ -synuclein signals (from blot shown in **C**) revealing a significant decrease in  $\alpha$ -synuclein protein levels after LIMP-2 expression. The protein level was normalised to NSE and expressed as percentage of mock transfected control. A two-sided, independent Student's t-test was applied with \* indicating  $p < 0.05$ ; n=3.

These data suggest an accelerated clearance of  $\alpha$ -synuclein after overexpression of LIMP-2 by increasing lysosomal GC activity. The results could be obtained in a murine (N2a) as well as a human cell line (H4) further emphasising the crucial role of LIMP-2 in the degradation and homeostasis of  $\alpha$ -synuclein.

#### 4.7.1 The LIMP-2-derived helix 5 peptide: a novel therapeutic target for PD?

Since it was shown that the enhancement of lysosomal GC and its enzymatic activity leads to a decrease in  $\alpha$ -synuclein protein levels, GC is increasingly regarded as a new therapeutic target for the treatment of synucleinopathies. As described above a significant increase of lysosomal GC activity could be achieved by overexpression of LIMP-2.

However, a more direct approach to enhance GC activity would be to target the enzyme directly. As shown in chapter 4.2.1, the LIMP-2-derived peptide (helix 5) was able to increase GC activity *in vitro* and also in cell culture (in J774E macrophages and GC-deficient fibroblasts). Consequently, the following study analyses the impact of the LIMP-2 peptide to also decrease intracellular  $\alpha$ -synuclein levels.

To optimise the cellular uptake, the LIMP-2-derived peptides were modified by a c-terminally linked cell-penetrating TAT-sequence, derived from the human immunodeficiency virus. This motif has been shown to facilitate transfer across the cell membrane via its amphiphatic structure (Frankel and Pabo 1988, Green and Loewenstein 1988). In addition a KFERQ-sequence to support chaperone-mediated autophagy (CMA) and thus lysosomal import was n-terminally linked (Horst, Knecht et al. 1999) (for peptide sequences see material and methods 3.2.2.1).

First, the effects of the uptake-optimised TAT peptides on GC activity were verified *in vitro* by co-incubation with recombinant GC. A similar increase (~3.5 fold) of recombinant GC (Cerezyme ®) activity as described for the unmodified peptides was observed (compare Figure 4.15 A and Figure 4.53 A). A control peptide including the triple aspartate (3xD) motif was used (Table 4.1) exhibiting no effect on GC activity (Figure 4.53 A).

The ability of the TAT-peptides to decrease  $\alpha$ -synuclein levels by cellular uptake and enhancement of GC activity was assessed. The  $\alpha$ -synuclein overexpressing human neuroglioma cell line (H4 under a tetracycline-off promotor system) was used. H4 cells were incubated with the LIMP-2-derived TAT-peptide as well as the control TAT-peptide (3xD) and simultaneously treated with doxycycline (Dox) to suppress further *de novo*  $\alpha$ -synuclein protein expression (Figure 4.53 B). Cells were harvested after 16, 24, 48 and 74 hours and showed enhanced clearance of  $\alpha$ -synuclein when the helix 5 LIMP-2 TAT-peptide was present (Figure 4.53 B, D). This effect correlated with an increased intracellular GC activity

(Figure 4.53). In contrast the control 3xD TAT-peptide did not show an increase in GC activity over time (Figure 4.53 C).

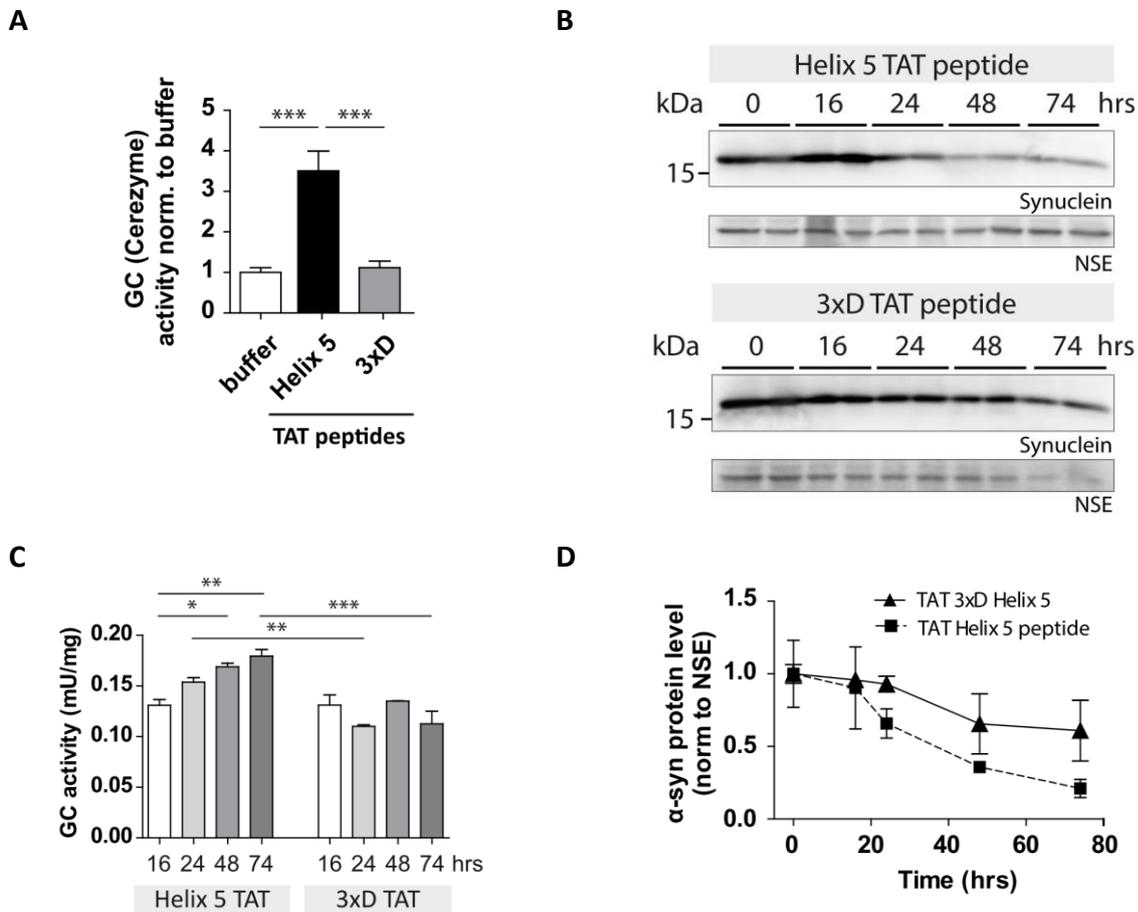


**Figure 4.53: Uptake of LIMP-2-derived TAT peptides and their effects on intracellular  $\alpha$ -synuclein levels.** **A)** *In vitro* activity assay of recombinant GC (Cerezyme<sup>®</sup>) incubated with uptake-optimised TAT-peptides (helix 5 and 3xD). GC activity was normalised to the buffer control. **B)** TAT-peptides (helix 5 and 3xD) were utilised for uptake in human neuroglioma cells (H4) and treated with doxycycline to stop *de novo* synthesis of  $\alpha$ -synuclein. Immunoblots showing duplicates of samples harvested after 0, 16, 24, 48 and 72 hours of incubation with the peptides. An anti- $\alpha$ -synuclein antibody (LB509) was utilised to detect  $\alpha$ -synuclein protein levels and the neuronspecific enolase (NSE) was used as a loading control. **C)** GC activity of H4 cell lysates after uptake of TAT-peptides (helix 5 and 3xD) indicating an increase of GC activity over time after incubation with the helix 5 TAT-peptide. **D)** Quantification of  $\alpha$ -synuclein protein signals (immunoblot shown in **B**) revealing decreased  $\alpha$ -synuclein levels starting from 24 hours after incubation with the helix 5 TAT-peptide compared to 3xD control peptide. The  $\alpha$ -synuclein signal was normalised to the loading control NSE and the values are expressed relative to the starting point incubation (0 hours). A one-way ANOVA with a subsequent Tukey-Kramer posthoc test was utilised for statistical analyses. \*, \*\*, \*\*\* denote  $p < 0.05$ ; 0.01; 0.001;  $n = 3$ .

In conclusion these findings demonstrate that the LIMP-2-derived helix 5 peptide is able to reduce intracellular  $\alpha$ -synuclein levels in a cell culture-based disease model. This indicates that the peptide-induced enhancement of GC activity is sufficient to reverse intracellular  $\alpha$ -synuclein accumulation, suggesting a therapeutic application of such a peptide.

## 5 Discussion

Since LIMP-2 was described as the transport receptor of GC in the year 2007 (Reczek, Schwake et al. 2007), little progress has been made to identify details of their interaction. In 2013 the crystal structure of the LIMP-2 ectodomain was solved by Neculai *et al.*, revealing important information about LIMP-2 function and GC trafficking in the cell. Novel putative functions of LIMP-2 as well as structural properties important for the interaction with GC could be drawn from this protein model. Interestingly, the LIMP-2 protein structure uncovered the existence of a cavity traversing the entire length of molecule suggesting a potential function of the lysosomal membrane protein in intramolecular transport processes, such as lipid transport. In 2014 an independent structure analysis of the luminal domain of LIMP-2 was published (Zhao, Ren et al. 2014), claiming an M6P-dependent transport of LIMP-2 in complex with GC. To evaluate the impact of the putative M6P-tag on the cellular transport of LIMP-2, different cellular and *in vivo* experimental approaches were performed in this study.

Interestingly, the LIMP-2 crystal structure exhibits an exposed helical bundle, which is important for GC binding. Interestingly, one single helix of the identified helical interaction site of LIMP-2 is sufficient to facilitate binding to GC. This LIMP-2-derived peptide displayed a positive effect on GC activity.

### 5.1 New insights on LIMP-2 trafficking and function

Recently, crystallographic studies revealed the protein structure of the ectodomain of LIMP-2 (Neculai, Schwake et al. 2013, Zhao, Ren et al. 2014). The description of the three-dimensional structure improved our understanding of the molecular and structural properties of the protein. It enabled the performance of site-directed mutagenic studies to investigate details in ligand binding and gain knowledge about potential new roles of the protein. In general both protein structures (PDB: 4F7B (Neculai, Schwake et al. 2013) and PDB: 4Q4F (Zhao, Ren et al. 2014)) exhibit high similarities (see overlay Figure 1.7). In the study by Zhao and co-workers a putative mannose 6-phosphate (M6P) residue attached to the carbohydrate chain linked to N325 was identified. Based on this finding a lysosomal transport of LIMP-2 by interaction with the M6P-receptor was suggested possibly building a heterotrimeric complex together with a bound GC molecule (Figure 5.1). Additionally, plasmon resonance experiments were performed in this study suggesting binding of LIMP-2 to the

cation-independent (CI)-M6P receptor. Further evidence for the interaction of LIMP-2 and CI-MPR was provided by fluorescence lifetime imaging microscopy in living cells (Zhao, Ren et al. 2014). Altogether this study questions the accepted view of an M6P-independent lysosomal transport of LIMP-2 and GC (Bonifacino and Traub 2003, Reczek, Schwake et al. 2007, Braulke and Bonifacino 2009).

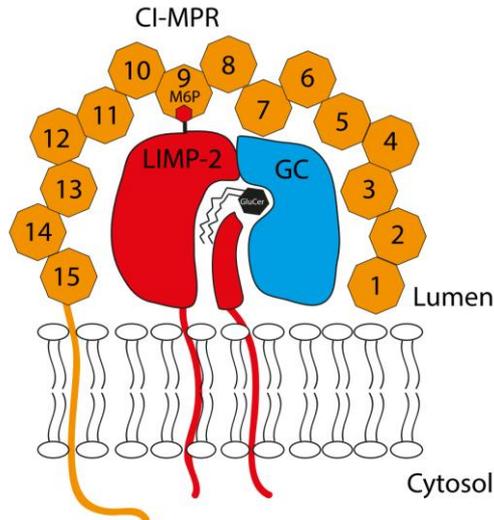


**Figure 5.1: Hetero-trimeric complex of LIMP-2 bound to GC and to the CI-MPR.**

A cartoon depicting LIMP-2 (red) associated with the CI-MPR (orange) by binding of a mannose 6-phosphate residue (M6P) attached to the LIMP-2 carbohydrate chain linked to amino acid residue N325. The 15 homologue domains of the CI-MPR are labelled and shown in orange octagons. A GC (blue) bound to LIMP-2 is shown with the glucosylceramide (GluCer) shown in black. The picture was adapted from Zhao *et al.*, 2014.

To resolve the apparent paradox between the previous studies (Bonifacino and Traub 2003, Reczek, Schwake et al. 2007) and the data from Zhao *et al.*, the impact of the putative M6P-modification on LIMP-2 trafficking was analysed in more detail. It could be demonstrated that LIMP-2 was able to reach the lysosomes independent of the existence of MPRs (cation-dependent or -independent). Also in fibroblasts lacking M6P-residues due to the absence of the N-acetylglucosamine-1-phosphotransferase (GlcNAc-1PT) endogenous LIMP-2 was present in lysosomal compartments. Additionally, LIMP-2 as well as GC could be found in purified lysosomal fractions of livers from GlcNAc-1PT-deficient animals. These results match published data showing lysosomal localisation of GC in fibroblasts lacking both MPRs (Reczek, Schwake et al. 2007). Since trafficking of LIMP-2 and GC is tightly linked, Reczek and co-workers already suggested an M6P-independent lysosomal sorting of LIMP-2. Moreover, Zhao *et al.* did not address the unchanged lysosomal transport of GC in human fibroblasts of I-cell disease patients (van Dongen, Willemsen et al. 1985, Aerts, Schram et al. 1988). These patients lack M6P-containing lysosomal enzymes due to a defective phosphotransferase (Dittmer, Ulbrich et al. 1999, S. Kornfeld 2001). Hence, it was concluded

that GC is trafficked to lysosomes by an M6P-independent transport. In 2007, LIMP-2 was identified as the transporter protein responsible for shuttling GC to the lysosomes (Reczek, Schwake et al. 2007). The studies performed by Zhao and co-workers neglect these important aspects and fail to provide experimental evidence, which is based on cell biological experiments. Since studies in human and murine fibroblasts and purified lysosomes did not indicate a M6P-dependent transport of LIMP-2, the physiological role of the described M6P-tag found on the lysosomal membrane protein is questioned. Although the finding of a M6P-residue in the crystal structure of Zhao *et al.* may be valid, it does not implicate that it is needed for the lysosomal trafficking of LIMP-2 and GC. The reported discrepancies in the two crystal structures could be due to the employment of different cell systems for the extraction of the recombinant protein. Zhao *et al.* used human HEK293S cells whereas Neculai *et al.* exploited SF-9 insect cells, which lack the GlcNAc-1-phosphotransferase (Aeed and Elhammer 1994).

In an additional experiment, which was performed in collaboration with the laboratory of Prof. Thomas Braulke (University Hospital Hamburg), it is questioned that LIMP-2 is M6-phosphorylated at all. It was not possible to precipitate LIMP-2 from mouse fibroblasts using immobilised anti-M6P antibodies. Even in the absence of the lysosomal acid phosphatase Acp2 and 5, which under normal conditions dephosphorylate the proteins upon arrival in the lysosomes (Makrypidi, Damme et al. 2012), LIMP-2 failed to bind to the M6P antibodies (data not shown). In comparison cathepsin Z, a lysosomal cysteine proteinase suspected to be transported to the lysosomal compartment in an M6P-dependent manner (Santamaria, Velasco et al. 1998), could be precipitated indicating the presence of a M6P residue (data not shown).

The recent understanding of the lysosomal sorting of transmembrane proteins has been proposed to be mediated by signals within the cytosolic domains of the proteins. Also LIMP-2 exhibits a dileucine-based signal ([DE]XXXL[LI]), which interact with components of the clathrin coats such as adaptor protein complexes (AP-1 and AP-3) (Honing, Sandoval et al. 1998, Janvier, Kato et al. 2003, Braulke and Bonifacino 2009).

Interestingly, another theory of lysosomal LIMP-2 trafficking was proposed, describing two phosphatidylinositol 4-kinases (PI4Ks) to play a role in the trafficking pathway of LIMP-2 and GC (Jovic, Kean et al. 2012). It remains unclear if the lysosomal targeting of LIMP-2 is mediated directly by the kinases or by their substrates, the phosphatidylinositol 4-phosphate (PtdIns4P). Both components have been shown to be crucial for the exit of LIMP-2 and GC from Golgi compartments. However, Jovic and co-workers also suggests an M6P-independent

transport of LIMP-2 but further claim the importance of the transmembrane or luminal domain of the lysosomal membrane protein in this trafficking pathway (Jovic, Kean et al. 2012). Although the detailed mechanisms of the intracellular LIMP-2/GC transport still need to be further addressed, the results of the above mentioned experiments show that the M6P-residue is not crucial for lysosomal trafficking of LIMP-2.

### 5.1.1 Speculations about the function of the tunnel structure in the LIMP-2 protein

The structure information of the LIMP-2 luminal domain (Neculai, Schwake et al. 2013, Zhao, Ren et al. 2014), also exhibited similarities including an unexpected finding within the core of the protein structure. Remarkably, a cavity traversing the entire length of the molecule was found in both crystal structures. This indicates a potential additional function of the lysosomal membrane protein besides its well-described role in the transport of GC. Since other members of the CD36 superfamily (the scavenger class BI (SR-BI) and CD36) are known as important regulators of lipid metabolism (Canton, Neculai et al. 2013), a possible function of LIMP-2 in lipid transport processes was evaluated in this study. The cavity within LIMP-2 predominantly exhibits a hydrophobic nature, which further supports the idea of mediating lipid transport (Neculai, Schwake et al. 2013). On the basis of the LIMP-2 crystal structure Neculai and co-workers homology modelled the protein structures of SR-BI and CD36. Subsequent mutagenesis of SR-BI suggests the transport of cholesterol(esters) from high-density lipoproteins (HDL) to the plasma membrane through the identified cavity (Gu, Trigatti et al. 1998, Gaidukov, Nager et al. 2011). Moreover, Neculai *et al.* show a direct interaction of SR-BI and CD36 with fluorescent high-density lipoprotein (HDL) and proposed that the identified tunnel moderates the selective lipid transfer of SR-BI and CD36 (Neculai, Schwake et al. 2013).

Even though it is known that lysosomes have a function in the recycling of cholesterol, the mechanisms underlying intracellular cholesterol trafficking are still largely unknown. It is proposed that cholesterol gets unesterified through hydrolysis in lysosomes and is transported back to the ER where it gets redistributed within the cell (Brown and Goldstein 1986, Chang, Chang et al. 2006). Interestingly, a recent study additionally revealed an additional role of peroxisomes in intracellular cholesterol transport (Chu, Liao et al. 2015). However, the mechanisms how cholesterol leaves the lysosomes and moves to other organelles (e.g. ER or peroxisome) still remain elusive. It is conceivable that LIMP-2 can serve a second function involving cholesterol transport after having released GC to the lysosomal lumen.

So far, two proteins have been shown to be important for the lysosomal cholesterol export: Niemann-Pick C1 and C2 (NPC1 and NPC2). Hereby, NPC2 is proposed to deliver free cholesterol to the membrane-bound NPC1 for further transport of the lipid through the lysosomal membrane (Storch and Cheruku 2005). Although the actual details of the cholesterol transport mechanisms by NPC1 across the lysosomal membrane remain unknown, patients exhibiting mutations in either NPC-protein reveal strong lysosomal cholesterol accumulation (Tangemo, Weber et al. 2011). Initial studies in murine LIMP-2-deficient fibroblast as well as liver sections did not reveal any abnormal cholesterol levels (Figure 4.3 and data not shown). To further verify a putative role of LIMP-2 in cholesterol transport, cells exhibiting aberrant cholesterol storage were utilised. Indeed, a significant decrease in the amount of lysosomal cholesterol could be observed in NPC patients fibroblasts after transfection of LIMP-2. Additionally, the same effect was observed when lysosomal cholesterol storage was generated artificially by treating cells with U18666A, a blocker for the lysosomal cholesterol exit. Cells positive for overexpressed LIMP-2 revealed a significant decrease in lysosomal cholesterol levels. Furthermore, cholesterol accumulation has been described in late endosomes and lysosomes of fibroblasts deficient for the two lysosomal membrane proteins LAMP-1 and LAMP-2 (Eskelinen, Schmidt et al. 2004, Schneede, Schmidt et al. 2011). Comparable to the other cell systems a reduction of the intra-lysosomal cholesterol levels could be observed after overexpression of LIMP-2 in LAMP-1/2 double-deficient cells. However, since there was no initial abnormality of intracellular cholesterol levels seen in the absence of LIMP-2, it rather points to a minor effect of the lysosomal membrane protein on the intracellular cholesterol distribution. The results lead to the conclusion that other proteins, e.g. NPC1 and NPC2 are more important for the cholesterol transport, whereas LIMP-2 is able to additionally support the efflux of cholesterol when the cell is stressed and cannot keep up with the intracellular amounts of cholesterol.

To verify if the effect of LIMP-2 on cholesterol trafficking is indirect, as suspected for LAMP-2 (Schneede, Schmidt et al. 2011), or if the cholesterol transport is mediated directly through the proposed cavity, a ‘tunnel mutant’ was designed. A point mutation within the cavity results into a sterically block of the tunnel (A379W and V415W). After controlling the lysosomal localisation of the mutants, the effect on lysosomal cholesterol efflux was abolished in a preliminary study. The actual impact of LIMP-2 in the lysosomal export of cholesterol has to be further addressed. Also, a more sensitive cholesterol read-out other than the performed filipin stainings would be of help. For instance establishing a fluorescence-

activated cell sorting (FACS) protocol to stain and sort for free cholesterol could improve the experimental validity.

Cholesterol is not the only hydrophobic molecule which could possibly be delivered to the cavity of the LIMP-2 protein. In this regard, LIMP-2 might not only transport the lysosomal hydrolase GC to lysosomes, but may also facilitate its catalytic reaction. The tunnel in the LIMP-2 protein may interact with the hydrophobic parts of the substrate (ceramide) presenting the hydrophilic part (glucose-residue) to the enzyme. An interaction of LIMP-2 together with GC and its substrate glucosylceramide has been proposed by Zhao *et al.* (see cartoon in Figure 5.1). In cooperation with the laboratory of Prof. Joost Holthuis (Molecular Cell Biology Division, University of Osnabrück), preliminary results analysing an interaction of LIMP-2 with glucosylceramide as well as with ceramide were generated by using bifunctional fatty acids (Haberkant and Holthuis 2014). For this experimental approach photo-activated-and-clickable lipids (pacLipids) were mixed with the recombinant GC and subsequently subjected to UV-light in order to crosslink the lipids to the interacting protein. This step was followed by a ‘click-chemistry’ reaction, where the pacLipids got labelled with a fluorophore, which then could be visualised in-gel after subjecting the samples to SDS-PAGE. The intensities of the fluorescent signals on the gel indicate the strength of interaction to the lipids. For LIMP-2 a strong positive signal could be observed after interacting with ceramide. Surprisingly, GC did not bind to any lipid. Only when the pH was decreased below seven an interaction of GC with glucosylceramide was detectable (data not shown). Indeed, the preliminary data indicates an interaction of LIMP-2 with ceramide as well as glucosylceramide. This interaction emphasises a putative role of LIMP-2 in facilitating enzymatic turnover of GC. A stronger interaction of LIMP-2 with the reaction product (ceramide) after the hydrolysis of glucosylceramide, might be supportive for the catalytic reaction. To fully understand and interpret the data additional experiments will have to be performed. For example mass spectroscopic analysis after covalently linking the lipids to the recombinant proteins are currently performed and will help to identify the lipid binding sites of the lipids of LIMP-2 and GC.

Interestingly, a recent study describes the crucial impact of the hydrophobic tunnel in uncoating the enterovirus EV71 after binding of the virus to the apical helical bundle of LIMP-2 (Dang, Wang *et al.* 2014). This emphasises the functional importance of the two structural striking characteristics revealed by the LIMP-2 protein crystal structure: the apical helical bundle and the hydrophobic cavity. Hence, it is likely that the tunnel and its

hydrophobic nature mediate more functions within the cellular metabolism as for example facilitating GC activity or lysosomal cholesterol export.

## 5.2 The interaction of LIMP-2 and GC

### 5.2.1 Analysing the GC binding site on the LIMP-2 protein

Studies in I-cell disease patient's fibroblasts, that lack M6P-containing lysosomal enzymes due to a defective phosphotransferase, revealed an unchanged transport of GC to lysosomes (Dittmer, Ulbrich et al. 1999, S. Kornfeld 2001). This supported the conclusion that a lysosomal trafficking mechanism exists, which is mediated by an M6P-independent transporter. This receptor remained elusive until 2007. Reczek and co-workers found LIMP-2 as a specific binding partner of GC in an affinity-chromatography experiment (Reczek, Schwake et al. 2007). Since then a highly conserved coiled-coil motif (His150-Leu167) within the luminal domain of LIMP-2 has been described as an interaction interface for binding GC (Reczek, Schwake et al. 2007, Blanz, Groth et al. 2010, Zachos, Blanz et al. 2012). A disruption of this coiled-coil motif abolished the interaction with GC (Reczek, Schwake et al. 2007). An ER-resident LIMP-2 mutant still shows binding to GC, implicating an early association of both proteins in the ER at neutral pH (Reczek, Schwake et al. 2007, Blanz, Groth et al. 2010, Zachos, Blanz et al. 2012). The recently solved LIMP-2 crystal structure revealed the genuine nature of this coiled-coil motif. It is part of an exposed helical bundle consisting of three  $\alpha$ -helices: helix 4 (Asn137-Gln148), helix 5 (Val149-Gln164) and helix 7 (Lys181-Pro193) (Figure 5.2). The previously identified coiled-coil domain contains helix 5. Since the name coiled-coil implicates an interaction of one coiled structure to another coiled region with identical structural properties, which GC does not exhibit, this terminology is no longer applicable and will be referred to as helix 5 in the following studies. The crystal structure does not only verify the previous findings, but it also allowed the design of specific LIMP-2 mutants. Site-directed mutagenesis was performed within the exposed helical bundle of LIMP-2 to verify its impact in GC binding. Protein surface exposed amino acids were substituted by charged aspartate-residues (D) in order to abolish the highly hydrophobic property of this protein region. It was observed that all point mutations in helix 5, but also in helix 7 of LIMP-2 greatly impaired binding to GC. Surprisingly, the K166D mutant -located at the distal apical protein site, but outside the helical bundle- showed a rescue in GC activity similar to the wild-type (Figure 4.10). This result is in apparent contrast to the Co-IP study, where interaction with GC of this mutant was completely abolished. Such differences show the difficulties of overexpression studies and demonstrate the necessity to verify results in

different cell systems. The observed discrepancy in the behaviour of the K166D mutant may be explained by differences of the employed cell lines (Cos7 for CoIP and murine MEF cells for rescue experiment). Despite this uncertainty all other data clearly underline the important function of the apical helix 5 and 7 of LIMP-2 in binding GC. Both helices are part of an exposed helical bundle, which exhibits highly hydrophobic characteristics, suggesting ligand binding mediated by hydrophobic interactions (Figure 4.25 and Figure 5.2). The exposed and hydrophobic nature of the apical helical bundle has been shown to be important for mediating a variety of specific functions, including binding of the enterovirus EV71 before cellular uptake (Dang, Wang et al. 2014). Furthermore, the two other CD36 family members (SR-BI and CD36) show binding of HDL as well as oxidised low-density lipoprotein (oxLDL) mediated by the hydrophobic helical patch (Neculai, Schwake et al. 2013).

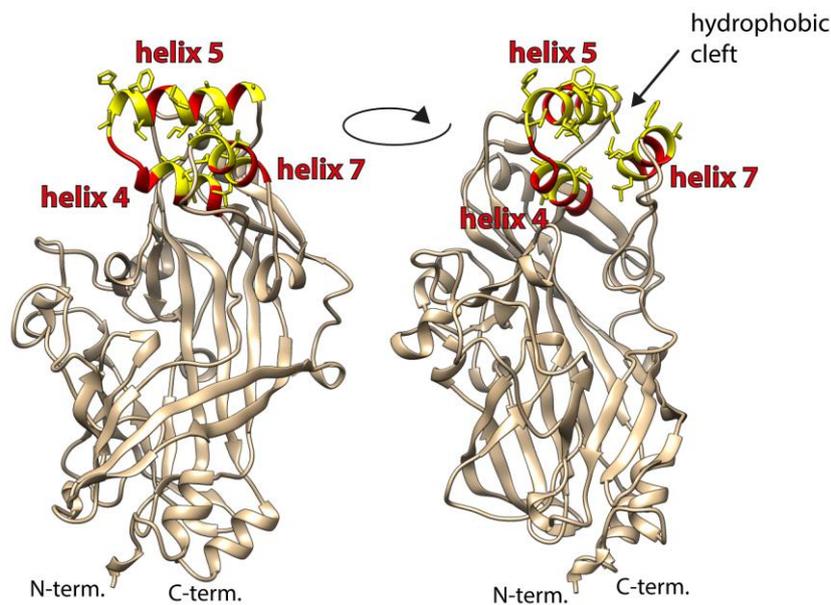


**Figure 5.2: LIMP-2 protein model with highlighted hydrophobic interaction site.**

LIMP-2 protein structure with helical bundle indicated in red consisting of helix 4, 5 and 7. This area has been proposed to mediate ligand binding by hydrophobic amino acids, which are indicated in yellow forming a hydrophobic cleft. The structural illustration was performed with UCSF Chimera (PDB: 4F7B).

To date only ten mutations have been described in the *SCARB2* gene encoding for LIMP-2 causing myoclonus epilepsy (AMRF) (Berkovic, Dibbens et al. 2008, Dardis, Filocamo et al. 2009, Dibbens, Michelucci et al. 2009, Dibbens, Karakis et al. 2011). The majority of the *SCARB2* mutations are null mutations and associated with a truncation of the LIMP-2 protein, clearly affecting normal protein function including lysosomal transport of GC (Blanz, Groth et al. 2010). Only one missense mutation located outside of the helical bundle has been described (H363N) (Dardis, Filocamo et al. 2009, Dibbens, Karakis et al. 2011). Human mutations in *SCARB2* are rare possibly due to the severity of the phenotype. Nevertheless,

LIMP-2 mutants, which are incapable of binding GC, might be a powerful tool to study potential additional role of the lysosomal protein independent of its GC-transport function via the helical bundle. For example a transgenic mouse overexpressing a GC-binding deficient LIMP-2 variant could exhibit novel functions of LIMP-2, which are independent of an intact helical bundle. Since, the major function of LIMP-2 is restricted to GC transport, the appearing phenotypes in this mouse model will mainly correlate to functions of LIMP-2 other than interaction and trafficking of GC.

Further validation of the GC-interaction site of LIMP-2 was provided by interaction studies with a small LIMP-2-derived peptide (helix 5). The 24 amino acids long  $\alpha$ -helix was able to specifically mediate the interaction *in vitro* to recombinant GC (Cerezyme®), as well as to endogenous enzyme from cell lysate. Hence, the peptide shows a great potential to be exploited for further GC-precipitation assays.

### 5.2.2 Analysis of the LIMP-2 binding site on the GC protein

Due to difficulties in the initial purification of recombinant LIMP-2 the identification of the LIMP-2 binding site on GC was not possible by a co-crystallisation approach with the two recombinant proteins (LIMP-2 and GC). Hence, the LIMP-2-derived peptide (helix 5), which was shown to mediate a specific interaction to GC, was used instead of the entire LIMP-2 protein for co-crystallisation experiments. Highly purified GC, clinically used for enzyme replacement therapy (Cerezyme®, Genzyme, USA) was co-incubated with the peptide. An existing crystal structure of fully glycosylated GC (Cerezyme®) was published in 2006 and exhibits three N-glycosylation sites (Figure 1.9) (Brumshtein, Wormald et al. 2006). To obtain co-crystals of the recombinant GC and the small helical peptide two different strategies were applied. Firstly, the peptide was added to existing crystals of GC. Secondly, recombinant GC and peptide were incubated in solution before seeding for crystallisation. Although it was possible to obtain good quality crystals (high diffraction and resolution), both approaches failed since the peptide could not be visualised. A possible explanation for this failure could be related to the tight crystal-packaging of GC (Brumshtein, Wormald et al. 2006). Most likely the interaction of single GC molecules is stronger than the binding of GC to the peptide. In future studies deglycosylation of the GC protein beforehand may help to increase the space between single GC molecules. Future co-crystallisation approaches may be performed using Cerezyme® together with the recently obtained entire LIMP-2 ectodomain (Zhao, Ren et al. 2014).

Since the co-crystallisation approach was not successful, a different strategy was applied to study the LIMP-2 binding site on the GC protein. Potential sites of interaction were identified using the knowledge about the LIMP-2 crystal structure (PDB: 4F7B). As mentioned earlier the highly hydrophobic characteristic of the helical bundle in LIMP-2 suggests ligand binding via hydrophobic interactions. Therefore, the GC protein structure was analysed for surface charges. Similar to LIMP-2 a hydrophobic patch was observed (Figure 4.25). The hydrophobic protein region in GC exhibits a distinctive fold of  $\alpha$ -helices, similar to the helical bundle found in LIMP-2. The helical patch of GC consists of one long angled helix 1 (Thr86-Ser110) and one short helix 2 (Pro150-Ala168) (Figure 5.3). Furthermore, the orientation of the hydrophobic amino acids within the helical bundle show a distinct hydrophobic cavity, exhibiting a perfect interaction site for an exposed hydrophobic  $\alpha$ -helical structure as found on the apex of LIMP-2.

To analyse the impact of this particular protein region of GC on the binding of LIMP-2, site-directed mutagenesis was performed. The three hydrophobic leucins (L) on position 91, 94 and 156 were individually substituted with highly charged glutamic acids (E) in order to lower the hydrophobic characteristics of the interaction site (Figure 5.3). Although all three mutants lost the ability to bind LIMP-2 in a co-precipitation approach, the mutants slightly differed in their binding behaviour. To study the properties of each GC mutant, a number of additional assays were applied, including subcellular localisation studies (immunofluorescence with lysosomal and ER markers), endoglycosidase digestion assays and LIMP-2 co-expression studies. The later experiment was designed to further verify the interaction site on GC protein and to evaluate if an increased LIMP-2 expression may be of potential benefit to facilitate transport of GC and its mutants to the lysosome.

A mild interaction of the GC L94E mutant with LIMP-2 could be observed, whereas L91E and L156E were incapable of binding LIMP-2. Furthermore, the L94E mutant showed a slight increase in GC activity after additional LIMP-2 overexpression. Therefore the leucine residue at position 94 may play a minor role compared to the leucines at position 91 and 156 in binding of LIMP-2. Thus, the integrity and hydrophobicity of the upper part of the helical bundle, where the leucines 91 and 156 are located, appear to be more important in mediating GC's interaction with LIMP-2 (Figure 5.3).

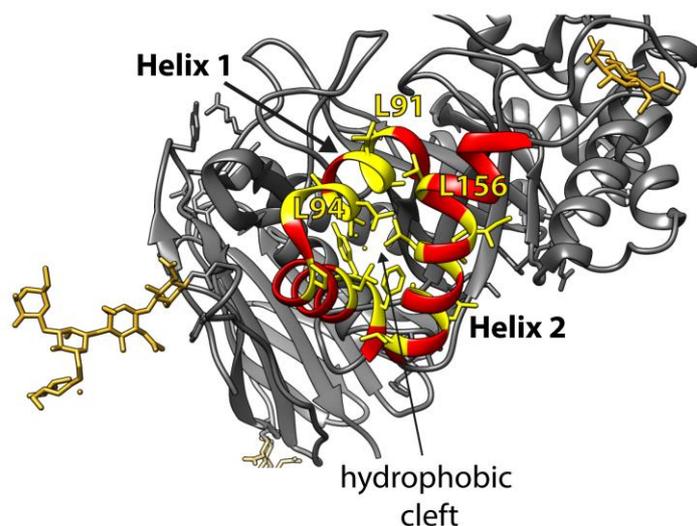


**Figure 5.3: The potential LIMP-2 interaction site on the GC protein exhibits hydrophobic characteristics.** Structural model of GC with the helical bundle highlighted in red and all hydrophobic amino acids marked in yellow. For the experiments described in this study the three leucines located at position 91, 94 (in helix 1) and 156 (in helix 2) were substituted with glutamic acid in order to destroy the hydrophobic nature of the helical bundle. The structural illustration was created using UCSF Chimera (PDB: 2J25).

Using GC mutants (L91E, L94E, L156E), the hydrophobic properties that play a critical role in LIMP-2 binding were identified. To further validate the binding site of LIMP-2, clinical GC mutants were included in this study. Interestingly, only 13 out of almost 300 mutations that cause Gaucher disease have been reported in the potential LIMP-2 binding site affecting only 9 different amino acids (green amino acids in Figure 5.4) (Hruska, LaMarca et al. 2008, Malini, Grossi et al. 2014). Additionally, most of these patients present with a mild phenotype, mostly resembling type 1 Gaucher disease characterised by splenectomy and bone phenotypes but no neuropathological symptoms (Cormand, Harboe et al. 1998, Demina and Beutler 1998). Only two patients with mutations in the predicted interaction site (S107L, I161S) were described presenting neurological impairments (Demina and Beutler 1998, Goker-Alpan, Lopez et al. 2008). Interestingly, the consequences of the I161 mutation are diverse, resulting in either type 1 (Cormand, Harboe et al. 1998) or the neuronopathic type 3 Gaucher disease (Goker-Alpan, Schiffmann et al. 2004). An explanation for Gaucher patients with comparable mild phenotypes in the potential interaction site, may be that the enzyme is recaptured from the extracellular space. Since the binding-deficient GC mutants are still enzymatically active, the amount of GC reaching lysosomes indirectly may be sufficient for several cell types to degrade sphingolipids.

Similarly, the ability of cells in taking up molecules and even whole proteins is exploited for enzyme replacement therapy in Gaucher disease (Sly, Kaplan et al. 1978, Stahl, Rodman et al. 1978, Pastores, Weinreb et al. 2004). Hence, macrophages, which are most effected in

Gaucher disease due to their high metabolic rate (Pastores 1997), efficiently engulf small substrates, molecules and even whole cells (Weissleder, Nahrendorf et al. 2014).

In this study, the two clinical associated and enzymatically active GC mutations located in the putative interaction site (P159L and I161S) failed to bind LIMP-2. A structural explanation for this behaviour might be the decrease of the hydrophobicity of the helical bundle of GC when substituting isoleucine to serine (I161S). The P159L mutant possibly interferes with the secondary structure of the helical bundle and potentially neighbouring protein structures.

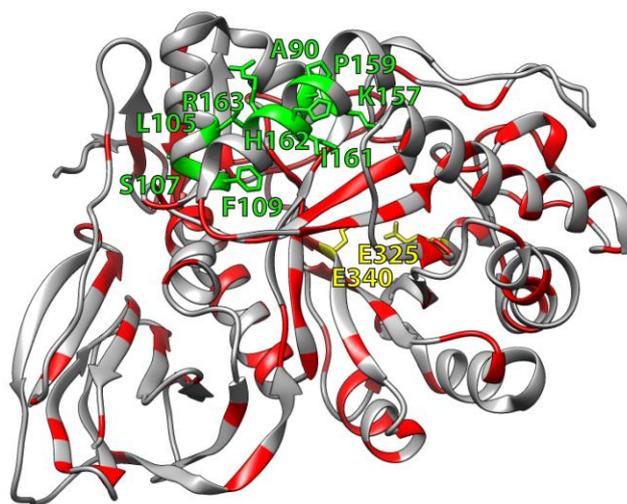


**Figure 5.4: GC protein model indicating all existing disease causing missense mutations.**

The GC protein exhibits almost 300 unique mutations (including 203 missense mutations shown here in red/green). The green amino acids indicate the nine amino acids, which might result in clinical missense mutations located in the LIMP-2 interaction site. The catalytic cavity is labelled in yellow (E325 and E340). The widely spread location of the occurring mutations indicates functional importance of the whole protein for optimal enzymatic function. The structural illustration was created using UCSF Chimera (PDB: 2J25).

The hydrophobic helical bundle is found opposite of the catalytic cavity (E325 and E340 indicated in yellow, figure 5.4 and 5.5) as well opposite of proposed saposin C binding site (green, figure 5.5) (Atrian, Lopez-Vinas et al. 2008, Lieberman 2011). Saposin C is an important cofactor for GC (Vaccaro, Tatti et al. 1994, Wilkening, Linke et al. 1998). For optimal enzyme activity GC has been shown to associate with negatively charged lipids residing in the limiting membrane of the lysosome (Mueller and Rosenberg 1979, Osiecki-Newman, Fabbro et al. 1987, Grace, Newman et al. 1994). The structural model of GC (Figure 5.5) highlights all functionally important protein regions and thus displays the unrestricted accessibility of the hydrophobic interaction site of GC, further supporting its role in facilitating its interaction with LIMP-2.

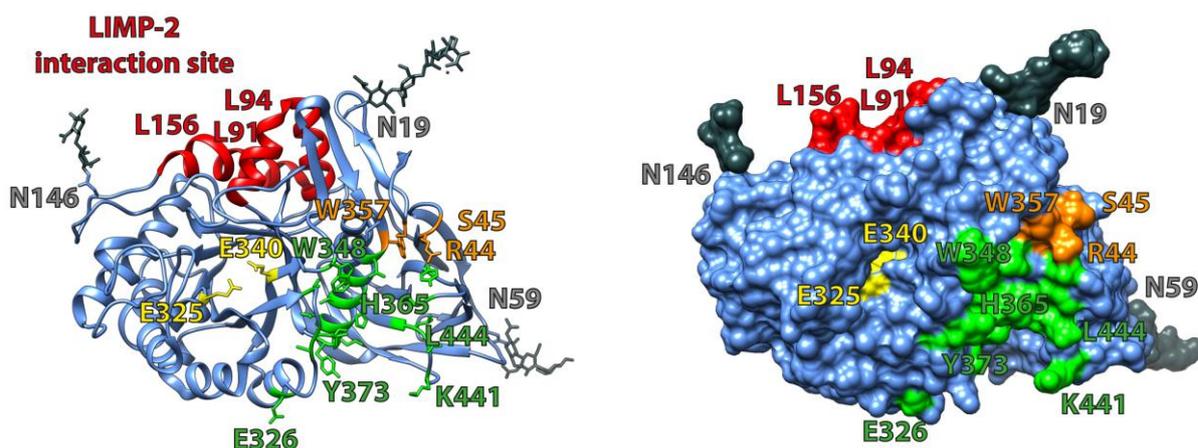


**Figure 5.5: Structural model of GC indicating functionally important regions.**

The protein model of GC with highlighted areas important for protein function: Glycosylation chains (grey), active site (yellow), saposin C (green) and lipid interaction site (orange). The potential LIMP-2 interaction site is indicated in red, showing its good accessibility with all functionally important regions located on the opposite side of the protein. In addition, the carbohydrate residues are arranged in favour for an interaction with LIMP-2. The structural illustration was done using UCSF Chimera (PDB: 2J25).

To exclude secondary effects of the inserted mutations, it is important to check the protein integrity before performing structural analysis. For enzymes the activity can be used as a measurement of protein integrity. Only those GC mutants exhibiting considerable enzymatic activity were used in the interaction studies with LIMP-2. However, it should be noted that the specific activity was generally low, even for mutations within regions not involved in the catalytic function of the enzyme. Even mutations within the proposed LIMP-2 interaction site, which is located at the opposite side of the catalytic cavity (Figure 5.5), show reductions in GC activity. The L94E and N188S GC mutants showed ~60% and ~50% residual enzyme activity compared to the wild-type (Figure 4.26), similar to reports for the N188S mutant (Tajima, Ohashi et al. 2010). In general minor changes to the GC sequence by single point mutations lead to changes in activity highlighting the sensitivity and complex arrangement of the enzyme. In general, the rate of GC activity does not correlate with the severity of the Gaucher disease. This further highlights the complexity and the necessary contribution of other factors to the clinical manifestation of the disease. Considering the tight interaction and dependence of GC on its transport receptor LIMP-2, it was hypothesised that also mutations in *SCARB2* could modulate the phenotype in Gaucher disease. In fact, mutations in the LIMP-2 protein were found to modify Gaucher disease (Velayati, DePaolo et al. 2011).

Recently, another study addressed the LIMP-2 binding site on GC (Liou, Haffey et al. 2014). In order to locate the interaction site, the authors designed truncation mutants of GC. Taking in account the profound effects of single point mutations on GC activity as described here and

elsewhere in literature (Pasmanik-Chor, Laadan et al. 1996, Liou, Kazimierczuk et al. 2006, Tajima, Ohashi et al. 2010), this approach seems questionable. Liou *et al.* proposed that the GC binding sequence on LIMP-2 consists of an 11 amino acid long stretch (Liou, Haffey et al. 2014), which forms a surface accessible loop and is in close vicinity to the helical bundle reported here. However, most of the mutated residues within this loop (D399-D409) point towards the interior of GC (Figure 5.6). Thus, the data rather suggest a secondary effect of the introduced mutants on the structure of surrounding areas, such as the helical bundle. It seems unlikely that the reported loop of GC is directly involved in LIMP-2 binding. This view is supported by the fact that single mutations in this region were unable to completely disrupt GC binding to LIMP-2 (Liou, Haffey et al. 2014). As indicated in figure 5.6 only amino acids I406-D409 exhibit surface exposure (yellow; Figure 5.6). Liou *et al.* further mutated T407 and D409 to alanine (A) and observed impaired LIMP-2 binding. However, as illustrated in figure 5.6 B this effect might also be indirect by affecting the structural properties of the helical bundle. The aspartic acid may stabilise the surrounding protein region, including the helical bundle. Thus, the acid-derived proton may interact with a serine in the helical bundle (S97). A substitution of the aspartic acid to an alanine (D409A), a small hydrophobic amino acid, does not allow this kind of acid-base interaction and might lead to a collapse of the overall protein structure. Therefore, the identified loop might rather have an important function in protein stabilisation than directly affecting the binding to LIMP-2.

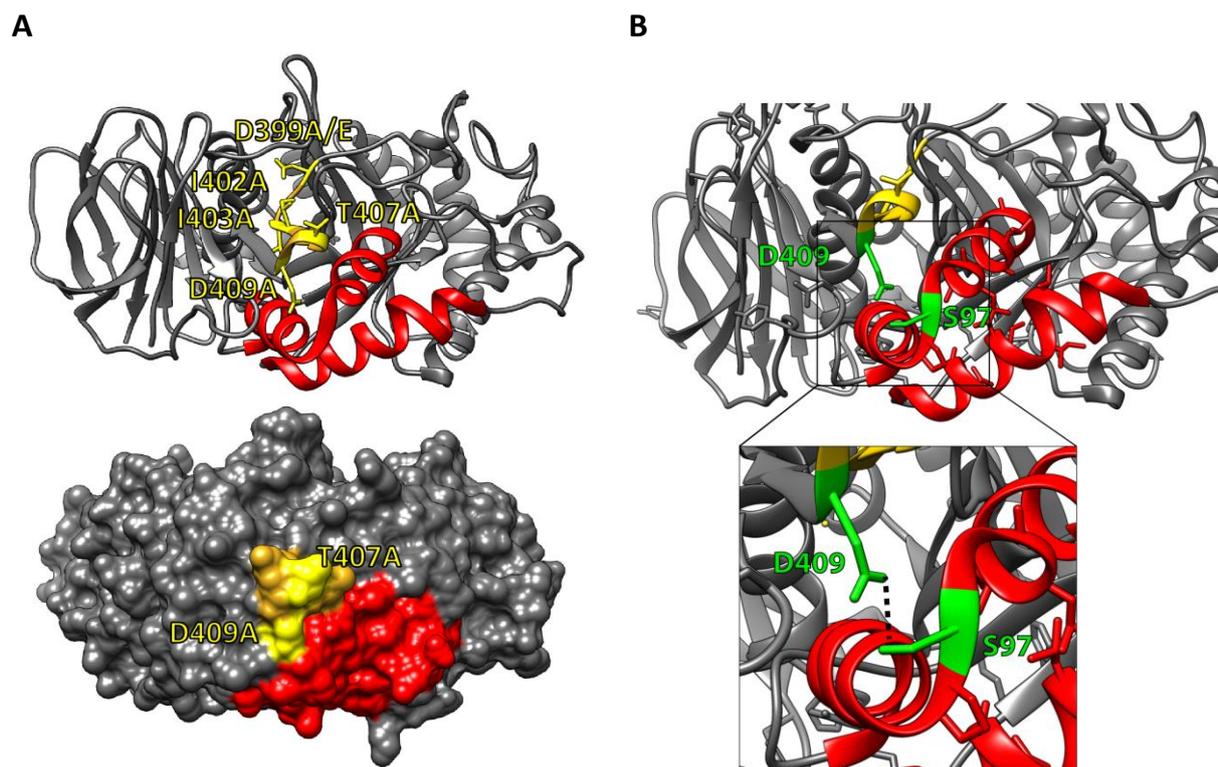


**Figure 5.6: Structural analysis of the described interaction sites in the GC protein.**

**A)** Structural model of GC with the highlighted proposed LIMP-2 interaction sites: helical bundle (red) and the 11 amino acid long loop (orange; with introduced point mutations from Liou *et al.*, 2014 in yellow). Amino acids D399, I402 and I403 were hypothesised to be involved in the interaction with LIMP-2. As indicated in the surface view only amino acids I406-D409 are exposed on the surface. **B)** In addition Liou *et al.* substituted D409 to alanine. A possible interaction between the aspartic acid and a serine (S97) in the helical bundle might be responsible for the stabilisation of this protein region, which is lost when the acid is exchanged to an alanine (D409A). The structural illustration was performed using UCSF Chimera (PDB: 2J25).

### 5.2.3 The overall picture: combining all data about the LIMP-2 and GC interaction

The determination of the binding sites of LIMP-2 and GC with the help of the single crystal structures of both proteins (Brumshtein, Wormald *et al.* 2006, Neculai, Schwake *et al.* 2013) provided a deeper understanding in to how this receptor/ligand protein complex may form. It suggests that LIMP-2 and GC interact through contact of their helical bundles in a 1:1 stoichiometry, which is consistent with previous crosslinking experiments obtained after co-expression of LIMP-2 and GC in Cos7 cells (Reczek, Schwake *et al.* 2007).

Our interaction model (Figure 5.7) of LIMP-2 and GC reveals that the glycosylation patterns of both proteins are also arranged in favour for an interaction at the proposed sites. The carbohydrate chains may even exert an auxiliary function contributing to the stabilisation of the LIMP-2-GC protein complex. Furthermore, the importance of intact glycosylation in LIMP-2 is supported by the fact that an absence of a carbohydrate moiety at position N325,

which is in close proximity to the helical bundle, leads to a retention of the mutant in the ER (Neculai, Schwake et al. 2013).

As another interesting feature of LIMP-2 is its role as a receptor on the plasma membrane that binds enteroviruses (e.g. EV71), the causative pathogen of hand, food and mouth disease (Yamayoshi, Yamashita et al. 2009). Importantly, the helical bundle of LIMP-2 is involved in the association and uncoating of the EV71 virus (Yamayoshi and Koike 2011, Dang, Wang et al. 2014). Therefore, the hydrophobic characters of helix 5 and 7 in the LIMP-2 binding interface seem to mediate this specific interaction. In addition, the glycosylation pattern of LIMP-2 is described to play a key role in the binding and uncoating events of the EV71 virus (Dang, Wang et al. 2014).

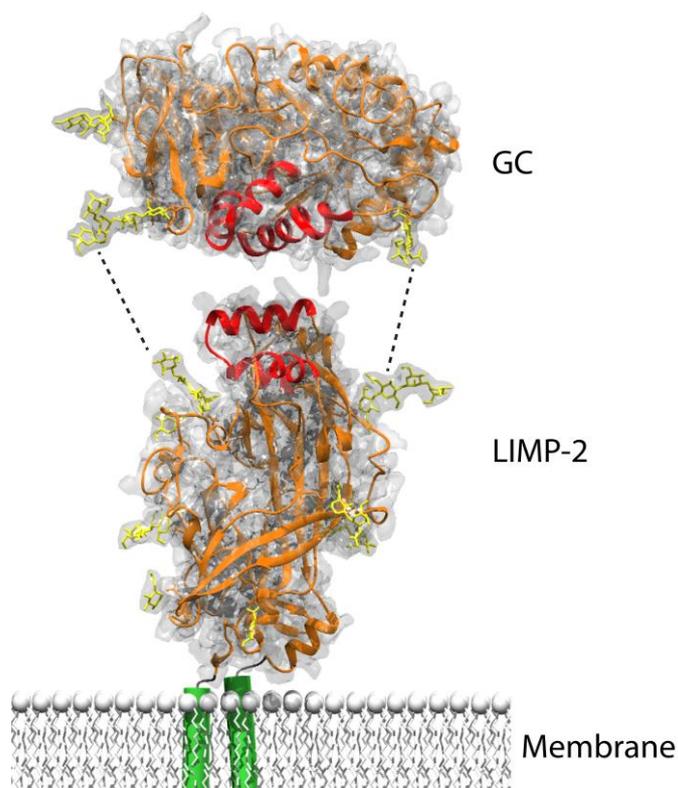


**Figure 5.7: Structural model of LIMP-2 and GC showing their interaction.**

LIMP-2 and GC structural models indicate binding in a 1:1 stoichiometry by interaction of both helical bundles (red). The oligosaccharide chains are indicated in yellow. Their arrangements around the proposed interaction site also suggest an interaction and thus stabilisation of the whole protein complex. The structural illustration was created using UCSF Chimera (PDB: 2J25; 4F7B) with the transmembrane domains (green) and membrane modelled subsequently to the protein model.

A small peptide derived from the binding site of LIMP-2 (helix 5: L152-E175) was able to mediate interaction with GC. This primarily verified the specificity of the LIMP-2 interaction site, but the peptide was also used to confirm the binding site on GC. Less interaction with the peptide was seen for the LIMP-2-binding impaired GC mutants.

### 5.3 The LIMP-2-derived helix 5 peptide: a therapeutic target?

One important finding from this study is that helix 5 in the helical bundle of LIMP-2 is apparently sufficient for GC binding. This was shown for recombinant GC in an *in vitro* approach as well as for endogenous and overexpressed GC from Cos7 and N2a cell lysate, respectively. In contrast, the apical helix 7 was not able to mediate interaction with GC as efficiently. This might be due a less exposed position of helix 7 in comparison to helix 5 in the LIMP-2 protein (Figure 5.2). It rather suggests a supportive role of the helix 7 in ligand binding than its direct interaction with GC. A non-binding peptide with a substitution of three aspartic acids (3xD) within the helix 5 amino acid structure was used to control for the specificity of binding. The inability of a LIMP-2 mutant with this 3xD motif to bind GC was previously shown in cell-based experiments (Blanz, Groth et al. 2010).

Intravenous enzyme replacement is currently the accepted standard treatment for Gaucher disease. The recombinant GC is expressed in different cell systems and efficient purification relies on an extensive protocol (Jayapal, Wlaschin et al. 2007, Shaaltiel, Bartfeld et al. 2007, Starzyk, Richards et al. 2007, Zimran, Loveday et al. 2007, Weinreb 2008, Pastores 2010). The specific interaction of the LIMP-2-derived peptide with GC may be of impact, since it may be used as an alternative strategy to efficiently purify GC from cells or cell lysates. Further studies are necessary to assess how to optimise the enzyme purification.

Although enzyme replacement therapy is very costly and the intravenously applied enzyme is not able to cross the blood-brain barrier (Altarescu, Hill et al. 2001), this therapy is still the therapy of choice to treat Gaucher disease. Other therapeutic strategies employ substrate reduction, gene therapy and small molecules (Cabrera-Salazar, Novelli et al. 2002, Cox 2005, Sawkar, D'Haese et al. 2006, Sidransky, LaMarca et al. 2007).

Chemical chaperones are small molecules, which are able to bind proteins and assist their correct folding (Perlmutter 2002). The hypothesised molecular mechanisms of the compounds involve their competitive binding to the active site of the protein. This is thought to facilitate proper folding of the enzymes and assures their trafficking to lysosomes where the small molecule is substituted by the substrate. To date, the two chemical chaperones of GC, isofagomine and the imino sugar N-butyldeoxynojirimycin (NB-DNJ, miglustat) have been described and shown to bind within the active site of the protein (Alfonso, Pampin et al. 2005, Brumshtein, Greenblatt et al. 2007, Lieberman, Wustman et al. 2007, Kornhaber, Tropak et al. 2008). The presence of isofagomine and miglustat is thought to decrease the degradation of

GC, which subsequently leads to higher lysosomal levels of the enzyme (Alfonso, Pampin et al. 2005, Shen, Edwards et al. 2008).

In this study the LIMP-2-derived helix 5 peptide increased recombinant GC enzyme activity about 4-fold. The detailed mechanism of the helix 5-mediated GC activation is unknown. However, a stabilisation of the enzyme at 37°C and pH7 after incubation with the peptide could be assessed. A chaperone-like function of the helix 5 peptide similar to the above mentioned chemical chaperones could be an explanation for the stability effect. The LIMP-2-derived peptide appears not to bind within the active site of GC, as shown for the described chemical chaperones of GC. Since the LIMP-2 binding site has been shown to be located opposite to the active site (Figure 5.5 and Figure 5.8), it is likely that the LIMP-2-derived peptide, which resembles the interacting  $\alpha$ -helix, binds to the same protein region. Thus, the chaperone-like stabilisation and activation of the enzyme by the LIMP-2-derived peptide appears not to be due to a competitive inhibitory effect.

The characterisation of a GC activator, which does not simultaneously exhibit an inhibitory effect, could be of advantage for a therapeutic use since it is easier to control and adjust. For example, the consequences of applying a wrong concentration of a non-inhibitory activator (like the helix 5 peptide) would not be as disastrous as for an inhibitory molecule, which can potentially block the complete enzyme function.

Considering that the LIMP-2-derived peptide binds to the same protein region as the LIMP-2 protein, it further opens the possibility to design small molecules to target this particular protein domain (Figure 5.8). The development of small non-inhibitory molecules, which in addition are able to cross the blood-brain barrier and thus be able to target the neurological pathologies in certain cases of Gaucher disease.

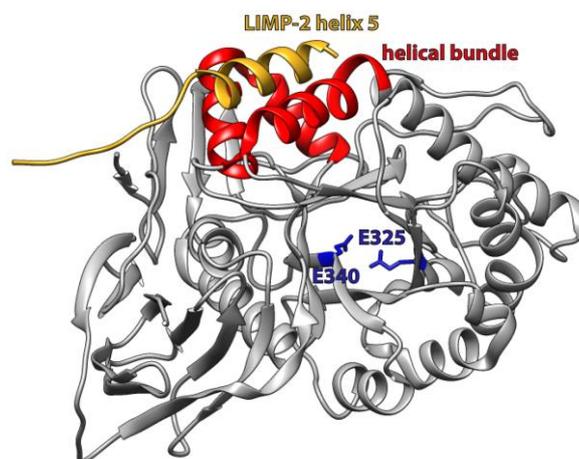


**Figure 5.8: GC protein structure with LIMP-2 helix 5 peptide bound to the helical bundle.**

The GC protein structure with highlighted helical bundle (red) interacting with the LIMP-2 helix 5 peptide (yellow). The active centre on the opposite side of the protein is indicated in blue by the two catalytically active amino acids E340 and E325. The structural illustration was done using UCSF Chimera (PDB: 2J25).

To study the effects of the LIMP-2-derived peptides on GC activity *in vivo*, the uptake of recombinant GC (Cerezyme®) that was preincubated with the peptides was assessed in GC-deficient MEF cells. These cells exhibit the perfect read-out system for the uptake of recombinant GC, since they do not have endogenous GC. After efficient internalisation of Cerezyme® preincubated with the helix 5 peptide, an increased intracellular GC activity was observed in comparison to cells treated with Cerezyme® only. This suggests a strong interaction of the peptide with GC, since the complex appears to stay stable even after uptake by the cells. It could be shown, that the helix 5 peptide has a stabilising effect on the GC protein, steadily enhancing its activity when incubated at 37°C and neutral pH. It is conceivable, that GC is preincubated with the helix 5 peptide, leading to stabilisation and an increase in enzyme activity before applying the recombinant enzyme by intravenous infusion. This initially higher activity of GC could reduce the amounts of required enzyme leading to a reduction of costs for this highly expensive form of therapy.

Furthermore, the effect of the helix 5 peptide on endogenous GC after incubation with cells was assessed. Murine macrophages (J774E) as well as human brain neuroglioma cells (H4) were able to efficiently incorporate the LIMP-2-derived peptides, which led to an increase in intracellular GC activity. For further optimisation of the cellular and lysosomal uptake, the peptides were altered through addition of a cell-penetrating TAT-motif (Frankel and Pabo 1988, Green and Loewenstein 1988) and a chaperone-mediated-autophagy marker sequence (Horst, Knecht et al. 1999). These modifications made the cellular uptake of the peptides more efficient and significantly reduced the amount of the applied peptide (from 50 µM to 1 µM) necessary to reach comparable levels of activity when compared to the unmodified sequence.

Future studies are needed to address if the helix 5 peptide shows similar positive effects on GC activity *in vivo* tested in animals. Additionally it remains unclear if the helix 5-induced boost of GC activity is sufficient to lead to a reduction of its substrate glucosylceramide. The lack of suitable animal models, which accurately recapitulate the clinical manifestations of human Gaucher disease, makes it difficult to further study the therapeutic effect of the LIMP-2 peptide *in vivo*.

The increase in GC activity *in vitro* as well as in cell culture induced by the LIMP-2 peptide indicates that helix 5 may be able to act as a direct activator. Additionally, recombinant GC showed increased activity when incubated with the purified luminal domain of LIMP-2, which further emphasises a role in direct protein stabilisation by LIMP-2. However, it is

described in literature that the enzyme dissociates from its transport receptor LIMP-2 in a pH-dependent manner (Reczek, Schwake et al. 2007, Zachos, Blanz et al. 2012). That would implicate a stabilising function of LIMP-2 before this pH-dependent dissociation from GC takes place. But what is the benefit of stabilising GC in the ER when the enzyme is actually fulfilling its function within lysosomes? Facilitating enzymatic activity within the ER may be important in order to regulate hydrolysis processes, since it cannot be excluded that GC has additional, not yet identified, functions within the ER or anywhere else besides the lysosome. In addition it has to be mentioned, that all performed GC activity assays were carried out at low pH (~5). Since the helix 5 peptide as well as the luminal domain of LIMP-2 revealed a positive effect on GC function under these conditions, it indicates a permanent interaction of the enzyme with both molecules. This seems to be in contrast to the situation in the cell. In a recent study a histidine (H171) located in close proximity to the helical bundle has been described to be crucial for pH-dependent dissociation of ligands (Zachos, Blanz et al. 2012). Since this histidine is included in the helix 5 peptide sequence, it seems likely that conformational changes induced by this histidine are not sufficient to lead to a dissociation of the peptide and GC. Thus, a different study lately postulated that a different histidine close to the helix 5 (H150) is responsible for acting as a pH sensor to regulate ligand binding (Dang, Wang et al. 2014, Zhao, Ren et al. 2014). This amino acid is not included in the peptide structure and may explain the association of peptide and enzyme even at a low pH. A further explanation might be that the actual dissociation of LIMP-2/helix5 peptide and GC in lysosomes is incomplete.

#### **5.4 The role of LIMP-2 in $\alpha$ -synuclein homeostasis**

Besides the well-described role of LIMP-2 as a transporter for GC to lysosomes, little is known about its function in the central nervous system. In addition to the structural data provided in this study, this work addresses the role of LIMP-2 in the regulation of the cellular homeostasis of  $\alpha$ -synuclein. Dysfunction of GC causes the most common lysosomal storage disorder Gaucher disease (Brady, Kanfer et al. 1966). Recently mutations in the *GBA1* gene encoding for GC have also been associated with Parkinson disease (Westbroek, Gustafson et al. 2011) and other synucleinopathies such as Lewy body disease (Goker-Alpan, Giasson et al. 2006, Clark, Kartsaklis et al. 2009). At a molecular level it could be shown that the loss of GC activity and the simultaneous accumulation of its substrate glucosylceramide lead to the development of PD (Mazzulli, Xu et al. 2011, Gegg, Burke et al. 2012).

Since lysosomal activity of GC is tightly linked with the expression of its transport receptor LIMP-2,  $\alpha$ -synuclein levels were analysed in murine brain of LIMP-2-deficient mice. For this study mice were backcrossed into the C57BL/6N background. In a previous study animals in the background of a C57BL/6J Harlan strain have failed to show any signs of synucleinopathy, since this strain is deficient in  $\alpha$ -synuclein (Specht and Schoepfer 2001, Gamp, Tanaka et al. 2003).

#### 5.4.1 Consequences of LIMP-2 deficiency on lysosomal function in murine brain

Biochemical analyses of the midbrain and pons of LIMP-2-deficient animals showed a complete absence of the LIMP-2 protein and significant reduction in the steady-state levels of GC accompanied by a dramatic decrease of enzyme activity. Since LIMP-2 is the only described transport receptor for the lysosomal enzyme a cellular missorting of the enzyme seems to be a logical consequence. In a previous study deficiency of LIMP-2 led to the secretion of GC in fibroblasts and primary macrophages (Reczek, Schwake et al. 2007). A further approach using a fluorescent probe specifically targeting active GC (Inhibody®) (Witte, Kallemeijn et al. 2010) confirmed the significant reduction of active enzyme in LIMP-2 deficient brain (Rothaug, Zunke et al. 2014).

The deficiency of GC activity in patients with GD type 2 and 3 leads to neurological symptoms (Sidransky, Sherer et al. 1992, Sidransky, Tayebi et al. 1996, Enquist, Lo Bianco et al. 2007, Xu, Reboulet et al. 2008, Mazzulli, Xu et al. 2011). However, patients with type 1 GD are not affected by neurological impairments. Recently, the view of Gaucher typ 1 as a non-neuronopathic form has been questioned since aberrant function of GC became linked to an increased risk to develop PD (Hruska, Goker-Alpan et al. 2006, Westbroek, Gustafson et al. 2011).

Efficient degradation of cellular metabolites is essential for neuronal survival. An impairment of lysosomal GC activity was found in post-mortem brain obtained from PD patients (Chu, Dodiya et al. 2009, Dehay, Bove et al. 2010). This indicates the importance of the lysosomal pathway in the development of neurodegenerative diseases (Nixon 2013).

In this study an impairment of lysosomal clearance could be identified in the brain of LIMP-2-deficient mice. The initial consequence of the drastically reduced GC activity is an apparent accumulation of glucosylceramide. Since there are no specific antibodies against the glycolipid available, indirect detection methods were used. Electron micrographs indicated dense storage material and lipid droplets in neurons of the pons and additional analysis of primary neurons of LIMP-2-deficient mice exhibited an increase in lipid droplet formation

indicated by staining of neutral lipids (including glucosylceramide) (Rothaug, Zunke et al. 2014). It would be of interest to further characterise the storage material found in the brain of LIMP-2-deficient mice e.g. by mass spectroscopical analyses.

#### 5.4.2 Reasons for $\alpha$ -synuclein accumulation mediated by the LIMP-2 deficiency

The loss of GC activity as well as the accumulation of its substrate glucosylceramide may promote  $\alpha$ -synuclein accumulation and aggregation (Mazzulli, Xu et al. 2011, Westbroek, Gustafson et al. 2011, Gegg, Burke et al. 2012). However, the molecular mechanisms leading to this pathology are still poorly understood. The depletion of LIMP-2 resulted in elevated levels of  $\alpha$ -synuclein as shown in this study. In immunoblot analyses of midbrain samples such increased  $\alpha$ -synuclein levels were found in the soluble and insoluble fraction. In addition, three different antibodies against  $\alpha$ -synuclein were utilised since the protein can appear in different aggregating stages. Each antibody recognises preferably a different form. Although the molecular weight of the monomer of  $\alpha$ -synuclein has been found to be around 14 kDa by mass spectrometry, the protein exhibits an apparent weight of 17-19 kDa on SDS-PAGE (Weinreb, Zhen et al. 1996). This deviation in size had been explained by the highly charged c-terminus of  $\alpha$ -synuclein, which leads to a low binding of SDS (Ueda, Fukushima et al. 1993).

In midbrain of LIMP-2-deficient mice no increase in the protein level of monomeric  $\alpha$ -synuclein was observed. In contrast the 23 and 58 kDa species were both elevated in LIMP-2-deficient samples. Most likely the 23 kDa band is a dimer of  $\alpha$ -synuclein, but it could also be an ubiquitinated form of the protein (Shimura, Schlossmacher et al. 2001). The 58 kDa band most likely representing an oligomeric form of  $\alpha$ -synuclein. An  $\alpha$ -synuclein knockout control was used to control for the specificity of the antibodies. Rothaug and co-workers performed size-exclusion-chromatography (SEC) to better assess the presence of oligomeric  $\alpha$ -synuclein forms. Two different antibodies (C-20 and Syn-1) were utilised showing increased high molecular  $\alpha$ -synuclein protein levels in LIMP-2 knockout samples (Rothaug, Zunke et al. 2014).

This is in agreement with recent literature where loss-of-function mutations in the *GBA1* gene were linked to aberrant  $\alpha$ -synuclein degradation (Westbroek, Gustafson et al. 2011). Also cell-based and *in vivo* data in mice demonstrated that dysfunction of GC activity leads to the formation of  $\alpha$ -synuclein aggregates (Mazzulli, Xu et al. 2011, Osellame, Rahim et al. 2013, Ginns, Mak et al. 2014).

There are several hypotheses published describing how the link between mutated GC and  $\alpha$ -synuclein could be mediated. Some studies show a direct interaction of the mutant GC with

$\alpha$ -synuclein thus promoting the aggregation of the neuronal protein (Cullen, Sardi et al. 2011, Yap, Gruschus et al. 2011). Another theory implies an involvement of the ER associated degradation (ERAD) of the mutated enzyme resulting in increased cell stress (Ron and Horowitz 2005, Mu, Ong et al. 2008). Supporting this view increased levels of ERAD-markers have been found in brains of PD patients with and without mutations in *GBA1*, indicating a rather general role for the ERAD-pathway in PD (Rocha, Smith et al. 2015). These gain-of-function theories, which imply a direct effect of the mutant GC on  $\alpha$ -synuclein levels, do not explain the observed elevation of  $\alpha$ -synuclein in LIMP-2-deficient mice or in mouse models where an inhibitor of GC was applied (CBE) (Manning-Bog, Schule et al. 2009, Xu, Sun et al. 2011). Hence it seems likely that a loss-of-function in GC results in an imbalance in the  $\alpha$ -synuclein homeostasis. The dysfunction of GC may lead to a progressive built-up of glucosylceramide or glycosylsphingosine. In addition, *in vitro* experiments indicate that this glucosylceramide interacts with  $\alpha$ -synuclein leading to stabilisation (Mazzulli, Xu et al. 2011). Surprisingly, a recent study reveals no evidence for substrate (glucosylceramide) accumulation in post-mortem brains of PD patients with *GBA1* mutations (Gegg, Sweet et al. 2015). This emphasises that the mechanisms by which GC deficiency increases the risk for developing PD are still unclear.

To date a direct effect of the LIMP-2 protein on  $\alpha$ -synuclein homeostasis cannot be ruled out completely. So far only one study showed an interaction of  $\alpha$ -synuclein with LIMP-2 (Gegg, Burke et al. 2012), which could not be reproduced by coimmunoprecipitation approaches in our laboratory (data not shown).

#### 5.4.3 Consequences of $\alpha$ -synuclein accumulation in mouse and human CNS

This work suggests a distinct relationship between the expression levels of LIMP-2 and  $\alpha$ -synuclein clearance. As outlined in this study, the presence of endogenous levels of  $\alpha$ -synuclein in LIMP-2-deficient mice (in the C57/BL6N background) led to a severe neurological phenotype, which was not observed when LIMP-2 knockout mice were kept in the  $\alpha$ -synuclein deficient background (C57/BL6J). This clearly suggests a link between the severity of disease and the abundance of  $\alpha$ -synuclein. Furthermore, a dosage-dependent relationship between  $\alpha$ -synuclein levels and disease progression has been shown in transgenic mice overexpressing  $\alpha$ -synuclein (Rieker, Dev et al. 2011).

Consequently, accumulating  $\alpha$ -synuclein has shown to be toxic exhibiting severe effects on neuronal cell viability (Karpinar, Baliya et al. 2009, Winner, Jappelli et al. 2011). In PD mouse models as well as in patients astrogliosis and microgliosis have been observed (Hirsch, Hunot et al. 2005, Zhang, Wang et al. 2005). A similar disease progression could be described

in the pons and midbrain of LIMP-2-deficient mice. Immunostainings revealed an increased number of GFAP and CD68-positive cells indicating highly progressive astro- as well as microgliosis. Furthermore an elevation of apoptotic cells accompanied by a shrinkage of tyrosine hydroxylase positive cells within the midbrain of LIMP-2-deficient mice (Rothaug, Zunke et al. 2014) indicated the severe progression of disease.

Similar as in patients, these  $\alpha$ -synuclein accumulation also resulted in severe behavioural abnormalities in the LIMP-2-deficient mice (Rothaug, Zunke et al. 2014). This was indicated by motor deficits, hind limb clasping, weight loss and premature death. Since these phenotypes resemble the course of disease in a PD mouse model expressing the highly accumulation-prone A53T mutant of  $\alpha$ -synuclein (Giasson, Duda et al. 2002), it further underlines that the observed neuropathological impairments are mediated by the deficiency of LIMP-2.

Whether the loss of LIMP-2 also leads to a comparable elevation of  $\alpha$ -synuclein levels in AMRF-patients, lacking functional LIMP-2, still has to be evaluated. Further studies will be necessary to assess if aggregation of  $\alpha$ -synuclein contributes to the neuropathic characteristics in AMRF patients. However, patients that lack LIMP-2 expression die young and may not be old enough to allow accumulation of  $\alpha$ -synuclein (Balreira, Gaspar et al. 2008). Fibroblasts derived from AMRF patients indicated a loss of LIMP-2 and decreased levels and activity of lysosomal GC (Figure 4.48). To validate if the loss of GC consequently leads to  $\alpha$ -synuclein accumulation post-mortem analysis of brains from AMRF patients will be necessary. Another approach would be to characterise neuronal cell types derived from induced pluripotent stem cells (iPSC) from fibroblasts of AMRF patients.

Furthermore, it was assessed if and to what extent  $\alpha$ -synuclein influences GC activity. Recent studies in PD patients show reduced GC-activity in brain regions with increased  $\alpha$ -synuclein levels (Gegg, Burke et al. 2012, Murphy, Gysbers et al. 2014). In this work the effect of  $\alpha$ -synuclein on lysosomal activity in iPSC-derived dopaminergic neurons from human midbrain was investigated. The results suggest that not only decreased GC activity results in an accumulation of  $\alpha$ -synuclein, but also vice versa, that  $\alpha$ -synuclein negatively influences GC function. A direct interaction of  $\alpha$ -synuclein with GC resulting in enzyme inhibition may be a possible explanation (Yap, Gruschus et al. 2011). Another reason for this negative effect on GC activity could result from intracellular trafficking deficiencies. Recent studies reveal that oligomeric  $\alpha$ -synuclein is able to block ER-Golgi delivery. This could be verified in yeast, mammalian cells and PD brain lysates (Cooper, Gitler et al. 2006, Thayanidhi, Helm et al. 2010, Mazzulli, Xu et al. 2011). The impairment of intracellular transport has extensive

consequences, since the transport, maturation and thus function of lysosomal enzymes and potentially other -so far undescribed- proteins is affected. This trafficking deficit results in dysfunction of lysosomal GC and creates a negative feedback loop, which further supports  $\alpha$ -synuclein accumulation (Figure 5.10).

#### 5.4.4 The role of LIMP-2 in the development and correction of synucleinopathies: identification of novel therapeutic targets

The importance of LIMP-2 in  $\alpha$ -synuclein homeostasis is further supported by the identification of increased levels of the lysosomal membrane protein in post-mortem brain of PD patients (Rothaug, Zunke et al. 2014). This might indicate a compensatory effect to overcome an impaired lysosomal targeting of GC. Single nucleotide polymorphisms (SNPs) in the *SCARB2* gene encoding for LIMP-2 have been described as genetic risk factors for the development of PD (Do, Tung et al. 2011, Hopfner, Schulte et al. 2013). However, for further validation of this finding a larger cohort of PD patients will be needed for genetic screens (Maniwang, Tayebi et al. 2013). It was shown in a recent study that the *SCARB2* locus is associated with dementia with Lewy body (DLB) indicating the involvement of LIMP-2 in the development of synucleinopathies (Bras, Guerreiro et al. 2014). In addition, mutations within *SCARB2* were recently shown to modify the neurological presentation of GD (Velayati, DePaolo et al. 2011).

Data described in this study emphasise an important reciprocal role for LIMP-2 in  $\alpha$ -synuclein homeostasis (Figure 5.9). Although the molecular details of this interaction still remain elusive, it could be shown that a depletion of LIMP-2 leads to  $\alpha$ -synuclein accumulation in murine brain. This is most likely due to an impaired lysosomal transport and activity of GC. Decreased GC activity leads to the accumulation of its substrate glucosylceramide. This glycosphingolipid may directly interact with and stabilise  $\alpha$ -synuclein, which also has been shown to inhibit intracellular trafficking, further affecting the delivery of lysosomal enzymes to lysosomes (Cooper, Gitler et al. 2006, Thayanidhi, Helm et al. 2010, Mazzulli, Xu et al. 2011) (Figure 5.9 and Figure 5.10).

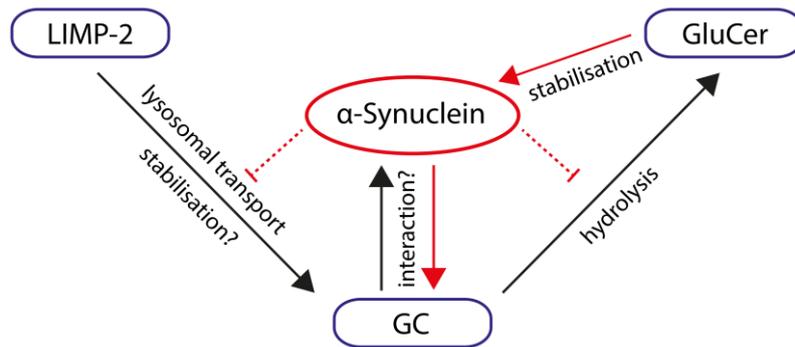


**Figure 5.9: Schematic interaction between LIMP-2, GC and  $\alpha$ -synuclein.**

LIMP-2 transports GC to the lysosome, where it hydrolyses glucosylceramide (GluCer) to glucose and ceramide. GluCer seems to interact with  $\alpha$ -synuclein leading to its stabilisation. Increased levels of  $\alpha$ -synuclein impair intracellular trafficking, which leads to reduced lysosomal levels of GC. Furthermore,  $\alpha$ -synuclein might directly interact with GC, negatively influencing its enzymatic function. This creates a negative feedback loop, where the accumulating substrate of GC (GluCer) further stabilises the aggregating  $\alpha$ -synuclein thereby accelerating its negative effects on GC transport and activity.

Thus, methods that overcome the  $\alpha$ -synuclein-induced ER-Golgi transport defect and that increase the delivery of GC to lysosomes have been suggested as a therapeutic strategy (Figure 5.10). Since LIMP-2 is the only reported transporter of GC it is an attractive target to influence lysosomal transport of GC.

As already described by Reczek *et al.*, a known disease causing mutant of GC (L444P) that is retained in the ER, was transported to the lysosomal compartments after LIMP-2 overexpression, highlighting the high affinity of the enzyme for its receptor (Reczek, Schwake *et al.* 2007). This data and the positive effects of LIMP-2 expression on the lysosomal GC localisation further emphasises the role of LIMP-2 in targeting wild-type as well as aberrant GC to lysosomes, where the enzyme is most active.

Furthermore, the GC activity in the whole cell as well as in the lysosomal fraction only could be increased after overexpression of LIMP-2. Since GC already exhibits activity while in the ER, it is important to control that the activity is actually increased in the target organelle of GC, the lysosome.

Besides its trafficking function LIMP-2 might also act as a chaperone, stabilising and thus activating GC directly. As described in this study, the elevated lysosomal activity of GC resulted in an accelerated  $\alpha$ -synuclein degradation in the presence of auxiliary LIMP-2. This effect could also be shown in a time-dependent manner.

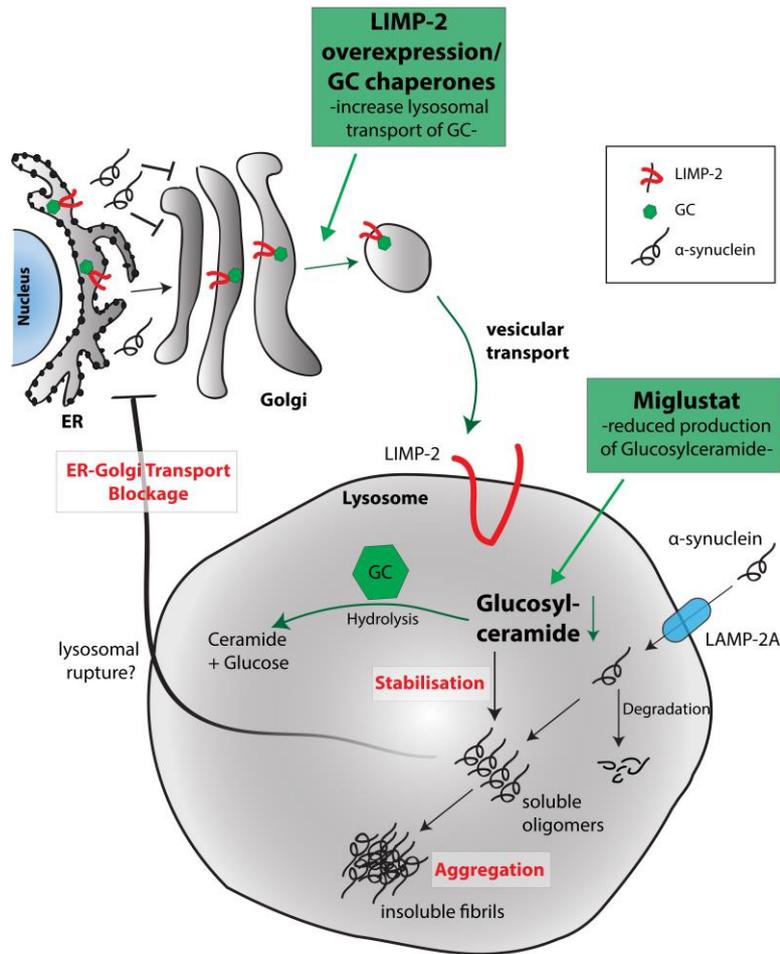


**Figure 5.10: Overview of strategies to reduce the accumulation of  $\alpha$ -synuclein.**

GC gets transported to the lysosome by interaction with LIMP-2. Both proteins associate in the ER and dissociate pH-dependently in the lysosome. The lysosomal transport of GC can be enhanced by overexpression of LIMP-2 or GC chaperones. Increased levels of lysosomal GC result in a boost of GC activity followed by a decrease in glucosylceramide levels. Another way to reduce the concentration of the glycosphingolipid is the substrate reduction therapy by miglustat. Since glucosylceramide has been shown to interact and stabilise  $\alpha$ -synuclein, reduction of the lipid will also reduce  $\alpha$ -synuclein accumulation. A decreased concentration of soluble  $\alpha$ -synuclein oligomers is followed by reduced blockage of the ER-Golgi transport. In summary, either increased lysosomal transport of GC or direct substrate reduction may lead to a decrease in  $\alpha$ -synuclein levels reducing cellular toxicity and decline of cellular trafficking defects.

In order to exploit the benefit of the positive effect of LIMP-2 on  $\alpha$ -synuclein levels for therapy, strategies to increase the protein level of the lysosomal membrane protein should be considered (Figure 5.10). In this respect, gene therapy may be an option, but remaining issues of the viral vector safety are still an obstacle in the clinical application (Sands and Davidson 2006, Aronovich and Hackett 2015). Another approach would be to analyse the promoter region of LIMP-2 to identify new therapeutic targets, which increase the expression of the lysosomal membrane protein on a transcriptional level. A high-throughput screening of small molecules evaluating changes in LIMP-2 transcription could help to discover novel effectors for treatment of synucleinopathies like PD.

Pathology and behavioural abnormalities induced by  $\alpha$ -synuclein accumulation can be reversed in a mouse model of dementia with Lewy body (DLB) (Lim, Kehm et al. 2011). This indicates that methods, which enhance  $\alpha$ -synuclein clearance, are able to reverse already existent symptoms and may provide a therapeutic benefit. Increasing the activity of GC is one strategy that might downregulate  $\alpha$ -synuclein levels and thus may prevent further disease progression in synucleinopathies including PD. Recent studies show a decline in  $\alpha$ -synuclein accumulation as well as CNS impairment after introducing GC adenovirus-mediated into PD mouse brains (Sardi, Clarke et al. 2013).

Small molecules directly targeting and activating GC are of interest. As shown in this work the LIMP-2-derived helix 5 peptide was able to increase GC activity *in vitro* as well as in cell culture based studies. Furthermore, it was assessed if the peptide-induced augmentation of GC activity is sufficient to reduce  $\alpha$ -synuclein levels. Indeed, enhanced  $\alpha$ -synuclein clearance could be observed after adding the helix 5 peptide to the media of stably  $\alpha$ -synuclein overexpressing H4 cell line. This effect was accompanied by an increase of intracellular GC activity, indicating that the positive effect on the  $\alpha$ -synuclein levels is due to the peptide-mediated increase of GC activity. Since,  $\alpha$ -synuclein is the accumulating protein in Parkinson disease (Polymeropoulos, Lavedan et al. 1997), this broadens the field of a potential therapeutic application of the LIMP-2-derived peptide. In further studies, the effect and potency of the helix 5 peptide on GC activity and subsequently on  $\alpha$ -synuclein levels will need to be assessed *in vivo*. However, a critical point will be the ability of the peptide to cross the blood-brain barrier. This is of interest for the treatment of synucleinopathies but also for the neuropathological forms of Gaucher disease (type II and III).

Another strategy to potentially reduce  $\alpha$ -synuclein levels may be the substrate reduction therapy (SRT). Since the compound miglustat has been shown to target the glucosylceramide synthase leading to reduced levels of glucosylceramide (Platt, Neises et al. 1994), the decline in glycosphingolipid levels may reduce the stabilisation of  $\alpha$ -synuclein oligomers (Figure 5.10). However to date, no effect of miglustat treatment on neurological phenotypes could be observed. So far, therapeutic benefits were perceived particularly in liver and spleen size as well as in platelet count (Cox, Lachmann et al. 2000, Elstein, Hollak et al. 2004).

## 5.5 Conclusion and outlook

This study describes the structural characteristics of the interaction of LIMP-2 with GC and its auxiliary effect on GC activity. After describing the GC binding site on the LIMP-2 protein, a small peptide resembling helix 5 of this interaction site was shown to specifically interact with GC. Interestingly, the peptide was also able to enhance GC activity *in vitro* as well as in cells. Furthermore, this work shows a distinct relationship between LIMP-2 expression, GC-activity and  $\alpha$ -synuclein homeostasis. However, the detailed molecular mechanisms of this interaction still remain unclear. Since activators of GC accelerate the clearance of  $\alpha$ -synuclein and thus prevent further disease progression in synucleinopathies, future experiments are necessary to address the impact of the LIMP-2-derived peptide *in vivo*. Since it was also possible to identify the LIMP-2 binding site on GC, found opposite of the catalytic cavity, this interaction domain is of interest for a rational drug design. Small molecules targeting this specific protein region may be considered as therapeutic approach for Gaucher disease and synucleinopathies like Parkinson disease.

## 6 References

- Abumrad, N., C. Harmon and A. Ibrahimi (1998). "Membrane transport of long-chain fatty acids: evidence for a facilitated process." *J Lipid Res* **39**(12): 2309-2318.
- Aeed, P. A. and A. P. Elhammer (1994). "Glycosylation of recombinant prorenin in insect cells: the insect cell line Sf9 does not express the mannose 6-phosphate recognition signal." *Biochemistry* **33**(29): 8793-8797.
- Aerts, J. M., A. W. Schram, A. Strijland, W. S. van, L. M. Jonsson, J. M. Tager, S. H. Sorrell, E. I. Ginns, J. A. Barranger and G. J. Murray (1988). "Glucocerebrosidase, a lysosomal enzyme that does not undergo oligosaccharide phosphorylation." *Biochim.Biophys.Acta* **964**(3): 303-308.
- Alattia, J. R., J. E. Shaw, C. M. Yip and G. G. Prive (2006). "Direct visualization of saposin remodelling of lipid bilayers." *J Mol Biol* **362**(5): 943-953.
- Alattia, J. R., J. E. Shaw, C. M. Yip and G. G. Prive (2007). "Molecular imaging of membrane interfaces reveals mode of beta-glucosidase activation by saposin C." *Proc Natl Acad Sci U S A* **104**(44): 17394-17399.
- Alfonso, P., S. Pampin, J. Estrada, J. C. Rodriguez-Rey, P. Giraldo, J. Sancho and M. Pocovi (2005). "Miglustat (NB-DNJ) works as a chaperone for mutated acid beta-glucosidase in cells transfected with several Gaucher disease mutations." *Blood Cells Mol Dis* **35**(2): 268-276.
- Altarescu, G., S. Hill, E. Wiggs, N. Jeffries, C. Kreps, C. C. Parker, R. O. Brady, N. W. Barton and R. Schiffmann (2001). "The efficacy of enzyme replacement therapy in patients with chronic neuronopathic Gaucher's disease." *J Pediatr* **138**(4): 539-547.
- Aronovich, E. L. and P. B. Hackett (2015). "Lysosomal storage disease: gene therapy on both sides of the blood-brain barrier." *Mol Genet Metab* **114**(2): 83-93.
- Atrian, S., E. Lopez-Vinas, P. Gomez-Puertas, A. Chabas, L. Vilageliu and D. Grinberg (2008). "An evolutionary and structure-based docking model for glucocerebrosidase-saposin C and glucocerebrosidase-substrate interactions - Relevance for Gaucher disease." *Proteins-Structure Function and Bioinformatics* **70**(3): 882-891.
- Baba, M., S. Nakajo, P. H. Tu, T. Tomita, K. Nakaya, V. M. Lee, J. Q. Trojanowski and T. Iwatsubo (1998). "Aggregation of alpha-synuclein in Lewy bodies of sporadic Parkinson's disease and dementia with Lewy bodies." *Am J Pathol* **152**(4): 879-884.
- Badhwar, A., S. F. Berkovic, J. P. Dowling, M. Gonzales, S. Narayanan, A. Brodtmann, L. Berzen, J. Caviness, C. Trenkwalder, J. Winkelmann, J. Rivest, M. Lambert, O. Hernandez-Cossio, S. Carpenter, F. Andermann and E. Andermann (2004). "Action myoclonus-renal failure syndrome: characterization of a unique cerebro-renal disorder." *Brain* **127**(Pt 10): 2173-2182.
- Bainton, D. F. (1981). "The discovery of lysosomes." *J Cell Biol* **91**(3 Pt 2): 66s-76s.
- Balreira, A., P. Gaspar, D. Caiola, J. Chaves, I. Beirao, J. L. Lima, J. E. Azevedo and M. C. Miranda (2008). "A nonsense mutation in the LIMP-2 gene associated with progressive myoclonic epilepsy and nephrotic syndrome." *Hum.Mol.Genet.* **17**(14): 2238-2243.
- Beavan, M. S. and A. H. Schapira (2013). "Glucocerebrosidase mutations and the pathogenesis of Parkinson disease." *Ann Med* **45**(8): 511-521.
- Bendikov-Bar, I. and M. Horowitz (2012). "Gaucher disease paradigm: from ERAD to comorbidity." *Hum Mutat* **33**(10): 1398-1407.
- Berg-Fussman, A., M. E. Grace, Y. Ioannou and G. A. Grabowski (1993). "Human acid beta-glucosidase. N-glycosylation site occupancy and the effect of glycosylation on enzymatic activity." *J Biol Chem* **268**(20): 14861-14866.

- Berkovic, S. F., L. M. Dibbens, A. Oshlack, J. D. Silver, M. Katerelos, D. F. Vears, R. Lullmann-Rauch, J. Blanz, K. W. Zhang, J. Stankovich, R. M. Kalnins, J. P. Dowling, E. Andermann, F. Andermann, E. Faldini, R. D'Hooge, L. Vadlamudi, R. A. Macdonell, B. L. Hodgson, M. A. Bayly, J. Savige, J. C. Mulley, G. K. Smyth, D. A. Power, P. Saftig and M. Bahlo (2008). "Array-based gene discovery with three unrelated subjects shows SCARB2/LIMP-2 deficiency causes myoclonus epilepsy and glomerulosclerosis." *Am.J.Hum.Genet.* **82**(3): 673-684.
- Blanz, J., J. Groth, C. Zachos, C. Wehling, P. Saftig and M. Schwake (2010). "Disease-causing mutations within the lysosomal integral membrane protein type 2 (LIMP-2) reveal the nature of binding to its ligand beta-glucocerebrosidase." *Hum.Mol.Genet.* **19**(4): 563-572.
- Blanz, J., S. Stroobants, R. Lullmann-Rauch, W. Morelle, M. Ludemann, R. D'Hooge, H. Reuterwall, J. C. Michalski, J. Fogh, C. Andersson and P. Saftig (2008). "Reversal of peripheral and central neural storage and ataxia after recombinant enzyme replacement therapy in alpha-mannosidosis mice." *Hum.Mol.Genet.* **17**(22): 3437-3445.
- Bonifacino, J. S. and L. M. Traub (2003). "Signals for sorting of transmembrane proteins to endosomes and lysosomes." *Annu Rev Biochem* **72**: 395-447.
- Brady, R. O. (2006). "Enzyme replacement for lysosomal diseases." *Annu Rev Med* **57**: 283-296.
- Brady, R. O., J. N. Kanfer, R. M. Bradley and D. Shapiro (1966). "Demonstration of a deficiency of glucocerebrosidase-cleaving enzyme in Gaucher's disease." *J Clin Invest* **45**(7): 1112-1115.
- Bras, J., R. Guerreiro, L. Darwent, L. Parkkinen, O. Ansorge, V. Escott-Price, D. G. Hernandez, M. A. Nalls, L. N. Clark, L. S. Honig, K. Marder, W. M. Van Der Flier, A. Lemstra, P. Scheltens, E. Rogaeva, P. St George-Hyslop, E. Londos, H. Zetterberg, S. Ortega-Cubero, P. Pastor, T. J. Ferman, N. R. Graff-Radford, O. A. Ross, I. Barber, A. Braae, K. Brown, K. Morgan, W. Maetzler, D. Berg, C. Troakes, S. Al-Sarraj, T. Lashley, Y. Compta, T. Revesz, A. Lees, N. Cairns, G. M. Halliday, D. Mann, S. Pickering-Brown, D. W. Dickson, A. Singleton and J. Hardy (2014). "Genetic analysis implicates APOE, SNCA and suggests lysosomal dysfunction in the etiology of dementia with Lewy bodies." *Hum Mol Genet* **23**(23): 6139-6146.
- Braulke, T. (1999). "Type-2 IGF receptor: a multi-ligand binding protein." *Horm Metab Res* **31**(2-3): 242-246.
- Braulke, T. and J. S. Bonifacino (2009). "Sorting of lysosomal proteins." *Biochim Biophys Acta* **1793**(4): 605-614.
- Brown, M. S. and J. L. Goldstein (1986). "A receptor-mediated pathway for cholesterol homeostasis." *Science* **232**(4746): 34-47.
- Brumshtein, B., H. M. Greenblatt, T. D. Butters, Y. Shaaltiel, D. Aviezer, I. Silman, A. H. Futerman and J. L. Sussman (2007). "Crystal structures of complexes of N-butyl- and N-nonyl-deoxynojirimycin bound to acid beta-glucosidase: insights into the mechanism of chemical chaperone action in Gaucher disease." *J Biol Chem* **282**(39): 29052-29058.
- Brumshtein, B., M. R. Wormald, I. Silman, A. H. Futerman and J. L. Sussman (2006). "Structural comparison of differently glycosylated forms of acid-beta-glucosidase, the defective enzyme in Gaucher disease." *Acta Crystallogr.D.Biol.Crystallogr.* **62**(Pt 12): 1458-1465.
- Buccoliero, R., J. Bodennec and A. H. Futerman (2002). "The role of sphingolipids in neuronal development: lessons from models of sphingolipid storage diseases." *Neurochem Res* **27**(7-8): 565-574.
- Burre, J., M. Sharma, T. Tsetsenis, V. Buchman, M. R. Etherton and T. C. Sudhof (2010). "Alpha-synuclein promotes SNARE-complex assembly in vivo and in vitro." *Science* **329**(5999): 1663-1667.
- Cabrera-Salazar, M. A., E. Novelli and J. A. Barranger (2002). "Gene therapy for the lysosomal storage disorders." *Curr Opin Mol Ther* **4**(4): 349-358.
- Calvo, D., J. Dopazo and M. A. Vega (1995). "The CD36, CLA-1 (CD36L1), and LIMPII (CD36L2) gene family: cellular distribution, chromosomal location, and genetic evolution." *Genomics* **25**(1): 100-106.

- Canton, J., D. Neculai and S. Grinstein (2013). "Scavenger receptors in homeostasis and immunity." *Nat Rev Immunol* **13**(9): 621-634.
- Canuel, M., A. Korkidakis, K. Konnyu and C. R. Morales (2008). "Sortilin mediates the lysosomal targeting of cathepsins D and H." *Biochem Biophys Res Commun* **373**(2): 292-297.
- Chakravarthy, B. R., M. W. Spence, J. T. Clarke and H. W. Cook (1985). "Rapid isolation of neuroblastoma plasma membranes on Percoll gradients. Characterization and lipid composition." *Biochim Biophys Acta* **812**(1): 223-233.
- Chandra, S., F. Fornai, H. B. Kwon, U. Yazdani, D. Atasoy, X. Liu, R. E. Hammer, G. Battaglia, D. C. German, P. E. Castillo and T. C. Sudhof (2004). "Double-knockout mice for alpha- and beta-synucleins: effect on synaptic functions." *Proc Natl Acad Sci U S A* **101**(41): 14966-14971.
- Chandra, S., G. Gallardo, R. Fernandez-Chacon, O. M. Schluter and T. C. Sudhof (2005). "Alpha-synuclein cooperates with CSPalpha in preventing neurodegeneration." *Cell* **123**(3): 383-396.
- Chang, T. Y., C. C. Chang, N. Ohgami and Y. Yamauchi (2006). "Cholesterol sensing, trafficking, and esterification." *Annu Rev Cell Dev Biol* **22**: 129-157.
- Chaudhuri, K. R., D. G. Healy, A. H. Schapira and E. National Institute for Clinical (2006). "Non-motor symptoms of Parkinson's disease: diagnosis and management." *Lancet Neurol* **5**(3): 235-245.
- Chu, B. B., Y. C. Liao, W. Qi, C. Xie, X. Du, J. Wang, H. Yang, H. H. Miao, B. L. Li and B. L. Song (2015). "Cholesterol Transport through Lysosome-Peroxisome Membrane Contacts." *Cell* **161**(2): 291-306.
- Chu, Y., H. Dodiya, P. Aebischer, C. W. Olanow and J. H. Kordower (2009). "Alterations in lysosomal and proteasomal markers in Parkinson's disease: relationship to alpha-synuclein inclusions." *Neurobiol Dis* **35**(3): 385-398.
- Clark, L. N., L. A. Kartsaklis, R. Wolf Gilbert, B. Dorado, B. M. Ross, S. Kisselev, M. Verbitsky, H. Mejia-Santana, L. J. Cote, H. Andrews, J. P. Vonsattel, S. Fahn, R. Mayeux, L. S. Honig and K. Marder (2009). "Association of glucocerebrosidase mutations with dementia with lewy bodies." *Arch Neurol* **66**(5): 578-583.
- Conway, K. A., S. J. Lee, J. C. Rochet, T. T. Ding, R. E. Williamson and P. T. Lansbury, Jr. (2000). "Acceleration of oligomerization, not fibrillization, is a shared property of both alpha-synuclein mutations linked to early-onset Parkinson's disease: implications for pathogenesis and therapy." *Proc Natl Acad Sci U S A* **97**(2): 571-576.
- Cooper, A. A., A. D. Gitler, A. Cashikar, C. M. Haynes, K. J. Hill, B. Bhullar, K. Liu, K. Xu, K. E. Strathearn, F. Liu, S. Cao, K. A. Caldwell, G. A. Caldwell, G. Marsischky, R. D. Kolodner, J. Labeaer, J. C. Rochet, N. M. Bonini and S. Lindquist (2006). "Alpha-synuclein blocks ER-Golgi traffic and Rab1 rescues neuron loss in Parkinson's models." *Science* **313**(5785): 324-328.
- Cormand, B., T. L. Harboe, L. Gort, C. Campoy, M. Blanco, N. Chamoles, A. Chabas, L. Vilageliu and D. Grinberg (1998). "Mutation analysis of Gaucher disease patients from Argentina: high prevalence of the RecNcil mutation." *Am J Med Genet* **80**(4): 343-351.
- Cox, T., R. Lachmann, C. Hollak, J. Aerts, S. van Weely, M. Hrebicek, F. Platt, T. Butters, R. Dwek, C. Moyses, I. Gow, D. Elstein and A. Zimran (2000). "Novel oral treatment of Gaucher's disease with N-butyldeoxyojirimycin (OGT 918) to decrease substrate biosynthesis." *Lancet* **355**(9214): 1481-1485.
- Cox, T. M. (2005). "Substrate reduction therapy for lysosomal storage diseases." *Acta Paediatr Suppl* **94**(447): 69-75; discussion 57.
- Cuervo, A. M., L. Stefanis, R. Fredenburg, P. T. Lansbury and D. Sulzer (2004). "Impaired degradation of mutant alpha-synuclein by chaperone-mediated autophagy." *Science* **305**(5688): 1292-1295.
- Cullen, V., M. Lindfors, J. Ng, A. Paetau, E. Swinton, P. Kolodziej, H. Boston, P. Saftig, J. Woulfe, M. B. Feany, L. Myllykangas, M. G. Schlossmacher and J. Tyynela (2009). "Cathepsin D expression level affects alpha-synuclein processing, aggregation, and toxicity in vivo." *Mol Brain* **2**: 5.

- Cullen, V., S. P. Sardi, J. Ng, Y. H. Xu, Y. Sun, J. J. Tomlinson, P. Kolodziej, I. Kahn, P. Saftig, J. Woulfe, J. C. Rochet, M. A. Glicksman, S. H. Cheng, G. A. Grabowski, L. S. Shihabuddin and M. G. Schlossmacher (2011). "Acid beta-glucosidase mutants linked to Gaucher disease, Parkinson disease, and Lewy body dementia alter alpha-synuclein processing." *Ann Neurol* **69**(6): 940-953.
- Dang, M., X. Wang, Q. Wang, Y. Wang, J. Lin, Y. Sun, X. Li, L. Zhang, Z. Lou, J. Wang and Z. Rao (2014). "Molecular mechanism of SCARB2-mediated attachment and uncoating of EV71." *Protein Cell* **5**(9): 692-703.
- Dardis, A., M. Filocamo, S. Grossi, G. Ciana, S. Franceschetti, S. Dominissini, G. Rubboli, R. M. Di and B. Bembi (2009). "Biochemical and molecular findings in a patient with myoclonic epilepsy due to a mistarget of the beta-glucosidase enzyme." *Mol.Genet.Metab* **97**(4): 309-311.
- Davidson, W. S., A. Jonas, D. F. Clayton and J. M. George (1998). "Stabilization of alpha-synuclein secondary structure upon binding to synthetic membranes." *J Biol Chem* **273**(16): 9443-9449.
- Davie, C. A. (2008). "A review of Parkinson's disease." *Br Med Bull* **86**: 109-127.
- De Duve, C. and H. Beaufay (1959). "Tissue fractionation studies. 10. Influence of ischaemia on the state of some bound enzymes in rat liver." *Biochem J* **73**: 610-616.
- De Duve, C., B. C. Pressman, R. Gianetto, R. Wattiaux and F. Appelmans (1955). "Tissue fractionation studies. 6. Intracellular distribution patterns of enzymes in rat-liver tissue." *Biochem J* **60**(4): 604-617.
- de la Llera-Moya, M., G. H. Rothblat, M. A. Connelly, G. Kellner-Weibel, S. W. Sakr, M. C. Phillips and D. L. Williams (1999). "Scavenger receptor BI (SR-BI) mediates free cholesterol flux independently of HDL tethering to the cell surface." *J Lipid Res* **40**(3): 575-580.
- Dehay, B., J. Bove, N. Rodriguez-Muela, C. Perier, A. Recasens, P. Boya and M. Vila (2010). "Pathogenic lysosomal depletion in Parkinson's disease." *J Neurosci* **30**(37): 12535-12544.
- Demina, A. and E. Beutler (1998). "Six new Gaucher disease mutations." *Acta Haematol* **99**(2): 80-82.
- DeWitt, D. C. and E. Rhoades (2013). "alpha-Synuclein can inhibit SNARE-mediated vesicle fusion through direct interactions with lipid bilayers." *Biochemistry* **52**(14): 2385-2387.
- Dibbens, L. M., I. Karakis, M. A. Bayly, D. J. Costello, A. J. Cole and S. F. Berkovic (2011). "Mutation of SCARB2 in a patient with progressive myoclonus epilepsy and demyelinating peripheral neuropathy." *Arch Neurol* **68**(6): 812-813.
- Dibbens, L. M., R. Michelucci, A. Gambardella, F. Andermann, G. Rubboli, M. A. Bayly, T. Joensuu, D. F. Vears, S. Franceschetti, L. Canafoglia, R. Wallace, A. G. Bassuk, D. A. Power, C. A. Tassinari, E. Andermann, A. E. Lehesjoki and S. F. Berkovic (2009). "SCARB2 mutations in progressive myoclonus epilepsy (PME) without renal failure." *Ann Neurol* **66**(4): 532-536.
- Dittmer, F., E. J. Ulbrich, A. Hafner, W. Schmahl, T. Meister, R. Pohlmann and K. von Figura (1999). "Alternative mechanisms for trafficking of lysosomal enzymes in mannose 6-phosphate receptor-deficient mice are cell type-specific." *J Cell Sci* **112** ( Pt 10): 1591-1597.
- Do, C. B., J. Y. Tung, E. Dorfman, A. K. Kiefer, E. M. Drabant, U. Francke, J. L. Mountain, S. M. Goldman, C. M. Tanner, J. W. Langston, A. Wojcicki and N. Eriksson (2011). "Web-based genome-wide association study identifies two novel loci and a substantial genetic component for Parkinson's disease." *PLoS Genet* **7**(6): e1002141.
- Dvir, H., M. Harel, A. A. McCarthy, L. Toker, I. Silman, A. H. Futerman and J. L. Sussman (2003). "X-ray structure of human acid-beta-glucosidase, the defective enzyme in Gaucher disease." *EMBO Rep.* **4**(7): 704-709.
- Ebrahimi-Fakhari, D., I. Cantuti-Castelvetri, Z. Fan, E. Rockenstein, E. Masliah, B. T. Hyman, P. J. McLean and V. K. Unni (2011). "Distinct roles in vivo for the ubiquitin-proteasome system and the autophagy-lysosomal pathway in the degradation of alpha-synuclein." *J Neurosci* **31**(41): 14508-14520.

- Elstein, D., C. Hollak, J. M. Aerts, S. van Weely, M. Maas, T. M. Cox, R. H. Lachmann, M. Hrebicek, F. M. Platt, T. D. Butters, R. A. Dwek and A. Zimran (2004). "Sustained therapeutic effects of oral miglustat (Zavesca, N-butyldeoxynojirimycin, OGT 918) in type I Gaucher disease." *J Inherit Metab Dis* **27**(6): 757-766.
- Enquist, I. B., C. Lo Bianco, A. Ooka, E. Nilsson, J. E. Mansson, M. Ehinger, J. Richter, R. O. Brady, D. Kirik and S. Karlsson (2007). "Murine models of acute neuronopathic Gaucher disease." *Proc Natl Acad Sci U S A* **104**(44): 17483-17488.
- Erickson, A. H., E. I. Ginns and J. A. Barranger (1985). "Biosynthesis of the lysosomal enzyme glucocerebrosidase." *J Biol Chem* **260**(26): 14319-14324.
- Eskelinen, E. L., C. K. Schmidt, S. Neu, M. Willenborg, G. Fuertes, N. Salvador, Y. Tanaka, R. Lullmann-Rauch, D. Hartmann, J. Heeren, K. von Figura, E. Knecht and P. Saftig (2004). "Disturbed cholesterol traffic but normal proteolytic function in LAMP-1/LAMP-2 double-deficient fibroblasts." *Mol Biol Cell* **15**(7): 3132-3145.
- Eskelinen, E. L., Y. Tanaka and P. Saftig (2003). "At the acidic edge: emerging functions for lysosomal membrane proteins." *Trends Cell Biol.* **13**(3): 137-145.
- Eyal, N., N. Firon, S. Wilder, E. H. Kolodny and M. Horowitz (1991). "Three unique base pair changes in a family with Gaucher disease." *Hum Genet* **87**(3): 328-332.
- Fiani, M. L., J. Beitz, D. Turvy, J. S. Blum and P. D. Stahl (1998). "Regulation of mannose receptor synthesis and turnover in mouse J774 macrophages." *J Leukoc Biol* **64**(1): 85-91.
- Filocamo, M., R. Mazzotti, M. Stroppiano, S. Grossi, C. Dravet and R. Guerrini (2004). "Early visual seizures and progressive myoclonus epilepsy in neuronopathic Gaucher disease due to a rare compound heterozygosity (N188S/S107L)." *Epilepsia* **45**(9): 1154-1157.
- Frankel, A. D. and C. O. Pabo (1988). "Cellular uptake of the tat protein from human immunodeficiency virus." *Cell* **55**(6): 1189-1193.
- Fuller, M., P. J. Meikle and J. J. Hopwood (2006). *Epidemiology of lysosomal storage diseases: an overview. Fabry Disease: Perspectives from 5 Years of FOS.* A. Mehta, M. Beck and G. Sunder-Plassmann. Oxford.
- Gaidukov, L., A. R. Nager, S. Xu, M. Penman and M. Krieger (2011). "Glycine dimerization motif in the N-terminal transmembrane domain of the high density lipoprotein receptor SR-BI required for normal receptor oligomerization and lipid transport." *J Biol Chem* **286**(21): 18452-18464.
- Gamp, A. C., Y. Tanaka, R. Lullmann-Rauch, D. Wittke, R. D'Hooge, P. P. De Deyn, T. Moser, H. Maier, D. Hartmann, K. Reiss, A. L. Illert, F. K. von and P. Saftig (2003). "LIMP-2/LGP85 deficiency causes ureteric pelvic junction obstruction, deafness and peripheral neuropathy in mice." *Hum.Mol.Genet.* **12**(6): 631-646.
- Gegg, M. E., D. Burke, S. J. Heales, J. M. Cooper, J. Hardy, N. W. Wood and A. H. Schapira (2012). "Glucocerebrosidase deficiency in substantia nigra of parkinson disease brains." *Ann Neurol* **72**(3): 455-463.
- Gegg, M. E., L. Sweet, B. H. Wang, L. S. Shihabuddin, S. P. Sardi and A. H. Schapira (2015). "No evidence for substrate accumulation in Parkinson brains with GBA mutations." *Mov Disord.*
- George, J. M. (2002). "The synucleins." *Genome Biol* **3**(1): REVIEWS3002.
- Ghosh, P., N. M. Dahms and S. Kornfeld (2003). "Mannose 6-phosphate receptors: new twists in the tale." *Nat Rev Mol Cell Biol* **4**(3): 202-212.
- Giasson, B. I., J. E. Duda, S. M. Quinn, B. Zhang, J. Q. Trojanowski and V. M. Lee (2002). "Neuronal alpha-synucleinopathy with severe movement disorder in mice expressing A53T human alpha-synuclein." *Neuron* **34**(4): 521-533.
- Gieselmann, V. (1995). "Lysosomal storage diseases." *Biochim.Biophys.Acta* **1270**(2-3): 103-136.
- Ginns, E. I., S. K. Mak, N. Ko, J. Karlgren, S. Akbarian, V. P. Chou, Y. Guo, A. Lim, S. Samuelsson, M. L. LaMarca, J. Vazquez-DeRose and A. B. Manning-Bog (2014). "Neuroinflammation and alpha-synuclein

- accumulation in response to glucocerebrosidase deficiency are accompanied by synaptic dysfunction." Mol Genet Metab **111**(2): 152-162.
- Goker-Alpan, O., B. I. Giasson, M. J. Eblan, J. Nguyen, H. I. Hurtig, V. M. Lee, J. Q. Trojanowski and E. Sidransky (2006). "Glucocerebrosidase mutations are an important risk factor for Lewy body disorders." Neurology **67**(5): 908-910.
- Goker-Alpan, O., G. Lopez, J. Vithayathil, J. Davis, M. Hallett and E. Sidransky (2008). "The spectrum of parkinsonian manifestations associated with glucocerebrosidase mutations." Arch Neurol **65**(10): 1353-1357.
- Goker-Alpan, O., R. Schiffmann, M. E. LaMarca, R. L. Nussbaum, A. McInerney-Leo and E. Sidransky (2004). "Parkinsonism among Gaucher disease carriers." J Med Genet **41**(12): 937-940.
- Grabowski, G. A., S. Gatt and M. Horowitz (1990). "Acid beta-glucosidase: enzymology and molecular biology of Gaucher disease." Crit Rev Biochem Mol Biol **25**(6): 385-414.
- Grace, M. E., K. M. Newman, V. Scheinker, A. Berg-Fussman and G. A. Grabowski (1994). "Analysis of human acid beta-glucosidase by site-directed mutagenesis and heterologous expression." J Biol Chem **269**(3): 2283-2291.
- Green, M. and P. M. Loewenstein (1988). "Autonomous functional domains of chemically synthesized human immunodeficiency virus tat trans-activator protein." Cell **55**(6): 1179-1188.
- Greenwalt, D. E., R. H. Lipsky, C. F. Ockenhouse, H. Ikeda, N. N. Tandon and G. A. Jamieson (1992). "Membrane glycoprotein CD36: a review of its roles in adherence, signal transduction, and transfusion medicine." Blood **80**(5): 1105-1115.
- Griffiths, G. M. (2007). "Gaucher disease: forging a new path to the lysosome." Cell **131**(4): 647-649.
- Gu, X., B. Trigatti, S. Xu, S. Acton, J. Babitt and M. Krieger (1998). "The efficient cellular uptake of high density lipoprotein lipids via scavenger receptor class B type I requires not only receptor-mediated surface binding but also receptor-specific lipid transfer mediated by its extracellular domain." J Biol Chem **273**(41): 26338-26348.
- Haberkant, P. and J. C. Holthuis (2014). "Fat & fabulous: bifunctional lipids in the spotlight." Biochim Biophys Acta **1841**(8): 1022-1030.
- Han, H., P. H. Weinreb and P. T. Lansbury, Jr. (1995). "The core Alzheimer's peptide NAC forms amyloid fibrils which seed and are seeded by beta-amyloid: is NAC a common trigger or target in neurodegenerative disease?" Chem Biol **2**(3): 163-169.
- Hara, T., K. Nakamura, M. Matsui, A. Yamamoto, Y. Nakahara, R. Suzuki-Migishima, M. Yokoyama, K. Mishima, I. Saito, H. Okano and N. Mizushima (2006). "Suppression of basal autophagy in neural cells causes neurodegenerative disease in mice." Nature **441**(7095): 885-889.
- He, G. S., M. E. Grace and G. A. Grabowski (1992). "Gaucher disease: four rare alleles encoding F213I, P289L, T323I, and R463C in type 1 variants." Hum Mutat **1**(5): 423-427.
- Hirsch, E. C., S. Hunot and A. Hartmann (2005). "Neuroinflammatory processes in Parkinson's disease." Parkinsonism Relat Disord **11 Suppl 1**: S9-S15.
- Hla, T. and A. J. Dannenberg (2012). "Sphingolipid signaling in metabolic disorders." Cell Metab **16**(4): 420-434.
- Hodanova, K., M. Hrebicek, M. Cervenkova, L. Mrazova, L. Veprekova and J. Zemen (1999). "Analysis of the beta-glucocerebrosidase gene in Czech and Slovak Gaucher patients: mutation profile and description of six novel mutant alleles." Blood Cells Mol Dis **25**(5-6): 287-298.
- Honing, S., I. V. Sandoval and K. von Figura (1998). "A di-leucine-based motif in the cytoplasmic tail of LIMP-II and tyrosinase mediates selective binding of AP-3." EMBO J **17**(5): 1304-1314.

- Hopfner, F., B. Schormair, F. Knauf, A. Berthele, T. R. Tolle, R. Baron, C. Maier, R. D. Treede, A. Binder, C. Sommer, C. Maihofner, W. Kunz, F. Zimprich, U. Heemann, A. Pfeufer, M. Nabauer, S. Kaab, B. Nowak, C. Gieger, P. Lichtner, C. Trenkwalder, K. Oexle and J. Winkelmann (2011). "Novel SCARB2 mutation in action myoclonus-renal failure syndrome and evaluation of SCARB2 mutations in isolated AMRF features." BMC.Neurol. **11**: 134.
- Hopfner, F., E. C. Schulte, B. Mollenhauer, B. Bereznoi, F. Knauf, P. Lichtner, A. Zimprich, D. Haubenberger, W. Pirker, T. Brucke, A. Peters, C. Gieger, G. Kuhlenbaumer, C. Trenkwalder and J. Winkelmann (2013). "The role of SCARB2 as susceptibility factor in Parkinson's disease." Mov Disord **28**(4): 538-540.
- Horowitz, M. and A. Zimran (1994). "Mutations causing Gaucher disease." Hum Mutat **3**(1): 1-11.
- Horst, M., E. C. Knecht and P. V. Schu (1999). "Import into and degradation of cytosolic proteins by isolated yeast vacuoles." Mol Biol Cell **10**(9): 2879-2889.
- Hruska, K. S., O. Goker-Alpan and E. Sidransky (2006). "Gaucher disease and the synucleinopathies." J Biomed Biotechnol **2006**(3): 78549.
- Hruska, K. S., M. E. LaMarca, C. R. Scott and E. Sidransky (2008). "Gaucher disease: mutation and polymorphism spectrum in the glucocerebrosidase gene (GBA)." Hum Mutat **29**(5): 567-583.
- Ikonen, E. (2006). "Mechanisms for cellular cholesterol transport: defects and human disease." Physiol Rev **86**(4): 1237-1261.
- Ikonen, E. (2008). "Cellular cholesterol trafficking and compartmentalization." Nat Rev Mol Cell Biol **9**(2): 125-138.
- Infante, R. E., A. Radhakrishnan, L. Abi-Mosleh, L. N. Kinch, M. L. Wang, N. V. Grishin, J. L. Goldstein and M. S. Brown (2008). "Purified NPC1 protein: II. Localization of sterol binding to a 240-amino acid soluble luminal loop." J Biol Chem **283**(2): 1064-1075.
- Janvier, K. and J. S. Bonifacino (2005). "Role of the endocytic machinery in the sorting of lysosome-associated membrane proteins." Mol Biol Cell **16**(9): 4231-4242.
- Janvier, K., Y. Kato, M. Boehm, J. R. Rose, J. A. Martina, B. Y. Kim, S. Venkatesan and J. S. Bonifacino (2003). "Recognition of dileucine-based sorting signals from HIV-1 Nef and LIMP-II by the AP-1 gamma-sigma1 and AP-3 delta-sigma3 hemicomplexes." J Cell Biol **163**(6): 1281-1290.
- Jayapal, K. R., K. F. Wlaschin, W. S. Hu and M. G. S. Yap (2007). "Recombinant protein therapeutics from CHO cells - 20 years and counting." Chemical Engineering Progress **103**(10): 40-47.
- Jovic, M., M. J. Kean, Z. Szentpetery, G. Polevoy, A. C. Gingras, J. A. Brill and T. Balla (2012). "Two phosphatidylinositol 4-kinases control lysosomal delivery of the Gaucher disease enzyme, beta-glucocerebrosidase." Mol Biol Cell **23**(8): 1533-1545.
- Kamp, F., N. Exner, A. K. Lutz, N. Wender, J. Hegermann, B. Brunner, B. Nuscher, T. Bartels, A. Giese, K. Beyer, S. Eimer, K. F. Winklhofer and C. Haass (2010). "Inhibition of mitochondrial fusion by alpha-synuclein is rescued by PINK1, Parkin and DJ-1." EMBO J **29**(20): 3571-3589.
- Karpinar, D. P., M. B. Balija, S. Kugler, F. Opazo, N. Rezaei-Ghaleh, N. Wender, H. Y. Kim, G. Taschenberger, B. H. Falkenburger, H. Heise, A. Kumar, D. Riedel, L. Fichtner, A. Voigt, G. H. Braus, K. Giller, S. Becker, A. Herzig, M. Baldus, H. Jackle, S. Eimer, J. B. Schulz, C. Griesinger and M. Zweckstetter (2009). "Pre-fibrillar alpha-synuclein variants with impaired beta-structure increase neurotoxicity in Parkinson's disease models." EMBO J **28**(20): 3256-3268.
- Katzenstein, I. P., A. M. Spielvogel and A. W. Norman (1974). "Stoichiometry of interaction of the polyene antibiotic, filipin, with free and liposomal-bound cholesterol." J Antibiot (Tokyo) **27**(12): 943-951.
- Kawame, H. and Y. Eto (1991). "A new glucocerebrosidase-gene missense mutation responsible for neuronopathic Gaucher disease in Japanese patients." Am J Hum Genet **49**(6): 1378-1380.

- Ketcham, C. M. and S. Kornfeld (1992). "Characterization of UDP-N-acetylglucosamine:glycoprotein N-acetylglucosamine-1-phosphotransferase from *Acanthamoeba castellanii*." J Biol Chem **267**(16): 11654-11659.
- Kim, J. W., B. B. Liou, M. Y. Lai, E. Ponce and G. A. Grabowski (1996). "Gaucher disease: identification of three new mutations in the Korean and Chinese (Taiwanese) populations." Hum Mutat **7**(3): 214-218.
- Kitada, T., S. Asakawa, N. Hattori, H. Matsumine, Y. Yamamura, S. Minoshima, M. Yokochi, Y. Mizuno and N. Shimizu (1998). "Mutations in the parkin gene cause autosomal recessive juvenile parkinsonism." Nature **392**(6676): 605-608.
- Kollmann, K., M. Damme, S. Markmann, W. Morelle, M. Schweizer, I. Hermans-Borgmeyer, A. K. Rochert, S. Pohl, T. Lubke, J. C. Michalski, R. Kakela, S. U. Walkley and T. Braulke (2012). "Lysosomal dysfunction causes neurodegeneration in mucopolipidosis II 'knock-in' mice." Brain **135**(Pt 9): 2661-2675.
- Komatsu, M., S. Waguri, T. Chiba, S. Murata, J. Iwata, I. Tanida, T. Ueno, M. Koike, Y. Uchiyama, E. Kominami and K. Tanaka (2006). "Loss of autophagy in the central nervous system causes neurodegeneration in mice." Nature **441**(7095): 880-884.
- Kornfeld, R., M. Bao, K. Brewer, C. Noll and W. Canfield (1999). "Molecular cloning and functional expression of two splice forms of human N-acetylglucosamine-1-phosphodiester alpha-N-acetylglucosaminidase." J Biol Chem **274**(46): 32778-32785.
- Kornfeld, R. and S. Kornfeld (1985). "Assembly of asparagine-linked oligosaccharides." Annu Rev Biochem **54**: 631-664.
- Kornfeld, S. (1992). "Structure and function of the mannose 6-phosphate/insulinlike growth factor II receptors." Annu.Rev.Biochem. **61**: 307-330.
- Kornfeld, S. and I. Mellman (1989). "The biogenesis of lysosomes." Annu.Rev.Cell Biol. **5**: 483-525.
- Kornhaber, G. J., M. B. Tropak, G. H. Maegawa, S. J. Tuske, S. J. Coales, D. J. Mahuran and Y. Hamuro (2008). "Isogagamine induced stabilization of glucocerebrosidase." Chembiochem **9**(16): 2643-2649.
- Korschen, H. G., Y. Yildiz, D. N. Raju, S. Schonauer, W. Bonigk, V. Jansen, E. Kremmer, U. B. Kaupp and D. Wachten (2013). "The non-lysosomal beta-glucosidase GBA2 is a non-integral membrane-associated protein at the endoplasmic reticulum (ER) and Golgi." J Biol Chem **288**(5): 3381-3393.
- Kriks, S., J. W. Shim, J. Piao, Y. M. Ganat, D. R. Wakeman, Z. Xie, L. Carrillo-Reid, G. Auyeung, C. Antonacci, A. Buch, L. Yang, M. F. Beal, D. J. Surmeier, J. H. Kordower, V. Tabar and L. Studer (2011). "Dopamine neurons derived from human ES cells efficiently engraft in animal models of Parkinson's disease." Nature **480**(7378): 547-551.
- Kuronita, T., E. L. Eskelinen, H. Fujita, P. Saftig, M. Himeno and Y. Tanaka (2002). "A role for the lysosomal membrane protein LGP85 in the biogenesis and maintenance of endosomal and lysosomal morphology." J.Cell Sci. **115**(Pt 21): 4117-4131.
- Kuronita, T., T. Hatano, A. Furuyama, Y. Hirota, N. Masuyama, P. Saftig, M. Himeno, H. Fujita and Y. Tanaka (2005). "The NH(2)-terminal transmembrane and luminal domains of LGP85 are needed for the formation of enlarged endosomes/lysosomes." Traffic. **6**(10): 895-906.
- Lashuel, H. A. and P. T. Lansbury, Jr. (2006). "Are amyloid diseases caused by protein aggregates that mimic bacterial pore-forming toxins?" Q Rev Biophys **39**(2): 167-201.
- Lashuel, H. A., B. M. Pette, J. Wall, M. Simon, R. J. Nowak, T. Walz and P. T. Lansbury, Jr. (2002). "Alpha-synuclein, especially the Parkinson's disease-associated mutants, forms pore-like annular and tubular protofibrils." J Mol Biol **322**(5): 1089-1102.
- Lazzarino, D. A. and C. A. Gabel (1988). "Biosynthesis of the mannose 6-phosphate recognition marker in transport-impaired mouse lymphoma cells. Demonstration of a two-step phosphorylation." J Biol Chem **263**(21): 10118-10126.

- Lefrancois, S., J. Zeng, A. J. Hassan, M. Canuel and C. R. Morales (2003). "The lysosomal trafficking of sphingolipid activator proteins (SAPs) is mediated by sortilin." *EMBO J* **22**(24): 6430-6437.
- Leroy, E., R. Boyer, G. Auburger, B. Leube, G. Ulm, E. Mezey, G. Harta, M. J. Brownstein, S. Jonnalagada, T. Chernova, A. Dehejia, C. Lavedan, T. Gasser, P. J. Steinbach, K. D. Wilkinson and M. H. Polymeropoulos (1998). "The ubiquitin pathway in Parkinson's disease." *Nature* **395**(6701): 451-452.
- Lesage, S., M. Anheim, C. Condroyer, P. Pollak, F. Durif, C. Dupuits, F. Viallet, E. Lohmann, J. C. Corvol, A. Honore, S. Rivaud, M. Vidailhet, A. Durr, A. Brice and G. French Parkinson's Disease Genetics Study (2011). "Large-scale screening of the Gaucher's disease-related glucocerebrosidase gene in Europeans with Parkinson's disease." *Hum Mol Genet* **20**(1): 202-210.
- Lieberman, R. L. (2011). "A Guided Tour of the Structural Biology of Gaucher Disease: Acid-beta-Glucosidase and Saposin C." *Enzyme Res* **2011**: 973231.
- Lieberman, R. L., B. A. Wustman, P. Huertas, A. C. Powe, Jr., C. W. Pine, R. Khanna, M. G. Schlossmacher, D. Ringe and G. A. Petsko (2007). "Structure of acid beta-glucosidase with pharmacological chaperone provides insight into Gaucher disease." *Nat Chem Biol* **3**(2): 101-107.
- Lim, Y., V. M. Kehm, E. B. Lee, J. H. Soper, C. Li, J. Q. Trojanowski and V. M. Lee (2011). "alpha-Syn suppression reverses synaptic and memory defects in a mouse model of dementia with Lewy bodies." *J Neurosci* **31**(27): 10076-10087.
- Liou, B., W. D. Haffey, K. D. Greis and G. A. Grabowski (2014). "The LIMP-2/SCARB2 Binding Motif on Acid beta-Glucosidase: BASIC AND APPLIED IMPLICATIONS FOR GAUCHER DISEASE AND ASSOCIATED NEURODEGENERATIVE DISEASES." *J Biol Chem* **289**(43): 30063-30074.
- Liou, B., A. Kazimierczuk, M. Zhang, C. R. Scott, R. S. Hegde and G. A. Grabowski (2006). "Analyses of variant acid beta-glucosidases: effects of Gaucher disease mutations." *J Biol Chem* **281**(7): 4242-4253.
- Liscum, L. and J. R. Faust (1989). "The intracellular transport of low density lipoprotein-derived cholesterol is inhibited in Chinese hamster ovary cells cultured with 3-beta-[2-(diethylamino)ethoxy]androst-5-en-17-one." *J Biol Chem* **264**(20): 11796-11806.
- Liu, B. and M. Krieger (2002). "Highly purified scavenger receptor class B, type I reconstituted into phosphatidylcholine/cholesterol liposomes mediates high affinity high density lipoprotein binding and selective lipid uptake." *J Biol Chem* **277**(37): 34125-34135.
- Ludwig, T., B. R. Le and B. Hoflack (1995). "Roles for mannose-6-phosphate receptors in lysosomal enzyme sorting, IGF-II binding and clathrin-coat assembly." *Trends Cell Biol* **5**(5): 202-206.
- Lwin, A., E. Orvisky, O. Goker-Alpan, M. E. LaMarca and E. Sidransky (2004). "Glucocerebrosidase mutations in subjects with parkinsonism." *Mol Genet Metab* **81**(1): 70-73.
- Mak, S. K., A. L. McCormack, A. B. Manning-Bog, A. M. Cuervo and D. A. Di Monte (2010). "Lysosomal degradation of alpha-synuclein in vivo." *J Biol Chem* **285**(18): 13621-13629.
- Makrypidi, G., M. Damme, S. Muller-Loennies, M. Trusch, B. Schmidt, H. Schluter, J. Heeren, T. Lubke, P. Saftig and T. Braulke (2012). "Mannose 6 dephosphorylation of lysosomal proteins mediated by acid phosphatases Acp2 and Acp5." *Mol Cell Biol* **32**(4): 774-782.
- Malini, E., S. Grossi, M. Deganuto, C. Rosano, R. Parini, S. Dominisini, R. Cariati, S. Zampieri, B. Bembi, M. Filocamo and A. Dardis (2014). "Functional analysis of 11 novel GBA alleles." *Eur J Hum Genet* **22**(4): 511-516.
- Maniwang, E., N. Tayebi and E. Sidransky (2013). "Is Parkinson disease associated with lysosomal integral membrane protein type-2?: challenges in interpreting association data." *Mol Genet Metab* **108**(4): 269-271.
- Manning-Bog, A. B., B. Schule and J. W. Langston (2009). "Alpha-synuclein-glucocerebrosidase interactions in pharmacological Gaucher models: a biological link between Gaucher disease and parkinsonism." *Neurotoxicology* **30**(6): 1127-1132.

- Markmann, S., M. Thelen, K. Cornils, M. Schweizer, N. Brocke-Ahmadinejad, T. Willnow, J. Heeren, V. Gieselmann, T. Braulke and K. Kollmann (2015). "Lrp1/LDL Receptor Play Critical Roles in Mannose 6-Phosphate-Independent Lysosomal Enzyme Targeting." *Traffic* **16**(7): 743-759.
- Matern, H., H. Boermans, F. Lottspeich and S. Matern (2001). "Molecular cloning and expression of human bile acid beta-glucosidase." *J Biol Chem* **276**(41): 37929-37933.
- Mazella, J., N. Zsuzsger, V. Navarro, J. Chabry, M. Kaghad, D. Caput, P. Ferrara, N. Vita, D. Gully, J. P. Maffrand and J. P. Vincent (1998). "The 100-kDa neurotensin receptor is gp95/sortilin, a non-G-protein-coupled receptor." *J Biol Chem* **273**(41): 26273-26276.
- Mazzulli, J. R., Y. H. Xu, Y. Sun, A. L. Knight, P. J. McLean, G. A. Caldwell, E. Sidransky, G. A. Grabowski and D. Krainc (2011). "Gaucher disease glucocerebrosidase and alpha-synuclein form a bidirectional pathogenic loop in synucleinopathies." *Cell* **146**(1): 37-52.
- McArthur, M. J., B. P. Atshaves, A. Frolov, W. D. Foxworth, A. B. Kier and F. Schroeder (1999). "Cellular uptake and intracellular trafficking of long chain fatty acids." *J Lipid Res* **40**(8): 1371-1383.
- McNeill, A., R. Duran, D. A. Hughes, A. Mehta and A. H. Schapira (2012). "A clinical and family history study of Parkinson's disease in heterozygous glucocerebrosidase mutation carriers." *J Neurol Neurosurg Psychiatry* **83**(8): 853-854.
- Miao, S., J. D. McCarter, M. E. Grace, G. A. Grabowski, R. Aebersold and S. G. Withers (1994). "Identification of Glu340 as the active-site nucleophile in human glucocerebrosidase by use of electrospray tandem mass spectrometry." *J Biol Chem* **269**(15): 10975-10978.
- Montfort, M., A. Chabas, L. Vilageliu and D. Grinberg (2004). "Functional analysis of 13 GBA mutant alleles identified in Gaucher disease patients: Pathogenic changes and "modifier" polymorphisms." *Hum Mutat* **23**(6): 567-575.
- Mu, T. W., D. S. Ong, Y. J. Wang, W. E. Balch, J. R. Yates, 3rd, L. Segatori and J. W. Kelly (2008). "Chemical and biological approaches synergize to ameliorate protein-folding diseases." *Cell* **134**(5): 769-781.
- Mueller, O. T. and A. Rosenberg (1979). "Activation of membrane-bound glucosylceramide: beta-glucosidase in fibroblasts cultured from normal and glucosylceramidotic human skin." *J Biol Chem* **254**(9): 3521-3525.
- Murphy, K. E., A. M. Gysbers, S. K. Abbott, N. Tayebi, W. S. Kim, E. Sidransky, A. Cooper, B. Garner and G. M. Halliday (2014). "Reduced glucocerebrosidase is associated with increased alpha-synuclein in sporadic Parkinson's disease." *Brain* **137**(Pt 3): 834-848.
- Nakamura, K., V. M. Nemani, F. Azarbal, G. Skibinski, J. M. Levy, K. Egami, L. Munishkina, J. Zhang, B. Gardner, J. Wakabayashi, H. Sesaki, Y. Cheng, S. Finkbeiner, R. L. Nussbaum, E. Masliah and R. H. Edwards (2011). "Direct membrane association drives mitochondrial fission by the Parkinson disease-associated protein alpha-synuclein." *J Biol Chem* **286**(23): 20710-20726.
- Nakata, T., N. Nakahara, K. Sohmiya, F. Okamoto, T. Tanaka, K. Kawamura and K. Shimamoto (1999). "Scintigraphic evidence for a specific long-chain fatty acid transporting system deficit and the genetic background in a patient with hypertrophic cardiomyopathy." *Jpn Circ J* **63**(4): 319-322.
- Neculai, D., M. Schwake, M. Ravichandran, F. Zunke, R. F. Collins, J. Peters, M. Neculai, J. Plumb, P. Loppnau, J. C. Pizarro, A. Seitova, W. S. Trimble, P. Saftig, S. Grinstein and S. Dhe-Paganon (2013). "Structure of LIMP-2 provides functional insights with implications for SR-BI and CD36." *Nature* **504**(7478): 172-176.
- Nielsen, M. S., C. Jacobsen, G. Olivecrona, J. Gliemann and C. M. Petersen (1999). "Sortilin/neurotensin receptor-3 binds and mediates degradation of lipoprotein lipase." *J Biol Chem* **274**(13): 8832-8836.
- Nilsson, O. and L. Svennerholm (1982). "Accumulation of glucosylceramide and glucosylsphingosine (psychosine) in cerebrum and cerebellum in infantile and juvenile Gaucher disease." *J Neurochem* **39**(3): 709-718.
- Nixon, R. A. (2013). "The role of autophagy in neurodegenerative disease." *Nat Med* **19**(8): 983-997.

- Nozaki, S., T. Tanaka, S. Yamashita, K. Sohmiya, T. Yoshizumi, F. Okamoto, Y. Kitaura, C. Kotake, H. Nishida, A. Nakata, T. Nakagawa, K. Matsumoto, K. Kameda-Takemura, S. Tadokoro, Y. Kurata, Y. Tomiyama, K. Kawamura and Y. Matsuzawa (1999). "CD36 mediates long-chain fatty acid transport in human myocardium: complete myocardial accumulation defect of radiolabeled long-chain fatty acid analog in subjects with CD36 deficiency." Mol Cell Biochem **192**(1-2): 129-135.
- Ohkuma, S., Y. Moriyama and T. Takano (1982). "Identification and characterization of a proton pump on lysosomes by fluorescein-isothiocyanate-dextran fluorescence." Proc Natl Acad Sci U S A **79**(9): 2758-2762.
- Orengo, C. A., A. D. Michie, S. Jones, D. T. Jones, M. B. Swindells and J. M. Thornton (1997). "CATH--a hierarchic classification of protein domain structures." Structure **5**(8): 1093-1108.
- Osellame, L. D., A. A. Rahim, I. P. Hargreaves, M. E. Gegg, A. Richard-Londt, S. Brandner, S. N. Waddington, A. H. Schapira and M. R. Duhen (2013). "Mitochondria and quality control defects in a mouse model of Gaucher disease--links to Parkinson's disease." Cell Metab **17**(6): 941-953.
- Osiecki-Newman, K., D. Fabbro, G. Legler, R. J. Desnick and G. A. Grabowski (1987). "Human acid beta-glucosidase: use of inhibitors, alternative substrates and amphiphiles to investigate the properties of the normal and Gaucher disease active sites." Biochim Biophys Acta **915**(1): 87-100.
- Park, J. K., E. Orvisky, N. Tayebi, C. Kaneski, M. E. Lamarca, B. K. Stubblefield, B. M. Martin, R. Schiffmann and E. Sidransky (2003). "Myoclonic epilepsy in Gaucher disease: genotype-phenotype insights from a rare patient subgroup." Pediatr Res **53**(3): 387-395.
- Pasmanik-Chor, M., S. Laadan, O. Elroy-Stein, A. Zimran, A. Abrahamov, S. Gatt and M. Horowitz (1996). "The glucocerebrosidase D409H mutation in Gaucher disease." Biochem Mol Med **59**(2): 125-133.
- Pastores, G. M. (1997). "Gaucher's Disease. Pathological features." Baillieres Clin Haematol **10**(4): 739-749.
- Pastores, G. M. (2010). "Velaglucerase alfa, a human recombinant glucocerebrosidase enzyme replacement therapy for type 1 Gaucher disease." Curr Opin Investig Drugs **11**(4): 472-478.
- Pastores, G. M., N. J. Weinreb, H. Aerts, G. Andria, T. M. Cox, M. Giralt, G. A. Grabowski, P. K. Mistry and A. Tytki-Szymanska (2004). "Therapeutic goals in the treatment of Gaucher disease." Semin Hematol **41**(4 Suppl 5): 4-14.
- Patterson, M. C., M. T. Vanier, K. Suzuki, J. A. Morris, E. Carsteu and E. B. Neufeld (2001). Niemann-Pick disease type C. A lipid trafficking disorder, McGraw-Hill.
- Periquet, M., T. Fulga, L. Myllykangas, M. G. Schlossmacher and M. B. Feany (2007). "Aggregated alpha-synuclein mediates dopaminergic neurotoxicity in vivo." J Neurosci **27**(12): 3338-3346.
- Perlmutter, D. H. (2002). "Chemical chaperones: a pharmacological strategy for disorders of protein folding and trafficking." Pediatr Res **52**(6): 832-836.
- Petersen, C. M., M. S. Nielsen, A. Nykjaer, L. Jacobsen, N. Tommerup, H. H. Rasmussen, H. Roigaard, J. Gliemann, P. Madsen and S. K. Moestrup (1997). "Molecular identification of a novel candidate sorting receptor purified from human brain by receptor-associated protein affinity chromatography." J Biol Chem **272**(6): 3599-3605.
- Platt, F. M., B. Boland and A. C. van der Spoel (2012). "The cell biology of disease: lysosomal storage disorders: the cellular impact of lysosomal dysfunction." J Cell Biol **199**(5): 723-734.
- Platt, F. M., G. R. Neises, R. A. Dwek and T. D. Butters (1994). "N-butyldeoxynojirimycin is a novel inhibitor of glycolipid biosynthesis." J Biol Chem **269**(11): 8362-8365.
- Polymeropoulos, M. H., C. Lavedan, E. Leroy, S. E. Ide, A. Dehejia, A. Dutra, B. Pike, H. Root, J. Rubenstein, R. Boyer, E. S. Stenroos, S. Chandrasekharappa, A. Athanassiadou, T. Papapetropoulos, W. G. Johnson, A. M. Lazzarini, R. C. Duvoisin, G. Di Iorio, L. I. Golbe and R. L. Nussbaum (1997). "Mutation in the alpha-synuclein gene identified in families with Parkinson's disease." Science **276**(5321): 2045-2047.

- Qiao, L., S. Hamamichi, K. A. Caldwell, G. A. Caldwell, T. A. Yacoubian, S. Wilson, Z. L. Xie, L. D. Speake, R. Parks, D. Crabtree, Q. Liang, S. Crimmins, L. Schneider, Y. Uchiyama, T. Iwatsubo, Y. Zhou, L. Peng, Y. Lu, D. G. Standaert, K. C. Walls, J. J. Shacka, K. A. Roth and J. Zhang (2008). "Lysosomal enzyme cathepsin D protects against alpha-synuclein aggregation and toxicity." *Mol Brain* **1**: 17.
- Reczek, D., M. Schwake, J. Schroder, H. Hughes, J. Blanz, X. Jin, W. Brondyk, P. S. Van, T. Edmunds and P. Saftig (2007). "LIMP-2 is a receptor for lysosomal mannose-6-phosphate-independent targeting of beta-glucocerebrosidase." *Cell* **131**(4): 770-783.
- Rieker, C., K. K. Dev, K. Lehnhoff, S. Barbieri, I. Ksiazek, S. Kauffmann, S. Danner, H. Schell, C. Boden, M. A. Ruegg, P. J. Kahle, H. van der Putten and D. R. Shimshek (2011). "Neuropathology in mice expressing mouse alpha-synuclein." *PLoS One* **6**(9): e24834.
- Rigotti, A., H. E. Miettinen and M. Krieger (2003). "The role of the high-density lipoprotein receptor SR-BI in the lipid metabolism of endocrine and other tissues." *Endocr Rev* **24**(3): 357-387.
- Rijnboutt, S., H. M. Aerts, H. J. Geuze, J. M. Tager and G. J. Strous (1991). "Mannose 6-phosphate-independent membrane association of cathepsin D, glucocerebrosidase, and sphingolipid-activating protein in HepG2 cells." *J Biol Chem* **266**(8): 4862-4868.
- Rijnboutt, S., A. J. Kal, H. J. Geuze, H. Aerts and G. J. Strous (1991). "Mannose 6-phosphate-independent targeting of cathepsin D to lysosomes in HepG2 cells." *J Biol Chem* **266**(35): 23586-23592.
- Roces, D. P., R. Lullmann-Rauch, J. Peng, C. Balducci, C. Andersson, O. Tollersrud, J. Fogh, A. Orlacchio, T. Beccari, P. Saftig and K. von Figura (2004). "Efficacy of enzyme replacement therapy in alpha-mannosidosis mice: a preclinical animal study." *Hum Mol Genet* **13**(18): 1979-1988.
- Rocha, E. M., G. A. Smith, E. Park, H. Cao, E. Brown, P. Hallett and O. Isacson (2015). "Progressive decline of glucocerebrosidase in aging and Parkinson's disease." *Ann Clin Transl Neurol* **2**(4): 433-438.
- Rodriguez-Lafresse, C., R. Rousson, P. G. Pentchev, P. Louisot and M. T. Vanier (1994). "Free sphingoid bases in tissues from patients with type C Niemann-Pick disease and other lysosomal storage disorders." *Biochim Biophys Acta* **1226**(2): 138-144.
- Rodrigueza, W. V., S. T. Thuahnai, R. E. Temel, S. Lund-Katz, M. C. Phillips and D. L. Williams (1999). "Mechanism of scavenger receptor class B type I-mediated selective uptake of cholesteryl esters from high density lipoprotein to adrenal cells." *J Biol Chem* **274**(29): 20344-20350.
- Rohrbach, M. and J. T. Clarke (2007). "Treatment of lysosomal storage disorders : progress with enzyme replacement therapy." *Drugs* **67**(18): 2697-2716.
- Ron, I. and M. Horowitz (2005). "ER retention and degradation as the molecular basis underlying Gaucher disease heterogeneity." *Hum Mol Genet* **14**(16): 2387-2398.
- Rothaug, M., F. Zunke, J. R. Mazzulli, M. Schweizer, H. Altmeppen, R. Lullmann-Rauch, W. W. Kallemeijn, P. Gaspar, J. M. Aerts, M. Glatzel, P. Saftig, D. Krainc, M. Schwake and J. Blanz (2014). "LIMP-2 expression is critical for beta-glucocerebrosidase activity and alpha-synuclein clearance." *Proc Natl Acad Sci U S A* **111**(43): 15573-15578.
- Rubboli, G., S. Franceschetti, S. F. Berkovic, L. Canafoglia, A. Gambardella, L. M. Dibbens, P. Riguzzi, C. Campieri, A. Magaudo, C. A. Tassinari and R. Michelucci (2011). "Clinical and neurophysiologic features of progressive myoclonus epilepsy without renal failure caused by SCARB2 mutations." *Epilepsia* **52**(12): 2356-2363.
- S. Kornfeld, W. S. S. (2001). I-cell disease and pseudo-Hurler polydystrophy: disorders of lysosomal enzyme phosphorylation and localization, . New York, McGraw-Hill.
- Saftig, P. and J. Klumperman (2009). "Lysosome biogenesis and lysosomal membrane proteins: trafficking meets function." *Nat.Rev.Mol.Cell Biol.* **10**(9): 623-635.

- Sands, M. S. and B. L. Davidson (2006). "Gene therapy for lysosomal storage diseases." *Mol Ther* **13**(5): 839-849.
- Santamaria, I., G. Velasco, A. M. Pendas, A. Fueyo and C. Lopez-Otin (1998). "Cathepsin Z, a novel human cysteine proteinase with a short propeptide domain and a unique chromosomal location." *J Biol Chem* **273**(27): 16816-16823.
- Sardi, S. P., J. Clarke, C. Kinnecom, T. J. Tamsett, L. Li, L. M. Stanek, M. A. Passini, G. A. Grabowski, M. G. Schlossmacher, R. L. Sidman, S. H. Cheng and L. S. Shihabuddin (2011). "CNS expression of glucocerebrosidase corrects alpha-synuclein pathology and memory in a mouse model of Gaucher-related synucleinopathy." *Proc Natl Acad Sci U S A* **108**(29): 12101-12106.
- Sardi, S. P., J. Clarke, C. Viel, M. Chan, T. J. Tamsett, C. M. Treleaven, J. Bu, L. Sweet, M. A. Passini, J. C. Dodge, W. H. Yu, R. L. Sidman, S. H. Cheng and L. S. Shihabuddin (2013). "Augmenting CNS glucocerebrosidase activity as a therapeutic strategy for parkinsonism and other Gaucher-related synucleinopathies." *Proc Natl Acad Sci U S A* **110**(9): 3537-3542.
- Sawkar, A. R., W. D'Haese and J. W. Kelly (2006). "Therapeutic strategies to ameliorate lysosomal storage disorders--a focus on Gaucher disease." *Cell Mol Life Sci* **63**(10): 1179-1192.
- Schapira, A. H., E. Bezdard, J. Brotchie, F. Calon, G. L. Collingridge, B. Ferger, B. Hengerer, E. Hirsch, P. Jenner, N. Le Novere, J. A. Obeso, M. A. Schwarzschild, U. Spampinato and G. Davidai (2006). "Novel pharmacological targets for the treatment of Parkinson's disease." *Nat Rev Drug Discov* **5**(10): 845-854.
- Schneede, A., C. K. Schmidt, M. Holtta-Vuori, J. Heeren, M. Willenborg, J. Blanz, M. Domansky, B. Breiden, S. Brodessa, J. Landgrebe, K. Sandhoff, E. Ikonen, P. Saftig and E. L. Eskelinen (2011). "Role for LAMP-2 in endosomal cholesterol transport." *J Cell Mol Med* **15**(2): 280-295.
- Schueler, U. H., T. Kolter, C. R. Kaneski, J. K. Blusztajn, M. Herkenham, K. Sandhoff and R. O. Brady (2003). "Toxicity of glucosylsphingosine (glucopsychosine) to cultured neuronal cells: a model system for assessing neuronal damage in Gaucher disease type 2 and 3." *Neurobiol Dis* **14**(3): 595-601.
- Schulze, H. and K. Sandhoff (2011). "Lysosomal lipid storage diseases." *Cold Spring Harb Perspect Biol* **3**(6).
- Schwake, M., B. Schroder and P. Saftig (2013). "Lysosomal membrane proteins and their central role in physiology." *Traffic* **14**(7): 739-748.
- Settembre, C., A. Fraldi, D. L. Medina and A. Ballabio (2013). "Signals from the lysosome: a control centre for cellular clearance and energy metabolism." *Nat Rev Mol Cell Biol* **14**(5): 283-296.
- Shaalit, Y., D. Bartfeld, S. Hashmueli, G. Baum, E. Brill-Almon, G. Galili, O. Dym, S. A. Boldin-Adamsky, I. Silman, J. L. Sussman, A. H. Futerman and D. Aviezer (2007). "Production of glucocerebrosidase with terminal mannose glycans for enzyme replacement therapy of Gaucher's disease using a plant cell system." *Plant Biotechnol J* **5**(5): 579-590.
- Shen, J. S., N. J. Edwards, Y. B. Hong and G. J. Murray (2008). "Isfagomine increases lysosomal delivery of exogenous glucocerebrosidase." *Biochem Biophys Res Commun* **369**(4): 1071-1075.
- Shimura, H., M. G. Schlossmacher, N. Hattori, M. P. Frosch, A. Trockenbacher, R. Schneider, Y. Mizuno, K. S. Kosik and D. J. Selkoe (2001). "Ubiquitination of a new form of alpha-synuclein by parkin from human brain: implications for Parkinson's disease." *Science* **293**(5528): 263-269.
- Sidransky, E., M. E. LaMarca and E. I. Ginns (2007). "Therapy for Gaucher disease: don't stop thinking about tomorrow." *Mol Genet Metab* **90**(2): 122-125.
- Sidransky, E., M. A. Nalls, J. O. Aasly, J. Aharon-Peretz, G. Annesi, E. R. Barbosa, A. Bar-Shira, D. Berg, J. Bras, A. Brice, C. M. Chen, L. N. Clark, C. Condroyer, E. V. De Marco, A. Durr, M. J. Eblan, S. Fahn, M. J. Farrer, H. C. Fung, Z. Gan-Or, T. Gasser, R. Gershoni-Baruch, N. Giladi, A. Griffith, T. Gurevich, C. Januario, P. Kropp, A. E. Lang, G. J. Lee-Chen, S. Lesage, K. Marder, I. F. Mata, A. Mirelman, J. Mitsui, I. Mizuta, G. Nicoletti, C. Oliveira, R. Ottman, A. Orr-Urtreger, L. V. Pereira, A. Quattrone, E. Rogava, A. Rolfs, H. Rosenbaum, R. Rozenberg, A. Samii, T. Samaddar, C. Schulte, M. Sharma, A. Singleton, M. Spitz, E. K. Tan, N.

- Tayebi, T. Toda, A. R. Troiano, S. Tsuji, M. Wittstock, T. G. Wolfsberg, Y. R. Wu, C. P. Zabetian, Y. Zhao and S. G. Ziegler (2009). "Multicenter analysis of glucocerebrosidase mutations in Parkinson's disease." N Engl J Med **361**(17): 1651-1661.
- Sidransky, E., D. M. Sherer and E. I. Ginns (1992). "Gaucher disease in the neonate: a distinct Gaucher phenotype is analogous to a mouse model created by targeted disruption of the glucocerebrosidase gene." Pediatr Res **32**(4): 494-498.
- Sidransky, E., N. Tayebi, B. K. Stubblefield, W. Eliason, A. Klineburgess, G. P. Pizzolato, J. N. Cox, J. Porta, A. Bottani and C. D. DeLozier-Blanchet (1996). "The clinical, molecular, and pathological characterisation of a family with two cases of lethal perinatal type 2 Gaucher disease." J Med Genet **33**(2): 132-136.
- Sillence, D. J. and F. M. Platt (2004). "Glycosphingolipids in endocytic membrane transport." Semin Cell Dev Biol **15**(4): 409-416.
- Sly, W. S., A. Kaplan, D. T. Achord, F. E. Brot and C. E. Bell (1978). "Receptor-mediated uptake of lysosomal enzymes." Prog Clin Biol Res **23**: 547-551.
- Specht, C. G. and R. Schoepfer (2001). "Deletion of the alpha-synuclein locus in a subpopulation of C57BL/6J inbred mice." BMC Neurosci **2**: 11.
- Spohn, M. and A. N. Davison (1972). "Cholesterol metabolism in myelin and other subcellular fractions of rat brain." J Lipid Res **13**(5): 563-570.
- Stahl, P. D., J. S. Rodman, M. J. Miller and P. H. Schlesinger (1978). "Evidence for receptor-mediated binding of glycoproteins, glycoconjugates, and lysosomal glycosidases by alveolar macrophages." Proc Natl Acad Sci U S A **75**(3): 1399-1403.
- Starzyk, K., S. Richards, J. Yee, S. E. Smith and W. Kingma (2007). "The long-term international safety experience of imiglucerase therapy for Gaucher disease." Mol Genet Metab **90**(2): 157-163.
- Storch, J. and S. Cheruku (2005). Lysosomes. Landes Bioscience/Eurekah.com.
- Tajima, A., T. Ohashi, S. Hamano, N. Higurashi and H. Ida (2010). "Gaucher disease patient with myoclonus epilepsia and a novel mutation." Pediatr Neurol **42**(1): 65-68.
- Tangemo, C., D. Weber, S. Theiss, E. Mengel and H. Runz (2011). "Niemann-Pick Type C disease: characterizing lipid levels in patients with variant lysosomal cholesterol storage." J Lipid Res **52**(4): 813-825.
- Thayanidhi, N., J. R. Helm, D. C. Nycz, M. Bentley, Y. Liang and J. C. Hay (2010). "Alpha-synuclein delays endoplasmic reticulum (ER)-to-Golgi transport in mammalian cells by antagonizing ER/Golgi SNAREs." Mol Biol Cell **21**(11): 1850-1863.
- Tiede, S., S. Storch, T. Lubke, B. Henrissat, R. Bargal, A. Raas-Rothschild and T. Bräulke (2005). "Mucopolipidosis II is caused by mutations in GNPTA encoding the alpha/beta GlcNAc-1-phosphotransferase." Nat Med **11**(10): 1109-1112.
- Tofaris, G. K., R. Layfield and M. G. Spillantini (2001). "alpha-synuclein metabolism and aggregation is linked to ubiquitin-independent degradation by the proteasome." FEBS Lett **509**(1): 22-26.
- Tsuji, A., K. Omura and Y. Suzuki (1988). "I-cell disease: evidence for a mannose 6-phosphate independent pathway for translocation of lysosomal enzymes in lymphoblastoid cells." Clin Chim Acta **176**(1): 115-121.
- Ueda, K., H. Fukushima, E. Masliah, Y. Xia, A. Iwai, M. Yoshimoto, D. A. Otero, J. Kondo, Y. Ihara and T. Saitoh (1993). "Molecular cloning of cDNA encoding an unrecognized component of amyloid in Alzheimer disease." Proc Natl Acad Sci U S A **90**(23): 11282-11286.
- Vaccaro, A. M., M. Tatti, F. Ciaffoni, R. Salvioli, A. Serafino and A. Barca (1994). "Saposin C induces pH-dependent destabilization and fusion of phosphatidylserine-containing vesicles." FEBS Lett **349**(2): 181-186.

- van Dongen, J. M., R. Willemsen, E. I. Ginns, H. J. Sips, J. M. Tager, J. A. Barranger and A. J. Reuser (1985). "The subcellular localization of soluble and membrane-bound lysosomal enzymes in I-cell fibroblasts: a comparative immunocytochemical study." Eur.J.Cell Biol. **39**(1): 179-189.
- Velayati, A., J. DePaolo, N. Gupta, J. H. Choi, N. Moaven, W. Westbroek, O. Goker-Alpan, E. Goldin, B. K. Stubblefield, E. Kolodny, N. Tayebi and E. Sidransky (2011). "A mutation in SCARB2 is a modifier in Gaucher disease." Hum Mutat **32**(11): 1232-1238.
- Verhoef, L. G., K. Lindsten, M. G. Masucci and N. P. Dantuma (2002). "Aggregate formation inhibits proteasomal degradation of polyglutamine proteins." Hum Mol Genet **11**(22): 2689-2700.
- Vielhaber, G., R. Hurwitz and K. Sandhoff (1996). "Biosynthesis, processing, and targeting of sphingolipid activator protein (SAP) precursor in cultured human fibroblasts. Mannose 6-phosphate receptor-independent endocytosis of SAP precursor." J Biol Chem **271**(50): 32438-32446.
- Vogiatzi, T., M. Xilouri, K. Vekrellis and L. Stefanis (2008). "Wild type alpha-synuclein is degraded by chaperone-mediated autophagy and macroautophagy in neuronal cells." J Biol Chem **283**(35): 23542-23556.
- Volles, M. J. and P. T. Lansbury, Jr. (2002). "Vesicle permeabilization by protofibrillar alpha-synuclein is sensitive to Parkinson's disease-linked mutations and occurs by a pore-like mechanism." Biochemistry **41**(14): 4595-4602.
- Webb, J. L., B. Ravikumar, J. Atkins, J. N. Skepper and D. C. Rubinsztein (2003). "Alpha-Synuclein is degraded by both autophagy and the proteasome." J Biol Chem **278**(27): 25009-25013.
- Weinreb, N. J. (2008). "Imiglucerase and its use for the treatment of Gaucher's disease." Expert Opin Pharmacother **9**(11): 1987-2000.
- Weinreb, N. J., J. Charrow, H. C. Andersson, P. Kaplan, E. H. Kolodny, P. Mistry, G. Pastores, B. E. Rosenbloom, C. R. Scott, R. S. Wappner and A. Zimran (2002). "Effectiveness of enzyme replacement therapy in 1028 patients with type 1 Gaucher disease after 2 to 5 years of treatment: a report from the Gaucher Registry." Am J Med **113**(2): 112-119.
- Weinreb, P. H., W. Zhen, A. W. Poon, K. A. Conway and P. T. Lansbury, Jr. (1996). "NACP, a protein implicated in Alzheimer's disease and learning, is natively unfolded." Biochemistry **35**(43): 13709-13715.
- Weissleder, R., M. Nahrendorf and M. J. Pittet (2014). "Imaging macrophages with nanoparticles." Nat Mater **13**(2): 125-138.
- Westbroek, W., A. M. Gustafson and E. Sidransky (2011). "Exploring the link between glucocerebrosidase mutations and parkinsonism." Trends Mol.Med. **17**(9): 485-493.
- Wilke, S., J. Krausze and K. Bussow (2012). "Crystal structure of the conserved domain of the DC lysosomal associated membrane protein: implications for the lysosomal glycocalyx." BMC Biol **10**: 62.
- Wilkening, G., T. Linke and K. Sandhoff (1998). "Lysosomal degradation on vesicular membrane surfaces. Enhanced glucosylceramide degradation by lysosomal anionic lipids and activators." J Biol Chem **273**(46): 30271-30278.
- Winner, B., R. Jappelli, S. K. Maji, P. A. Desplats, L. Boyer, S. Aigner, C. Hetzer, T. Loher, M. Vilar, S. Campioni, C. Tzitzilonis, A. Soragni, S. Jessberger, H. Mira, A. Consiglio, E. Pham, E. Masliah, F. H. Gage and R. Riek (2011). "In vivo demonstration that alpha-synuclein oligomers are toxic." Proc Natl Acad Sci U S A **108**(10): 4194-4199.
- Witte, M. D., W. W. Kallemeijn, J. Aten, K. Y. Li, A. Strijland, W. E. Donker-Koopman, A. M. van den Nieuwendijk, B. Bleijlevens, G. Kramer, B. I. Florea, B. Hooibrink, C. E. Hollak, R. Ottenhoff, R. G. Boot, G. A. van der Marel, H. S. Overkleeft and J. M. Aerts (2010). "Ultrasensitive in situ visualization of active glucocerebrosidase molecules." Nat.Chem.Biol. **6**(12): 907-913.
- Xia, Q., L. Liao, D. Cheng, D. M. Duong, M. Gearing, J. J. Lah, A. I. Levey and J. Peng (2008). "Proteomic identification of novel proteins associated with Lewy bodies." Front Biosci **13**: 3850-3856.

- Xilouri, M., T. Vogiatzi, K. Vekrellis and L. Stefanis (2008). "alpha-synuclein degradation by autophagic pathways: a potential key to Parkinson's disease pathogenesis." *Autophagy* **4**(7): 917-919.
- Xu, J., S. Y. Kao, F. J. Lee, W. Song, L. W. Jin and B. A. Yankner (2002). "Dopamine-dependent neurotoxicity of alpha-synuclein: a mechanism for selective neurodegeneration in Parkinson disease." *Nat Med* **8**(6): 600-606.
- Xu, Y. H., R. Reboulet, B. Quinn, J. Huelsken, D. Witte and G. A. Grabowski (2008). "Dependence of reversibility and progression of mouse neuronopathic Gaucher disease on acid beta-glucosidase residual activity levels." *Mol Genet Metab* **94**(2): 190-203.
- Xu, Y. H., Y. Sun, H. Ran, B. Quinn, D. Witte and G. A. Grabowski (2011). "Accumulation and distribution of alpha-synuclein and ubiquitin in the CNS of Gaucher disease mouse models." *Mol Genet Metab* **102**(4): 436-447.
- Yamayoshi, S. and S. Koike (2011). "Identification of a human SCARB2 region that is important for enterovirus 71 binding and infection." *J.Virol.* **85**(10): 4937-4946.
- Yamayoshi, S., Y. Yamashita, J. Li, N. Hanagata, T. Minowa, T. Takemura and S. Koike (2009). "Scavenger receptor B2 is a cellular receptor for enterovirus 71." *Nat Med* **15**(7): 798-801.
- Yap, T. L., J. M. Gruschus, A. Velayati, W. Westbroek, E. Goldin, N. Moaven, E. Sidransky and J. C. Lee (2011). "Alpha-synuclein interacts with Glucocerebrosidase providing a molecular link between Parkinson and Gaucher diseases." *J Biol Chem* **286**(32): 28080-28088.
- Yu, R. K., Y. Nakatani and M. Yanagisawa (2009). "The role of glycosphingolipid metabolism in the developing brain." *J Lipid Res* **50 Suppl**: S440-445.
- Yuasa-Kawase, M., D. Masuda, T. Yamashita, R. Kawase, H. Nakaoka, M. Inagaki, K. Nakatani, K. Tsubakio-Yamamoto, T. Ohama, A. Matsuyama, M. Nishida, M. Ishigami, T. Kawamoto, I. Komuro and S. Yamashita (2012). "Patients with CD36 deficiency are associated with enhanced atherosclerotic cardiovascular diseases." *J Atheroscler Thromb* **19**(3): 263-275.
- Zachos, C., J. Blanz, P. Saftig and M. Schwake (2012). "A critical histidine residue within LIMP-2 mediates pH sensitive binding to its ligand beta-glucocerebrosidase." *Traffic*. **13**(8): 1113-1123.
- Zervas, M., K. Dobrenis and S. U. Walkley (2001). "Neurons in Niemann-Pick disease type C accumulate gangliosides as well as unesterified cholesterol and undergo dendritic and axonal alterations." *J Neuropathol Exp Neurol* **60**(1): 49-64.
- Zhang, W., T. Wang, Z. Pei, D. S. Miller, X. Wu, M. L. Block, B. Wilson, W. Zhang, Y. Zhou, J. S. Hong and J. Zhang (2005). "Aggregated alpha-synuclein activates microglia: a process leading to disease progression in Parkinson's disease." *FASEB J* **19**(6): 533-542.
- Zhao, Y., J. Ren, S. Padilla-Parra, E. E. Fry and D. I. Stuart (2014). "Lysosome sorting of beta-glucocerebrosidase by LIMP-2 is targeted by the mannose 6-phosphate receptor." *Nat Commun* **5**: 4321.
- Zimran, A., K. Loveday, C. Fratazzi and D. Elstein (2007). "A pharmacokinetic analysis of a novel enzyme replacement therapy with Gene-Activated human glucocerebrosidase (GA-GCB) in patients with type 1 Gaucher disease." *Blood Cells Mol Dis* **39**(1): 115-118.

## 7 Appendix

### 7.1 Abbreviations

**Table 7.1: Abbreviations**

%	Percentage
-/-	Knockout
+/+	Wild-type
°C	Degree Celsius
AMRF	Action Myoclonus Renal Failure Syndrome
ANOVA	Analysis of variance
AP	Adaptor protein
Baf	Bafilomycin
BSA	bovines Serum Albumin
CBE	Conduritol B epoxide
CD	Circular dichroism
CD36	cluster of differentiation 36
CD-MPR	cation-dependent mannoe-6-phosphate receptor
Cer	Ceramide
CHO	Chinese Hamster Ovary
CI-MPR	cation-independent mannoe-6-phosphate receptor
CMA	Chaperone mediated autophagy
CNS	Central nervous system
Co-IP	Co-Immunoprecipitation
ctrl.	control
DAB	3,3'-Diaminobenzidine
ddH <sub>2</sub> O	double-distilled H <sub>2</sub> O
dKO	double knockout
DLS	Dynamic Light Scattering
DMSO	Dimethylsulfoxid
DNA	Deoxyribonucleic acid
EM	Electron micrograph
EndoH	Endoglycosidase H
ER	Endoplasmic reticulum
ERret.	Endoplasmic reticulum retention mutant
ERT	Enzyme replacement therapy
GC	β-glucocerebrosidase
GFAP	Glial fibrillary acid protein
GlcNac-1PT	N-acetylglucosamine-1-phosphotransferase
GluCer	Glucosylceramide
HPLC	High performance liquid chromatography
HRP	horseradish peroxidase
hGC	human β-glucocerebrosidase
hrs	hours
IF	Immunofluorescence
IP	Immunoprecipitation
iPSC	induced pluripotent stem cells
kDa	Kilodalton
KO	knockout
LAMAN	Lysosomal acid mannosidase (α-mannosidase)
LAMP	Lysosomal Associated Membrane Protein
LIMP	Lysosomal Integral Membrane Protein
LSD	Lysosomal storage disease
M6P	Mannose-6-Phosphate
MEF	mouse embryonic fibroblasts

MPR	Mannose-6-Phosphate Receptor
NeuN	Neuronal Nuclei: neuronal marker
nm	nanometer
norm.	normalised
NPC	Niemann-Pick Type C
NSE	Neuronal specific enolase
pacLipids	Photo-activated-and-clickable lipids
PAS	Periodic acid Schiff staining
PBS	Phosphate buffered saline
PDB	Protein data base
PDI	Protein disulfide isomerase
pH	Potential hydrogen
PME	progressive myoclonic epilepsy
PNGaseF	Peptide -N-Glycosidase F
s	second
SCARB	scavenger receptor class B
SDS	sodium dodecyl sulfate
SDS-PAGE	sodium dodecyl sulfate polyacrylamide gel electrophoresis
SNCA	$\alpha$ -synuclein gene
SR-BI	scavenger receptor class B type I
SRT	Substrate reduction therapy
TGN	Trans-Golgi-Network
TH	Tyrosine hydroxylase
Tris	Tris-(hydroxymethyl)-aminomethan
T-Sol.	Triton soluble
TUNEL	Terminal dUTP-biotin Nick End Labeling
WT	Wild-type
$\mu$ g	Mikrogramm
$\mu$ L	Mikroliter
$\mu$ M	Mikromolar

## 7.2 Equipment, chemicals, enzymes, kits and buffers

### 7.2.1 Machines

**Table 7.2: Overview of utilised machines.**

Description	Model	Company
96 well plate reader	Synergy HAT	BioTek, Bad-Friedrichshall, DE
Agarose gel imaging	Gel Jet Imager UV system	Intas, Göttingen, DE
Agarose running chamber	Sub-Cell®GT	Bio-Rad, Hercules, US
Autoclave	Tecnomara	Integra Biosciences, Fernwald, DE
Bacteria incubator	Multitron II	Infra-Hat, Sulzemoos, DE
Bench-top roller	RM5	Karl Hecht KG, Sondheim, DE
CD- spectropolarimeter	Jasco-J-720-CD	Japan Spectroscopic Company, JP
Cell culture incubator	HeraCell240	Heraeus, Hanau, DE
Chemiluminescence detection system	LAS4000	GE Healthcare, Munich, DE
Confocal laser scanning microscope	FV1000	Olympus. Hamburg, DE

DLS spectrometer	Laser-spectroscatter 201	RiNA GmbH Netwerk RNA-Technologie, Berlin DE
Electroporation device	Pulse controller gene pulser	Bio-Rad, Hercules, US
Fluorescence microscope	Axiovert 200M	Zeiss, Jena, DE
Electroporation device	Gene Pulser	Bio-Rad, Hercules, US
Heating block	Thermostat 5320	Eppendorf, Hamburg, DE
Light microscope	CKX41 & SZ61	Olympus, Hamburg, DE
Magnetic stirrer	IKAMAG RCT, REO	IKA, Staufen, DE
Micropipette	1 µl	Eppendorf, Hamburg, DE
	10 µl	Eppendorf, Hamburg, DE
	200 µl	Gilson, Limburg-Offheim, DE
	1000µl	Gilson, Limburg-Offheim, DE
PCR-Cycler	GenAmp 2400 PCR	Perkin Elmer, Rodgau-Jügesheim, DE
pH-Meter	Digital-pH-Meter 646	Krick, Langenselbold, DE
Pipette Boy	Accu-jet®Pro	Integra Bioscience, Fernwald, DE
Powerpack	Powerpack 200/300	Bio-Rad, Hercules, US
Pure water device	Milli-Q Plus	Millipore, Schwalbach, DE
SDS-Page Chamber	Mini-Protein 3- Electrophoresis system	Bio-Rad, Munich, DE
Sensitive scales	L420P	Sartorius AG, Göttingen, DE
Sterile hood	VFR1806	CLAUS DAMM A/S, Alleroed, DE
Tabletop centrifuge	EM 900	Eppendorf, Hamburg, DE
Tabletop cooling centrifuge	Fresco21	Thermo Fisher Scientific, Waltham, US
Tank blotting device	Criterion™	Bio-Rad, Hercules, US
Thermomixer	Thermomixer 5436	Eppendorf, Hamburg, DE
Tissue homogeniser	Precellys	PeqLab, Erlangen, DE
Ultracentrifuge	J2-HS	Beckman, Fullerton, US
UV-Table	Reprostar	Lamag, Berlin, DE
Vortexer	Vortex Genie	Bender & Hobein, Bruchsaal, DE
Waterbath	1083	GFL, Burgwedel, DE
Weighing scales	Kern 770	Kern & Son, Dürnwangen, DE

## 7.2.2 Consumables

**Table 7.3: Laboratory material.**

Description	Company
12-Well-Plates	Sarstedt, Nümbrecht, DE
6-Well-Plates	Sarstedt, Nümbrecht, DE
96-Well-Plates	Sarstedt, Nümbrecht, DE
96-Well-Plates (Crystallisation)	Hampton Research, Aliso Viejo, US
Coverslips	Assistent, Sondheim, DE
Cryo tubes	Sarstedt, Nümbrecht, DE
Electroporation cuvettes	Peqlab, Erlangen, DE
Filter Tips Biosphere	Sarstedt, Nümbrecht, DE
Glass beakers	Roth, Karlsruhe, DE
Gloves	Roth, Karlsruhe, DE
Graduated cylinders	Roth, Karlsruhe, DE
MicoMesh Mounts (400/50)	Jena Bioscience, Jena, DE
Needles	Becton Dickinson, Heidelberg, DE

Nitrocellulose membrane, Amersham Protran 0.2 µm NC	GE Healthcare, Munich, DE
Objectives (histology)	Marienfeld Laboratory Glassware, Lauda-Königshofen, DE
Objectives (tissue culture)	Menzel Glass GmbH & Co. KG, Braunschweig, DE
Parafilm	American National Can™, Chicago, IL, US
Pasteur pipettes	Assistant, Sondheim, DE
PCR tube strips (8x)	Sarstedt, Nümbrecht, DE
PCR tubes	Sarstedt, Nümbrecht, DE
Pipette tips	Sarstedt, Nümbrecht, DE
PVDF-membranes, Immobilon	Millipore, Schwalbach, DE
Reaction tubes	Eppendorf, Hamburg, DE
Sterile filter (0,2 µm pore size)	Sarstedt, Nümbrecht, DE
Sterile plastic tubes	Sarstedt, Nümbrecht, DE
Surgical preparation tools	FST, Heidelberg, DE
Surgical scalpel	Aesculap, Tuttlingen, DE
Syringes	Becton Dickinson, Heidelberg, DE
Tissue culture dishes	Sarstedt, Nümbrecht, DE
Transfer pipettes, 3,5 ml	Sarstedt, Nümbrecht, DE
Ultracentrifuge 1.5 ml tubes	Beckman, Fullerton, US
Vivaspin 500	Sartorius, stedim biotech, Göttingen, DE
Whatman paper	Roth, Karlsruhe, DE

### 7.2.3 Chemicals/Enzymes

**Table 7.4: Applied Chemicals and enzymes.**

<b>Description</b>	<b>Company</b>
1 X Trypsin/EDTA	PAA-Laboratories, Linz, AT
2-Mercaptoethanol (p.a.)	Roth, Karlsruhe, DE
30% Acrylamide / 0,8% bisacrylamide, rotiphorese 30	Roth, Karlsruhe, DE
Acetic acid	Sigma Aldrich, Steinheim, DE
Agarose	Lonza, Cologne, DE
Al's oil (Paraffin and Silicon 50:50)	Hampton Research, Aliso Viejo, US
Ammonium Persulfate (APS)	Roth, Karlsruhe, DE
Ampicillin	Melford Laboratories, Chelsworth, UK
Bafilomycin A1	Calbiochem/Merck, Darmstadt, DE
Bovine serum Albumin (BSA)	Sigma Aldrich, Steinheim, DE
Bromphenol blue	Canalco, Bethesda, US
Calcium Chloride dehydrated	Merck, Darmstadt, DE
Citric acid	Merck, Darmstadt, DE
Complete Protease Inhibitor Cocktail	Roche, Mannheim, DE
Coomassie Brilliant Blue R-250	Bio-Rad, Hercules, US
DAB (3,3 Diaminobenzidine tetrahydrochloride)	Sigma Aldrich, Steinheim, DE
DABCO (1,4-Diazobicyclo[2.2.2]octane)	Sigma Aldrich, Steinheim, DE
DAPI (4',6-Diamidine-2-phenylindol)	Sigma Aldrich, Steinheim, DE
Desoxyribonucleosidetrifosphates (NTPs) (2 mM/ 10 mM)	Thermo Fisher Scientific, Waltham, US
Di-Calcium-hydrogen-phosphate	Roth, Karlsruhe, DE
Di-Sodium hydrogen phosphate	Roth, Karlsruhe, DE
DMSO (Dimethylsulfoxide)	Serva, Heidelberg, DE
DNA-Ladder (100 bp, 1 kb)	Roche, Mannheim, DE
DNA-Loading Dye	Thermo Fisher Scientific, Waltham, US

DNA-Polymerase (Taq, Pfu)	Thermo Fisher Scientific, Waltham, US
DNase	Roche, Mannheim, DE
Doxycycline	Sigma Aldrich, Steinheim, DE
DTT (Dithiothreitol)	Sigma Aldrich, Steinheim, DE
Dynabeads	Invitrogen, Darmstadt, DE
Ethanol 99,8% p.a.	Roth, Karlsruhe, DE
Ethidiumbromide	Roth, Karlsruhe, DE
Ethylendiamintetra acetic acid (EDTA)	Roth, Karlsruhe, DE
Eukitt	Sigma Aldrich, Steinheim, DE
Fetal Bovine serum	Invitrogen, Darmstadt, DE
Filipin (F9765)	Sigma Aldrich, Steinheim, DE
Fetal calf serum (FCS)	PAA, Laboratories, Linz, AT
G418 (Geneticin)	InvivoGen, Toulouse, FR
Glucose	Sigma Aldrich, Steinheim, DE
Glycerol	Sigma Aldrich, Steinheim, DE
Glycine	Roth, Karlsruhe, DE
Haematoxylin by Harris	Roth, Karlsruhe, DE
Hydrogen peroxide (30 % H <sub>2</sub> O <sub>2</sub> )	Merck, Darmstadt, DE
Hygromycin	InvivoGen, Toulouse, FR
Isopropanol (p.a.)	Roth, Karlsruhe, DE
Izit ® staining	Hampton Research, Aliso Viejo, US
Magnesium chloride	Merck, Darmstadt, DE
Methanol (p.a.)	Roth, Karlsruhe, DE
Milk powder	Roth, Karlsruhe, DE
Mowiol	Calbiochem, La Jolla CA, US
N,N,N',N'-Tetramethylethylendiamine (TEMED) (p.a.)	Roth, Karlsruhe, DE
N-butyl-deoxynojirimycin (Miglustat)	Tocris biosciences, Bristol, UK
Page Ruler Prestained Protein Ladder Plus	Thermo Fisher Scientific, Waltham, US
Paraformaldehyde	Fluka, Buchs, Switzerland
Penicillin/Steptomycin	PAA-Laboratories, Linz, AT
PFB-FDGlu (5- (Pentafluorobenzoyl-amino) Fluorescein Di-β-D-Glucopyranoside)	Thermo Fisher Scientific, Waltham, US
Polyethylenimin (PEI)	Sigma Aldrich, Steinheim, DE
Potassium Chloride	Roth, Karlsruhe, DE
Potassium dihydrogen-phosphate	Roth, Karlsruhe, DE
Potassium-hydrogen carbonate	Roth, Karlsruhe, DE
Restriction enzymes and buffers	Thermo Fisher Scientific, Waltham, US
RotiHistol	Roth, Karlsruhe, DE
Sodium chloride	Roth, Karlsruhe, DE
sodium dodecyl sulfate (SDS)	Roth, Karlsruhe, DE
Sodium hydrogen carbonate	Roth, Karlsruhe, DE
Sodium hydroxide	Riedel-de-Haen, Seelze, DE
Sodiumcitrate	Merck, Darmstadt, DE
Streptavidin (High Capacity) beads	Thermo Fisher Scientific, Waltham, US
Tetracyclin	Merck, Darmstadt, DE
Tris(hydroxymethyl)-aminomethane (TRIS)	Roth, Karlsruhe, DE
Triton X-100	Sigma Aldrich, Steinheim, DE
Trypan blue 0.4 %	Invitrogen, Darmstadt, DE
Trypsin/EDTA	Invitrogen, Darmstadt, DE
Turbofect® transfection reagent	Thermo Fisher Scientific, Waltham, US
Tween 20	Sigma Aldrich, St Louis, US

U18666A Xylol	Cayman Chemicals, Ann Arbor, US Roth, Karlsruhe, DE
------------------	--

## 7.2.4 Kits

**Table 7.5: Overview of utilised kits.**

Description	Company
ApopTag® Peroxidase <i>In situ</i> Apoptosis Detection Kit	Millipore (Schwalbach, DE)
BCA-Protein Assay Kit	Pierce; Thermo Fisher Scientific, Waltham, US
ECL Advanced/Plus Western Blot Detection Kit	GE Healthcare, Munich, DE
Elite DAB staining kit	Enzo Life Sciences, Lörrach, DE
EndoH/PNGaseF digestion kit	New England Biolabs, Ipswich, US
High Pure PCR-Purification Kit	Roche, Mannheim, DE
NucleoSpin® RNA easy Kit	Macherey-Nagel, Düren, DE
PureYield Plasmid Midiprep System	Promega, Mannheim, DE
Plasmid Miniprep Kit	Thermo Fisher Scientific, Waltham, US
RevertAid™ First Strand cDNA Synthesis Kit	Thermo Fisher Scientific, Waltham, US
RNA-isolaton	Macherey-Nagel, Düren, DE
Vector Laboratories ABC kit	Enzo Life Sciences, Lörrach, DE

## 7.2.5 Buffer and solutions

**Table 7.6: Overview of general buffers.**

Name of buffer/solution	Reagents
0.1 M NaPhosphat buffer, pH7	Stock: 195 ml 0.2 M NaH <sub>2</sub> PO <sub>4</sub> (27.6 g NaH <sub>2</sub> PO <sub>4</sub> ·1H <sub>2</sub> O in 1L dH <sub>2</sub> O) 305 ml 0.2 M Na <sub>2</sub> HPO <sub>4</sub> (35.6 g Na <sub>2</sub> HPO <sub>4</sub> ·1H <sub>2</sub> O in 1L dH <sub>2</sub> O) 500 ml dH <sub>2</sub> O
EBC-buffer cell lysis buffer for Co-IP experiments	50mM Tris 120mM NaCl 0,5% NP40 pH 7,4 (HCl) 1 tablet Complete ®
LB-Agar	10 g Bacto-Trypton 5 g Bacto-yeast-Extrakt 10 g NaCl 15 g/L Bacto-agar Fill to 1000 ml dest. H <sub>2</sub> O; pH7 autoclave and pour into 10 ml sterile dishes
LB-medium	10 g Bacto-Trypton 5 g Bacto-yeast-Extrakt 10 g NaCl Fill to 1000 ml H <sub>2</sub> O; pH7.4

Phosphate buffer (0.1 M PB)	77.4 ml 1M Na <sub>2</sub> HPO <sub>4</sub> 22.6 ml 1M Na <sub>2</sub> HPO <sub>4</sub> Fill to 1L with ddH <sub>2</sub> O, pH 7.4
Phosphate buffered saline solution (PBS)	137 mM NaCl 2.7 mM KCl 4.3 mM Na <sub>2</sub> HPO <sub>4</sub> 1.4 mM KH <sub>2</sub> PO <sub>4</sub> Fill to 1L with H <sub>2</sub> O, pH 7.4
50 x TAE buffer	2 M Tris 2 M Glacial acetic acid 100 ml 0.5 M EDTA (pH 8.0-8.5) Fill to 1000 ml ddH <sub>2</sub> O

**Table 7.7: Solutions for cell culture.**

<b>Name of buffer/solution</b>	<b>Reagents</b>
Dulbecco's Modified Eagle Medium (DMEM) High Glucose (4.5 g/ml) general cell culture medium (GE Healthcare, Chalfont St. Giles, UK)	+ additives: 10 % FCS 1 % Penicillin/Streptomycin
Freezing medium	1 % Penicillin/Streptomycin 20% DMSO 30% FCS in DMEM/RPMI medium
Opti-MEM medium For H4 (human neuroglioma) (Thermo Fisher Scientific, Waltham, US)	+ additives: 5 % FCS 1 % Penicillin/Streptomycin 200 µg/ml G418 200 µg/ml Hygromycin
RPMI medium 1640 for human fibroblasts (GE Healthcare, Chalfont St. Giles, UK)	+ additives: 10 % FCS 1 % Penicillin/Streptomycin
SM1-neurobasal (NB) medium For human neurons (iPSC-derived) (Thermo Fisher Scientific, Waltham, US)	without phenol red + additives: 10 % FCS

**Table 7.8: Enzyme activity assay buffers.**

<b>Name of buffer/solution</b>	<b>Reagents</b>
Enzyme activity assay citrate buffer	0.2 M Sodium citrate 0.04 % NaN <sub>3</sub> 0.2 % BSA pH 4.6

Enzyme activity assay stop solution	0.4 M Glycine pH to 10.4 with NaOH
Enzyme activity assay: substrate	10 mM 4-Nitrophenyl $\beta$ -D-glucopyranoside (Sigma-Alderich N7006) 0.2 M Citrate buffer

**Table 7.9: Buffer for SDS-PAGE and Western-Blotting.**

<b>Name of buffer/solution</b>	<b>Reagents</b>
Blocking buffer (IF)	10 % FCS, 0.2 % saponin
Coomassie destaining solution	10 % Methanol 10 % Acetic acid (CH <sub>3</sub> COOH) in ddH <sub>2</sub> O
Lysis Buffer cell pellets	50 mM Tris-NaOH 150 mM NaCl 2 mM EDTA Complete™ 1 % Triton-x 100 2 mM MgCl <sub>2</sub> pH 7.4
SDS soluble buffer (Mazzulli <i>et al.</i> , 2006)	2 % SDS, 50 mM Tris-HCl-pH7.4
SDS-PAGE-buffer 10x	1.92 M Glycine 250 mM Tris-HCl 35 mM SDS
4x SDS-PAGE-loading buffer (Laemmli)	500 mM Tris/HCl pH6.8 4 % SDS 40 % Glycerol 0.02 % Bromophenol blue 400 mM DTT Fill to 10 ml with ddH <sub>2</sub> O
Stacking gel buffer	0.5 M Tris 0.4 % (w/v) SDS pH 6.8
Seperation gel buffer	1,5 M Tris 0.4 % (w/v) SDS pH 8.8
Stripping buffer (Glycine)	100 mM Glycine 20 mM Mg-Acetate 50 mM KCl pH 2.2 Fill to 1L with ddH <sub>2</sub> O
Stripping buffer ( $\beta$ -ME)	200 ml 10 % SDS stock solution 62.5 ml Tris/HCl pH 6.8 8.3 ml $\beta$ -mercaptoethanol ( $\beta$ -ME) Fill to 1L with ddH <sub>2</sub> O

Tank-Blot-Transfer-Buffer (10X)	250 mM Tris 2 M Glycine pH 8.3
Tank-Blot-Buffer (1X)	1 x Tank-Blot-Buffer 10x 20 % Methanol Fill to 1L with ddH <sub>2</sub> O
TBS-T	20 mM Tris HCl 150 mM NaCl pH 7.5 0.1 % Tween20
Triton soluble buffer (Mazzulli <i>et al.</i> , 2006)	1 % triton x-100  20 mM HEPES 150 mM NaCl 10 % glycerol 1 mM MgCl <sub>2</sub> 50 mM NaF 2 mM NaVO <sub>3</sub> Complete™ pH 7.4
Washing/permeabilisation buffer (IF)	PBS, 0.2 % saponin
Western-Blot blocking buffer	5 g Milk powder dissolved in TBS/T

**Table 7.10: Buffers and solutions used for immunofluorescence (IF) and histological sections (IH).**

<b>Name of buffer/solution</b>	<b>Reagents</b>
Blocking/antibody solution (IH)	0.25% Triton-x-100, 4% goat serum in PB
Blocking buffer (IF)	10 % FCS, 0.2% Saponin in PBS
Citric acid immunohistology unmasking solution (IH)	10 mM Citric acid (pH 6 - NaOH)
H <sub>2</sub> O <sub>2</sub> -solution (IH)	0.3 % H <sub>2</sub> O <sub>2</sub> in PB
Masking buffer (IF)	0.12 % Glycine, 0.2% Saponine in PBS
Fixation solution (IF)	PBS, 4 % PFA
Mounting IF/IH (immunofluorescence only)	1 ml Mowiol solution (17 % Mowiol/33 % Glycerol in PBS; pH 6-7) 100 µl DABCO (200 mg/ml Diazobicyclooctan; end conc. 50 mg/ml) 1 µl DAPI-solution (end conc. 1 µg/ml)
Washing /permeabilisation buffer (IF)	PBS, 0.2 % Saponin
Washing solution (IH)	0.25% Triton-x-100 in PB

**Table 7.11: Solutions for recombinant protein/peptide assays and crystallisation.**

Name of buffer/solution	Reagents
Crystallisation buffer	100 mM Bis-Tris, pH 4.9-5.1 Ammonium sulphate: 2.0 – 2.4 M
NaPhosphate buffer solution for recombinant proteins/peptides;  peptides were solved in 0.1 % HCl (in 10 vol. % of total buffer vol.)	50 mM NaPhosphate 150 mM NaCl pH7
MES buffer solution of recombinant protein/peptides for crystallisation	50 mM MES 100 mM NaCl

## 7.3 List of figures and tables

### 7.3.1 Figures

Figure 1.1: Overview of major lysosomal membrane proteins. ....	12
Figure 1.2: Structure of the two mannose-6-phosphate-receptors (MPR300 and MPR46).....	14
Figure 1.3: Transport routes to the lysosome: Mannose-6-phosphate dependent and independent. ....	15
Figure 1.4: Overview of sphingolipid degradation and sphingolipidoses. ....	17
Figure 1.5: Cholesterol transport in late endosomes: the role of NPC1 and 2. ....	19
Figure 1.6: Protein model of the human LIMP-2 with the protein cavity indicated.....	21
Figure 1.7: Comparison of two different LIMP-2 crystal structures.....	22
Figure 1.8: Enzymatic reaction catalysed by $\beta$ -glucocerebrosidase.....	24
Figure 1.9: Protein structure of GC subdivided in three domains. ....	24
Figure 1.10: Overview of pathological mutations in the GC protein. ....	26
Figure 1.11: Structure of the $\alpha$ -synuclein protein.....	28
Figure 1.12: The role of LIMP-2 and GC in lysosomal degradation and aggregation of $\alpha$ -synuclein. ....	31
Figure 3.1: Analysis of $\alpha$ -synuclein levels in mice of two different genetic backgrounds.....	35
Figure 3.2: Map of pfrog3 vector.....	38
Figure 3.3: Principle of fusion-PCR.....	41
Figure 3.4: Different brain regions in a sagittal murine brain section.....	44
Figure 3.5: Structure of the Ttds-linker.....	48
Figure 3.6: Characteristic CD-spectra of individual secondary structures. ....	51
Figure 3.7: Principle of dynamic light scattering technique.....	52
Figure 3.8: Side view of under oil crystallisation batches.....	53
Figure 3.9: Illustration of endoglycosidase H/PNGaseF cleavage. ....	56
Figure 3.10: Principle of Co-Immunoprecipitation. ....	57
Figure 3.11: Set-up of TANK-blot system.....	58
Figure 3.12: Principle of measuring and calculating lysosomal GC activity. ....	61
Figure 4.1: Subcellular localisation of endogenous LIMP-2 in dependence of MPR and M6P.....	68
Figure 4.2: Immunoblot analysis indicating MPR-independent transport of LIMP-2 to the lysosome.....	68
Figure 4.3: Filipin stainings in LIMP-2 KO and LAMP-1/2 double KO MEFs. ....	70
Figure 4.4: Filipin staining in HeLa, LAMP-1/2 dKO cells and NPC fibroblasts after overexpression of LIMP-2. ....	72
Figure 4.5: Filipin stainings in HeLa cells treated with U18666A after overexpression of LAMP-1.....	73
Figure 4.6: Mutational analysis of the LIMP-2 tunnel mutant (V415W, A379W). ....	74
Figure 4.7: Crystal structure of LIMP-2 with an exposed helical bundle. ....	75
Figure 4.8: Subcellular localisation study of LIMP-2-GC binding mutants. ....	76
Figure 4.9: Endoglycosidase H and PNGaseF digestion of LIMP-2 mutants. ....	77
Figure 4.10: Structural overview of LIMP-2 mutants and interaction studies to determine the binding site of LIMP-2 to GC.....	78
Figure 4.11: Circular dichroism (CD) spectroscopy of the LIMP-2-derived peptides.....	80
Figure 4.12: Pulldown experiment using LIMP-2 peptides and recombinant GC. ....	80
Figure 4.13: Specificity control: precipitation experiment of recombinant LAMAN and BSA.....	81
Figure 4.14: Pulldown experiment revealing endogenous GC-precipitation from Cos7 cellular lysate. ....	81
Figure 4.15: Activity assays of recombinant and endogenous enzymes after incubation with LIMP-2-derived peptides.....	82
Figure 4.16: Effect of the recombinant LIMP-2 ectodomain and the helix 5 peptide on GC activity.....	83
Figure 4.17: Impact of LIMP-2 peptides on protein stability and function.....	84
Figure 4.18: Stabilisation assay of GC after incubation at 37°C.....	85
Figure 4.19: GC activity assay after incubation with fragmented peptides derived from the helix 5 sequence. ...	86
Figure 4.20: Uptake and effect of helix 5 peptide in J774E mouse macrophages.....	86
Figure 4.21: Uptake and effect of GC pre-incubated with LIMP-2 peptides into GC KO MEFs. ....	87
Figure 4.22: Thermal protein stability: CD-analysis of GC after incubation with helix 5 peptide. ....	88
Figure 4.23: Dynamic light scattering (DLS) of GC in the presence or absence of the helix 5 peptide. ....	89
Figure 4.24: Crystallisation approach showing shape and properties of GC crystals. ....	90
Figure 4.25: Surface charge analysis of LIMP-2 and GC protein. ....	91
Figure 4.26: Structural and functional characterisation of GC mutants analysed in this study.....	93
Figure 4.27: Co-Immunoprecipitation studies of GC 'glutamic acid mutants'. ....	94
Figure 4.28: Co-Immunoprecipitation study of Gaucher patient mutants. ....	95
Figure 4.29: Analysis of cellular localisation of GC 'glutamic acid mutants' by immunofluorescence. ....	96

Figure 4.30: Triple stainings of GC constructs with LIMP-2 and an additional lysosomal marker LAMP-2.....	97
Figure 4.31: Analysis of cellular localisation of GC mutants by endoglycosidase H digestion.....	98
Figure 4.32: Analysis of cellular localisation of GC patient mutants by immunofluorescence microscopy.....	99
Figure 4.33: Triple stainings of GC patient mutants with LIMP-2 and LAMP-2.....	100
Figure 4.34: Analysis of cellular localisation of GC mutants by endoglycosidase H digestions.....	100
Figure 4.35: LIMP-2 co-expressed with GC leads to a molecular weight shift due to transport to lysosomes...	102
Figure 4.36: Biochemical analysis of the cellular localisation of the GC mutants by endoglycosidase H digestion. .....	103
Figure 4.37: Immunofluorescence microscopy to evaluate co-localisation of GC mutants and LIMP-2.....	104
Figure 4.38: Effect of LIMP-2 co-expression on GC activity.....	104
Figure 4.39: Pulldown of overexpressed GC mutants with LIMP-2-derived peptides from cell lysates.....	105
Figure 4.40: LIMP-2 deficiency causes decreased GC expression and activity in murine pons and midbrain...	106
Figure 4.41: Periodic-acid-Schiff staining (PAS) of brain sections at different ages.....	107
Figure 4.42: Electron micrographs indicating storage material in the pons of LIMP-2 KO mice.....	108
Figure 4.43: Immunoblot analysis revealing $\alpha$ -synuclein accumulation in the midbrain of LIMP-2-deficient animals.....	109
Figure 4.44: Immunohistochemical stainings of $\alpha$ -synuclein in midbrain and pons.....	110
Figure 4.45: DAB-immunohistochemistry showing highly progressive neurotoxic effects of $\alpha$ -synuclein.....	112
Figure 4.46: Effect of $\alpha$ -synuclein on lysosomal GC activity in human midbrain dopaminergic neurons.....	114
Figure 4.47: Immunohistological stainings of LIMP-2 in control and PD midbrain sections.....	114
Figure 4.48: Biochemical analyses of fibroblasts derived from AMRF patients.....	116
Figure 4.49: Whole cell and lysosomal GC activity is increased after LIMP-2 overexpression.....	117
Figure 4.50: LIMP-2 overexpression leads to a decrease in $\alpha$ -synuclein protein levels in murine N2a cells....	118
Figure 4.51: LIMP-2 overexpression leads to a decrease in $\alpha$ -synuclein protein levels in human H4 cells.....	118
Figure 4.52: Turn-over rate of $\alpha$ -synuclein after overexpression of LIMP-2 in human H4 cells.....	119
Figure 4.53: Uptake of LIMP-2-derived TAT peptides and their effects on intracellular $\alpha$ -synuclein levels....	121
Figure 5.1: Hetero-trimeric complex of LIMP-2 bound to GC and to the CI-MPR.....	123
Figure 5.2: LIMP-2 protein model with highlighted hydrophobic interaction site.....	129
Figure 5.3: The potential LIMP-2 interaction site on the GC protein exhibits hydrophobic characteristics.....	132
Figure 5.4: GC protein model indicating all existing disease causing missense mutations.....	133
Figure 5.5: Structural model of GC indicating functionally important regions.....	134
Figure 5.6: Structural analysis of the described interaction sites in the GC protein.....	136
Figure 5.7: Structural model of LIMP-2 and GC showing their interaction.....	137
Figure 5.8: GC protein structure with LIMP-2 helix 5 peptide bound to the helical bundle.....	139
Figure 5.9: Schematic interaction between LIMP-2, GC and $\alpha$ -synuclein.....	147
Figure 5.10: Overview of strategies to reduce the accumulation of $\alpha$ -synuclein.....	148

### 7.3.2 Tables

Table 3.1: Cell lines utilised in this study.....	33
Table 3.2: Overview of primary antibodies.....	35
Table 3.3: Overview of secondary antibodies.....	36
Table 3.4: Overview of primer for cloning and site-directed mutagenesis.....	37
Table 3.5: Overview of utilised expression constructs.....	38
Table 3.6: Standard-PCR procedure: Ingredients and protocol.....	40
Table 3.7: Protocol for PAS-staining of brain sections.....	47
Table 3.8: Overview and properties of utilised peptides.....	48
Table 3.9: Overview and description of utilised recombinant enzymes.....	49
Table 3.10: Settings of CD-spectrum measurements.....	52
Table 3.11: Properties of the BL14.1 beamline.....	54
Table 3.12: List of utilised software for data handling and analysis.....	65
Table 4.1: Overview of the three peptide sequences.....	79
Table 4.2: Overview of small peptide sequences.....	85
Table 4.3: X-ray parameters of the protein crystals.....	90
Table 4.4: Overview of the introduced GC point mutations.....	92
Table 7.1: Abbreviations.....	167
Table 7.2: Overview of utilised machines.....	168
Table 7.3: Laboratory material.....	169

---

Table 7.4: Applied Chemicals and enzymes. ....	170
Table 7.5: Overview of utilised kits. ....	172
Table 7.6: Overview of general buffers.....	172
Table 7.7: Solutions for cell culture. ....	173
Table 7.8: Enzyme activity assay buffers.....	173
Table 7.9: Buffer for SDS-PAGE and Western-Blotting. ....	174
Table 7.10: Buffers and solutions used for immunofluorescence (IF) and histological sections (IH). ....	175
Table 7.11: Solutions for recombinant protein/peptide assays and crystallisation.....	176

## 7.4 Curriculum Vitae

### *Friederike Zunke*

Gender: female  
Date/Place of birth: 27.09.1987, Neumünster, Germany

#### Education

- |                   |   |
|-------------------|---|
| From 10/2011      | <i>Doctoral training</i> in the DFG funded Research Training Group 1459:<br>Thesis: ‘Analysis of the lysosomal transport receptor (LIMP-2)’<br>Institute of Biochemistry, University of Kiel, Germany;<br>Prof. Dr. Paul Saftig, PD Dr. Michael Schwake |
| 01/2013 – 01/2015 | PhD project funded by the Boehringer Ingelheim Fonds  |
| 09/2010 - 09/2011 | <i>Master of Research in Biomedical Sciences</i><br>Thesis: ‘Role and function of Kv7.4 channels in vascular regulation’<br>Department of Cell Signalling, St. George’s University, London, UK;<br>Dr. Iain Greenwood                                   |
| 09/2007 - 09/2010 | <i>Bachelor of Science in Biochemistry</i><br>Thesis: ‘Structural and functional analysis of KCNQ1 and KCNE2’<br>Institute of Biochemistry and Institute of Physiology, University of Kiel;<br>PD Dr. Michael Schwake, Prof. Dr. Markus Bleich          |
| 1998 - 2007       | <i>Abitur (A-Levels)</i><br>Klaus-Groth-Schule, Neumünster, Germany   |

#### Practical Experiences during doctoral training

- |                   |  |
|-------------------|--|
| 11/2014           | Training in UV- crosslinking and click-chemistry of lipids<br>Department of molecular Cell Biology, University of Osnabrück,<br>Prof. Dr. Joost Holthuis           |
| 07/2013 – 10/2013 | Collaboration and training in iPS-technology cooperated in PhD studies<br>Department of Neurology, Harvard Medical School, Boston, USA,<br>Dimitri Krainc, MD, PhD |

## 7.5 Publications and scientific participations

### Publications

- 07/2015 *Sent to journal:* **Zunke F**, Wesseler S, Groth J, Arnold P, Rothaug, M, Saftig P, Schwake M: Unraveling the molecular architecture of the  $\beta$ -glucocerebrosidase/ lysosomal integral membrane protein type 2 complex. **Proceedings of the National Academy of Sciences (PNAS)**.
- 06/2015 *In revision:* Blanz J\*, **Zunke F\***, Markamm S, Damme M, Braulke T, Saftig P, Schwake M: Mannose-6-phosphate-independent Lysosomal Sorting of LIMP-2. **Traffic**. \* authors contributed equally
- 06/2015 *In revision:* Mazzulli J, **Zunke F**, Jeon S, Tsunemi T, Burbulla L, Patnaik S, Sidranski E, Marugan J, Sue C, Isacson O, Studer L, Krainc D: Alpha-Synuclein-induced Lysosomal Dysfunction is Reversible by Modulation of Glucocerebrosidase in Parkinson Patient Neurons. **Nature Communications**.
- 05/2015 Arnold P, Schmidt F, Prox J, **Zunke F**, Pietrzik C, Lucius R, Becker-Pauly C. Calcium negatively regulates meprin  $\beta$  activity and attenuates substrate cleavage. **FASEB J**. 2015 May 8.
- 01/2015 Rothaug M, Stroobants S, Schweizer M, Peters J, **Zunke F**, Allerding M, D Hooge R, Saftig P, Blanz J: LAMP-2 deficiency leads to hippocampal dysfunction but normal clearance of neuronal substrates of chaperone-mediated autophagy in a mouse model for Danon disease. **Acta Neuropathol Commun**.
- 01/2015 Peters J, Rittger A, Weisner R, Knabbe J, **Zunke F**, Rothaug M, Damme M, Berkovic SF, Blanz J, Saftig P, Schwake M: Lysosomal integral membrane protein type-2 (LIMP-2/SCARB2) is a substrate of cathepsin-F, a cysteine protease mutated in type-B-Kufs-disease. **Biochem Biophys Res Commun**.
- 10/2014 Rothaug M\*, **Zunke F\***, Mazzulli JR, Schweizer M, Altmepfen H, Lüllmann-Rauch R, Kallemeijn WW, Gaspar P, Aerts JM, Glatzel M, Saftig P, Krainc D, Schwake M, Blanz J: LIMP-2 expression is critical for  $\beta$ -glucocerebrosidase activity and  $\alpha$ -synuclein clearance. **Proceedings of the National Academy of Sciences (PNAS)**. \* authors contributed equally
- 01/2014 Gaspar P, Kallemeijn WW, Strijland A, Scheij S, Van Eijk M, Aten J, Overkleeft HS, Balreira A, **Zunke F**, Schwake M, Sá Miranda C, Aerts JM. Action myoclonus-renal failure syndrome: diagnostic applications of activity-based probes and lipid analysis. **Journal of Lipid Research**.
- 12/2013 Neculai D, Schwake M, Ravichandran M, **Zunke F**, Collins RF, Peters J, Neculai M, Plumb J, Loppnau P, Pizarro JC, Seitova A, Trimble WS, Saftig P, Grinstein S, Dhe-Paganon S: Structure of LIMP-2 provides functional insight with implications for SR-BI and CD36. **Nature**.
- 04/2012 Chadha PS, **Zunke F**, Zhu HL, Davis AJ, Jepps TA, Olesen SP, Cole WC, Moffatt JD, Greenwood IA: Reduced KCNQ4-encoded voltage-dependent potassium channel activity underlies impaired beta-adrenoceptor-mediated relaxation of renal arteries in hypertension. **Hypertension**.
- 01/2012 Chadha PS, **Zunke F**, Davis AJ, Jepps TA, Linders JT, Schwake M, Towart R, Greenwood IA: Pharmacological dissection of Kv 7.1 channels in systemic and pulmonary arteries. **British Journal of Pharmacology**.

**Scientific Participation**

- 03/2015 Gordon Conference and Seminar: Lysosomal storage diseases; Galveston, Texas, USA (Oral and poster presentation)
- 09/2014 International Symposium 'Protein Trafficking in Health and Disease', Hamburg, Germany (Poster presentation)
- 09/2014 Boehringer Ingelheim Annual Meeting, Hirschegg; Austria (Oral presentation)
- 11/2013 Society for Neuroscience, 43<sup>rd</sup> Annual Meeting; San Diego, CA, USA
- 09/2012 International Symposium 'Protein Trafficking in Health and Disease'; Hamburg, Germany (Poster presentation)
- 07/2011 Meeting of Physiological Society in Oxford, UK (Poster presentation)
- 04/2011 Experimental Biology; Washington D.C., USA (Poster)

**Scientific Awards**

- 03/2015 Poster selected for additional special oral presentation (Gordon Conference, Texas, USA)
- 09/2014 Poster prize: International Symposium 'Protein Trafficking in Health and Disease' (Hamburg, Germany)
- 01/2013 Boehringer Ingelheim stipend
- 09/2011 Master of Research poster prize (St. George's University of London)
- 02/2011 Student award (Holsteiner Studienpreis) by the University of Kiel for outstanding achievements and social commitment

## **7.6 Acknowledgments/Danksagung**

## 7.7 Declaration

Herewith I declare that:

- apart from the supervisor`s guidance, the content and design of this dissertation is my own work.
- this thesis has not been submitted partially or wholly as part of a doctoral degree to another examining body, but parts of this work have been published or submitted for scientific publication:

Published work:

- (1) Neculai D, Schwake M, Ravichandran M, **Zunke F**, Collins RF, Peters J, Neculai M, Plumb J, Loppnau P, Pizarro JC, Seitova A, Trimble WS, Saftig P, Grinstein S, Dhe-Paganon S. Structure of LIMP-2 provides functional insights with implications for SR-BI and CD36. *Nature*. 2013 Dec 5; 504(7478):172-6.
- (2) Rothaug M\*, **Zunke F\***, Mazzulli JR, Schweizer M, Altmeyen H, Lüllmann-Rauch R, Kallemeijn WW, Gaspar P, Aerts JM, Glatzel M, Saftig P, Krainc D, Schwake M, Blanz J.;  
\* shared first position  
LIMP-2 expression is critical for  $\beta$ -glucocerebrosidase activity and  $\alpha$ -synuclein clearance. *Proc Natl Acad Sci U S A (PNAS)*. 2014 Oct 28; 111(43):15573-8.

Work in revision at the following journals:

- (3) Blanz J\*, **Zunke F\***, Markamm S, Damme M, Bräulke T, Saftig P, Schwake M.  
\* shared first position  
Mannose-6-phosphate-independent Lysosomal Sorting of LIMP-2.  
*Traffic*. Send for revision: 06/29/15
- (4) Mazzulli J, **Zunke F**, Jeon S, Tsunemi T, Burbulla L, Patnaik S, Sidranski E, Marugan J, Sue C, Isacson O, Studer L, Krainc D.  
Alpha-Synuclein-induced Lysosomal Dysfunction is Reversible by Modulation of Glucocerebrosidase in Parkinson Patient Neurons.  
*Nature Communications*. Send for revision: 06/29/15

Script sent to the following journal:

- (5) **Zunke F**, Wessler S, Groth J, Arnold P, Rothaug, M, Saftig P, Schwake M.  
Unraveling the molecular architecture of the  $\beta$ -glucocerebrosidase/ lysosomal integral membrane protein type 2 complex.  
*Proc Natl Acad Sci USA (PNAS)*, send to journal 07/08/15

- this thesis has been prepared according to the Rules of Good Scientific Practice of the German Research Foundation.

Kiel, July 2015

Friederike Zunke

